NASA CR-132544

INFLUENCE OF PROPULSION SYSTEM SIZE, SHAPE, AND LOCATION ON SUPERSONIC AIRCRAFT DESIGN

Prepared by

Ellwood Bonner
Marshall H. Roe
Ray M. Tyson
Ronald Y. Mairs

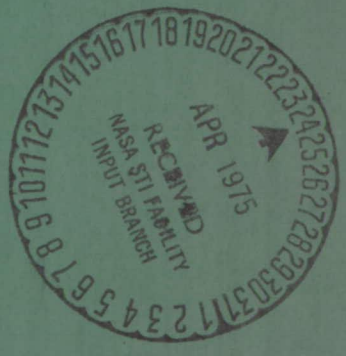

December 1974

Prepared Under Contract NAS1-13105
By Los Angeles Aircraft Division
ROCKWELL INTERNATIONAL CORPORATION
Los Angeles, California
For
LANGLEY RESEARCH CENTER
NATIONAL AERONAUTICS AND SPACE ADMINISTRATION

NASA CR-132544

INFLUENCE OF PROPULSION SYSTEM SIZE, SHAPE, AND LOCATION ON SUPERSONIC AIRCRAFT DESIGN

Prepared by

Ellwood Bonner
Marshall H. Roe
Ray M. Tyson
Ronald Y. Mairs

December 1974

Prepared Under Contract NAS1-13105
By Los Angeles Aircraft Division
ROCKWELL INTERNATIONAL CORPORATION
Los Angeles, California
For
LANGLEY RESEARCH CENTER
NATIONAL AERONAUTICS AND SPACE ADMINISTRATION

ABSTRACT

An investigation was made of the effects of various propulsion system parameters on the characteristics of a supersonic transport. The effects of arbitrarily scaling engine size on wave drag, friction drag, drag-due-to-lift, wing sizing, airplane balance, and airplane weight were studied. These evaluations were made for two families of nacelle shapes, resulting from typical turbojet and turbofan installations. Effects of nacelle location were examined, and the wing camber plane deformations required to cancel the nacelle interference pressure field at cruise Mach number (2.7 M) were determined.

The most drag-sensitive parameter was found to be nacelle shape. Similarly, wing deformation requirements were found to be primarily affected by nacelle shape. Effects of engine size variations were noted primarily in airplane gross weight.

TABLE OF CONTENTS

LIST OF ILLUSTRATIONS

LIST OF ILLUSTRATIONS (Continued)

LIST OF ILLUSTRATIONS (Continued)

LIST OF ILLUSTRATIONS (Continued)

LIST OF ILLUSTRATIONS (Continued)

LIST OF TABLES

LIST OF TABLES

INFLUENCE OF PROPULSION SYSTEM SIZE, SHAPE, AND LOCATION ON SUPERSONIC AIRCRAFT DESIGN

By Ellwood Bonner, Marshall H. Roe, Ray M. Tyson, and Ronald Y. Mairs
Los Angeles Aircraft Division, Rockwell International

SUMMARY

The objectives of this study were to determine in a parametric manner the overall effects on supersonic cruising aircraft design of the arbitrary scaling up and down of the propulsion package and to examine the sensitivity of these effects to nacelle shape. The study was made for nacelle shapes typical of a dry turbojet engine and a duct burning turbofan engine.

The NASA arrow-wing configuration was used as a baseline airframe, with only those changes being made that were necessary to the engine installation. Results of this study cannot be assumed to be applicable to other airframe configurations.

The turbojet engine used was the same as that used in a previous study (reference 1), wherein a turbojet and a variable-cycle engine were compared. In order to select the duct heating turbofan cycle for use in this study, 18 different turbofan cycles were examined, and one was selected that resulted in the lowest airplane weight to perform a given mission. The turbojet and the turbofan were then scaled over the range of airflows from 272 to 544 kg/sec (600 to 1200 lb/sec) at 45 kg/sec (100 lb/sec) increments. The effects of engine cycle and size on cruise drag, takeoff gross weight (TOGW) and wing camber plane deformation required for nacelle interference cancellation were then determined.

Quantitative results illustrate a sensitivity to engine cycle through the nacelle shaping, which is related to engine cycle parameters. The duct heating turbofan (DHTF) nacelle had an exhaust area very nearly equal to the maximum nacelle cross-sectional area, resulting in a very small boattail angle. This characteristic shape produces a pressure field which, when imposed on the aft portion of the wing, results in reduced wave drag at cruise Mach number. Because of the favorable shape and the favorable location, the larger the nacelle, the larger the favorable interference drag. The turbojet (TJ) cycle results in a nacelle shape with more boattailing and thus does not have the favorable interference effect demonstrated by the DHTF installation. Friction drag, of course, is directly related to the wetted area which increases with engine size. The magnitude of the friction drag component was larger than the cruise speed wave drag increments; therefore, the net effect on cruise drag was, in all cases, an increasing drag with increasing engine size.

The variation of wing camber plane deformation required to cancel the interference pressure field imposed on the wing by the nacelle was found to be within reasonable manufacturing techniques. The magnitude of the required deformations for the turbojet installation was greater than that for the turbofan installation, again due to differences in the shaping of the nacelles.

Airplane sizing studies were conducted to assess the overall effect of the engine size and cycle variations on the takeoff gross weight of vehicles designed to perform a given mission. This sizing process accounts for the variation of propulsion system weight, fuel consumption characteristics, airplane drag and airplane balance provisions. It does not include a possible variation of wing flutter weight penalty associated with the different engine sizes. These results show a high sensitivity of airplane weight to engine size, with the turbojet cycle having a higher sensitivity than the duct heating fan.

Because of the strong influence of cycle-related nacelle shaping, and to extend the data base for support of future supersonic airplane programs, it is recommended that the effects of variable-geometry components (variable-area turbines, variable fan inlet guide vanes, and additional variable compressor stators) for turbojet and turbofan cycles, and of variable-cycle engine parameters that affect nacelle shape, be examined on an overall airplane design basis.

INTRODUCTION

The National Aeronautics and Space Administration is conducting a continuing program of advanced supersonic technology studies with the objective of developing an adequate technology base to support development of future supersonic cruising aircraft. It is recognized in this program that one of the more sensitive problems in the synthesis of a successful supersonic cruising aircraft is that of airframe/engine integration. This process must investigate and properly manage the interactions between the technical disciplines of external aerodynamics, internal aerodynamics, engine cycle design, acoustics, mass properties, and structural design; and, it must be responsive to the practical considerations of fabrication, maintenance, and operation.

Although considerable effort has been expended on the problem of airframe/engine integration, it has been mostly in the nature of point-designs, which do not provide the sensitivity-type data needed for preliminary engine and airframe design studies. This need of sensitivity, or trend, data was the instigation of the present study. This study makes a systematic investigation of the effects of engine mass flow rate and the effects of engine cycle design on the cruise drag, takeoff weight, and wing camber plane deformation required for nacelle interference cancellation of a representative supersonic transport.

The study is limited to a Mach 2.7 cruise speed and two engine cycles - dry turbojet and duct heating turbofan - and does not analytically account for wing flutter effects. The study utilized the NASA-modified SCAT-15F as a baseline airframe on which to perform the parametric variations.

This work was performed by the Los Angeles Aircraft Division of Rockwell International under contract NAS1-13105 for the NASA Langley Research Center.

In addition to the authors noted, significant contributions to this study and report were made by Thomas P. Goebel and Bruce E. Moore, aerodynamics; Kenneth W. Williston, propulsion; Floyd D. Halferty, Jr., structural design; Lester D. Hendrix, configuration design; and David Chaloff, mass properties.

LIST OF SYMBOLS

NOTE: All aerodynamic coefficients are based on reference area of 929 sq m (10 000 sq ft) and reference chord of 50.3 m (1980 in.), unless noted otherwise.

A_c	Inlet capture area, sq m (sq in.)
ALT	Altitude, m (ft)
BP	Basepoint
C_D	Drag coefficient
C_{D_F}	Friction drag coefficient
C_{D_L}	Coefficient of drag due to lift
C_{D_P}	Profile drag coefficient
C_{D_W}	Wave drag coefficient
CG	Center of gravity
C_L	Lift coefficient
C_M	Pitching moment coefficient
C_P	Static-pressure coefficient
C_{REF}	Reference chord, 50.3 m (1980 in.)
D	Diameter, m, cm (in.)

daN	DecaNewton
dB	Decibel
DHTF	Duct heating turbofan
EPNL	Effective perceived noise level, EPNdB
FAR 36	Federal Aviation Regulation Part 36
F_G	Gross thrust, daN (lb)
FN	Net thrust, daN (LB)
FNE	Net propulsive effort, daN (lb)
h	Altitude, m (ft)
ℓ, L	Length, m, cm (ft)
L/D	Lift-to-drag ratio
M, M_o	Free-stream Mach number
m	Meter
OPR	Overall pressure ratio
P	Perimeter, m, cm (in.)
PNL	Perceived noise level, PNdB
R	Reference length = 2.54 cm (1 in.)
SFC	Specific fuel consumption, kg/hr/daN (lb/hr/lb)
S_{REF}	Reference area, sq m (sq ft),
S_W	Gross wing area
S_{WET}	Wetted area, sq m (sq ft)
$\bar{S}$	Average oblique projected area
S_π	Cross-sectional area
SL	Sideline distance
TOGW	Takeoff gross weight, kg (lb)

T-D	Thrust minus drag, daN (lb)
T/D	Thrust divided by drag
TJ	Turbojet
T/W	Thrust divided by weight, daN/kg (lb/lb)
V_1	Engine failure speed, km/hr (knots)
WF	Fuel flow, kg/hr (lb/hr)
W/S	Weight divided by wing area, kg/sq m (lb/sq ft)
X	Airplane longitudinal dimension, m (in.)
Y	Airplane lateral dimension, m (in.)
Y'	Nondimensional lateral station, Y/R
Z	Airplane vertical dimension, m (in.)
X_{NAC}	Nacelle longitudinal dimension, m (in.)
α	Angle of attack, degrees
Δ	Increment
$\Delta\Delta C_D$	Change in drag increment
$\Delta X'$	Nondimensional length increment = $\frac{\Delta X}{R}$
$\Delta Y'$	Nondimensional length increment = $\frac{\Delta Y}{R}$
$\Delta Z'$	Nondimensional length increment = $\frac{\Delta Z}{R}$

SUBSCRIPTS

C	Camber
MIN	Minimum value
MAX	Maximum value
REF	Reference
0	Free-stream or zero incidence value

NAC	Nacelle
EXIT	Nozzle exit
CAP, CAPTURE	Inlet mass flow ratio one stream tube
BP	Basepoint
Noz	Nozzle
i	Inboard nacelle
o	Outboard nacelle
W	Wing

STUDY PROCEDURE

Approach

The objectives of this investigation were to develop parametric data on the effects of engine mass flow rate on the cruise drag, takeoff gross weight, and wing camber plane deformation required to cancel the nacelle interference pressure field, for a representative supersonic transport configuration. Two engine cycles were specified - dry turbojet and duct heating turbofan.

Task description.- The general approach employed in pursuit of these objectives is illustrated in the task flow diagram shown in figure 1. Four major tasks were involved: (1) development of propulsion system data, (2) preliminary analysis - first-iteration wave drag and airplane sizing analyses, (3) refined analysis - second-iteration wave drag and airplane sizing analyses, and (4) wing camber plane deformation analysis.

Baseline airplane configuration characteristics and turbojet engine characteristics were obtained from the results of reference 1, which is a comparison of a variable-cycle engine and a turbojet engine installation in a supersonic transport.

An analysis was made to define an optimum duct heating turbofan cycle for the baseline airplane and for the design mission. Selection of engine cycle parameters was made on the basis of the minimum engine-plus-fuel weight to complete the mission, while meeting noise and structural temperature constraints. Following engine cycle definition, installed engine performance data and a

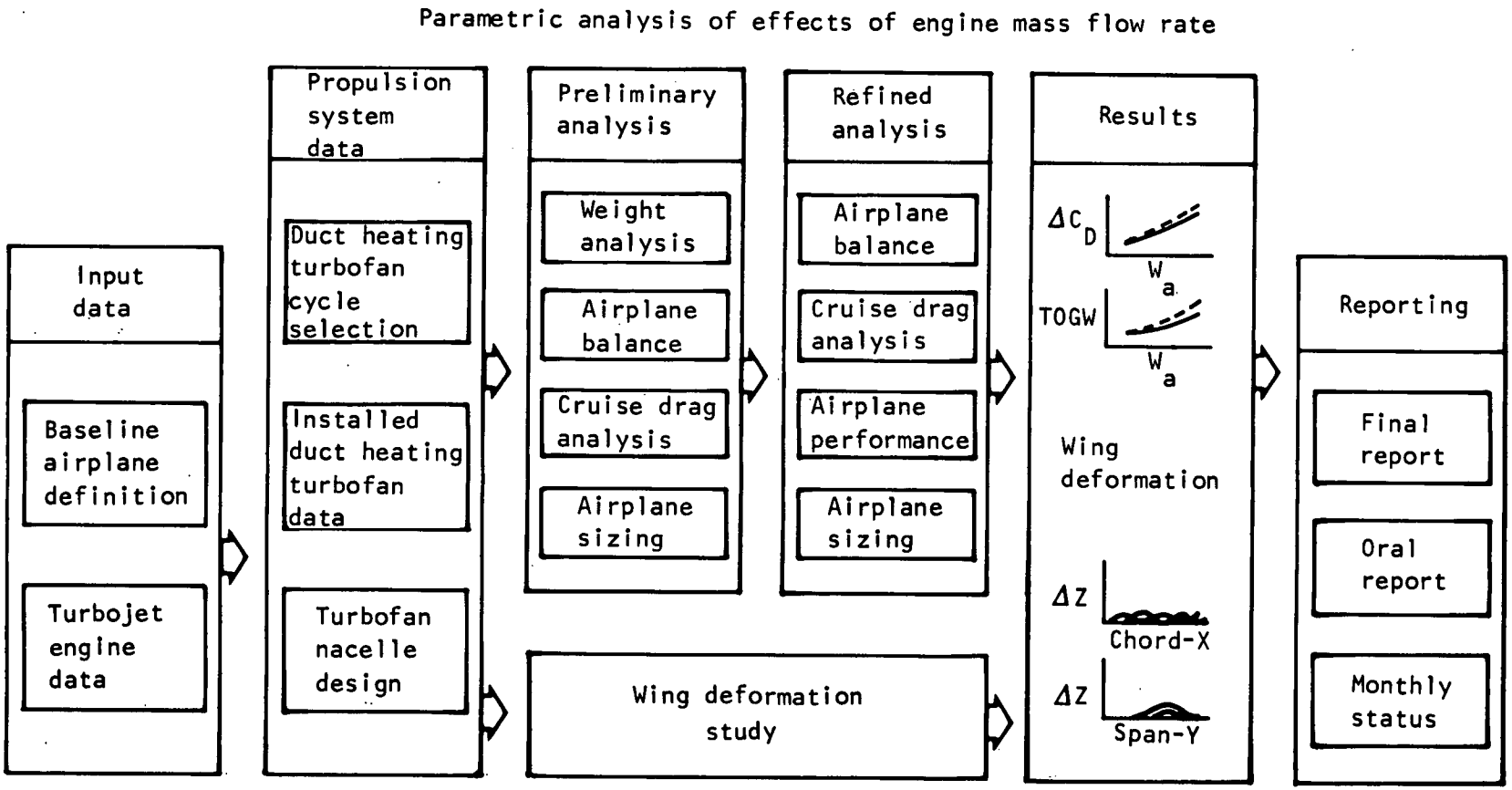

Figure 1.- Task flow diagram.

nacelle design were prepared for a nominal 408 kg/sec (900 lb/sec) engine. These were subsequently scaled over the range of 272 to 544 kg/sec (600 to 1200 lb/sec) for the required parametric analyses.

Following the fan engine analysis, preliminary sizing of the airplane was performed for the two engine cycles for 272, 408, and 544 kg/sec (600, 900, and 1200 lb/sec) airflow. This task involved estimation of the propulsion system weight and relocation of the wing to maintain airplane balance. For this first iteration of airplane sizing, wave drag estimates were based on wing and nacelle locations as defined for the baseline wing area of 995 sq m (10 713 sq ft)

In the refined analysis task, wing areas resulting from the first iteration sizing process were used for airplane rebalancing. These refined airplane geometry data were then used in the wave drag analysis. With these second-iteration drag data, sizing analyses were repeated to define takeoff weight required for the design range, as a function of engine mass flow rate.

Concurrently with the airplane sizing analyses, a study was conducted to define the wing camber plane deformation required to cancel the nacelle interface effects on cruise drag-due-to-lift. This analysis was performed for both engine cycles at 272, 408, and 544 kg/sec (600, 900, and 1200 lb/sec) airflow, with the nacelles installed on the baseline wing of 995 sq m (10 713 sq ft) area.

Ground rules.-

Baseline airframe: The reference configuration used in this study is a modification of the Mach 2.7 arrow-wing-design identified as model 969-336C in the Boeing Company report D6A11666-1. Characteristics of this airplane were supplied by NASA, including mass properties data, dimensional data, and aerodynamic data. These data were incrementally corrected to account for changes due to alternate propulsion systems. These resulting changes in weights and drag are given in detail under "Study Configuration Definitions."

Performance requirements: The performance requirements which were established as a standard for all final configurations are:

Range:	6482 km (3500 n. mi.) for the basic mission described following
Field length:	3200 m (10 500 ft), sea level, standard day; longer of balanced field length, or 115 percent of normal takeoff distance

Noise levels:	FAR 36
Cruise speed:	2.7 Mach number. This was specified in the definition of the baseline airplane.
Payload:	22 290 kg (49 140 lb) (234 passengers and luggage)
Thrust margin:	T/D ≥ 1.2 at 2.7 M, 18 300 m (60 000 ft) altitude, all engines operating, standard day
Mission:	The mission description used for calculating range, or fuel required for a given range, for each candidate configuration is illustrated in figure 2.
Fuel reserves:	As recommended in Lockheed report LR26 133 (ref. 2)
Alternate mission:	The mission description for the case of a critical engine failure at midmission is defined in figure 3.

Study Configuration Definition

Airframe.- The reference configuration used for the study is the Langley Research Center 340 000 kg (750 000 lb) TOGW, 234-passenger transport with 995 sq m(10 713 sq ft) two-segment leading edge arrow-wing and four axisymmetric pod-mounted 278 kg/sec (633 lb/sec) GE4/J5P turbojet engines along the trailing edge. The general arrangement of this configuration is presented in figure 4. The normal cross-sectional area distribution buildup and component wetted area summary are presented in figure 5 and table I, respectively.

Flaps and gear-down trimmed lift and drag characteristics used for airport performance analysis are presented in figure 6. These results were taken directly from reference 3, section 7.2.1. Adjustments for canard removal, use of the horizontal tail as the primary trim device, wing leading edge sweep modification, etc., were neglected, since the present study is concerned with relative as opposed to absolute performance. The lift-off lift coefficient of about 0.55 was assumed to be unaffected by increases in engine size or decreases in wing area. Although the flap effectiveness, C_{L_δ}, would be expected to be degraded by reduction in flap span as engine size increases, the lift-off angle of attack can be increased due to the aft movement of the wing. The variation of flap area and lift-off angle-of-attack limit is shown in table II as a function of engine size.

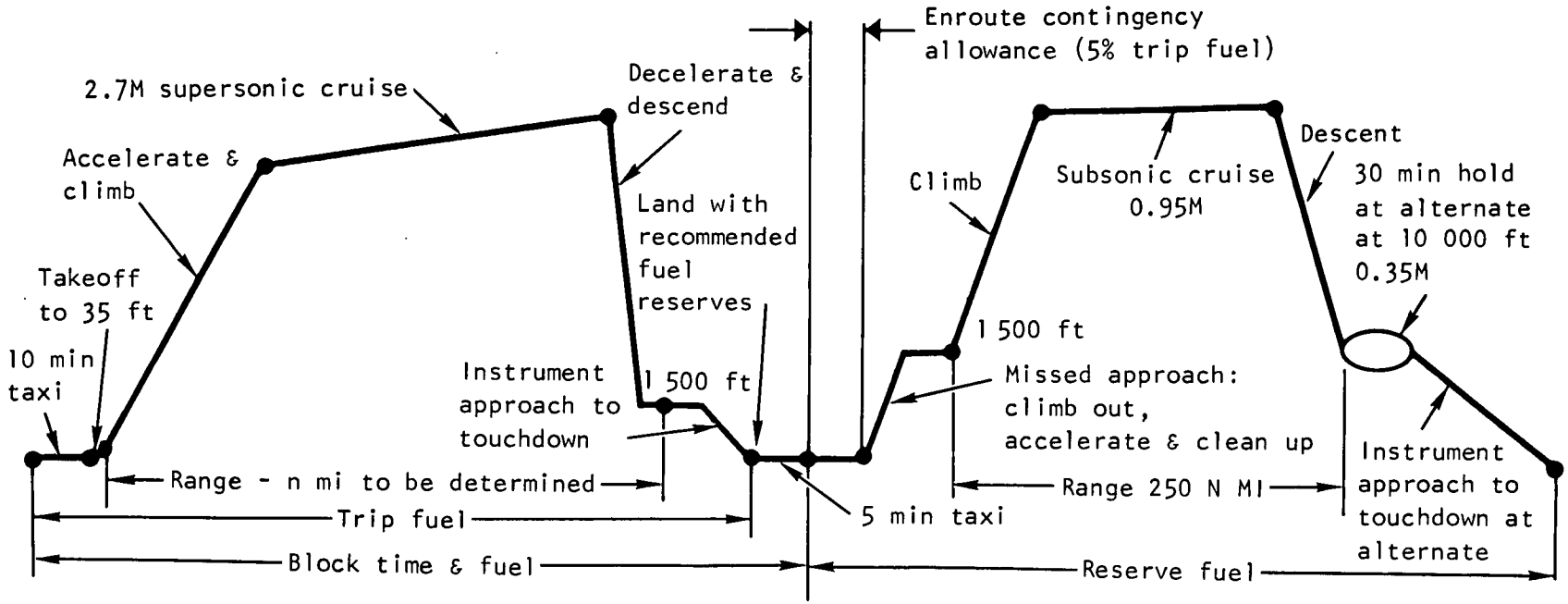

Figure 2.- Reference mission description.

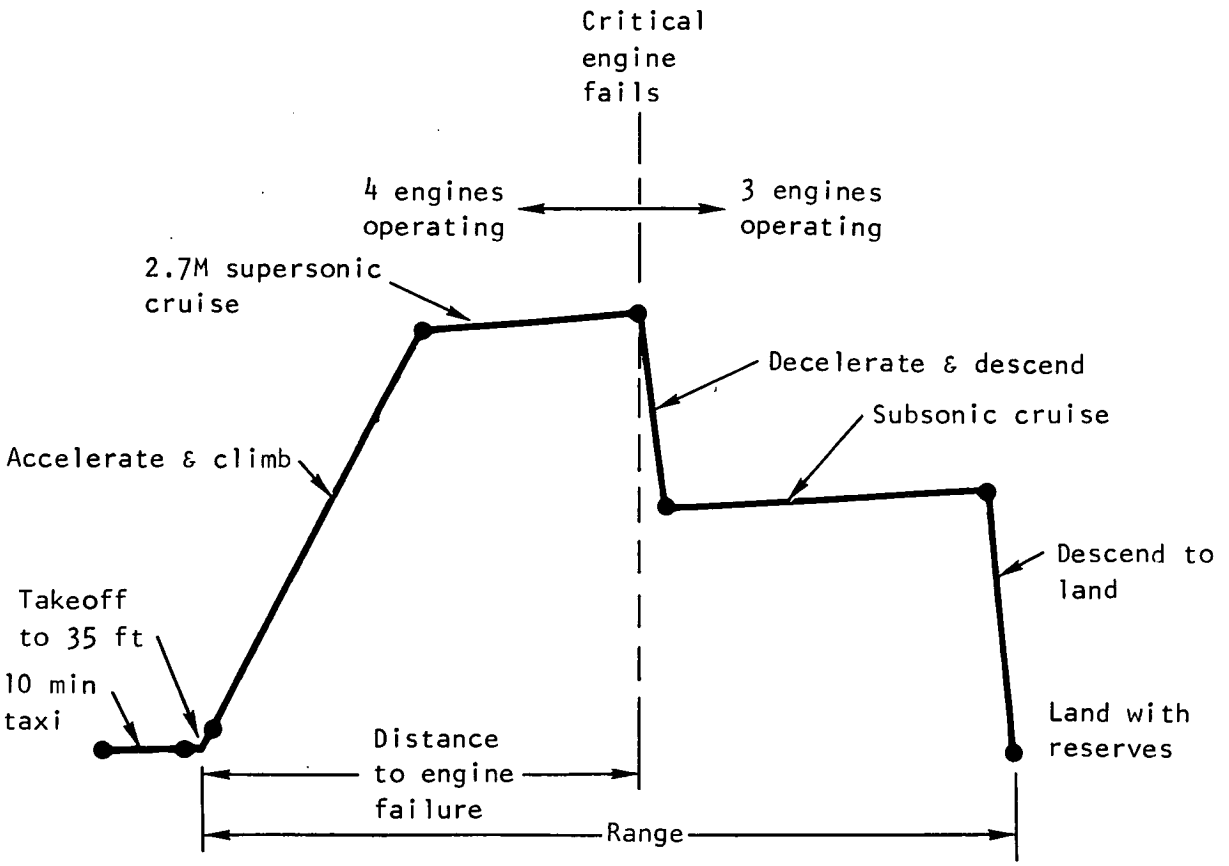

Figure 3.- Alternate mission.

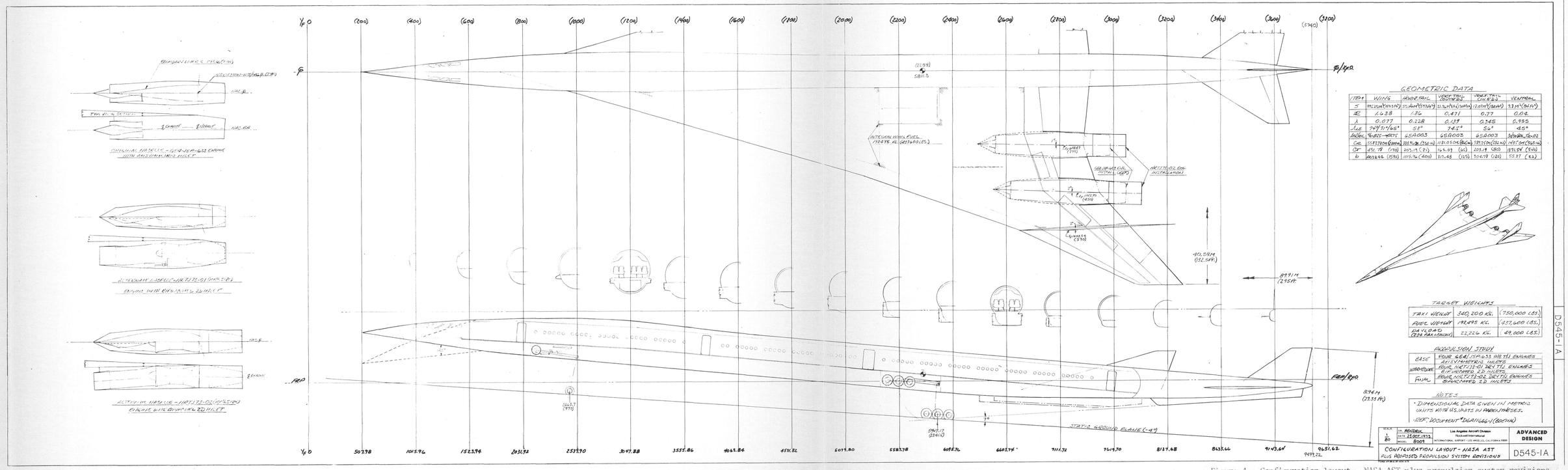

Figure 4.- Configuration layout - NASA AST plus propulsion system revisions.

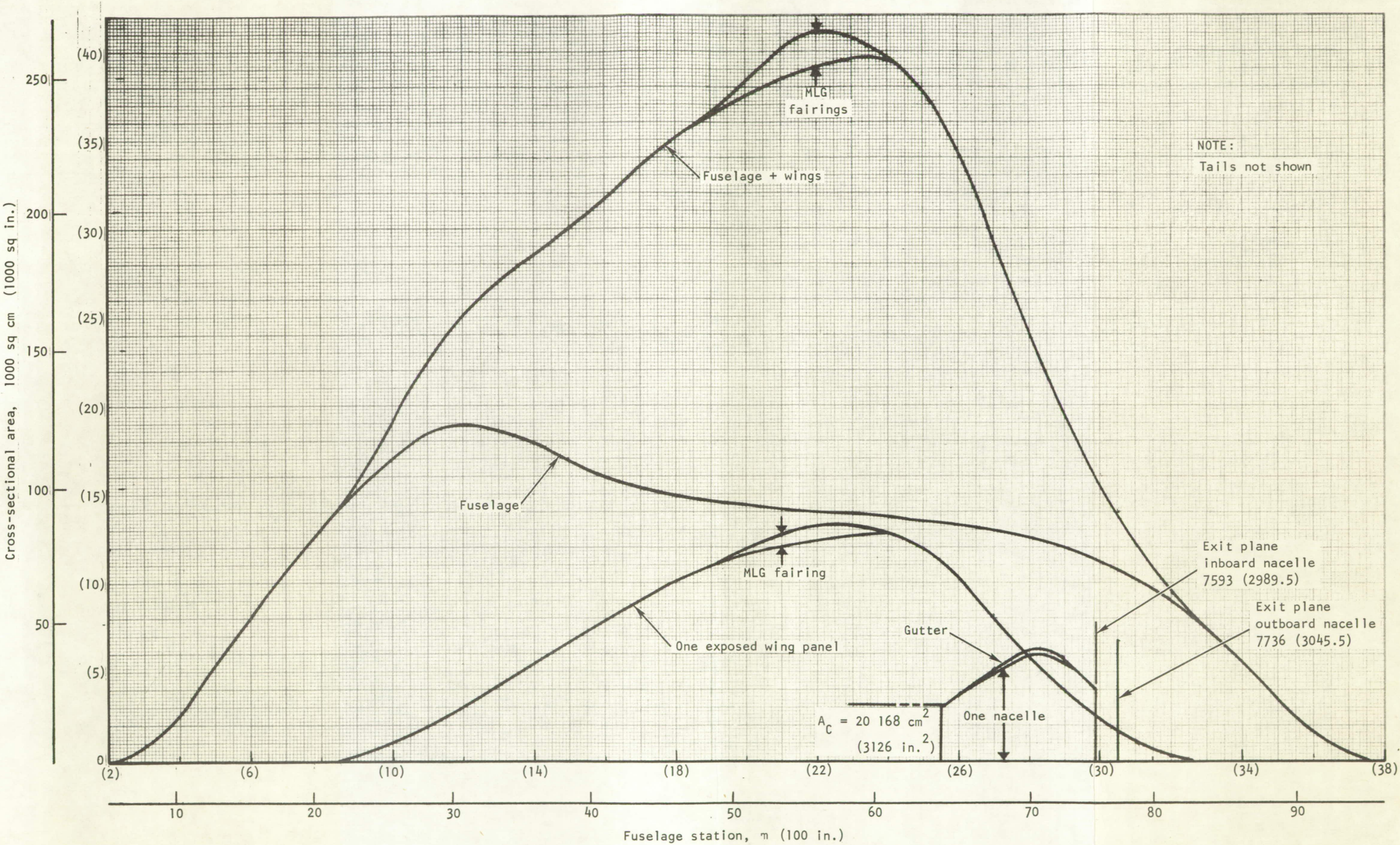

Figure 5.- Baseline vehicle cross-sectional area variation.

TABLE I.- REFERENCE CONFIGURATION WETTED AREA AND LENGTH SUMMARY

Component	S_{wet}, sq m (sq ft)	Length, m (ft)
Fuselage	753 (8 108)	90 (295)
Wing	1 630 (17 586)	22 (72)
Nacelles (4)	267 (2 870)	109 (35.8)
Center line vertical	24 (258)	4.3 (14.1)
Wing verticals	85 (920)	8.2 (26.8)
Ventral	16 (168)	14.2 (46.7)
Horizontal tail	84 (900)	10.9 (35.8)

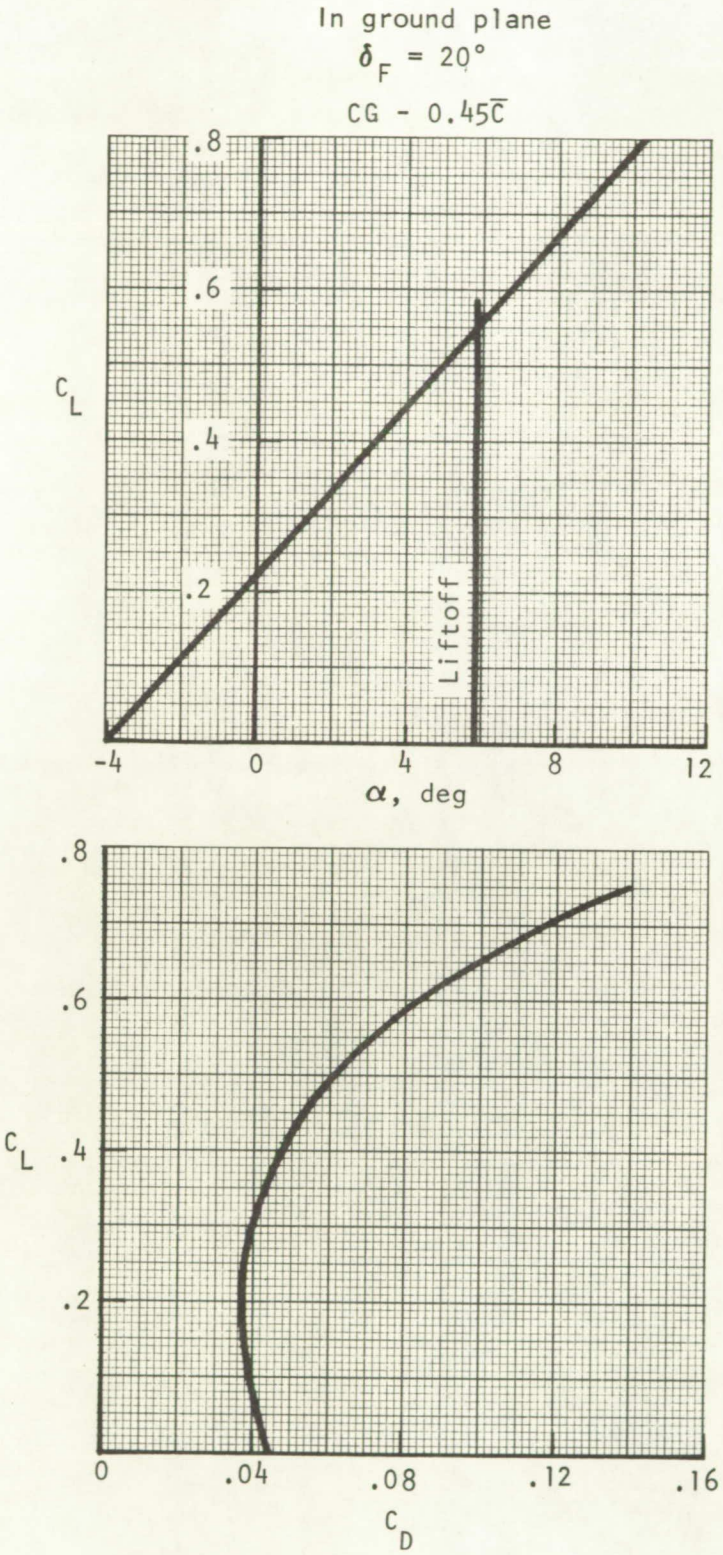

Figure 6.- Reference configuration takeoff characteristics.

The trimmed, clean, reference configuration drag polars are presented on figures 7 through 11. These data were provided to the contractor by Langley Research Center and will be subsequently incrementally corrected to account for the effect of engine and wing size and the repositioning of these components to satisfy aerodynamic balance consideration. For subsequent comparisons, the friction and wave drag characteristics of the reference configuration are summarized on table III. The former was evaluated for a fully turbulent, hydraulically smooth condition using the incompressible von Karman-Schoenherr variation (ref. 5) in conjunction with the adiabatic compressibility correction of Sommer and Short (ref. 4). Component characteristics length (e.g., the distance between the inlet lip and nozzle exit for the nacelle, the exposed wing mean aerodynamic chord, etc.) of table I and the altitude along the mission climb profile were used to evaluate length Reynolds numbers. The resulting flat plate skin friction drag was increased by 5 percent to allow for form losses. The wave drag due to thickness was evaluated using supersonic area rule theory (ref. 6 and 7) in conjunction with a transparent wing simulation. Nacelle preentry and postexit stream tubes were assumed to be equal to the inlet capture and nozzle exit area, respectively. The wing thickness distribution utilized in the analysis was established from wave drag card deck data provided to the contractor by Langley Research Center.

The reference configuration is assumed to be balanced to meet the stability and control requirements defined in reference 8, section VI-2, which include (1) rotation speed consistent with geometry-limited maximum lift coefficient in ground effect, (2) ability to provide nosedown pitching acceleration of 0.1 rad/sec^2 at the minimum demonstrated speed (determined from a 0.5 g incremental maneuver from trim at the approach speed) and maximum landing weight, and (3) satisfactory longitudinal short-period characteristics at approach using stability augmentation. For the remainder of the study, the configuration balance that resulted from these considerations was used, as opposed to the 10 individual criteria defined in reference 8. Specifically, all arrangements were aerodynamically balanced to a neutrally stable condition for takeoff, with tail sizes adjusted to offset wing movement and size changes such that the various tail volumes are constant.

The packaging and installation of the study propulsion system followed several general ground rules in order to maintain high aerodynamic cruise

TABLE II.- LIFT-OFF ANGLE AND FLAP AREA SUMMARY

	S_W			
	995.2 sq m (10 713 sq ft)		Resized wings	
Engine airflow, W_a kg/sec (lb/sec)	α_{LIM}	$\frac{S_{FLAP}}{S_W}$	α_{LIM}	$\frac{S_{FLAP}}{S_W}$
Reference	6.8	0.077	NA	NA
272 (600)	6.9	0.077	7.2	0.080
408 (900)	7.6	0.075	7.6	0.076
544 (1200)	8.4	0.071	7.9	0.069

NOTE Data are applicable to either turbojet or turbofan configurations.

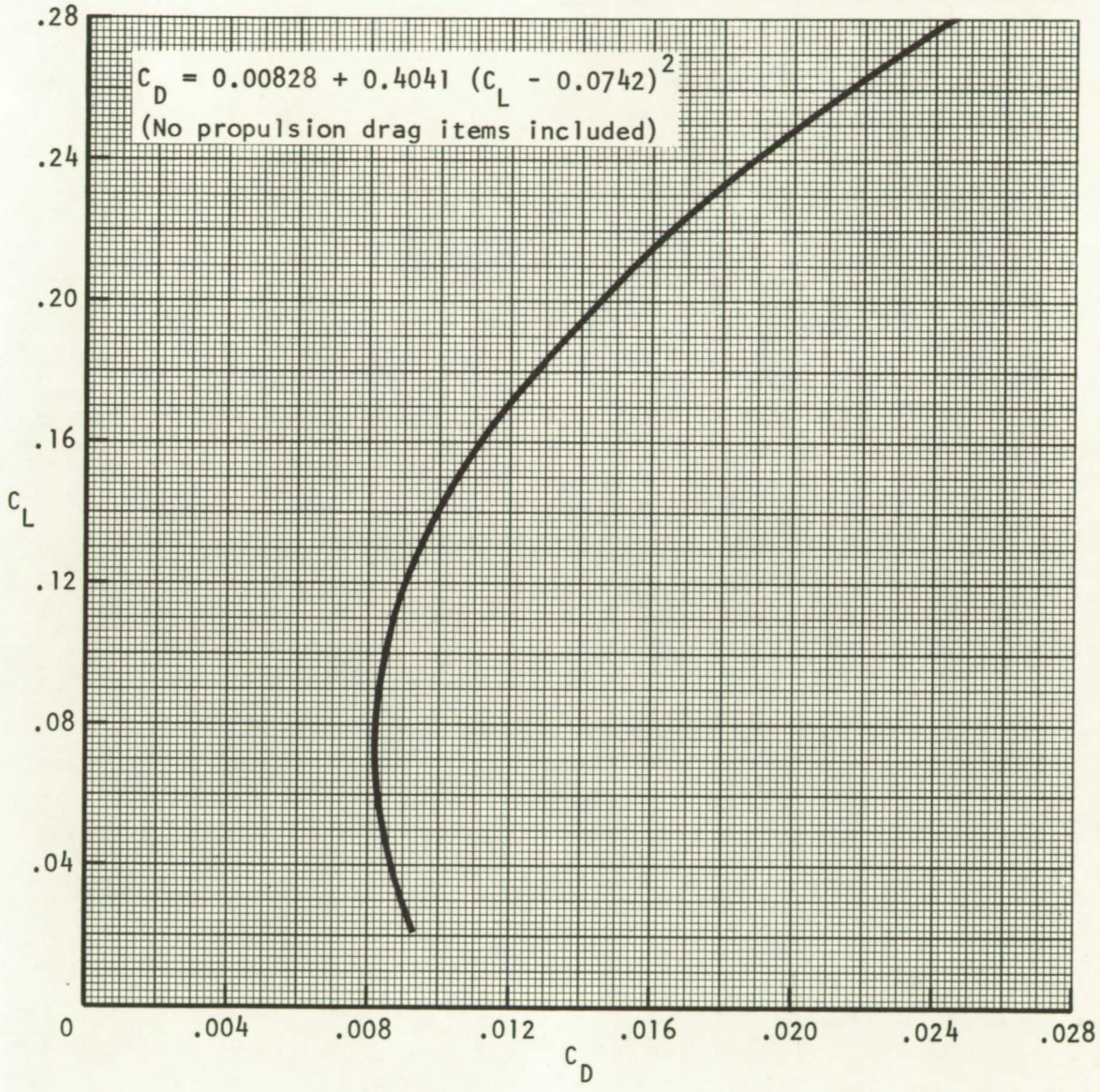

Figure 7.- Reference configuration drag polar at Mach 0.4, 457 meters (1500 feet).

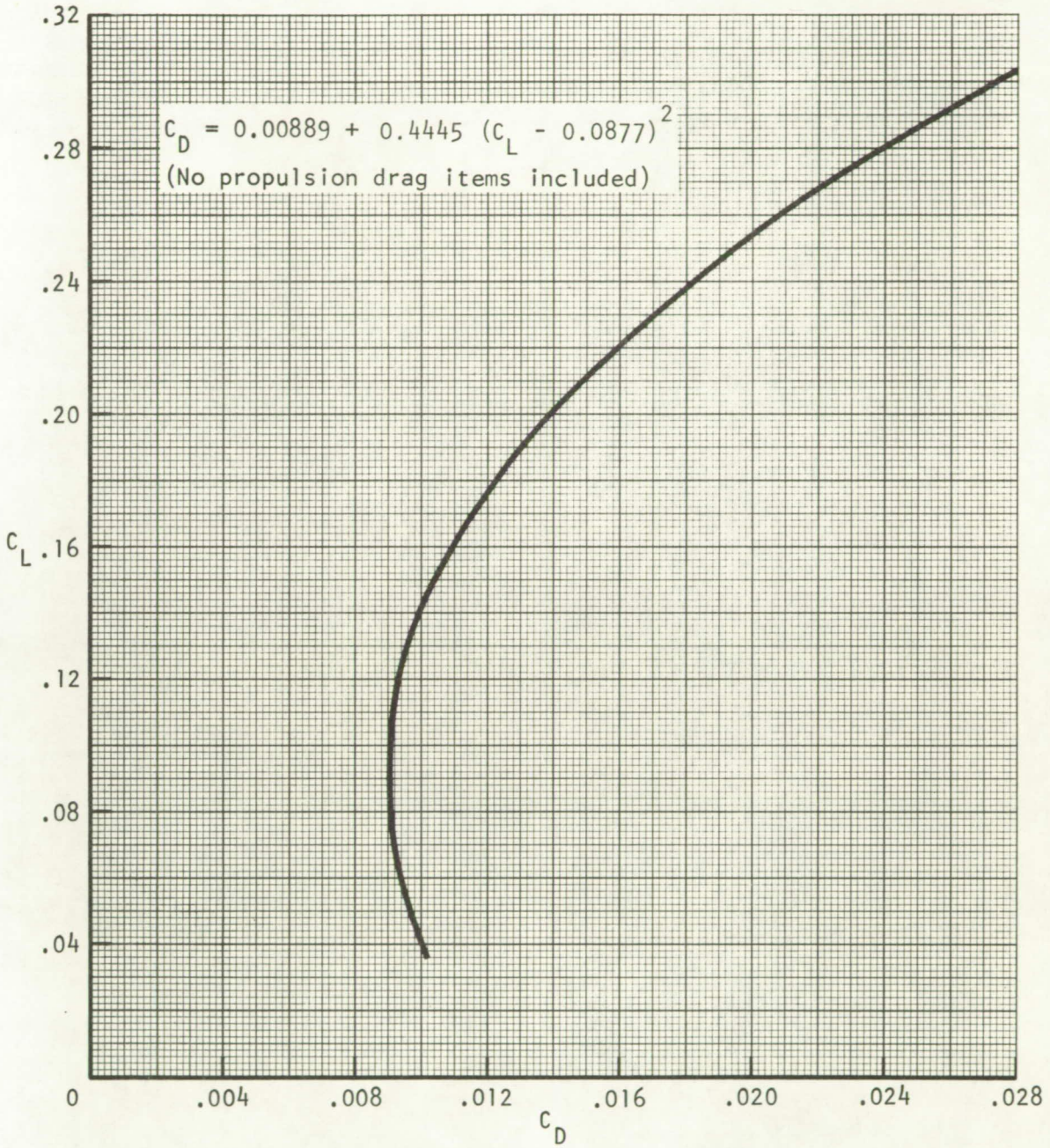

Figure 8.- Reference drag polar at Mach 0.95,
10 680 meters (35 000 feet).

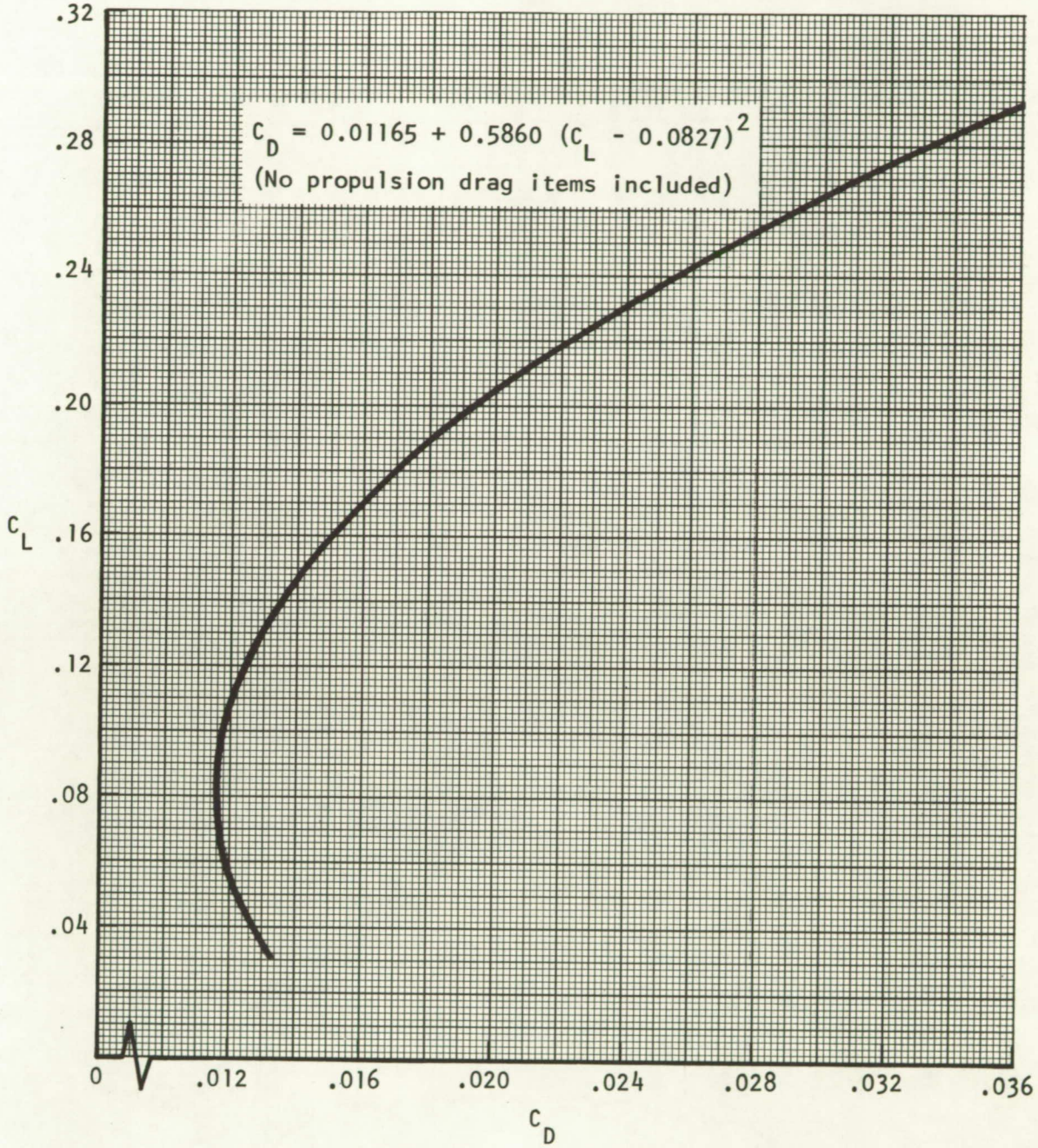

Figure 9.- Reference configuration drag polar at Mach 1.2, 10 510 meters (34 520 feet).

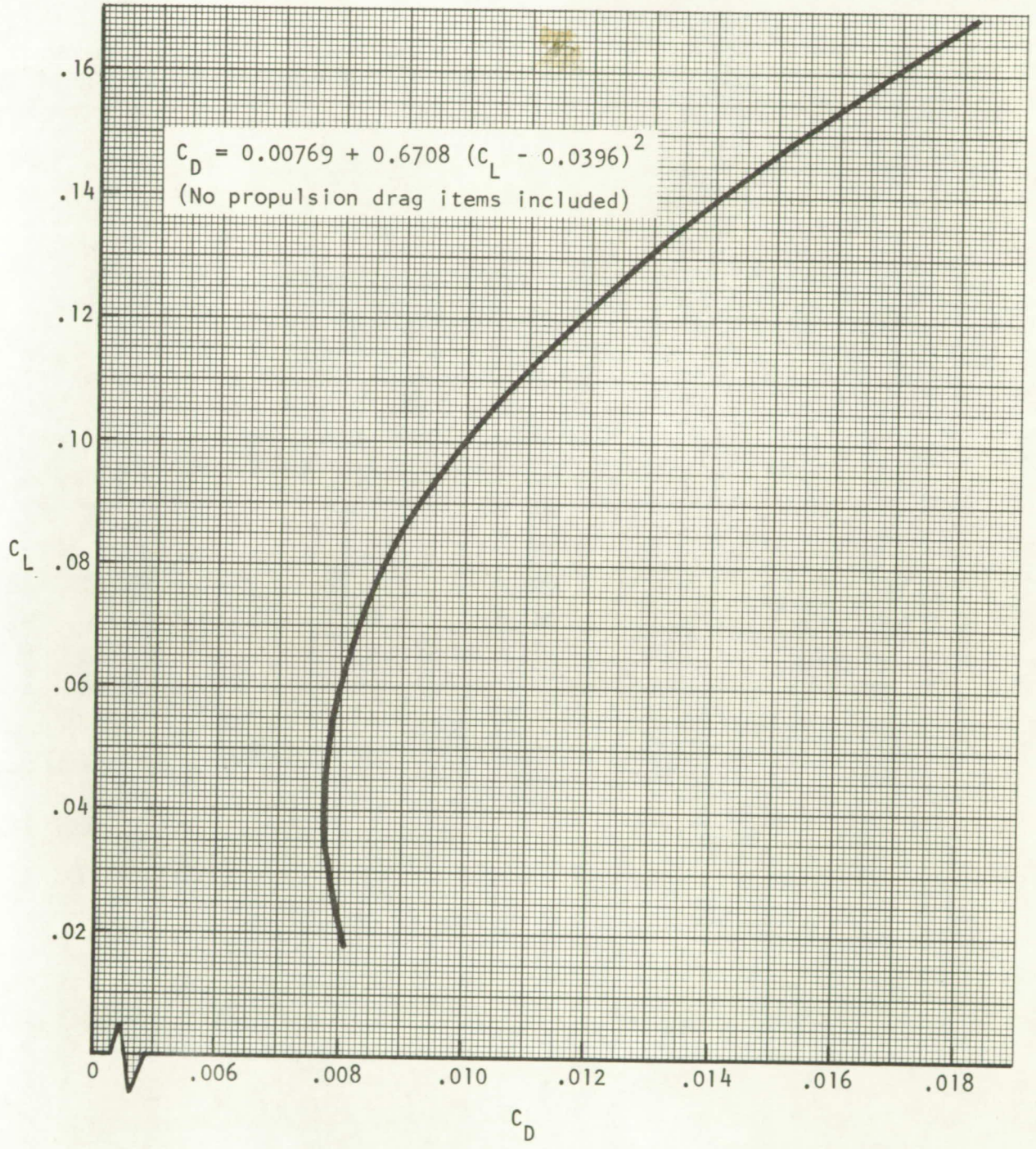

Figure 10.- Reference confuguration drag polar at Mach 2.2, 16 750 meters (55 000 feet).

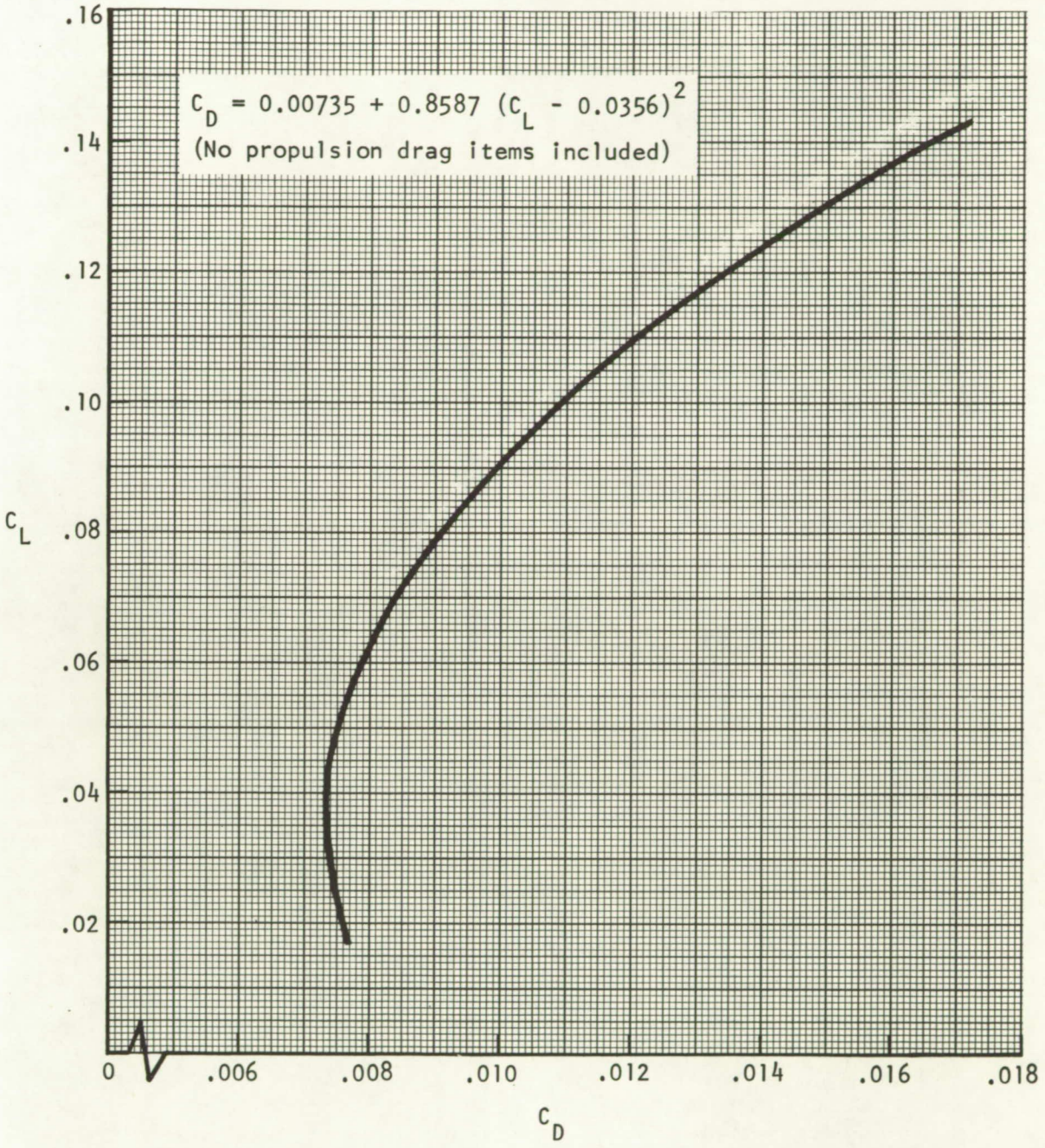

Figure 11.- Reference configuration drag polar at Mach 2.7, 18 310 meters (60 000 feet).

TABLE III.- REFERENCE CONFIGURATION ESTIMATED SKIN FRICTION AND WAVE DRAG CHARACTERISTICS, S_{ref} = 929 SQ M (10 000 SQ FT)

M	h	C_{D_P}	C_{D_W}	Nacelle	
				ΔC_{D_P}	ΔC_{D_W}
0.4	457.2 m (1 500 ft)	0.00586	—	0.00062	—
0.8	6 248 m (20 500 ft)	0.00555	—	0.00058	—
1.2	10 455 m (34 300 ft)	0.00531	0.00365	0.00056	0.00139
1.4	11 522 m (37 800 ft)	0.00514	0.00338	0.00054	0.00100
1.8	13 564 m (44 500 ft)	0.00472	0.00261	0.00050	0.00059
2.2	15 697 m (51 500 ft)	0.00433	0.00232	0.00046	0.00043
2.7	18 288 m (60 000 ft)	0.00399	0.00238	0.00042	0.00048

efficiency and provide consistent comparisons concerning the effects of engine size. They are:

1. The nozzle was operated at the ideal expansion area ratio in order to decrease the nacelle boattail area and increase internal nozzle efficiency at Mach 2.7 cruise.

2. Engine accessories were removed and located in the wing structure to reduce the maximum cross-sectional area of the nacelle. The engine was tucked up into the wing as necessary and allowable, for the same reason.

3. Nacelle relative volume allowances for structure were held constant.

4. Nacelle overhang of the wing trailing edge was limited to the baseline configuration value, for structural reasons.

5. The nacelle longitudinal distance between the outboard nacelle inlet face and wing leading edge and the inboard/outboard nacelle separation were preserved in order to maintain propulsion system flow quality.

6. The reference configuration philosophy of locating the propulsion system volume in a region of decreasing wing thickness was preserved.

Detailed nacelle layouts for a 408 kg/sec (900 lb/sec) engine (study baseline propulsion system), satisfying guidelines 1 through 3, are presented in figures 12 and 13 for the turbojet and turbofan cycles, respectively. Also, a direct overlay of the two nacelle envelopes is presented in figure 13a to facilitate comparison of the two engine packaging characteristics. The associated configuration drawings are presented in figures 14 and 15. A comparison of the normalized nacelle residual cross-sectional area distribution is presented in figure 16. (The reference configuration nacelle has been superimposed on this data for comparison purposes.) The maximum cross-sectional area relative to the capture and exit areas was much more easily controlled (and to a substantially greater degree) for the turbofan cycle in spite of effort to improve the area distribution of the turbojet by tucking into the wing, etc.

The increased rate of forebody cross-sectional area buildup of the turbojet nacelle is a result (figure 13a and table VIII) of the smaller inlet capture area relative to that of the engine front face and the associated more forward location of the engine relative to the inlet. A closer matching of these areas was obtained for the turbofan due to its higher airflow requirement at the design (Mach 2.7) cruise condition. The reduced boattail area of the turbofan is a result of the larger nozzle area relative to the engine

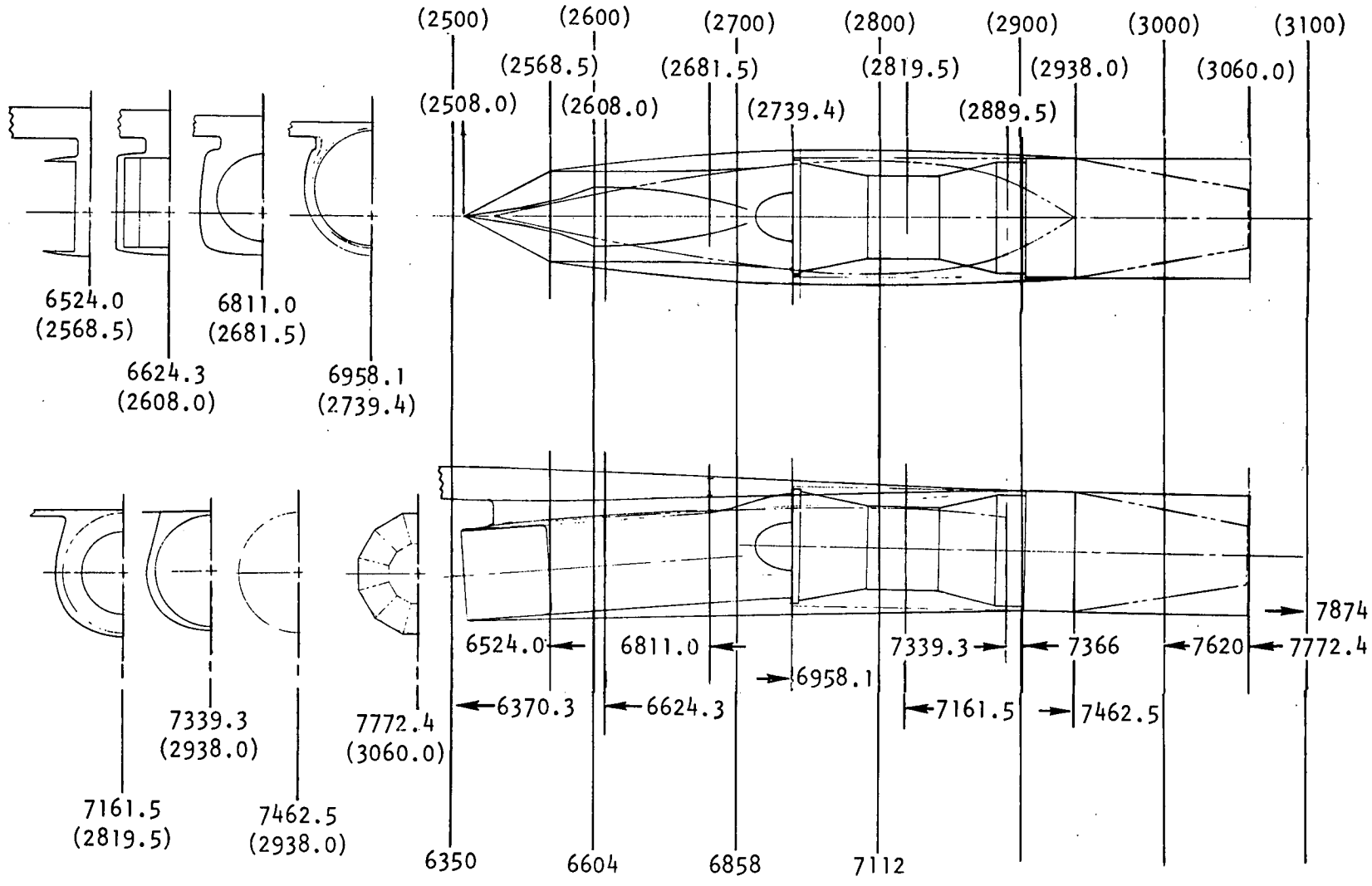

2. (XXXX.X) denotes inches.
1. XXXX.X denotes centimeters.

Figure 12.- Baseline propulsion pod.

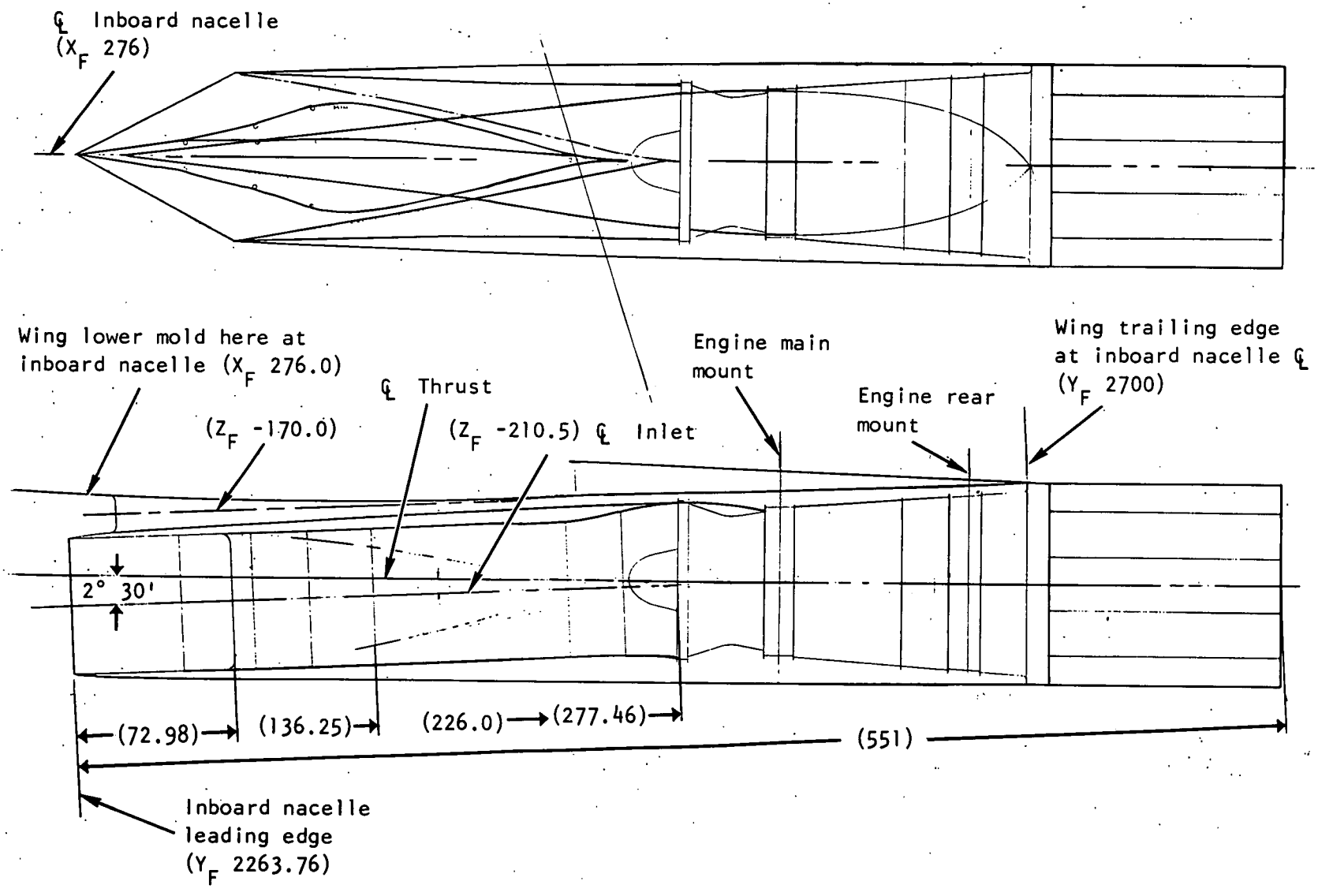

Figure 13.- Turbofan propulsion pod.

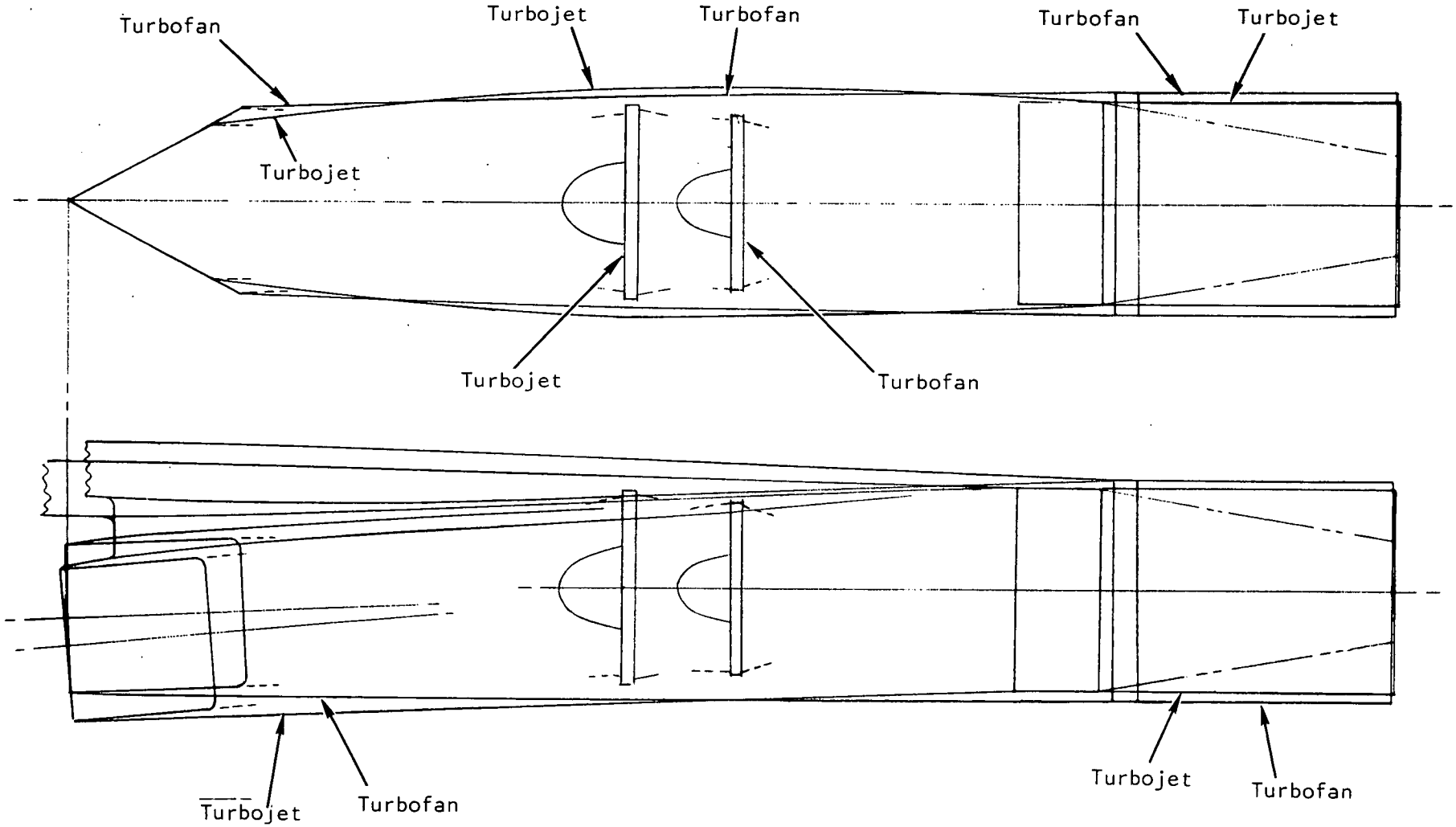

Figure 13a.- Comparison of turbojet and turbofan nacelle envelopes.

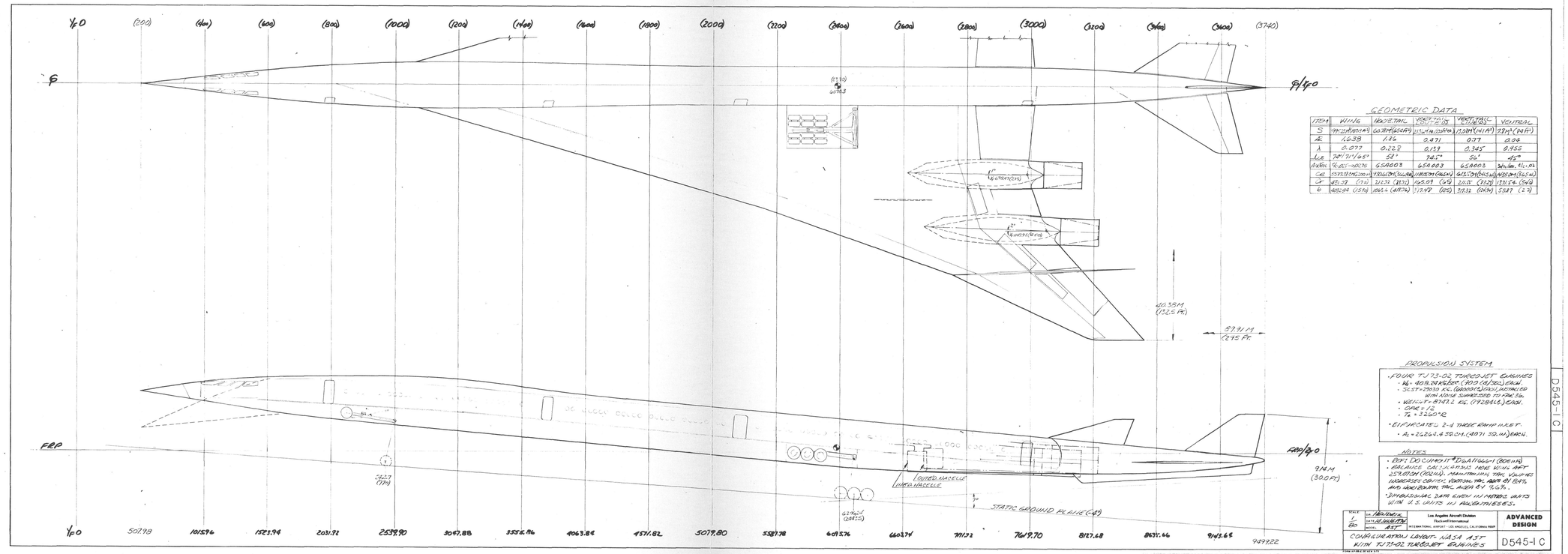

ITEM	WING	HORIZONTAL	VERTICAL (EXPOSED)	VERTICAL (EXPOSED)	VENTRAL
S	371.61 M² (4000 FT²)	60.39 M² (650 FT²)	21.5 M² (231.4 SQ. FT.)	17.09 M² (184 FT²)	22 M² (237 FT²)
AR	1.638	1.86	0.471	0.77	0.03
λ	0.077	0.223	0.139	0.345	0.455
Λ LE	74°/71°/45°	50°	74.7°	50°	45°
AIRFOIL	64-205-1.4005	64A203	64A203	64A003	64A006 MOD.
CR	37.71 M (123.75 FT.)	9.80 M (32.16 FT.)	11.18 M (36.7 FT.)	6.15 M (20.2 FT.)	4.88 M (16.0 FT.)
CT	8.23 M (27.0 FT.)	2.62 M (8.6 FT.)	1.65 M (5.4 FT.)	2.13 M (7.0 FT.)	1.73 M (5.68 FT.)
D	4.85 M (15.9 FT.)	1.65 M (5.41 FT.)	1.37 M (4.5 FT.)	1.37 M (4.5 FT.)	1.58 M (5.2 FT.)

Figure 14.- Configuration layout - NASA AST with TJ73-02 turbojet engines.

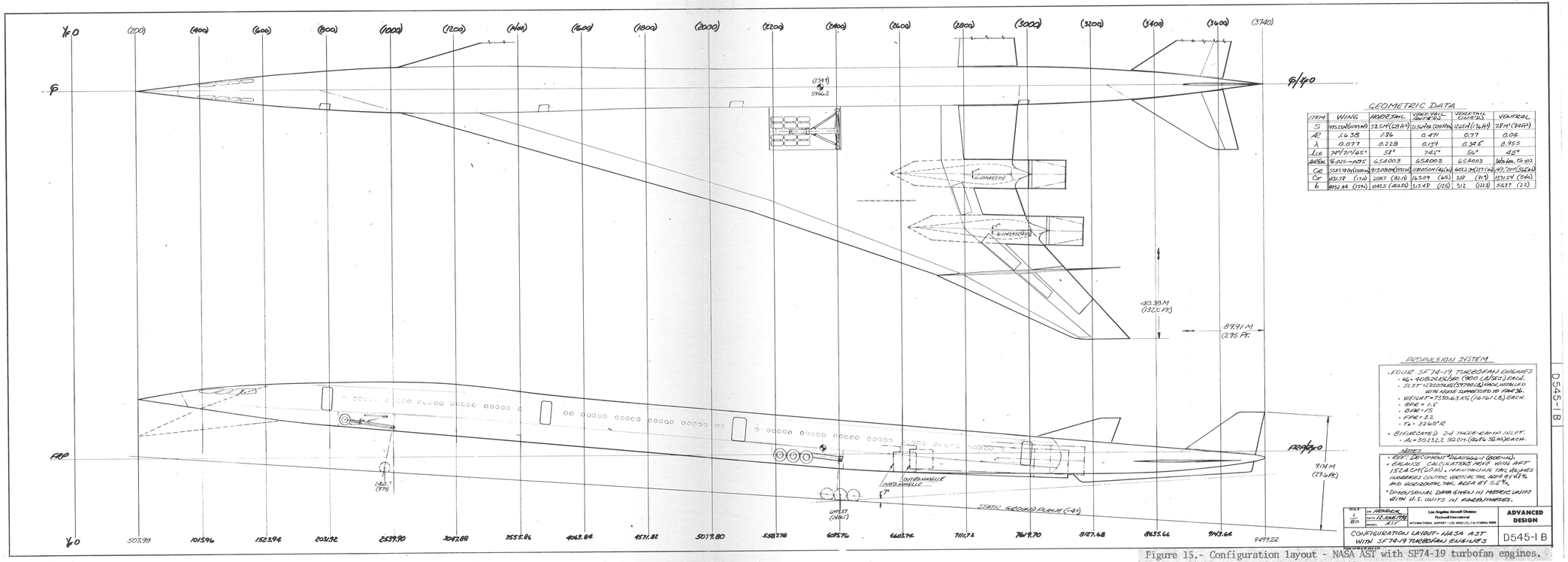

GEOMETRIC DATA

ITEM	WING	HORIZONTAL	VERTICAL OUTBOARD	VERTICAL INBOARD	VENTRAL
S	1171.23M²(12599 SQ FT)	51.5M² (554 FT²)	11.54M² (124 FT²)	11.62M² (125 FT²)	33M² (354 FT²)
AR	14.35	5.86	0.471	0.77	0.84
λ	0.077	0.228	0.139	0.345	0.455
Λ LE	74°/71°/65°	58°	74.5°	56°	45°
AIRFOIL	64-025-0.875	64A003	64A003	64A003	24% Elev. 64-012
CR	33.77M (110.8 FT)	9.73BOM (31.91 FT)	11.185M (36.7 FT)	6.02.3M (19.75 FT)	9.37M (30.74 FT)
CT	2.61M (8.56 FT)	2.08M (6.83 FT)	1.509 (4.95)	2.08 (6.83)	1.71M (5.6 FT)
b	69.2M (227 FT)	10.83 (35.53 FT)	3.749 (12.3)	3:12 (11.2)	5.87 (19.25)

PROPULSION SYSTEM

- FOUR SF74-19 TURBOFAN ENGINES
  - W_a = 408.2 KG/SEC (900 LB/SEC) EACH.
  - T_{SLS} = 13220 KG (29,700 LB) EACH, INSTALLED WITH NOISE SUPPRESSED TO FAR 36.
  - WEIGHT = 2530.3 KG (5,580 LB) EACH.
  - BPR = 1.5
  - OPR = 15
  - FPR = 2.2
  - T_4 = 3260°R
- BIFURCATED 2-D MACH 0.9 INLET
  - A_i = 10.232 SQ.M. (110.2 SQ. FT.) EACH.

NOTES:

- REF: DC CONCEPT DRAWING # (BOEING).
- BALANCE TAIL/ELEVATORS MOVE WING AFT 1.57 M (5.2 FT.), MAINTAINING TAIL VOLUMES INCREASES CONTROL VERTICAL TAIL AREA BY 44% AND HORIZONTAL TAIL AREA BY 5.5%.
- DIMENSIONAL DATA GIVEN IN METRIC UNITS WITH U.S. UNITS IN PARENTHESES.

SCALE	DRAWN	Los Angeles Aircraft Division	ADVANCED DESIGN
1/80	DATE 12 JUNE 1970	Rockwell International	
	MODEL AST	INTERNATIONAL AIRPORT • LOS ANGELES, CALIFORNIA 90009	
CONFIGURATION LAYOUT - NASA AST WITH SF74-19 TURBOFAN ENGINES			D545-1 B

D545-1-B

Figure 15.- Configuration layout - NASA AST with SF74-19 turbofan engines.

	Airflow, kg/sec (lb/sec)	Length, m (in.)	$S\pi_{cap}$ sq m (sq in.)
Reference	278 (633)	11.0 (435)	2.02 (3126)
TJ73-02	408 (900)	19.0 (551)	2.63 (4071)
SF74-19	408 (900)	14.9 (551)	3.02 (4686)

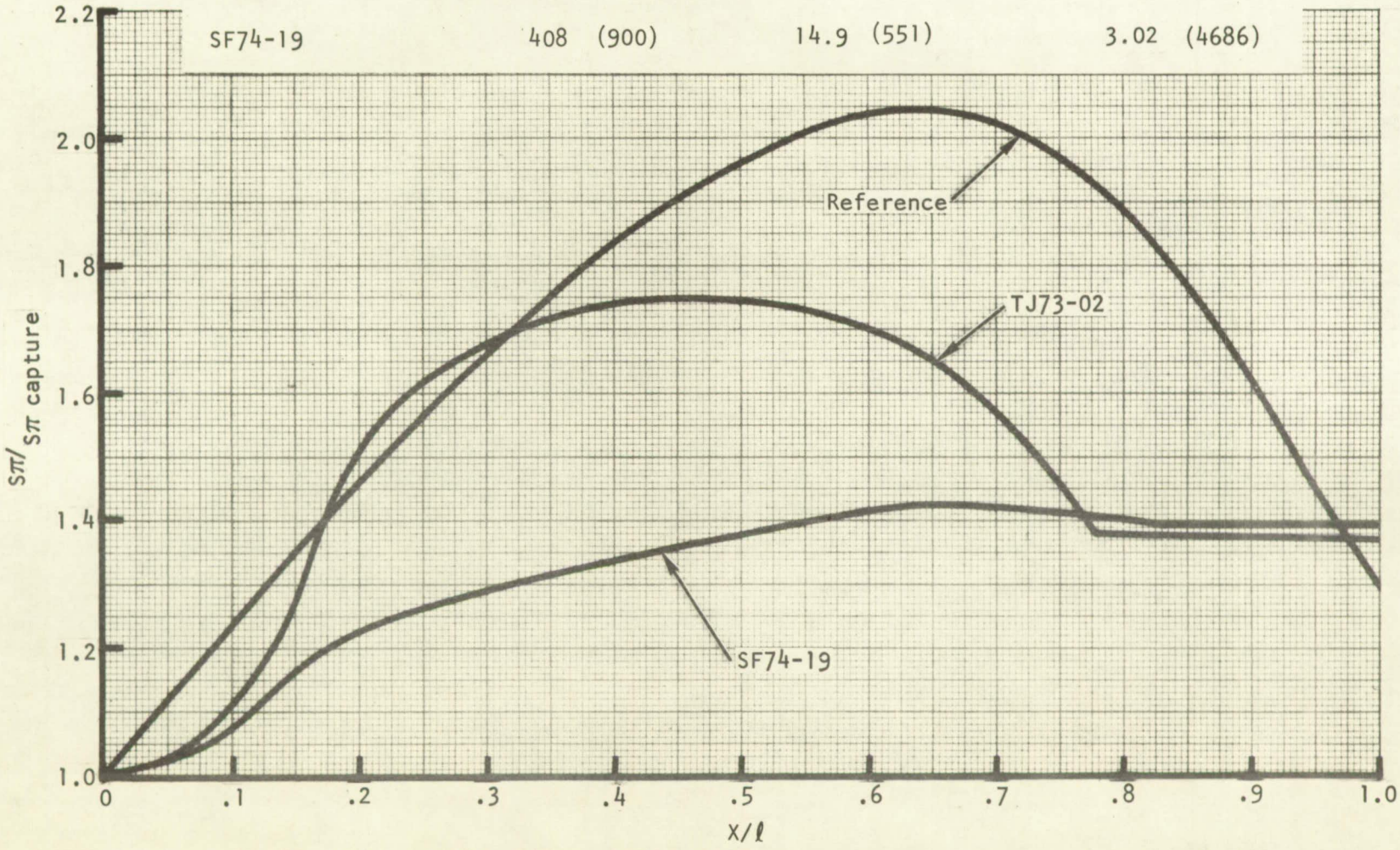

Figure 16.- Comparison of reference, turbojet, and turbofan normalized residual cross-sectional area distribution.

front face. This again is due primarily to the 15-percent greater airflow demand of the turbofan cycle.

It can be anticipated that engine cycle packaging differences will influence the study results as well as the engine size effects, which are the primary variables of the analysis. This is confirmed by the wave drag analysis of figure 17. The figure shows a significantly improved total configuration volumetric efficiency for the turbofan cycle throughout the supersonic Mach number range and a favorable pressure drag interference (relative to the nacelle off-configuration) above about Mach 1.9. An explanation of these results over and above the isolated nacelle shape is made with the aid of the Mach 2.7 total configuration average body area distribution of figure 18. The turbofan configuration has a smaller maximum cross section and a larger exhaust area than the turbojet, and consequently would be expected to have lower wave drag.

Detailed component geometric scaling was carried through for the minimum and maximum airflow of the study for the turbofan and turbojet cycles. It was found that various propulsion system characteristic dimensions changed essentially as the square root of the airflow. For example, if the 408 kg/sec (900 lb/sec) nacelle inlet dimensions, engine length, and maximum nozzle exit diameter are scaled up to the 544 kg/sec (1200 lb/sec) case or down to the 272 kg/sec (600 lb/sec) case, the deviations shown in table IV result. It is concluded that adjustment of the median-size nacelle detailed layout dimensions by square root of the airflow is reasonable over the range of airflows of the present study. This rule was utilized for all drag and nacelle flow field calculations reported in subsequent paragraphs of this report.

Propulsion. - Two engine types were studied in this program: turbojet and duct-burning turbofan. The baseline propulsion system (figure 12) consisted of a variable-ramp, two-dimensinal, mixed-compression, bifurcated-duct inlet and a single-spool, dry turbojet. The turbojet, designated TJ73-02, had a variable-area convergent-divergent nozzle with retractable noise suppressor and retractable thrust reverser. A noise suppressor with a maximum 10 dB suppression capability was used. The turbofan propulsion system (figure 13) used the same type of inlet, but had a 1.5 bypass ratio, dual-spool, separated flow, duct-burning turbofan engine. This engine, designated SF74-19, had variable-area convergent-divergent nozzles on the core and fan bypass. A retractable noise suppressor with a maximum of 5 dB suppression capability was used on the fan bypass flow only. The thrust reverser supplied reverse thrust of the fan bypass air only. The following paragraphs discuss the propulsion technology used, the method used for determining noise, the propulsion performance force accounting, the duct-heating turbofan selection process, and a comparison of the selected turbofan engine with the turbojet.

Propulsion system technology: Propulsion system characteristics were based on technology that could be demonstrated in 1975. All engine weights, dimensions, and propulsion system performance data were computed using the Rockwell steady-state propulsion analysis computer program. The propulsion system analysis computer program is basically an engine cycle analysis program extended to

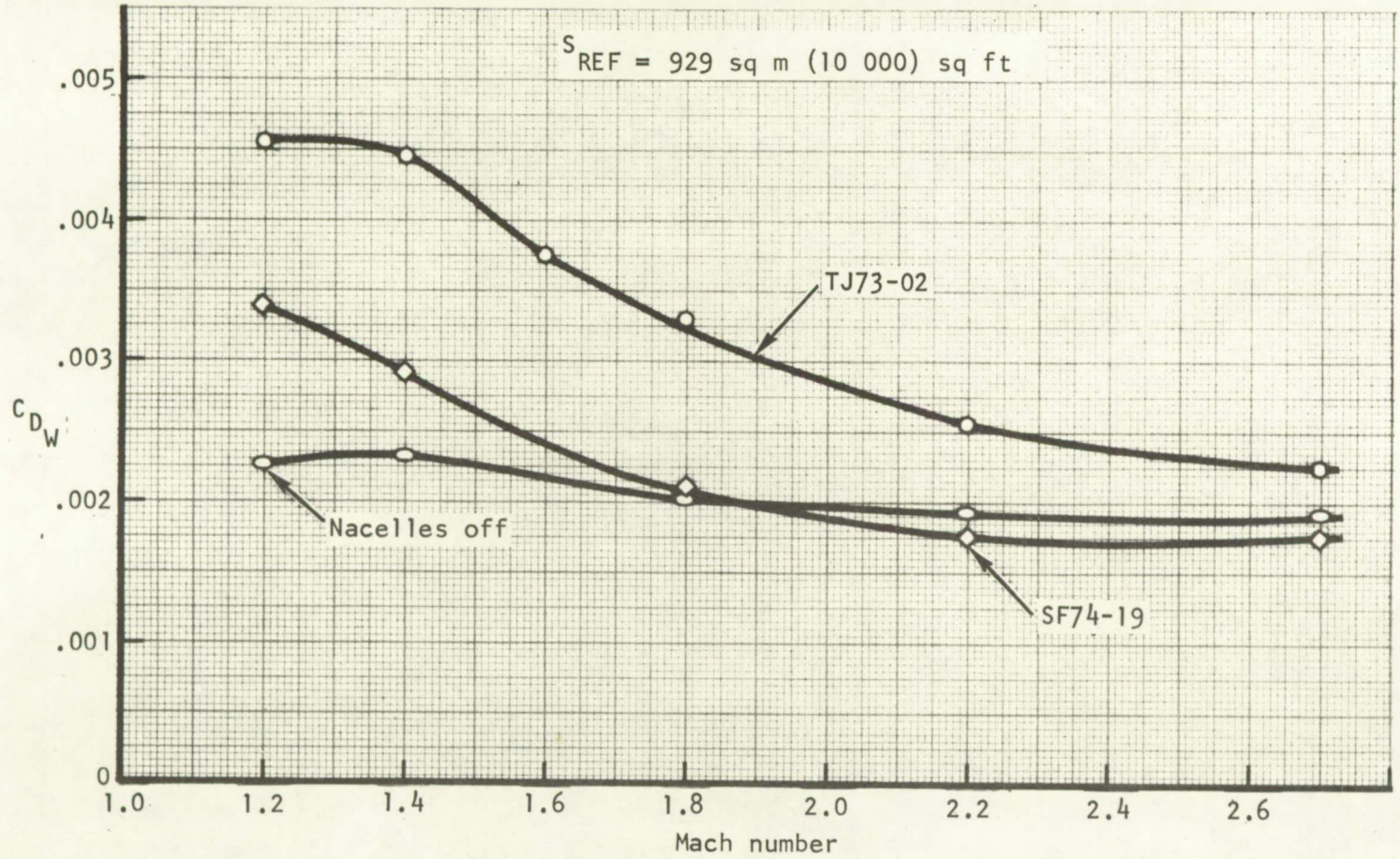

Figure 17.- Comparison of baseline configuration compressible drag, unbalanced.

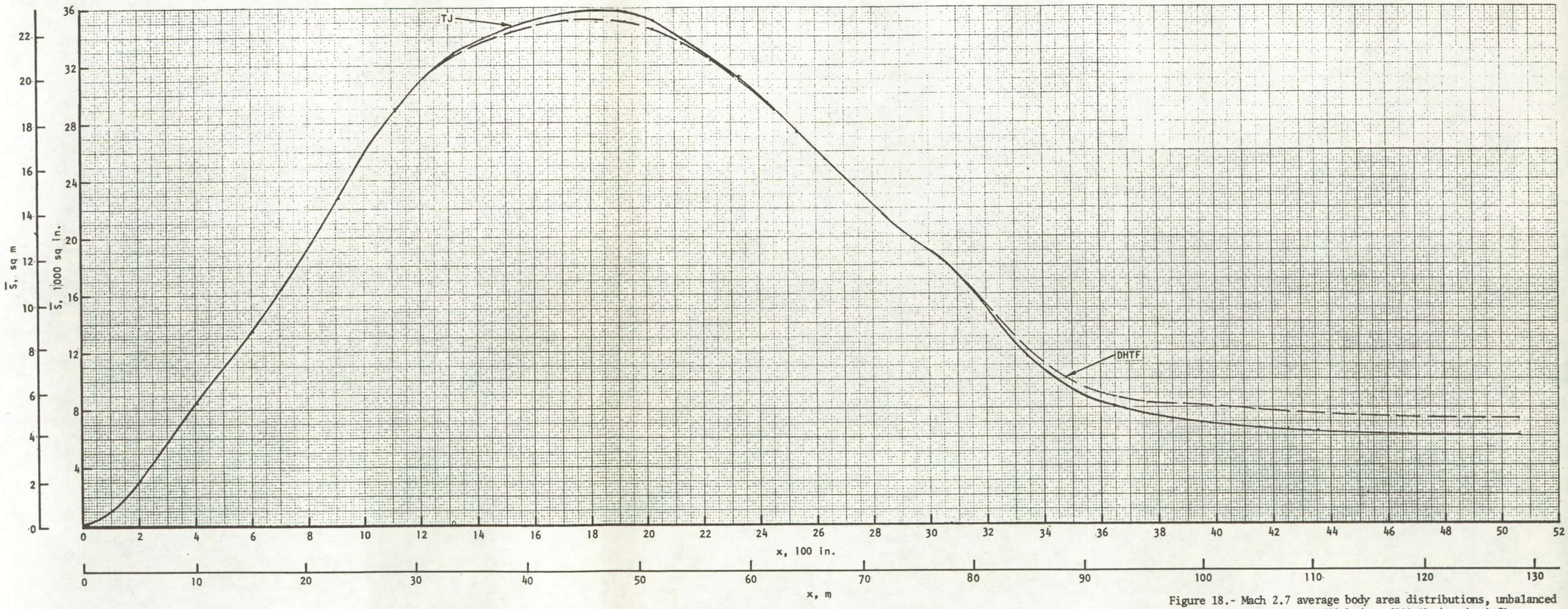

Figure 18.- Mach 2.7 average body area distributions, unbalanced configurations, 408 kg/sec (900 lb / sec) airflow.

TABLE IV.- DEVIATIONS IN NACELLE GEOMETRY DUE TO AIRFLOW SCALING

Engine	Airflow, kg/sec (lb/sec)	% deviation in A_c	% deviation in engine length	% deviation in $A_{noz_{max}}$
Turbojet	272 (600)	0	-3.2	-1.2
	408 (900)	-	-	-
	544 (1200)	0	+3.9	+0.4
Turbofan	272 (600)	0	-4.2	+0.7
	408 (900)	-	-	-
	544 (1200)	0	+2.6	+0.2

NOTE: Deviations are determined by the following:

$$\frac{P_{scaled} - P_{actual}}{P_{actual}} \times 100$$

where P indicates the parameter and the subscript "actual" refers to results obtained by a higher-order scaling.

compute overall propulsion system performance, including inlet and nozzle effects as shown schematically in figure 19. Real thermodynamic properties are included in curve fit form. All component characteristics, including inlet and nozzle, are input in map form. The basis of this program was developed under NASA contract NAS2-2985, "Study of Performance and Weight Analysis of Air Breathing Propulsion System for Hypersonic Aircraft." This computer program is capable of computing performance and engine weight and dimensions for several turbocycle engine configurations, including turbojet, turbofan, and turbo-derivative propulsion systems.

Component characteristics used in this study for the turbojet and the turbofan engines are compared in table V. The turbojet engine, the TJ73-02, is the same as that used in the study of reference 1. All engines used variable stators in their compressors, but had fixed-geometry turbines.

Noise determination: Perceived noise levels from jet exhaust were evaluated based on the SAE AIR 876 method. Perceived noise levels (PNL) were converted to effective perceived noise levels (EPNL) by correcting for aircraft Mach number (M_O), altitude (ALT), and sideline distance (SL), using figure 20, which was developed from empirical static exhaust noise data, and the method of FAR 36. The EPNL is determined, then, by:

$$EPNL = PNL - 10 \log\left(\frac{M_O}{0.3}\right) + \left[EPNL + 10 \log\left(\frac{M_O}{0.3}\right) - PNL \right] \quad \text{figure 20}$$

No reduction of noise level was assumed for coannular jets.

Noise suppression characteristics used are presented in figure 21. These data were developed from a survey of predicted suppression technology by engine manufacturing companies, with some consideration given to the relative risk of obtaining high levels of suppression. Application of noise suppression resulted in a gross thrust loss of 1 percent for each 2 dB reduction at the suppressor's design condition (i.e., 5 percent gross thrust loss at all operating conditions for a suppressor designed for 10 dB suppression). Weight of a 10 dB noise suppressor was assumed to be 50 percent of bare nozzle weight.

At approach flight conditions, inlet throat velocities were kept high by inlet ramp control to minimize machinery noise.

Integrated propulsion control: An integrated propulsion control system was assumed in the estimation of all installed performance. This control system provides increased performance through (1) closed-loop control of the inlet and engine airflow, and (2) elimination of those operating point compromises normally required to ensure stability during transient operation. The control allows smaller steady-state stability margins than conventional separated inlet and engine controls because it can provide increased stability margins when

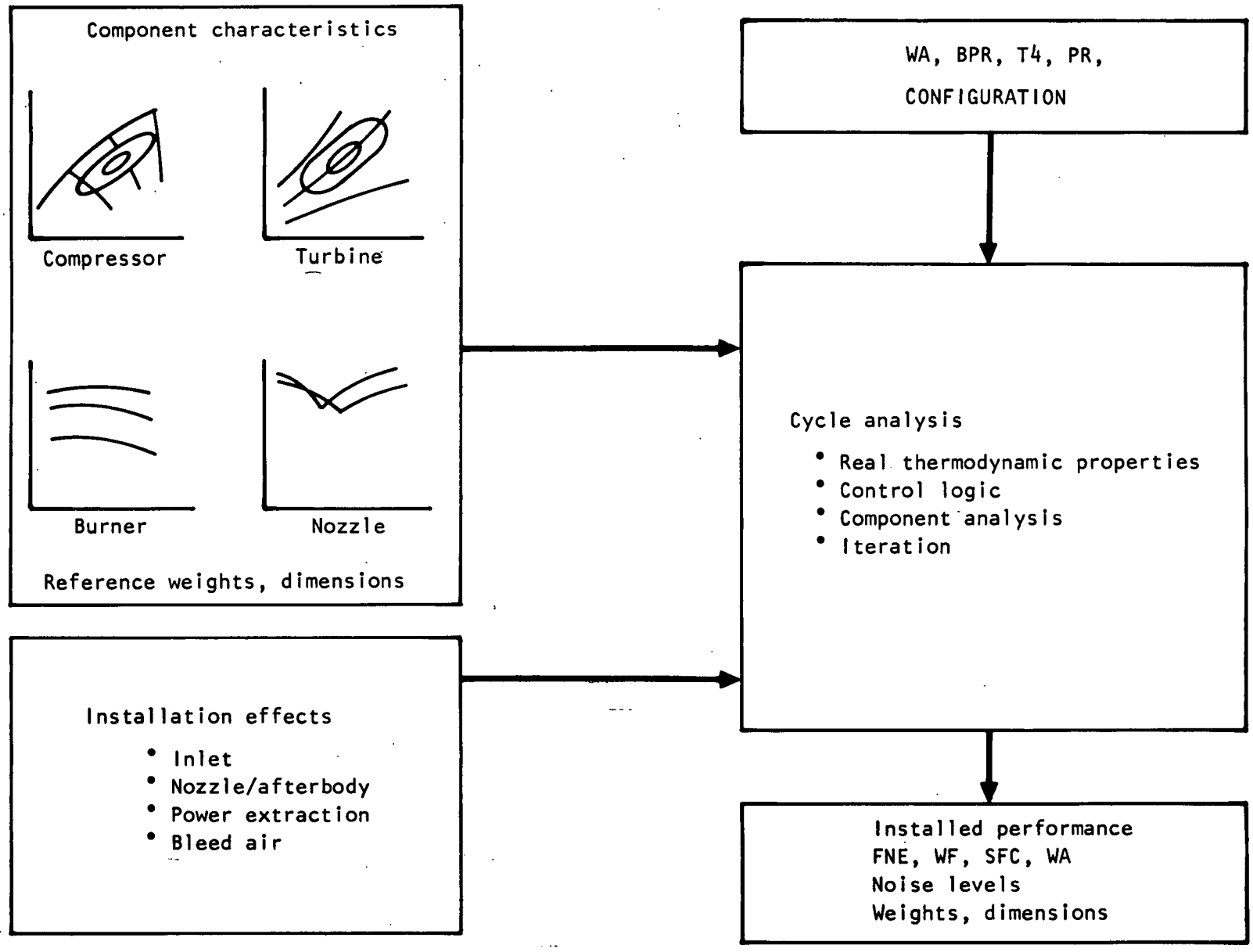

Figure 19.- Steady-state propulsion analysis program.

TABLE V.- ENGINE COMPONENT CHARACTERISTICS

Engine	Turbojet	Turbofan
Fan:		
Design point adiabatic efficiency	---	0.82
Peak adiabatic efficiency	---	0.862
Corrected speed control limit, %	---	105
Physical speed control limit, %	---	100
Inlet Mach number	---	0.55
Discharge Mach number	---	0.40
Tip speed, m/sec (ft/sec)	---	518 (1 700)
Design stall margin, %[a]	---	12.0
Minimum stall margin, %[a]	---	8.0
Hub/tip ratio	---	0.40
Compressor:		
Design point adiabatic efficiency	0.85	0.85
Peak adiabatic efficiency	0.865	0.865
Corrected speed control limit, %	105	105
Physical speed control limit, %	100	105
Inlet Mach number	0.53	0.50
Discharge Mach number	0.35	0.35
Tip speed, m/sec (ft/sec)	427 (1 400)	427 (1 400)
Design stall margin, %[a]	12.0	12.0
Minimum stall margin, %[a]	8.0	8.0
Hub/tip ratio	0.45	0.60
Maximum discharge pressure limit, N/sq cm (psia)	138 (200)	186 (270)
Maximum discharge temperature limit, °K (°R)	922 (1 660)	922 (1 660)
Combustor:		
Design point efficiency	0.985	0.985
Design point pressure drop, %	6.0	6.0
Fuel lower heating value, J/g (BTU/lb)	43 152 (18 560)	43 152 (18 560)
Maximum exit gas temperature, °K (°R)	1 810 (3 260)	1 810 (3 260)
High pressure turbine:		
Design point adiabatic efficiency	0.895	0.895
Peak adiabatic efficiency	0.898	0.895

TABLE V.- ENGINE COMPONENT CHARACTERISTICS - Continued

Engine	Turbojet	Turbofan
Rotor cooling flow %	7.5	7.5
Nozzle cooling flow %	7.5	7.5
Maximum rotor inlet gas temperature, °K (°R)	1 700 (3 060)	1 700 (3 060)
Design point discharge Mach number	0.45	0.45
Maximum discharge Mach number	0.55	0.55
Low-pressure turbine:		
Design point adiabatic efficiency	---	0.895
Peak adiabatic efficiency	---	0.897
Rotor cooling flow, %	---	2.5
Nozzle cooling flow, %	---	2.5
Design point discharge Mach number	---	0.45
Maximum discharge Mach number	---	0.55
Duct burner:		
Maximum exit temperature, °K (°R)	---	2 030 (3 660)
Peak efficiency	---	0.905
Design pressure loss, %	---	6.0
Design diffuser inlet Mach number	---	0.3
Design burner inlet Mach number	---	0.22
Minimum temperature rise, °C(°F)	---	278 (500)
Nozzle:		
Core secondary airflow, %	3.0	3.0
Core secondary airflow source	Compressor interstage	Fan bypass
Fan secondary airflow, %	---	0
Internal gross thrust		
Friction and leakage, %	1.5	1.5
Divergence and under expansion	Varies with nozzle position	

TABLE V.- ENGINE COMPONENT CHARACTERISTICS - Concluded

Engine	Turbojet	Turbofan
Maximum noise suppression, dB	10	5 (fan bypass only)

[a] Percent stall margin is defined as 100 x 1.0-PRo/PRs), where PRo is the operating pressure ratio and PRs is the stall pressure ratio at the same corrected speed.

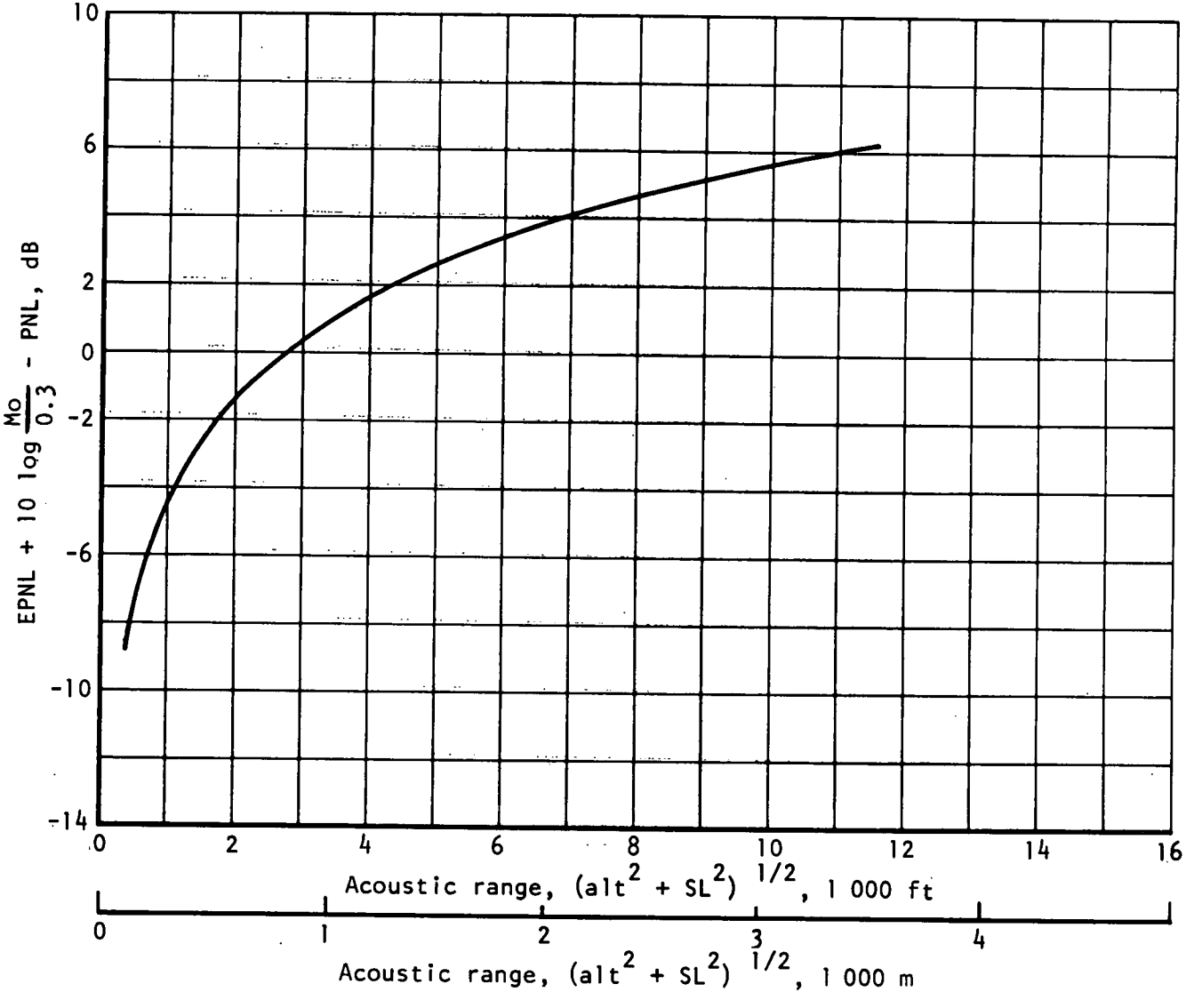

Figure 20.- Effective perceived noise level conversion.

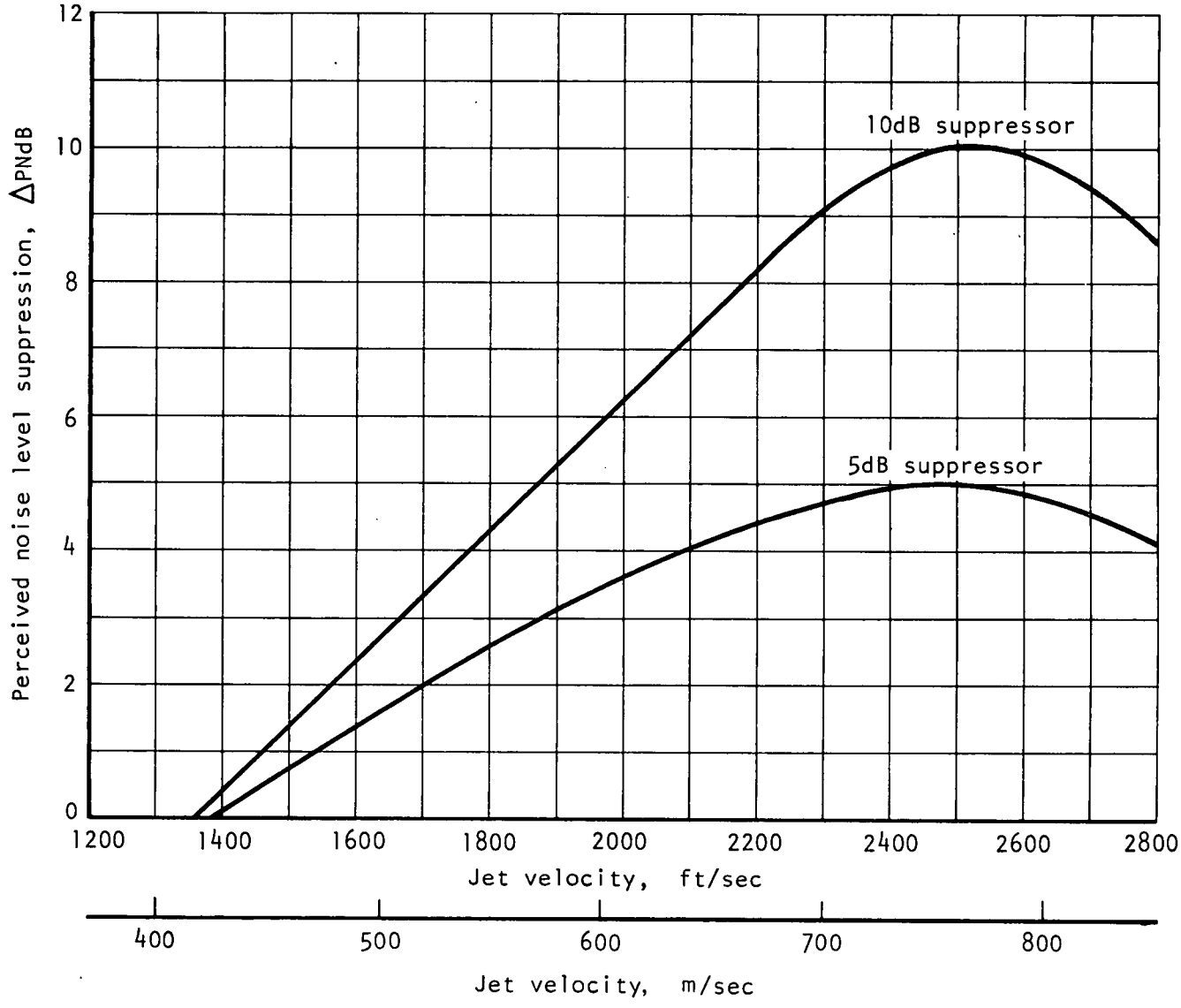

Figure 21.- Exhaust jet noise suppression.

throttle transients are commanded. The inlet capture area was sized at maximum power at Mach 2.7. However, at transonic and supersonic maximum power conditions, the engine and inlet were controlled to match airflow, unless a physical limit was encountered.

Propulsion performance force accounting: The determination of installed engine performance requires proper accounting of all forces and interactions between external and propulsion flow fields. Corrections are applied to propulsion system performance for the effect of these interactions. The propulsion installation effects represent corrections for the following:

- Inlet recovery: Subsonic diffuser and sharp lip losses plus shock losses at supersonic speeds
- Inlet drags: Additive or spillage drag, boundary layer control air momentum loss, bypass air momentum loss, and bypass door drag
- Afterbody drags: Scrubbing drag; nozzle exit blunt base drag; and effect of nozzle position and exhaust plume on external drag of the nacelle, nozzle, aft fuselage, and tail
- External flow effects on nozzle internal gross thrust
- Power extraction and compressor bleed

Thrust and drag forces which act upon the propulsion system are normally added as vectors to obtain magnitude and direction of the resultant force vector. Because propulsion gas flow is discharged at small angles to free-stream flow, the lift components of propulsion forces are negligible and are considered to be zero for the purpose of installed performance.

Inlet characteristics used are presented in reference 9.

The basic airplane drags are calculated with the exhaust nozzle position scheduled as a function of Mach number and the nozzle operating at a low-pressure ratio (~1.0). Thus, nozzle/afterbody drag increments used in propulsion performance account for effects of operating nozzle pressure ratio, any changes in nozzle position from the nominal schedule, and the blunt base drag due to the finite thickness of the nozzle exit. Nozzle/afterbody drags for the turbojet and turbofan installations are presented in references 9 and 10, respectively.

Compressor bleed-air extraction used was 0.68 kg/sec (1.5 lb/sec) per engine. Power extraction used was 148 kw (200 hp).

Duct heating turbofan cycle selection: Eighteen parametric turbofan engine cycles were selected for preliminary analysis. The cycles were chosen to show the effects of changing each major cycle parameter on noise level, performance, weight, and engine dimensions. These cycles were selected based on a review of engine technology level and on results of previous studies. The cycle characteristics of these 18 engines are presented in table VI. All engines were sized for 408kg/sec (900 lb/sec) design airflow. Installed performance was calculated for each cycle at flight conditions representative of those that are most important to vehicle performance. Data were calculated for a range of duct burner temperatures and for maximum dry power at takeoff, transonic acceleration, and at supersonic cruise. Installed performance and engine weight and dimensional data are presented in table VII. All engines were capable of meeting FAR 36 requirements with 10 dB, or less, suppression.

The aforementioned data were used to determine propulsion system weight increments for the 100-percent-size engines. The propulsion system weight increment includes the changes in engine and inlet weights and the change in cruise fuel (2 hours at Mach 2.7) relative to the SF74-12 propulsion system. The SF74-12 was selected as a reference because it had the largest propulsion system weight. The results of this analysis, presented in figure 22, show that systems with the largest weight decrease relative to the SF74-12 are those with bypass ratios in the range of 1.5 to 2.0.

Noise suppressors are limited to operation at or below exhaust temperatures of 1140° K (2060° R) because of suppressor material strength limitations. Thus, the engines had to be resized to meet takeoff requirements at the reduced duct burner temperatures. Figure 23 shows the engine size required to produce the same static thrust as the baseline TF73-02 engine at this limit temperature.

Because of the complexity of providing two noise suppressors on separated flow turbofans, it was decided to eliminate the noise suppressor on the core gas flow. With no suppression, exhaust gas velocities must be limited to about 640 m/sec (2100 ft/sec) to meet FAR 36 noise requirements. The smallest engine that meets FAR 36 requirements with no suppression on the core and with a duct burner temperature of 1140° K (2060° R) has a bypass ratio of 1.5, fan pressure ratio of 3.2, and combustor exit temperature of 1810° K (3260° R). The combination of 3.2 fan pressure ratio and duct burner temperature of 1140° K (2060° R) requires only 5 dB suppression to meet FAR 36 requirements. Thus, the SF74-19 engine cycle was selected for the propulsion system of the detailed study. Normal takeoff thrust is then defined by using duct burning to 1140° K (2060° R) and using 5 dB suppression on the fan bypass stream.

TABLE VI.- PRELIMINARY DUCT BURNING TURBOFANS

Engine designation	Bypass ratio	Fan pressure ratio	Overall pressure ratio	Turbine rotor inlet temp °K (°R)
SF74-02	1.0	4.0	15	1700 (3060)
SF74-03	1.0	3.2	15	1700 (3060)
SF74-04	1.0	3.2	12	1478 (2660)
SF74-05	2.0	3.2	15	1700 (3060)
SF74-06	2.0	2.7	15	1700 (3060)
SF74-07	2.0	2.7	15	1589 (2860)
SF74-08	2.0	2.7	12	1478 (2600)
SF74-09	3.0	2.7	15	1700 (3060)
SF74-10	3.0	2.4	15	1700 (3060)
SF74-11	3.0	2.4	15	1589 (2860)
SF74-12	3.0	2.4	12	1478 (2660)
SF74-13	1.0	2.7	15	1700 (3060)
SF74-14	1.5	2.7	15	1700 (3060)
SF74-15	2.5	2.7	15	1700 (3060)
SF74-16	2.0	2.4	15	1700 (3060)
SF74-17	2.0	2.7	15	1478 (2660)
SF74-18	1.5	2.4	15	1700 (3060)
SF74-19	1.5	3.2	15	1700 (3060)

TABLE VII.- TURBOFAN ENGINE CHARACTERISTICS

Engine	SF74-02	SF74-03	SF74-04	SF74-05	SF74-06	SF74-07	SF74-08	SF74-09	SF74-10
Length, m (in.)	7.45 (293)	7.67 (302)	7.42 (292)	7.56 (298)	7.21 (284)	7.12 (280)	7.00 (275)	7.12 (280)	7.37 (290)
Max diameter, m (in.)	2.01 (70)	2.11 (83)	2.13 (84)	2.18 (86)	2.06 (81)	2.06 (81)	2.08 (82)	2.13 (84)	2.18 (86)
Dry weight kg (lb)	7749 (17 060)	7 730 (17 010)	7 710 (16 980)	7 550 (16 640)	7 040 (15 510)	7 010 (15 440)	7 060 (15 570)	7 050 (15 550)	7 180 (15 810)
Capture area, sq m (sq in.)	2.91 (4 502)	3.03 (4 696)	3.08 (4 781)	3.02 (4 677)	3.12 (4 839)	3.10 (4 796)	3.18 (4 930)	3.18 (4 934)	3.20 (4 959)
Max thrust at Mach 2.7, 18 300 m (60 000 ft), daN (lb)	15 760 (35 460)	16 930 (38 070)	16 200 (36 390)	18 010 (40 500)	18 400 (41 380)	18 000 (40 380)	18 100 (40 670)	19 020 (42 780)	19 420 (43 640)
SFC at Mach 2.7, 18 300 m (60 000 ft), 9 000 daN (20 200 lb), kg/hr/daN (lb/hr/lb)	1.810 (1.775)	1.764 (1.730)	1.759 (1.723)	1.780 (1.746)	1.791 (1.757)	1.791 (1.757)	1.800 (1.764)	1.840 (1.803)	1.818 (1.782)

TABLE VII.- TURBOFAN ENGINE CHARACTERISTICS - Continued

Engine	SF74-02	SF74-03	SF74-04	SF74-05	SF74-06	SF74-07	SF74-08	SF74-09	SF74-10
Takeoff thrust, daN (lb) at duct burner temp of									
°K (°R)									
2 030(3 660)	33 800 (75 960)	33 100 (74 490)	30 600 (68 820)	31 600 (71 070)	31 000 (69 690)	29 950 (67 290)	28 350 (63 720)	29 050 (65 320)	28 600 (64 360)
1 140(2 060)	28 050 (63 070)	27 560 (62 190)	25 550 (57 310)	24 800 (55 680)	24 750 (55 560)	23 750 (53 400)	22 300 (50 190)	22 200 (49 960)	22 250 (50 020)
Engine	SF74-11	SF74-12	SF74-13	SF74-14	SF74-15	SF74-16	SF74-17	SF74-18	SF74-19
Length, m (in.)	7.25 (285)	6.61 (260)	7.35 (289)	7.65 (301)	7.45 (293)	6.96 (274)	7.06 (278)	7.37 (290)	7.30 (2.87)
Max diameter, m (in.)	2.18 (86)	2.08 (82)	2.01 (79)	2.16 (85)	2.18 (86)	2.01 (79)	2.08 (82)	2.08 (82)	2.06 (81)
Dry weight kg (lb)	7150 (15 730)	6740 (14 840)	7300 (16 100)	7550 (16 650)	7320 (16 110)	6740 (14 850)	7040 (15 510)	7230 (15 910)	7240 (15 960)
Capture Area, sq m (sq in.)	3.19 (4 943)	3.36 (5 212)	3.14 (4 855)	3.13 (4 849)	3.12 (4 833)	3.20 (4 962)	3.07 (4 756)	3.21 (4 969)	3.02 (4 686)

TABLE VII.- TURBOFAN ENGINE CHARACTERISTICS - Concluded

Engine	SF74-11	SF74-12	SF74-13	SF74-14	SF74-15	SF74-16	SF74-17	SF74-18	SF74-19
Max thrust at Mach 2.7, 18 300 m (60,000 ft) daN (lb)	19 100 (42 930)	19 100 (42 910)	17 380 (39 050)	18 410 (41 420)	18 860 (42 380)	18 500 (41 540)	17 420 (39 170)	18 650 (41 030)	17 450 (39 220)
SFC at Mach 2.7, 18 300 m (60 000 ft), 9000 daN (20 200 lb) kg/hr/daN (lb/hr/lb)	1.820 (1.784)	1.863 (1.828)	1.810 (1.774)	1.761 (1.728)	1.800 (1.765)	1.810 (1.773)	1.815 (1.780)	1.779 (1.744)	1.785 (1.750)
Takeoff thrust, daN (lb) at duct burner temp of °K (°R) 2 030 (3 660)	27 500 (61 800)	25 800 (57 940)	32 350 (72 660)	31 650 (71 130)	30 050 (67 590)	30 150 (67 820)	28 200 (63 450)	30 800 (69 290)	32 550 (73 130)
1 140 (2 060)	21 250 (47 850)	19 830 (44 540)	27 600 (62 010)	25 950 (58 380)	23 450 (52 690)	24 350 (54 760)	22 220 (50 000)	25 600 (57 550)	26 300 (59 110)

Propulsion weight includes fuel weight for 2 hours of supersonic cruise plus inlet and engine weights.
Weight increment is:
propulsion weight - SF74-12 propulsion weight

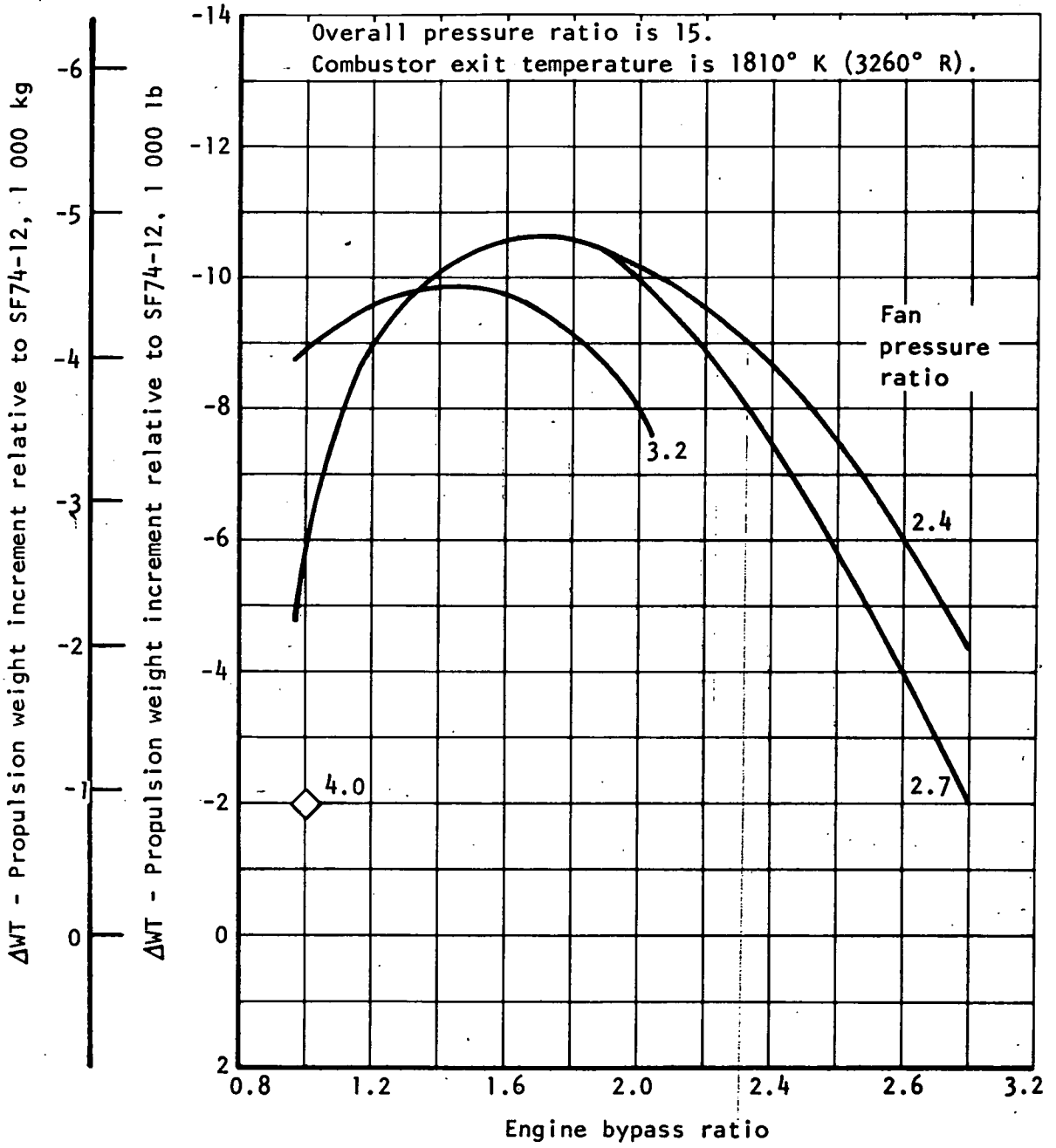

Figure 22.- Preliminary propulsion system weight increments.

Reference thrust is 28 400 kg (64 000 lb) at sea level static, standard day.

Overall pressure ratio is 15.
Combustor exit temperature is 1810° K (3260° R).
Duct burner temperature is 1140° K (2060° R).

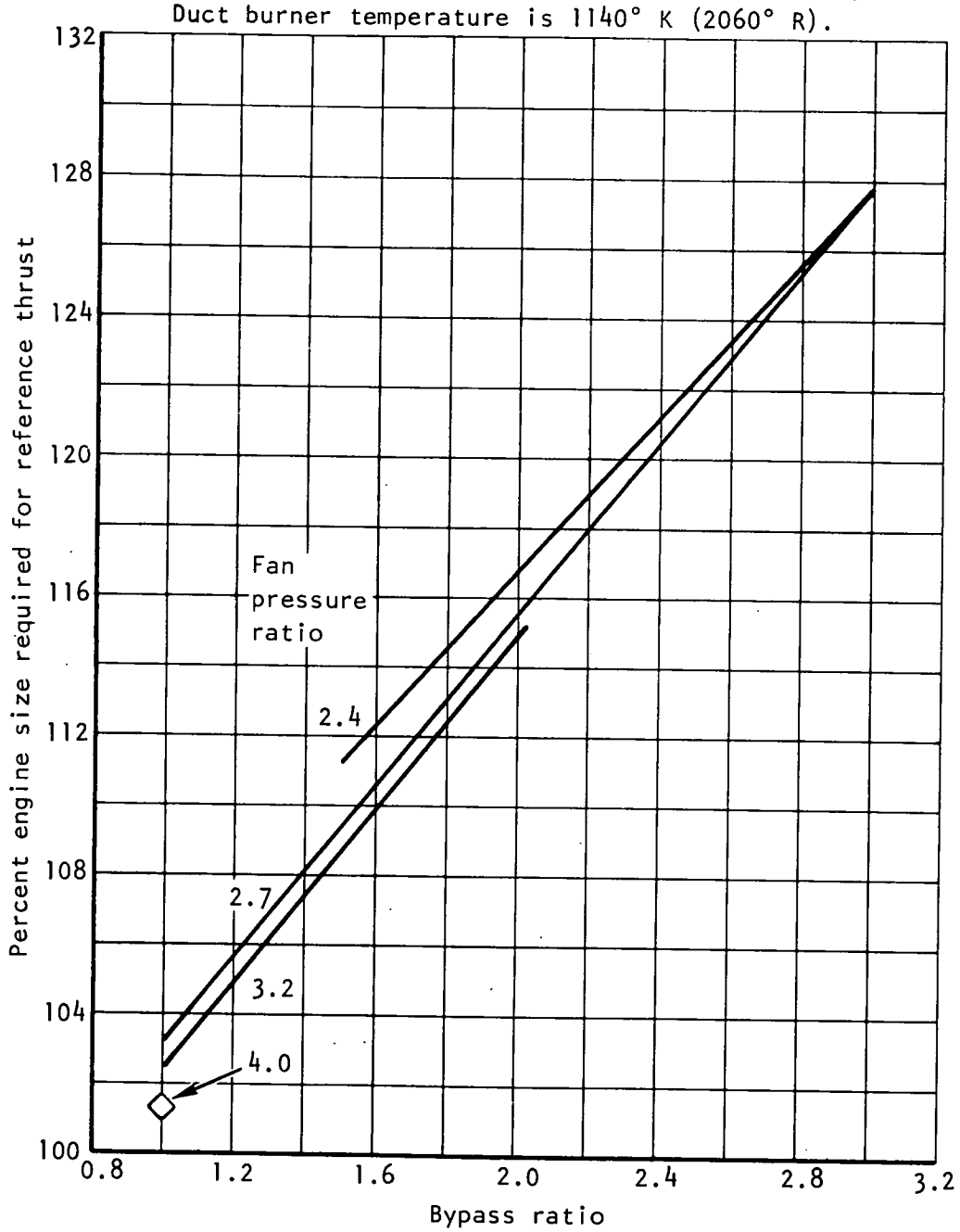

Figure 23.- Engine size required for reference thrust.

A study of the impact of changing exhaust nozzle size on propulsion and aircraft performance was also made. The nozzle of the SF74-19 was increased in diameter relative to the preliminary parametric engines for two reasons: (1) to improve supersonic cruise installed performance through complete expansion of exhaust gases, and (2) to reduce nacelle afterbody boattail drag at supersonic cruise. To determine the overall effect of this change, performance and weights with the original and with the larger nozzle diameters were determined. The system with the smaller nozzle was designated SF74-19A. The improved performance and reduced drag of the larger nozzle resulted in airplane weight reductions that more than offset the increased weight of the larger nozzle. The airplane weight reduction, for constant range, was approximately 2000 kg (4400 lb). All turbofan propulsion data are presented in reference 10.

Comparison of turbofan and turbojet: To ensure that the general characteristics of the turbofan engine were valid for this study, characteristics of the SF74-19 were compared to those of a Pratt & Whitney Aircraft (PWA) study engine with a slightly higher bypass ratio. Performance and general dimensional and weight characteristics of the PWA and SF74-19 engines compared very well, with only slight differences due to different bypass ratios.

Comparisons of installed performance of the turbojet and turbofans at typical supersonic and subsonic flight conditions are presented in figures 24 and 25, respectively, for 100-percent-size engines. Weight and dimensional data are compared in table VIII.

Nacelle design: The turbofan installation resulted in lower vehicle wave drag than the turbojet installation. Two engine-associated items were responsible for the differences. One is that the ratio of nacelle maximum cross-sectional area to capture area is smaller for the turbofan than for the turbojet. The fan, having a low-pressure ratio, demands more airflow at supersonic cruise than the high-pressure ratio compressor of the turbojet. This results in a 15-percent larger inlet capture area for the turbofan engine for the same sea-level design airflow. In addition, the turbofan engine face diameter is approximately 0.05 m (2 in.) less than that of the turbojet. (This is due to a slightly lower hub-to-tip ratio on the fan.) Thus, the turbofan engine has less cross-sectional area at this station. A direct comparison of the two nacelles is shown in figure 13a.

The other item which contributes to lower drags with the fan engine nacelle is the ratio of nacelle maximum cross-sectional area to nozzle exit area, which is smaller for the fan than for the turbojet engine. Thus, nacelle boattail angles are reduced.

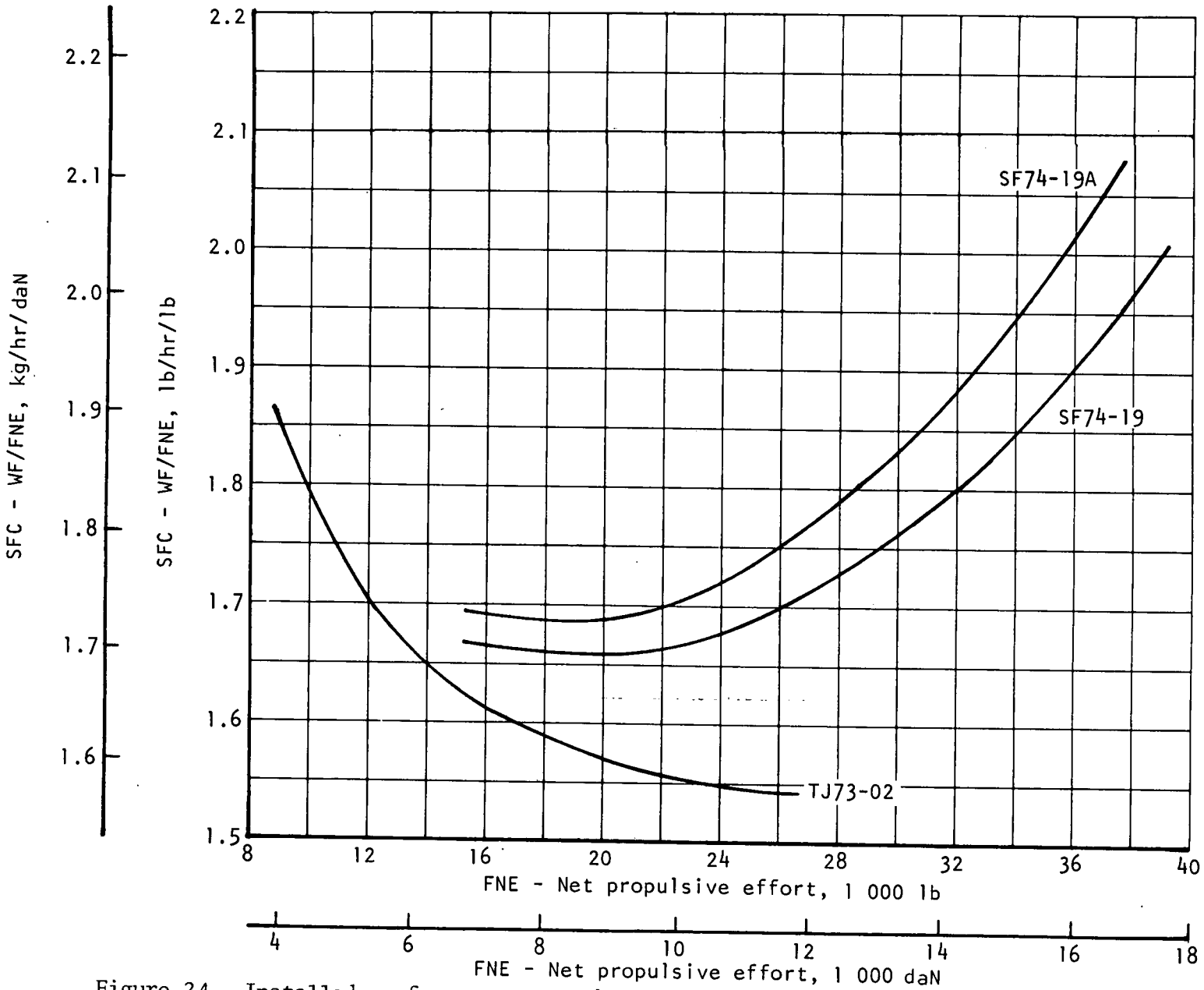

Figure 24.- Installed performance comparison at Mach 2.7, 18 300 meters (60 000 feet).

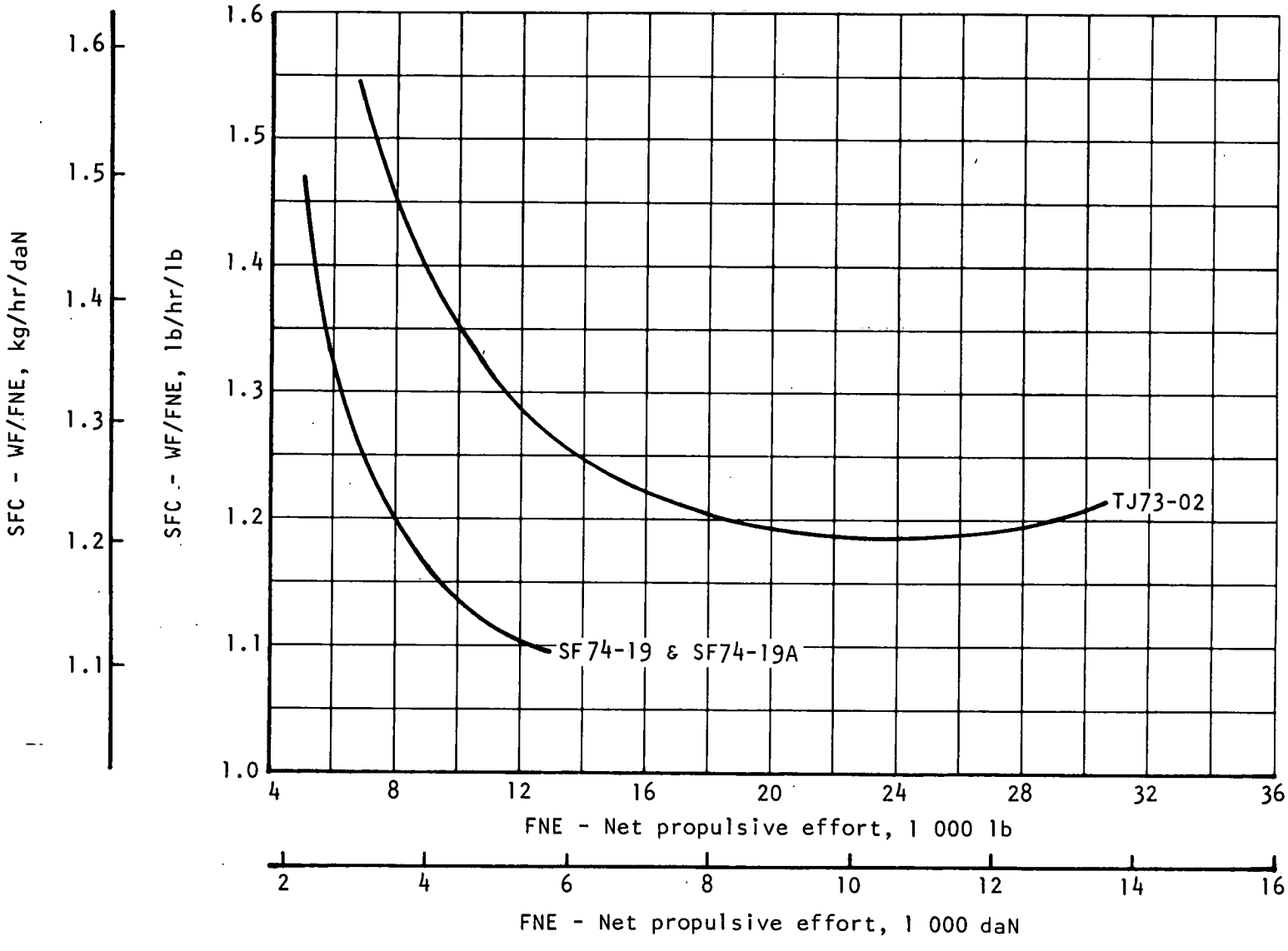

Figure 25.- Installed performance comparison at Mach 0.9, 11 000 meters (36 089 feet).

TABLE VIII.- COMPARISON OF TURBOFAN AND TURBOJET WEIGHTS AND DIMENSIONS FOR 408 KG/SEC (900 LB/SEC) AIRFLOW ENGINES

Engine	TJ73-02	SF74-19	SF74-19A
Length, m (in.)	8.15 (321)	7.30 (287)	7.30 (287)
Maximum diameter, m (in.) (at nozzle)	2.13 (84)	2.31 (91)	2.06 (81)
Engine inlet diameter, m (in.)	1.91 (75)	1.86 (73)	1.86 (73)
Dry weight, kg (lb)	8748 (19 285)	7330 (16 160)	7110 (15 680)
Inlet capture area, sq m (sq in.)	2.63 (4 071)	3.02 (4 686)	3.02 (4 686)

These items suggest areas which should be explored toward obtaining improved nacelle shapes. If the turbojet airflow could be increased at supersonic cruise, the inlet capture area could be increased. The airflow could be increased by (1) overspeeding the engine, (2) changing the engine cycle to lower pressure ratio, or (3) adding variable-geometry turbines. Any of these methods of increasing airflow would also allow increasing the nozzle exit area, which also reduces drag. Changes in engine geometry could reduce the maximum cross-sectional area of the nacelle. Reducing compressor hub-to-tip ratio or reducing flow areas (thus increasing flow velocities) in the engine would reduce engine diameters.

Mass Properties.- The weights of the NASA vehicle used as the basis for vehicle comparisons in this study and the basepoint 408 kg/sec (900 lb/sec) airflow turbojet propulsion/nacelle package weights are the same as those reported in the recently completed NASA study of reference 1. The methods used to scale the nacelle package weights with changes in engine size are presented in detail in reference 1. The basepoint 408 kg/sec (900 lb/sec) airflow turbofan nacelle package weight (table IX) was estimated from a layout drawing (figure 13), employing the same methodology as used for the turbojet installation, as described in reference 1.

The criterion selected to balance all configurations of this study was that of neutral stability in pitch (c.g., at 71.4% C_{ROOT}) for the takeoff (gear down) condition. This choice was based on the study results of reference 8, which indicate that this level was consistent with satisfying 10 individual static and dynamic low-speed longitudinal criteria. Parametric calculations (discussed later) indicate that the drag characteristics are relatively insensitive to modest changes in stability level used for balance.

The wing repositioning data defined in this section represent incremental movement of the wing relative to the 278 kg/sec (633 lb/sec) reference configuration. It is thus assumed that this arrangement satisfies the previous stability criteria.

The impact of engine size on the longitudinal wing location required to maintain neutral static pitch stability for the takeoff configuration with constant wing area of 995 sq m (10 713 sq ft) and takeoff gross weight of 340 000 kg (750 000 lb) is presented in figure 26. The nacelles were grown for this calculation such that their apex locations are coincident with the reference configuration in order to maintain the same location of the inlet to wing leading edge and nacelle thickness relative to the wing. One calculation point for an alternative assumption of maintaining the nacelle center-of-gravity location constant is shown for the 544 kg/sec (1200 lb/sec) turbojet

TABLE IX.- TURBOFAN BASEPOINT PROPULSION NACELLE PACKAGE WEIGHT FOR 408 KG/SEC (900 LB/SEC) ENGINE

Item	KG/NAC	LB/NAC
Nacelle structure	(1 388)	(3 060)
Lip to engine face	503	1 110
Engine face aft	885	1 950
Air induction system	(1 399)	(3 085)
Ducts (cowl lip to engine face)	302	665
Leading edge	68	150
Fixed ramp/splitter	39	85
Splitter/center beam	215	475
Ramps and actuation	567	1 250
Bypass and auxiliary inlet systems	136	300
Secondary air provisions	27	60
Controls	45	100
Engine (includes residual fluids)	7 375	16 260
Engine mounts	111	245
Total weight/nacelle	10 273	22 650

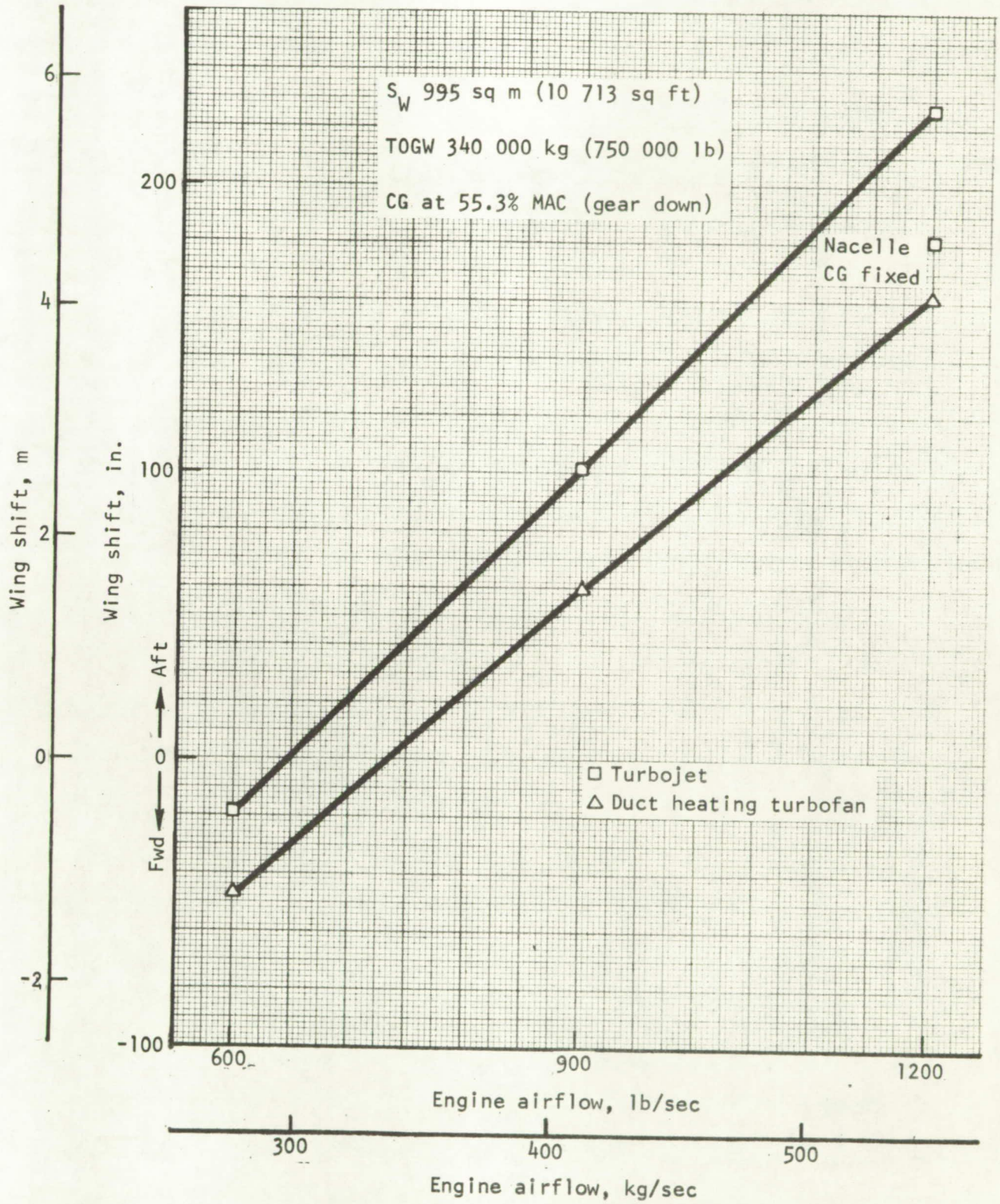

Figure 26.- Wing shift required for neutral longitudinal stability at takeoff as a function of engine size.

cycle in order to establish wing position sensitivity to nacelle growth rules. The turbofan cycle requires a smaller wing shift for all engine sizes, as a result of the considerably lighter nacelle installation relative to the turbojet. The engine weight is the principal component difference. Aerodynamic balance requires that the wing be shifted aft 1.52 m and 2.6 m (60 in. and 102 in.) for the basepoint 408 kg/sec (900 lb/sec) turbofan and turbojet cycles, respectively.

Balance of the minimum takeoff gross weight configurations was based on the first-iteration wing area and fuel weight sizing results under "Airplane Sizing," in conjunction with the nacelle-wing relocation data of "Drag Analysis." The fuel center-of-gravity was assumed to be the same as the reference configuration. The resulting impact on wing location is presented on table X.

Drag Analysis

The objective of this analysis was to provide incremental wave and skin friction drag corrections to the reference configuration drag polars of figures 7 through 11 for the effects of engine size. The specific methods which were used were defined previously in conjunction with the nacelle geometric airflow scaling procedure. The results for the constant TOGW performance analyses reflect the impact of engine size on 995 sq m (10 713 sq ft) wing-nacelle position required to maintain neutral aerodynamic balance. For the minimum TOGW performance evaluation, the analysis further reflects the change in wing size and the resultant effect on wing and nacelle location. In each case, (1) the propulsion system packaging and installation is in accordance with the guidelines discussed previously, and (2) the empennage size is adjusted to account for changes in wing area and tail arms such that the various tail volumes are held constant.

The trimmed drag-due-to-lift characteristics for the various configurations are assumed to be independent of wing area and the same as the reference configuration. At the supersonic cruise condition, the performance can be realized in principle (ref. 11 through 14) by rewarping the wing to cancel the interference flow field induced by nacelle thickness. Such incremental camber plane corrections are established as a function of engine size for both the turbofan and turbojet cycle under "Nacelle Interference Effects." An assessment of the drag-due-to-lift characteristics at off-design conditions (airplane Mach less than 2.7) requires wind tunnel tests and/or further nacelle flow field calculations for the modified wing camber shapes. Since such effort is beyond the scope of the present study, the previously indicated assumption was necessary. In order to assess the possible impact of this consideration on the study results,

TABLE X.- WING LOCATION SUMMARY FOR PRELIMINARY RESIZED CONFIGURATIONS

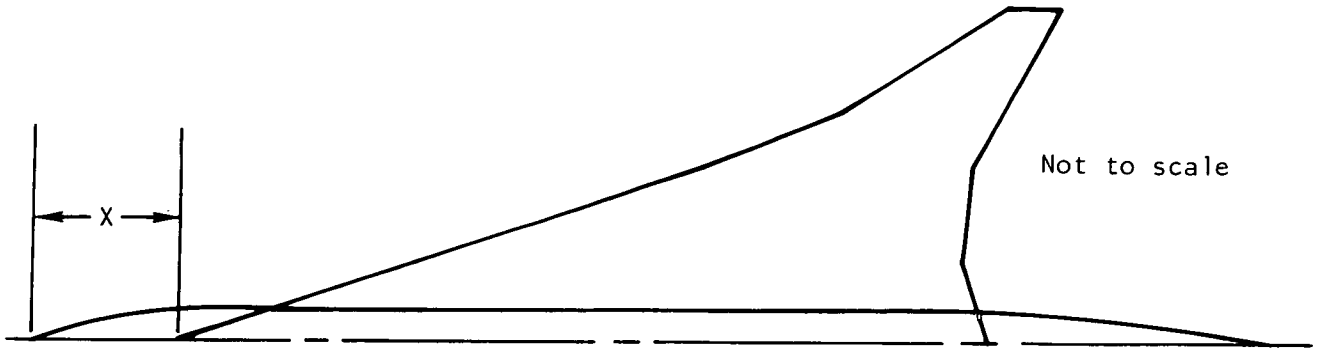

Cycle	W_a kg/sec (lb/sec)	S_W m^2 (ft^2)	X cm (in.)
Turbojet	272 (600)	776.2 (8 359)	2065 (813)
	408 (900)	868.7 (9 351)	2073 (816)
	544 (1200)	971.4 (10 456)	1951 (768)
Turbofan	272 (600)	789.3 (8 496)	1943 (765)
	408 (900)	860.9 (9 267)	1948 (767)
	544 (1200)	952.7 (10 255)	1824 (718)

a determination of the relative importance of drag uncertainties on constant TOGW performance was made. For this purpose, the range sensitivity for the median-size 408 kg/sec (900 lb/sec) turbojet reference configuration was evaluated at various assumed constant levels of drag change over the entire Mach number envelope and at the supersonic cruise point only. The results for this case indicated a 63 km (34 n. mi.) per drag count and 46 km (25 n. mi.) per drag count influence, respectively. Additional calculations indicated that the range performance was relatively insensitive to transonic drag changes. Uncertainties in drag due to lift, although not negligible at lower Mach numbers, are considerably less important than the Mach 2.7 cruise condition.

Prior to initiating the detailed drag calculations, a parametric analysis for the 272, 408, and 544 kg/sec (600, 900, and 1200 lb/sec) configurations with a constant wing area of 995 sq m (10 713 sq ft) was performed to assess the sensitivity of the wing-nacelle position (i.e., the specific aerodynamic balance criteria selected) on the Mach 2.7 wave drag. The results are presented in figure 27. A longitudinal aft wing movement of zero corresponds to the position of the Langley Research Center reference configuration. All wing locations considered resulted in a small favorable effect for both engine cycles. The use of an aerodynamic balance criteria moderately different (1%$\bar{c}$ corresponds to approximately 0.33 m or 13 in.) than neutral as proposed here does not appear to impact the cruise wave drag levels appreciably.

Aerodynamic balance requires that the 995 sq m (10 713 sq ft) wing be shifted aft 1.52 and 2.6 m (60 and 102 in.) for the study basepoint 408 kg/sec (900 lb/sec) turbofan and turbojet cycles, respectively. The resulting configuration layouts are presented in figures 14 and 15. The tail size increases required to maintain the same empennage volume are indicated in the lower right-hand block, but were not redrawn, as the differences are negligible at 1/80 scale. A comparison of the 408 kg/sec (900 lb/sec) turbojet nacelle installation to the 278 kg/sec (633 lb/sec) reference nacelle installation is presented in figure 4. The former is prior to the inclusion of wing shift. The impact of aerodynamic balance on the study basepoint wave drag is presented in table XI. The effect is favorable at most Mach numbers, with the turbofan generally benefitting the most. The average body area distribution comparison for the turbojet and turbofan basepoint layouts at Mach 2.7 is presented in figure 28. These data compare to similar information presented in figure 18, prior to inclusion of aerodynamic balance considerations. The basic reasons for the improved volumetric efficiency for the turbofan remain unchanged by wing relocation; i.e., smaller cross-sectional area, lower afterbody slope, and larger ratio of exhaust area to maximum cross-sectional area are sufficient in both cases to produce the indicated benefits of aft wing/nacelle movement.

The effect of engine size on the wave drag for the turbofan and turbojet cycles with the inclusion of aerodynamic balance considerations (in accordance with figure 26) is presented in figure 29. The major difference exhibited is due to engine cycle effects and is a result of the better matching of inlet to

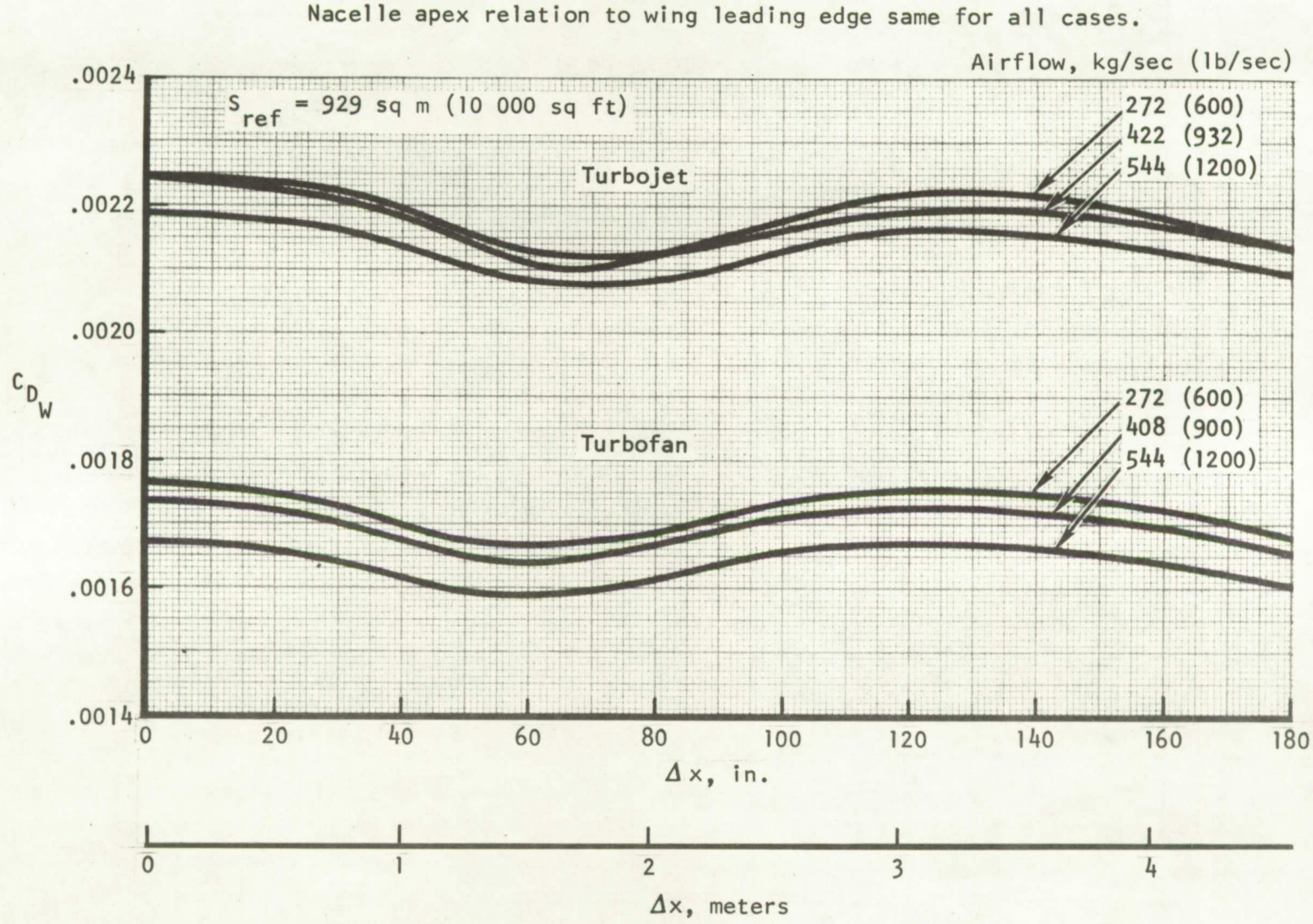

Figure 27.- Effect of wing shift on wave drag at Mach 2.7.

TABLE XI.- IMPACT OF BALANCE ON BASELINE CONFIGURATION WAVE DRAG

S_W = 995 sq m (10 713 sq ft)

W_a = 408 kg/sec (900 lb/sec)

M	Turbojet		Turbofan	
	C_{D_W}	C_{D_W}	C_{D_W}	C_{D_W}
	Δx = 0	Δx = 102 in.	Δx = 0	Δx = 60 in.
1.2	0.00458	0.00470	0.00337	0.00299
1.4	0.00445	0.00438	0.00291	0.00263
1.8	0.00328	0.00322	0.00208	0.00197
2.2	0.00256	0.00253	0.00174	0.00170
2.7	0.00225	0.00216	0.00174	0.00164

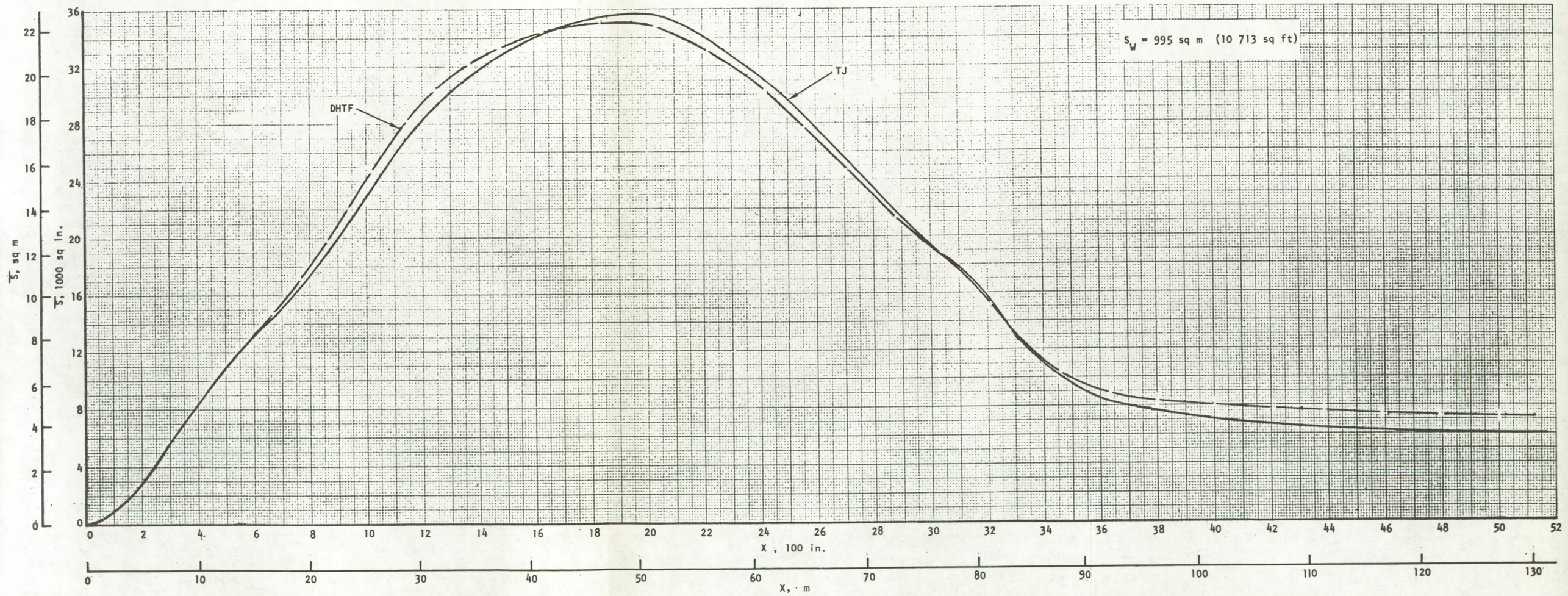

Figure 28.- Mach 2.7 average body area distributions, balanced configurations, 408 kg/sec (900 lb/sec) airflow.

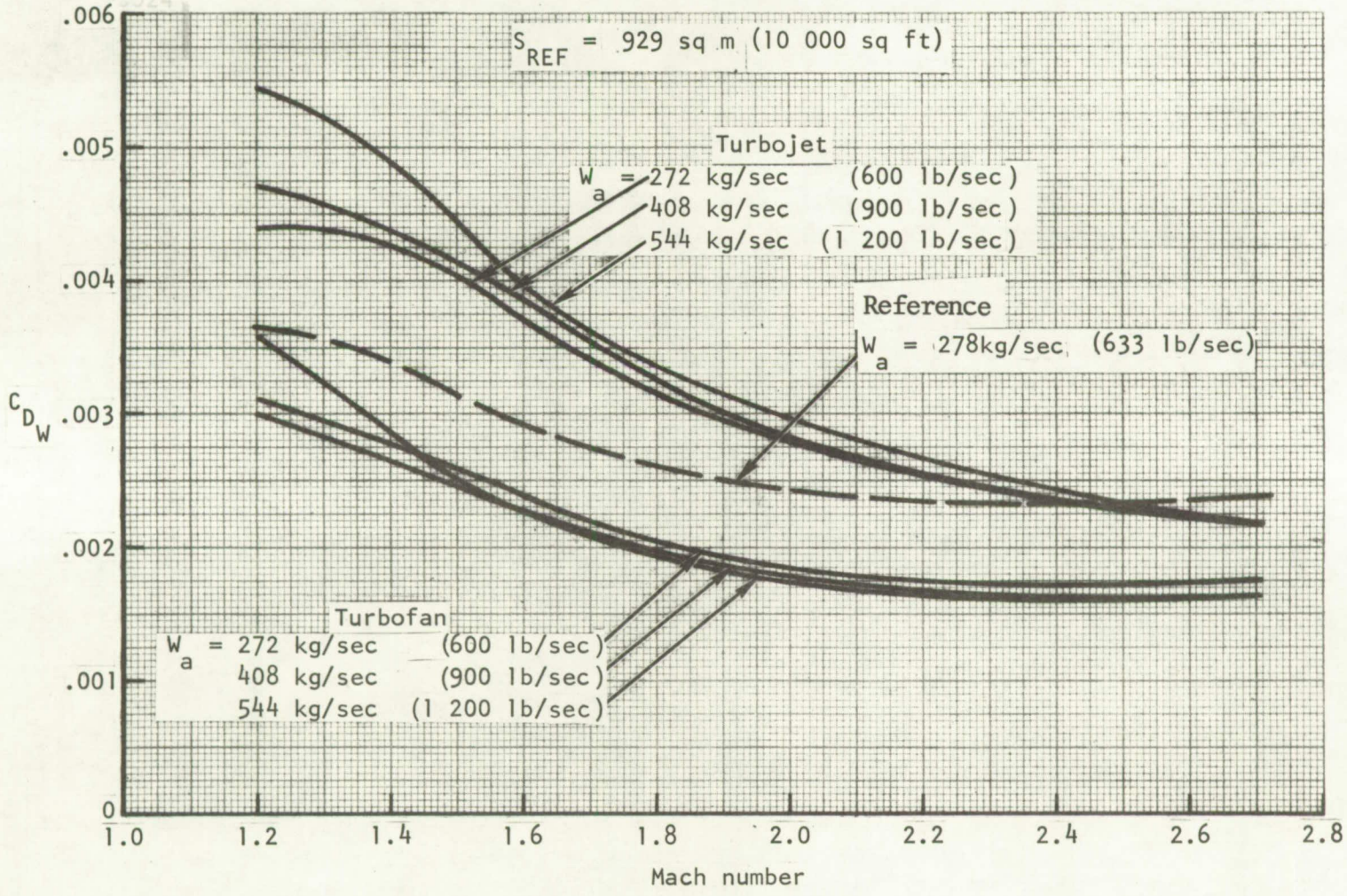

Figure 29.- Effect of engine cycle and size on wave drag.

compressor face area for the turbofan previously cited. The result of increasing turbojet engine size is to increase total configuration wave drag, with the largest variation occurring at low supersonic speeds and reducing to essentially nil effect at Mach 2.7. A reverse trend occurs for the turbofan cycle, except at the lower Mach numbers for the 544 kg/sec (1200 lb/sec) engine. The reference configuration has been superimposed on the data of figure 29 for comparison purposes. Inclusion of fully turbulent skin friction considerations on the impact of engine size is presented in figure 30. As might be anticipated, wetted area effects are such that the total configuration drag increases with increasing engine size for both cycles at all Mach numbers. The previously indicated favorable wave drag effects have been offset by frictional losses.

The detailed incremental corrections that were applied to the reference configuration drag polars of figures 7 through 11 to generate the constant TOGW performance under "Baseline Airplane Performance" are presented in tables XII through XVII.

Minimum TOGW, constant engine size, and 6482 km (3500 n. mi.) range performance were initially evaluated using balanced wing area of 995 sq m (10 713 sq ft) wave drag coefficient levels of figure 29, since the wing size and, consequently, location were not known apriori. Skin friction was varied with wetted area and chord, and the drag due to lift was assumed to be independent of wing size for this analysis.

The preliminary (i.e., "first pass") sizing results pertinent to the present discussion are summarized in the first three columns of table XVIII. The wing area for both cycles at all engine airflows was limited by fuel volume considerations. An examination of the compatibility between the wing and nacelle (in particular, the extent of wing trailing edge overhang) revealed that it would be necessary to shift the propulsion system inboard and forward in order to maintain a philosophy consistent with the study basepoint layouts of figures 14 and 15. The relocation was selected such that (1) the outboard nacelle occurred at the same wing percent chord, (2) the inboard nacelle apex was physically separated the same distance from the outboard nacelle, and (3) the nozzle overhang did not exceed the basepoint. The resulting nacelle locations relative to the wing are shown schematically in figures 31 and 32 and summarized in table XVIII. The basic intent here was to locate the propulsion system thickness relative to that of the wing consistently for each engine size, from a wave drag standpoint, subject to a qualitative structural/flutter constraint. The resulting wing-nacelle combination was longitudinally located on the fuselage in accordance with table X to produce neutral pitch stability at takeoff in order to satisfy aerodynamic balance consideration. Wave drag was reevaluated for the "second pass" resized and rebalanced 272, 408, and 544 kg/sec (600, 900 and 1200 lb/sec) configurations for subsequent refinement of the 6482 km (3500 n.mi) range performance. These results are presented in figure 33. The specific corrections applied to the reference configuration drag polars to reevaluate the minimum TOGW performance and sizing are presented in tables XIX through XXIV.

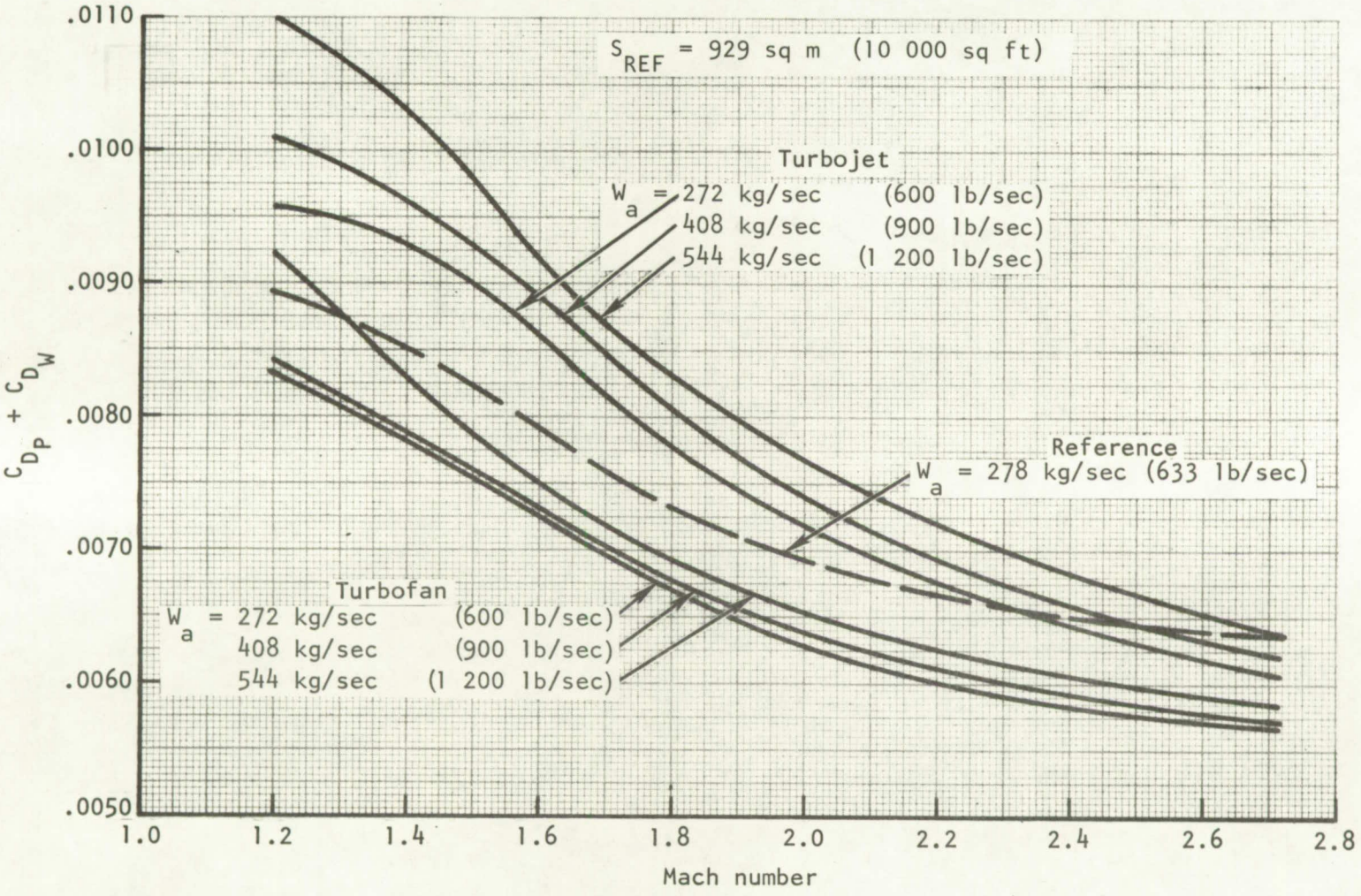

Figure 30.- Effect of engine cycle and size on friction plus wave drag.

TABLE XII.- AERODYNAMIC INCREMENTS FOR
272 KG/SEC (600 LB/SEC) TURBOJET
CONSTANT TOGW CONFIGURATION

S_W = 995.24 sq m (10 713 sq ft)

ΔX_W = -48.3 cm (-19 in.)

S_H = 41.06 sq m (442 sq ft)

S_V = 62.34 sq m (671 sq ft)

ΔS_{WET} = -56.11 sq m (-604 sq ft)

ℓ_{NAC} = 11.46 m (37.6 ft)

		Reference			Turbojet		
M	h m (ft)	C_{D_P}	C_{D_W}	$S_{\pi_{Exit}}$ sq m (sq in.)	ΔC_{D_P}	ΔC_{D_W}	$S_{\pi_{Exit}}$ sq m (sq in.)
0.4	457.2 (1 500)	0.00586	-	-	-0.00013	-	-
0.8	6 248 (20 500)	0.00555	-	-	-0.00012	-	-
1.2	10 455 (34 300)	0.00531	0.00365	2.51 (4050)	-0.00012	0.00073	1.22 (1888)
1.4	11 522 (37 800)	0.00514	0.00338	2.51 (4050)	-0.00011	0.00089	1.33 (2060)
1.8	13 564 (44 500	0.00472	0.00261	2.51 (4050)	-0.00010	0.00054	1.58 (2454)
2.2	15 697 (51 500)	0.00433	0.00232	2.51 (4050)	-0.00010	-0.00019	1.97 (3048)
2.7	18 288 (60 000)	0.00399	0.00238	2.51 (4050)	-0.00009	-0.00019	2.40 (3721)

NOTE: Aerodynamic coefficients based on reference area of 929.0 sq m (10 000 sq ft)

TABLE XIII.- AERODYNAMIC INCREMENTS FOR
408 KG/SEC (900 LB/SEC) TURBOJET
CONSTANT TOGW CONFIGURATION

S_W = 995.2 sq m (10 713 sq ft)

ΔX_W = 259.1 cm (102 in)

S_H = 45.71 sq m (492 sq ft)

S_V = 63.54 sq m (684 sq ft)

ΔS_{WET} = 61.78 sq m (665 sq ft)

ℓ_{NAC} = 14.02 m (46.0 ft)

M	h m (ft)	Reference			Turbojet		
		C_{D_P}	C_{D_W}	$S_{\pi_{Exit}}$ sq m (sq in.)	ΔC_{D_P}	ΔC_{D_W}	$S_{\pi_{Exit}}$ sq m (sq in.)
0.4	457.2 (1 500)	0.00586	-	-	0.00010	-	-
0.8	6 248 (20 500)	0.00555	-	-	0.00009	-	-
1.2	10 455 (34 300)	0.00531	0.00365	2.51 (4050)	0.00008	0.00105	1.83 (2832)
1.4	11 522 (37 800	0.00514	0.00338	2.51 (4050)	0.00008	0.00100	1.99 (3090)
1.8	13 564 (44 500)	0.00472	0.00261	2.51 (4050)	0.00008	0.00061	2.37 (3681)
2.2	15 697 (51 500)	0.00433	0.00232	2.51 (4050)	0.00007	0.00021	2.95 (4572)
2.7	18 288 (60 000)	0.00399	0.00238	2.51 (4050)	0.00006	-0.00022	3.60 (5582)

NOTE: Aerodynamic coefficients based on reference area of 929.0 sq m (10 000 sq ft)

TABLE XIV.- AERODYNAMIC INCREMENTS FOR
544 KG/SEC (1200 LB/SEC) TURBOJET
CONSTANT TOGW CONFIGURATION

S_W = 995.2 sq m (10 713 sq ft)

ΔX_W = 576.6 cm (227 in.)

S_H = 51.10 sq m (560 sq ft)

S_V = 66.03 sq m (700 sq ft)

ΔS_{WET} = 183.57 sq m (1976 sq ft)

ℓ_{NAC} = 16.22 m (53.2 ft)

		Reference			Turbojet		
M	h m (ft)	C_{D_P}	C_{D_W}	$S_{\pi_{Exit}}$ sq m (sq in.)	ΔC_{D_P}	ΔC_{D_W}	$S_{\pi_{Exit}}$ sq m (sq in.)
0.4	457.2 (1 500)	0.00586	-	-	0.00032	-	-
0.8	6 248 (20 500)	0.00555	-	-	0.00030	-	-
1.2	10 455 (34 300)	0.00531	0.00365	2.51 (4050)	0.00028	0.00177	2.44 (3776)
1.4	11 522 (37 800)	0.00514	0.00338	2.51 (4050)	0.00027	0.00152	2.65 (4120)
1.8	13 564 (44 500)	0.00472	0.00261	2.51 (4050)	0.00025	0.00072	3.16 (4908)
2.2	15 697 (51 500)	0.00433	0.00232	2.51 (4050)	0.00023	0.00033	3.93 (6096)
2.7	18 288 (60 000)	0.00399	0.00238	2.51 (4050)	0.00021	-0.00020	4.8 (7443)

NOTE: Aerodynamic coefficients based on reference area of 929.0 sq m (10 000 sq ft)

TABLE XV.- AERODYNAMIC INCREMENTS FOR
272 KG/SEC (600 LB/SEC) TURBOFAN
CONSTANT TOGW CONFIGURATION

S_W = 995.2 sq m (10,713 sq ft)

ΔX_W = -119.4 cm (-47 in)

S_H = 40.13 sq m (432 sq ft)

S_V = 62.14 sq m (669 sq ft)

ΔS_{WET} = -47.67 sq m (-514 sq ft)

ℓ_{NAC} = 11.46 m (37.6 ft)

		Reference			Turbofan		
M	h m (ft)	C_{D_P}	C_{D_W}	$S_{\pi_{Exit}}$ sq m (sq in.)	ΔC_{D_P}	ΔC_{D_W}	$S_{\pi_{Exit}}$ sq m (sq in.)
0.4	457.2 (1 500)	0.00586	-	-	-0.00011	-	-
0.8	6 248 (20 500)	0.00555	-	-	-0.00010	-	-
1.2	10 455 (34 300)	0.00531	0.00365	2.51 (4050)	-0.00009	-0.00066	1.75 (2717)
1.4	11 522 (37 800)	0.00514	0.00338	2.51 (4050)	-0.00009	-0.00075	1.97 (3053)
1.8	13 564 (44 500)	0.00472	0.00261	2.51 (4050)	-0.00008	-0.00064	2.47 (3833)
2.2	15 697 (51 500)	0.00433	0.00232	2.51 (4050)	-0.00008	-0.00062	2.80 (4336)
2.7	18 288 (60 000)	0.00399	0.00238	2.51 (4050)	-0.00007	-0.00074	2.80 (4336)

NOTE: Aerodynamic coefficients based on reference area of 929.0 sq m (10 000 sq ft)

TABLE XVI.- AERODYNAMIC INCREMENTS FOR
408 KG/SEC (900 LB/SEC) TURBOFAN
CONSTANT TOGW CONFIGURATION

S_W = 995.2 sq m (10,713 sq ft)

ΔX_W = 152.4 cm (60.0 in)

S_H = 43.85 sq m (472 sq ft)

S_V = 63.08 sq m (679 sq ft)

ΔS_{WET} = 73.02 sq m (786 sq ft)

ℓ_{NAC} = 14.02 m (46.0 ft)

		Reference			Turbofan		
M	h m (ft)	C_{D_P}	C_{D_W}	$S_{\pi_{Exit}}$ sq m (sq in.)	ΔC_{D_P}	ΔC_{D_W}	$S_{\pi_{Exit}}$ sq m (sq in.)
0.4	457.2 (1 500)	0.00586	-	-	0.00013	-	-
0.8	6 248 (20 500)	0.00555	-	-	0.00012	-	-
1.2	10 455 (34 300)	0.00531	0.00365	2.51 (4050)	0.00012	-0.00066	2.63 (4075)
1.4	11 522 (37 800)	0.00514	0.00338	2.51 (4050)	0.00011	-0.00075	2.95 (4580)
1.8	13 564 (44 500)	0.00472	0.00261	2.51 (4050)	0.00010	-0.00064	3.71 (5750)
2.2	15 697 (51 500)	0.00433	0.00232	2.51 (4050)	0.00010	-0.00062	4.20 (6504)
2.7	18 288 (60 000)	0.00399	0.00238	2.51 (4050)	0.00009	-0.00074	4.20 (6504)

NOTE: Aerodynamic coefficients based on reference area of 929.0 sq m (10 000 sq ft)

TABLE XVII.- AERODYNAMIC INCREMENTS FOR
544 KG/SEC (1200 LB/SEC) TURBOFAN
CONSTANT TOGW CONFIGURATION

S_W = 995.2 sq m (10,713 sq ft)

ΔX_W = 411.5 cm (162.0 sq in)

S_H = 48.49 sq in (522.0 sq ft

S_V = 64.19 sq in (691.0 sq ft)

ΔS_{WET} = 196.02 sq m (2110.0 sq ft)

ℓ_{NAC} = 16.22 m (53.2 ft)

		Reference			Turbofan		
M	h m (ft)	C_{D_P}	C_{D_W}	$S_{\pi_{Exit}}$ sq m (sq in.)	ΔC_{D_P}	ΔC_{D_W}	$S_{\pi_{Exit}}$ sq m (sq in.)
0.4	457.2 (1 500)	0.00586	-	-	0.00036	-	-
0.8	6 248 (20 500	0.00555	-	-	0.00034	-	-
1.2	10 455 (34 300)	0.00531	0.00365	2.51 (4050)	0.00032	-0.00005	3.51 (5433)
1.4	11 522 (37 800	0.00514	0.00338	2.51 (4050)	0.00031	-0.00054	3.93 (6107)
1.8	13 564 (44 500)	0.00472	0.00261	2.51 (4050)	0.00029	-0.00070	4.95 (7667)
2.2	15 697 (51 500)	0.00433	0.00232	2.51 (4050)	0.00027	-0.00066	5.60 (8672)
2.7	18 288 (60 000)	0.00399	0.00238	2.51 (4050)	0.00025	-0.00075	5.60 (8672)

NOTE: Aerodynamic coefficients based on reference area of 929.0 sq m (10 000 sq ft)

TABLE XVIII.- NACELLE LOCATION SUMMARY FOR PRELIMINARY RESIZED CONFIGURATIONS

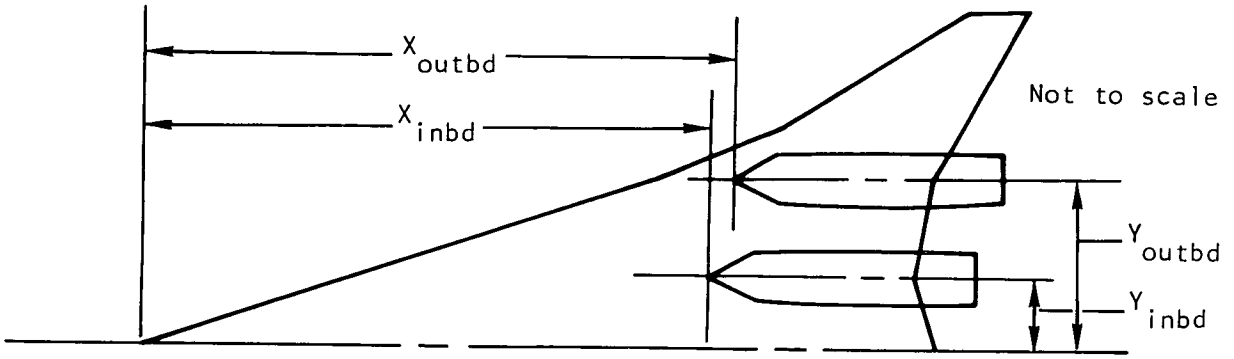

Cycle	W_a kg/sec (lb/sec)	S_W m^2, (ft^2)	X_{inbd} cm (in.)	Y_{inbd} cm (in.)	X_{outbd} cm (in.)	Y_{outbd} cm (in.)
Turbojet	272 (600)	776.6 (8 359)	4089 (1610)	620 (244)	4229 (1665)	1064 (419)
	408 (900)	868.7 (9 351)	4188 (1649)	584 (230)	4328 (1704)	1029 (405)
	544 (1200)	971.4 (10 456)	4227 (1664)	531 (209)	4366 (1719)	975 (384)
Turbofan	272 (600)	789.3 (8 496)	4166 (1640)	627 (247)	4305 (1695)	1072 (422)
	408 (900)	860.9 (9 267)	4173 (1643)	584 (230)	4313 (1698)	1029 (405)
	544 (1200)	952.7 (10 255)	4158 (1637)	508 (200)	4298 (1692)	952 (375)

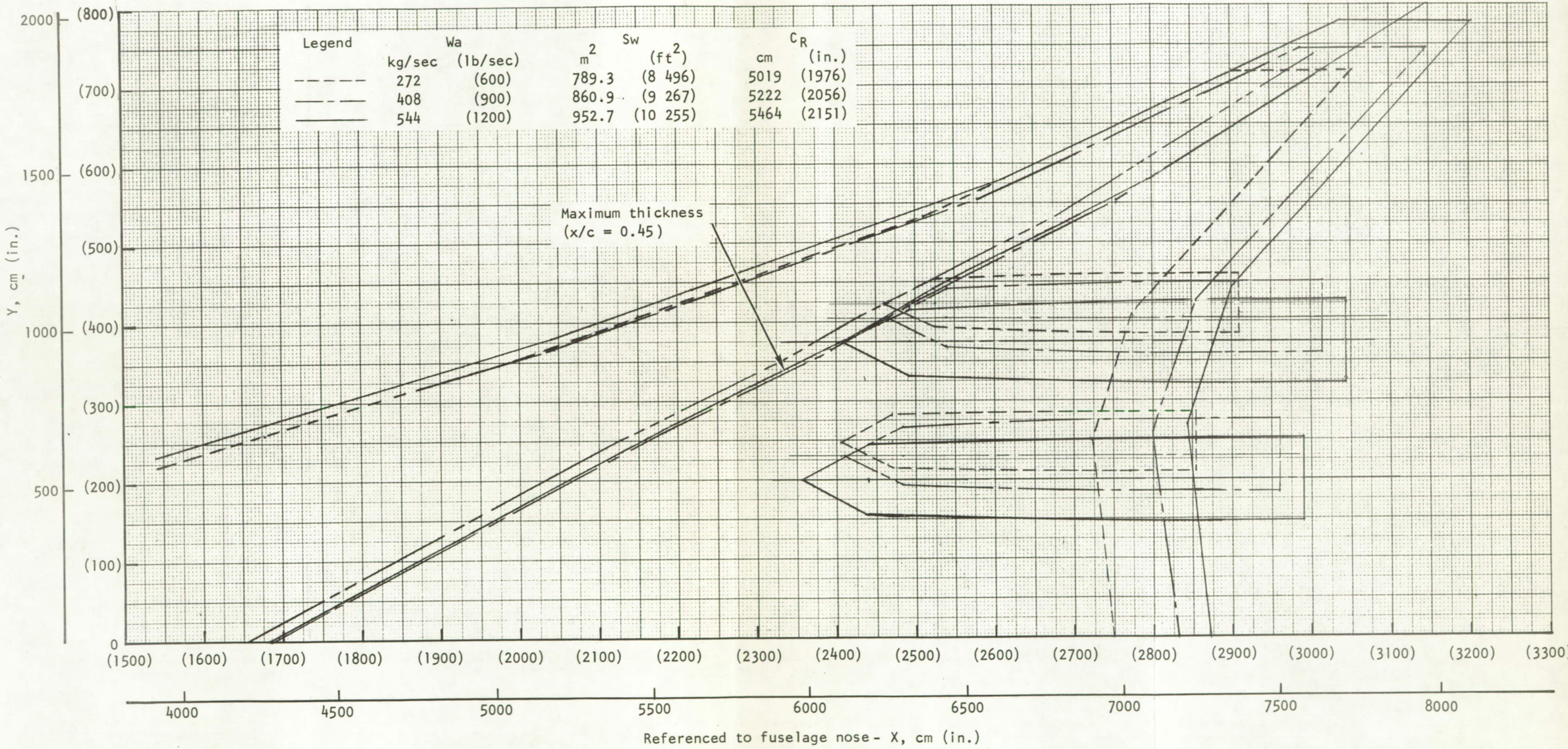

Figure 31.- Relative location of wing and nacelles for preliminary resized turbofan configurations.

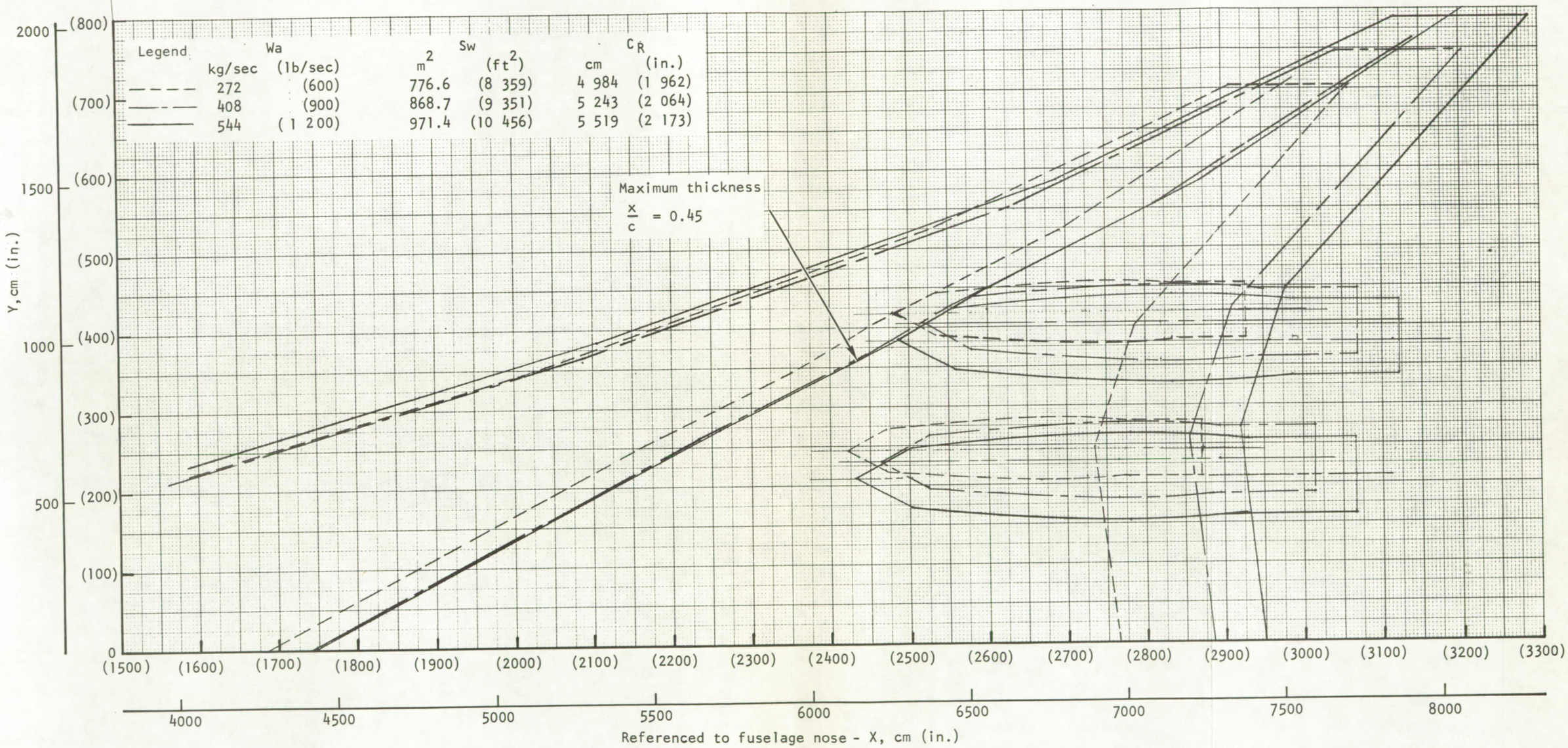

Figure 32.- Relative location of wing and nacelles for preliminary resized turbojet configurations.

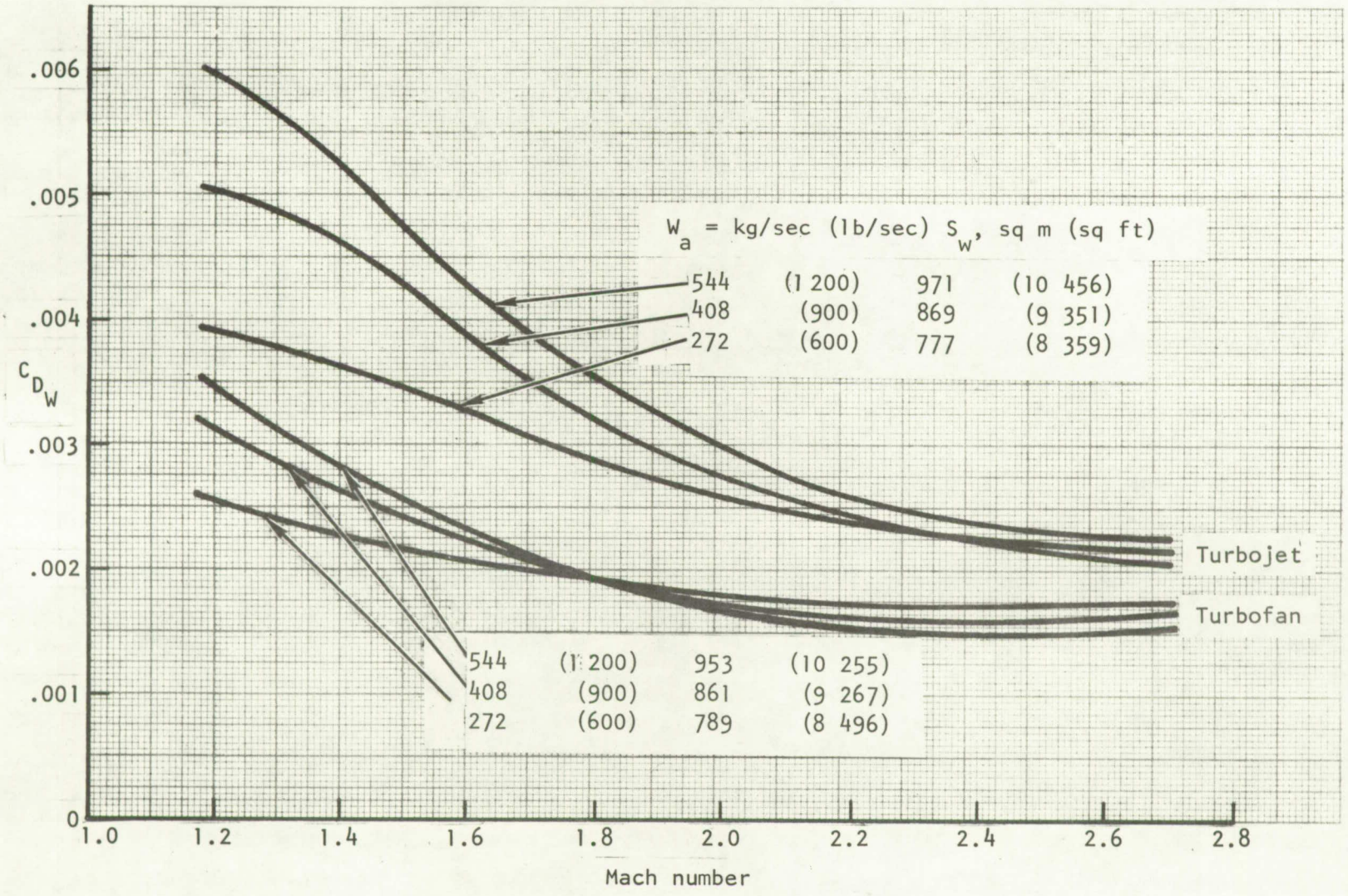

Figure 33.- Variation of wave drag with Mach number for resized configurations.

TABLE XIX.- AERODYNAMIC INCREMENTS FOR 272 KG/SEC (600 LB/SEC) TURBOJET RESIZED CONFIGURATION

S_W = 776.2 m^2 (8 359 ft^2)

ΔX_w = 749.3 cm (295 in.)

S_H = 28.8 m^2 (310 ft^2)

S_V = 43.1 m^2 (464 ft^2)

ΔS_{WET} = -413.1 m^2 (-4 447 ft^2)

ℓ_{NAC} = 11.46 m (37.6 ft)

M	h m (ft)	Reference			Turbojet		
		C_{D_P}	C_{D_W}	$S\pi_{EXIT}$ m^2 ($in.^2$)	ΔC_{D_P}	ΔC_{D_W}	$S\pi_{EXIT}$ m^2 ($in.^2$)
0.4	457.2 (1 500)	0.00586	-	-	-0.00089	-	-
0.8	6 248 (20 500)	0.00555	-	-	-0.00086	-	-
1.2	10 455 (34 300)	0.00531	0.00365	2.51 (4 050)	-0.00091	-0.00038	1.22 (1 888)
1.4	11 522 (37 800)	0.00514	0.00338	2.51 (4 050)	-0.00093	-0.00036	1.33 (2 060)
1.8	13 564 (44 500)	0.00472	0.00261	2.51 (4 050)	-0.00079	-0.00022	1.58 (2 454)
2.2	14 697 (51 500)	0.00433	0.00232	2.51 (4 050)	-0.00074	-0.00036	1.97 (3 048)
2.7	18 288 (60 000)	0.00399	0.00238	2.51 (4 050)	-0.00069	-0.00061	2.40 (3 721)

NOTE: Aerodynamic coefficients based on reference area of 929.0 m^2 (10 000 ft^2)

TABLE XX.- AERODYNAMIC INCREMENTS FOR 408 KG/SEC (900 LB/SEC) TURBOJET RESIZED CONFIGURATION

S_W = 868.7 (9 351 ft^2)

ΔX_W = 756.9 cm (298 in.)

S_H = 34.0 m^2 (366 ft^2)

S_V = 52.95 m^2 (570 ft^2)

ΔS_{WET} = -209.8 m^2 (-2 258 ft^2)

ℓ_{NAC} = 14.02 m (46.0 ft)

M	h m (ft)	Reference			TJ73-02		
		C_{D_P}	C_{D_W}	$S_{\pi_{EXIT}}$ m^2 ($in.^2$)	ΔC_{D_P}	ΔC_{D_W}	$S_{\pi_{EXIT}}$ m^2 ($in.^2$)
0.4	457.2 (1 500)	0.00586	-	-	-0.00017	-	-
0.8	6 248 (20 500)	0.00555	-	-	-0.00019	-	-
1.2	10 455 (34 300)	0.00531	0.00365	2.51 (4 050)	-0.00026	+0.00104	1.83 (2 832)
1.4	11 522 (37 400)	0.00514	0.00338	2.51 (4 050)	-0.00031	+0.00092	1.99 (3 090)
1.8	13 564 (44 500)	0.00472	0.00261	2.51 (4 050)	-0.00022	+0.00039	2.37 (3 681)
2.2	15 697 (51 500)	0.00433	0.00232	2.51 (4 050)	-0.00022	-0.00005	2.95 (4 572)
2.7	18 288 (60 000)	0.00399	0.00238	2.51 (4 050)	-0.00020	-0.00044	3.60 (5 582)

NOTE: Aerodynamic coefficients based on reference area of 929.0 m^2 (10 000 ft^2)

TABLE XXI.- AERODYNAMIC INCREMENTS FOR 544 KG/SEC (1 200 LB/SEC) TURBOJET RESIZED CONFIGURATION

S_W = 971.4 m^2 (10 456 ft^2)

ΔX_W = 635.0 cm (250 in.)

S_H = 40.23 m^2 (433 ft^2)

S_V = 60.39 m^2 (650 ft^2)

ΔS_{WET} = 107.4 m^2 (1 156 ft^2)

ℓ_{NAC} = 16.22 m (53.2 ft)

M	h m (ft)	Reference			Turbojet		
		C_{D_P}	C_{D_W}	$S_{\pi_{EXIT}}$ m^2 ($in.^2$)	ΔC_{D_P}	ΔC_{D_W}	$S_{\pi_{EXIT}}$ m^2 ($in.^2$)
0.4	457.2 (1 500)	0.00586	-	-	0.00057	-	-
0.8	6 248 (20 500)	0.00555	-	-	0.00050	-	-
1.2	10 455 (34 300)	0.00531	0.00365	2.51 (4 050)	0.00039	+0.00257	2.44 (3 776)
1.4	11 522 (37 800)	0.00514	0.00338	2.51 (4 050)	0.00031	+0.00206	2.65 (4 120)
1.8	13 564 (44 500)	0.00472	0.00261	2.51 (4 050)	0.00036	+0.00108	3.16 (4 908)
2.2	15 697 (51 500)	0.00433	0.00232	2.51 (4 050)	0.00032	+0.0037	3.93 (6 096)
2.7	18 288 (60 000)	0.00399	0.00238	2.51 (4 050)	0.00028	0.0	4.8 (7 443)

NOTE: Aerodynamic coefficients based on reference area of 929.0 m^2 (10 000 ft^2)

TABLE XXII.- AERODYNAMIC INCREMENTS FOR 272 KG/SEC (600 LB/SEC) TURBOFAN RESIZED CONFIGURATION

S_W = 789.13 m^2 (8496 ft^2)

ΔX_W = 627.40 m (247 in.)

S_H = 29.34 m^2 (317 ft^2)

S_V = 44.22 m^2 (476 ft^2)

ΔS_{WET} =-490.3 m^2 (-5278 ft^2)

ℓ_{NAC} = 11.46 m (37.6 ft)

M	h m (ft)	Reference			Turbofan		
		C_{D_P}	C_{D_W}	$S_{\pi_{exit}}$ m^2 ($in.^2$)	ΔC_{D_P}	ΔC_{D_W}	$S_{\pi_{exit}}$ m^2 ($in.^2$)
0.4	457.2 (1 500)	0.00586	-	-	-0.00074	-	-
0.8	6 248 (20 500)	0.00555	-	-	-0.00070	-	-
1.2	10 455 (34 300)	0.00531	0.00365	2.51 (4050)	-0.00076	-0.00146	1.75 (2717)
1.4	11 522 (37 800)	0.00514	0.00338	2.51 (4050)	-0.00084	-0.00145	1.97 (3053)
1.8	13 564 (44 500)	0.00472	0.00261	2.51 (4050)	-0.00066	-0.00098	2.47 (3833)
2.2	15 697 (51 500)	0.00433	0.00232	2.51 (4050)	-0.00062	-0.00085	2.8 (4336)
2.7	18 288 (60 000)	0.00399	0.00238	2.51 (4050)	-0.00057	-0.00090	2.8 (4336)

NOTE: Aerodynamic coefficients based on reference area of 292.0 m^2 (10 000 ft^2).

TABLE XXIII.- AERODYNAMIC INCREMENTS FOR 408 KG/SEC (900 LB/SEC) TURBOFAN RESIZED CONFIGURATION

S_W = 860.9 m^2 (9267 ft^2)
ΔX_W = 632.5 cm (249 in.)
S_H = 33.54 m^2 (361 ft^2)
S_V = 50.35 m^2 (542 ft^2)
ΔS_{WET} = 240.8 m^2 (-2592 ft^2)
ℓ_{NAC} = 14.02 m (46.0 ft)

M	h m (ft)	Reference			Turbofan		
		C_{D_P}	C_{D_W}	$S_{\pi_{exit}}$ m^2 ($in.^2$)	ΔC_{D_P}	ΔC_{D_W}	$S_{\pi_{exit}}$ m^2 ($in.^2$)
0.4	457.2 (1 500)	0.00586	-	-	-0.00017	-	-
0.8	6 248 (20 500)	0.00555	-	-	-0.00020	-	-
1.2	10 455 (34 300)	0.00531	0.00365	2.51 (4050)	-0.00026	-0.00074	2.63 (4075)
1.4	11 522 (37 800)	0.00514	0.00338	2.51 (4050)	-0.00036	-0.00095	2.95 (4580)
1.8	13 564 (44 500)	0.00472	0.00261	2.51 (4050)	-0.00021	-0.00085	3.71 (5750)
2.2	15 697 (51 500)	0.00433	0.00232	2.51 (4050)	-0.00020	-0.00080	4.20 (6504)
2.7	18 288 (60 000)	0.00399	0.00238	2.51 (4050)	-0.00021	-0.00084	4.20 (6504)

NOTE: Aerodynamic coefficients based on reference area of 929.0 m^2 (10 000 ft^2).

TABLE XXIV.- AERODYNAMIC INCREMENTS FOR 544 KG/SEC (1 200 LB/SEC) TURBOFAN RESIZED CONFIGURATION

S_W = 952.7 m^2 (10255 ft^2)
ΔX_W = 508.0 cm (200 in.)
S_H = 39.11 m^2 (421 ft^2)
S_V = 58.62 m^2 (631 ft^2)
ΔS_{WET} = 48.96 m^2 (527 ft^2)
ℓ_{NAC} = 16.22 m (53.2 ft)

M	h m (ft)	Reference			Turbofan		
		C_{D_P}	C_{D_W}	$S_{\pi_{exit}}$ m^2 ($in.^2$)	ΔC_{D_P}	ΔC_{D_W}	$S_{\pi_{exit}}$ m^2 ($in.^2$)
0.4	457.2 (1 500)	0.00586	-	-	0.00044	-	-
0.8	6248 (20 500)	0.00555	-	-	0.00039	-	-
1.2	10 455 (34 300)	0.00531	0.00365	2.51 (4050)	0.00028	-0.00010	3.51 (5433)
1.4	11 522 (37 800)	0.00514	0.00338	2.51 (4050)	0.00021	-0.00051	3.93 (6107)
1.8	13 564 (44 500)	0.00472	0.00261	2.51 (4050)	0.00026	-0.00067	4.95 (7667)
2.2	15 697 (51 500)	0.00433	0.00232	2.51 (4050)	0.00027	-0.00070	5.6 (8672)
2.7	18 288 (60 000)	0.00399	0.00238	2.51 (4050)	0.00020	-0.00077	5.6 (8672)

NOTE: Aerodynamic coefficients based on reference area of 929.0 m^2 (10 000 ft^2).

A comparison of the first- and second-pass sizing data summarized in table XXV reveals that further aerodynamic iteration is not indicated, since wing area changes are less than 1%. The rate of analysis convergence indicates that changes in wing area and associated wing-nacelle position did not appreciably alter the wave drag coefficient levels assumed for the first-pass analysis. Comparison of figures 29 and 33 confirms this.

Nacelle Interference Effects

In order to maintain the design trimmed drag-due-to-lift efficiency of the Mach 2.7 wing-body configuration, the disturbance induced on the wing by the nacelle thickness should be canceled to restore the original wing load shape (ref. 11 and 13).* This can be accomplished in principle by locally deforming the wing camber plane in the affected area. The analysis to accomplish this is composed of two basic steps. The first is associated with defining the interference field induced on the wing by the nacelle thickness. The second is concerned with the determination of the camber surface deformation required to eliminate this disturbance field. In order to simplify the presentation of the results of the following paragraphs, all lineal dimensions are treated as normalized (by 1 in., or 2.54 cm) quantities.

The Mach 2.7 induced flow field was evaluated for the 408 kg/sec (900 lb/sec) turbojet and turbofan nacelle simulations of figures 34 and 35 using a steady nonlinear finite difference analysis (ref. 15). The incident flow was assumed to be uniform and equal to the free stream. The inlet was treated as swallowing air supersonically (i.e., operating at a mass flow ratio of one), and thus the ramp shock terminated at the cowl. The wing was treated as a reflection plane by adding an image to the physical nacelle. The calculated results are presented in the form of isobar plots in figures 36 and 37 for turbojet and turbofan cycle. Examination of these data reveals that the bow shock is much stronger and more highly curved for the turbojet, and is a result of the increased rate of buildup of nacelle frontal area (figure 16) and boundary layer diverter width (figures 36 and 37) associated with the smaller ratio of capture-to-engine compressor face area and burying of the engine into the wing.

The wing deformation required to cancel the local induced nacelle pressures was calculated by use of a direct numerical formulation of linearized lifting surface theory (ref. 16). For convenience (and because solutions can be linearly superimposed), the inboard and outboard nacelle disturbance fields were treated separately. Typical solution paneling density for the region outboard of the outboard nacelle is shown in figure 38. The largest number of chordwise and

---

*Lifting efficiency changes due to far-field wave drag interference between the restored wing-body design load shape and the nacelle thickness have been totally neglected. Later calculations indicated that this assumption was conservative by $\Delta C_{D_{NAC}}$ = -0.00012 and -0.00007 at C_L = 0.1 for the 900 lb/sec turbojet and turbofan baseline configurations, respectively.

TABLE XXV.- EFFECT OF WAVE DRAG REEVALUATION ON MINIMUM TOGW AND WING SIZE

Cycle	Airflow, kg/sec (lb/sec)	TOGW, kg (lb)		S_W, sq m (sq ft)	
		1st pass	2nd pass	1st pass	2nd pass
Turbojet	272 (600)	271 400 (597 700)	267 700 (589 600)	777 (8 359)	766 (8 247)
	408 (900)	318 400 (701 300)	320 400 (705 700)	869 (9 351)	874 (9 410)
	544 (1200)	375 000 (826 000)	379 000 (834 900)	971 (10 456)	982 (10 568)
Turbofan	272 (600)	271 900 (599 000)	274 800 (605 300)	789 (8 496)	798 (8 585)
	408 (900)	311 400 (685 800)	313 900 (691 500)	861 (9 267)	868 (9 344)
	544 (1200)	358 500 (789 600)	359 100 (790 900)	953 (10 255)	954 (10 271)

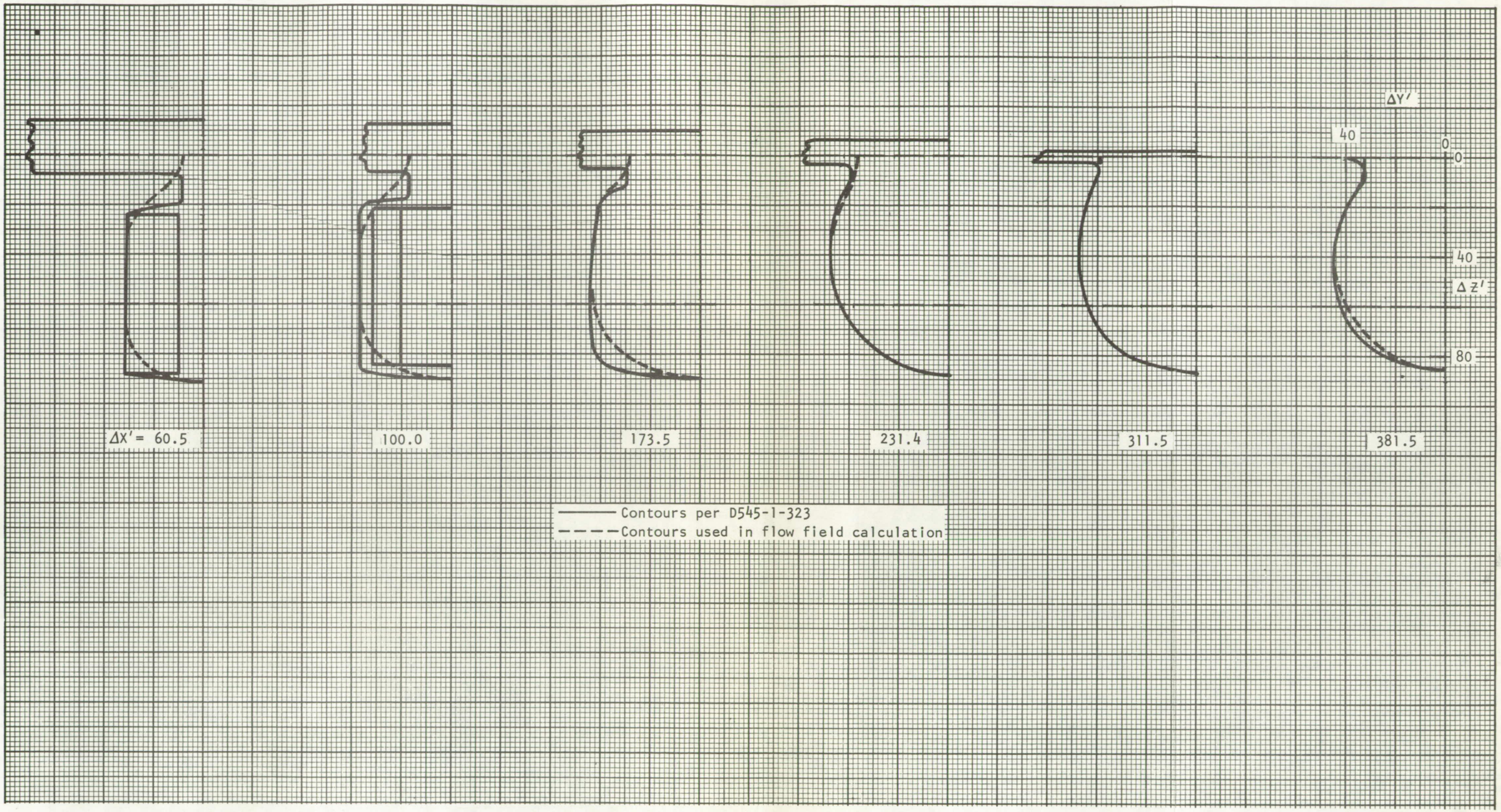

Figure 34.- Simulation of 408 kg/sec (900 lb/sec) turbojet nacelle.

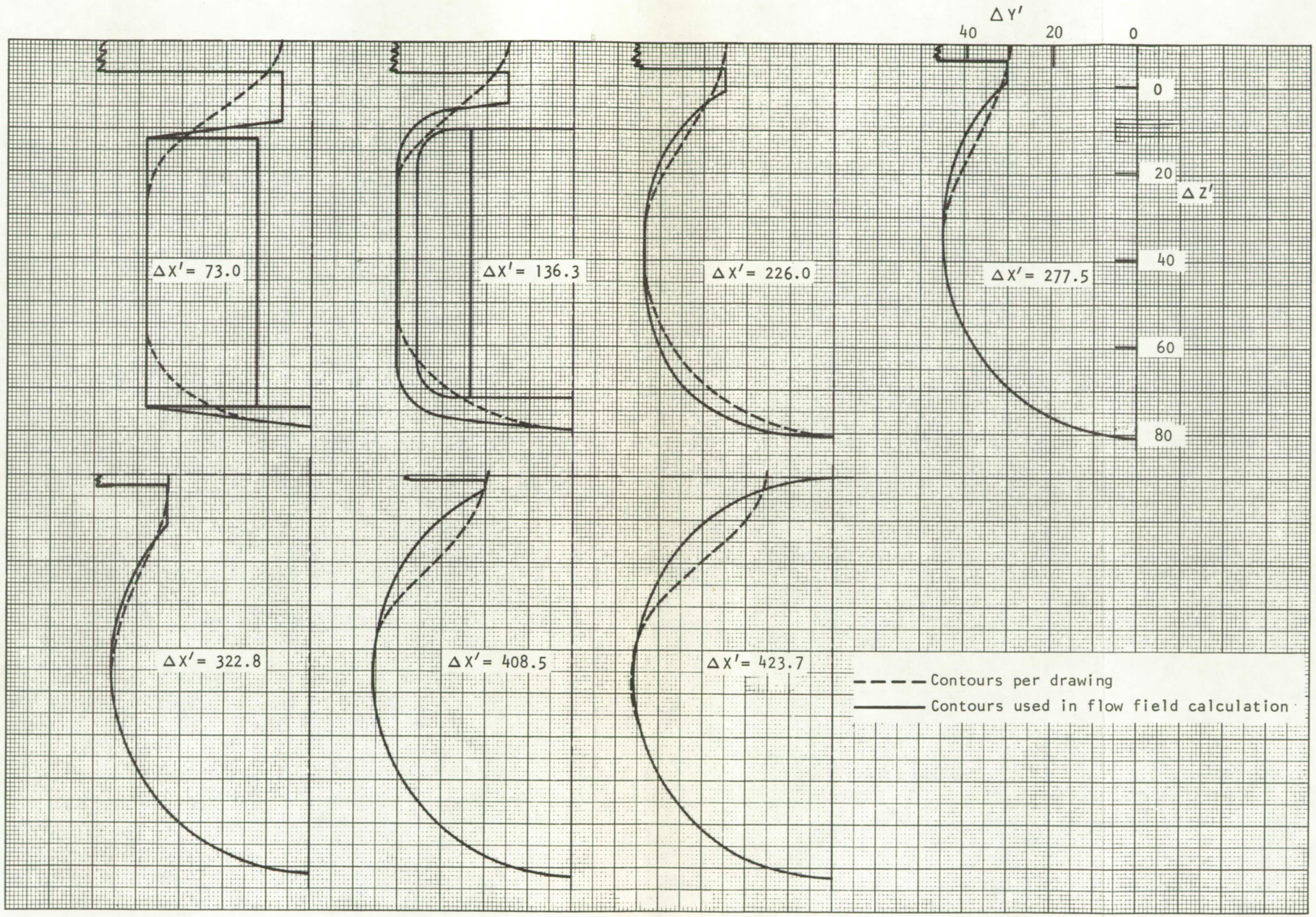

Figure 35.- Simulation of 900 lb/sec (408 kg/sec) turbofan nacelle.

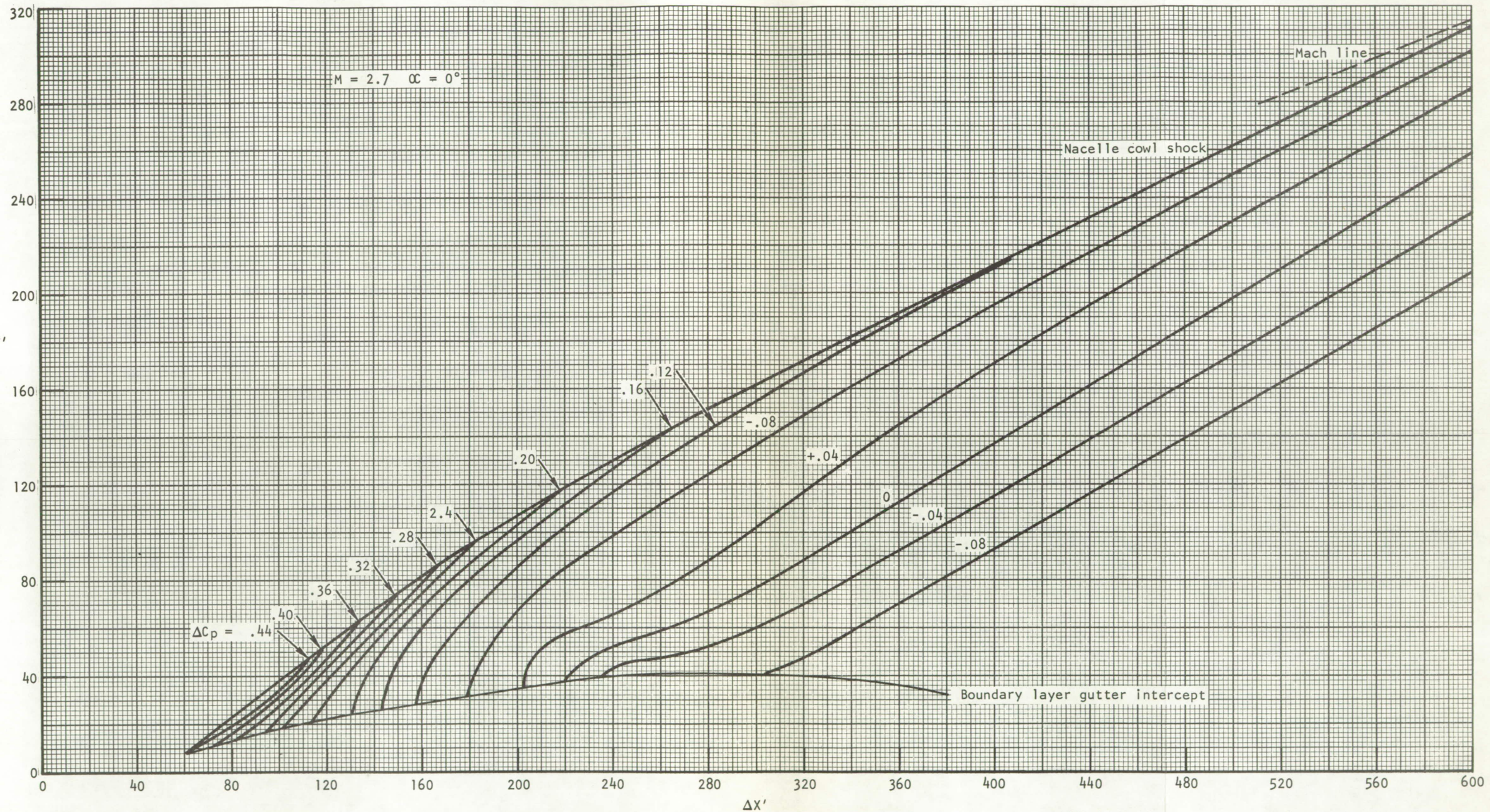

Figure 36.- Underwing pressure coefficients due to 408 kg/sec (900 lb/sec) turbojet nacelle.

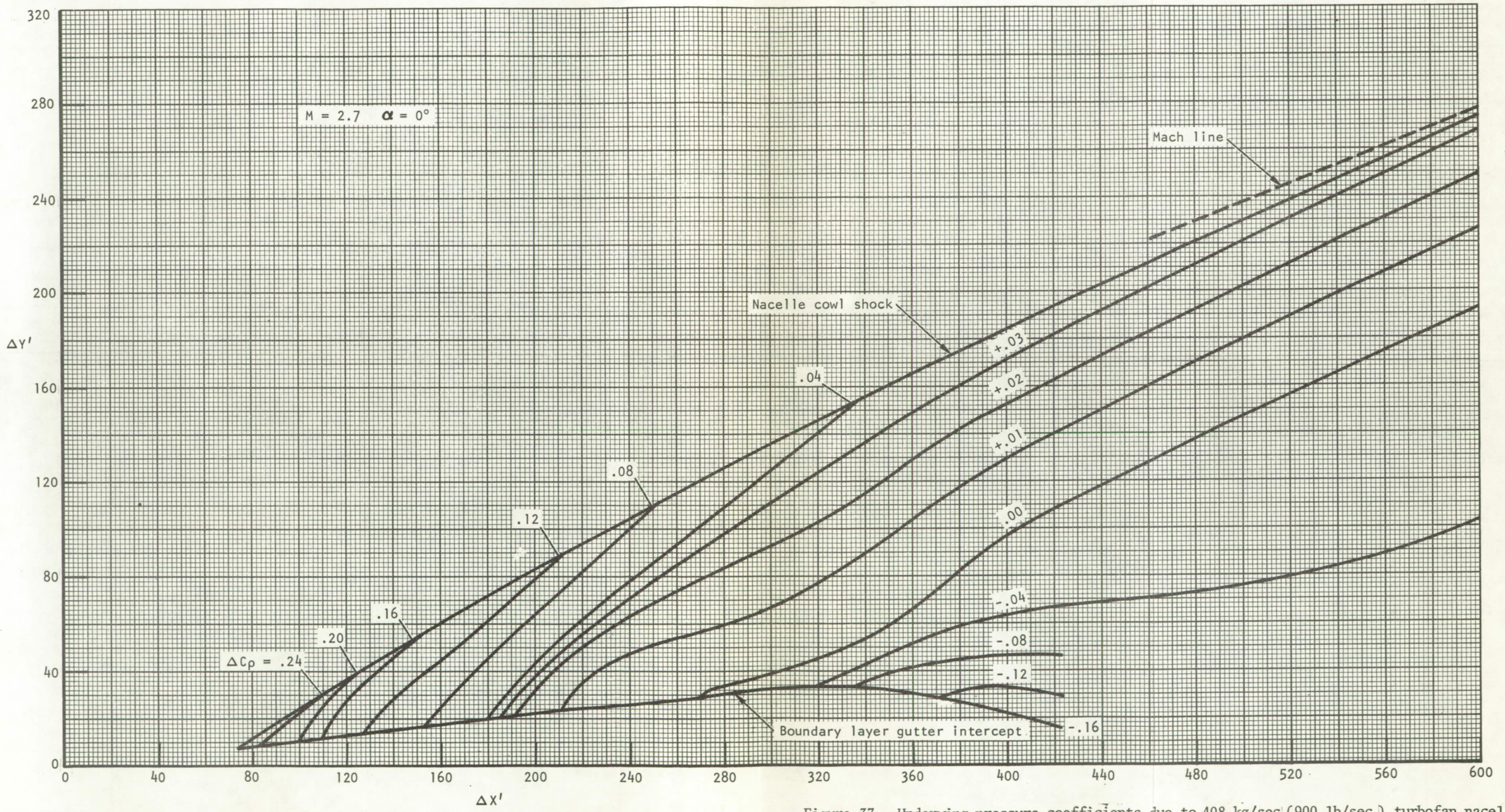

Figure 37.- Underwing pressure coefficients due to 408 kg/sec (900 lb/sec) turbofan nacelle.

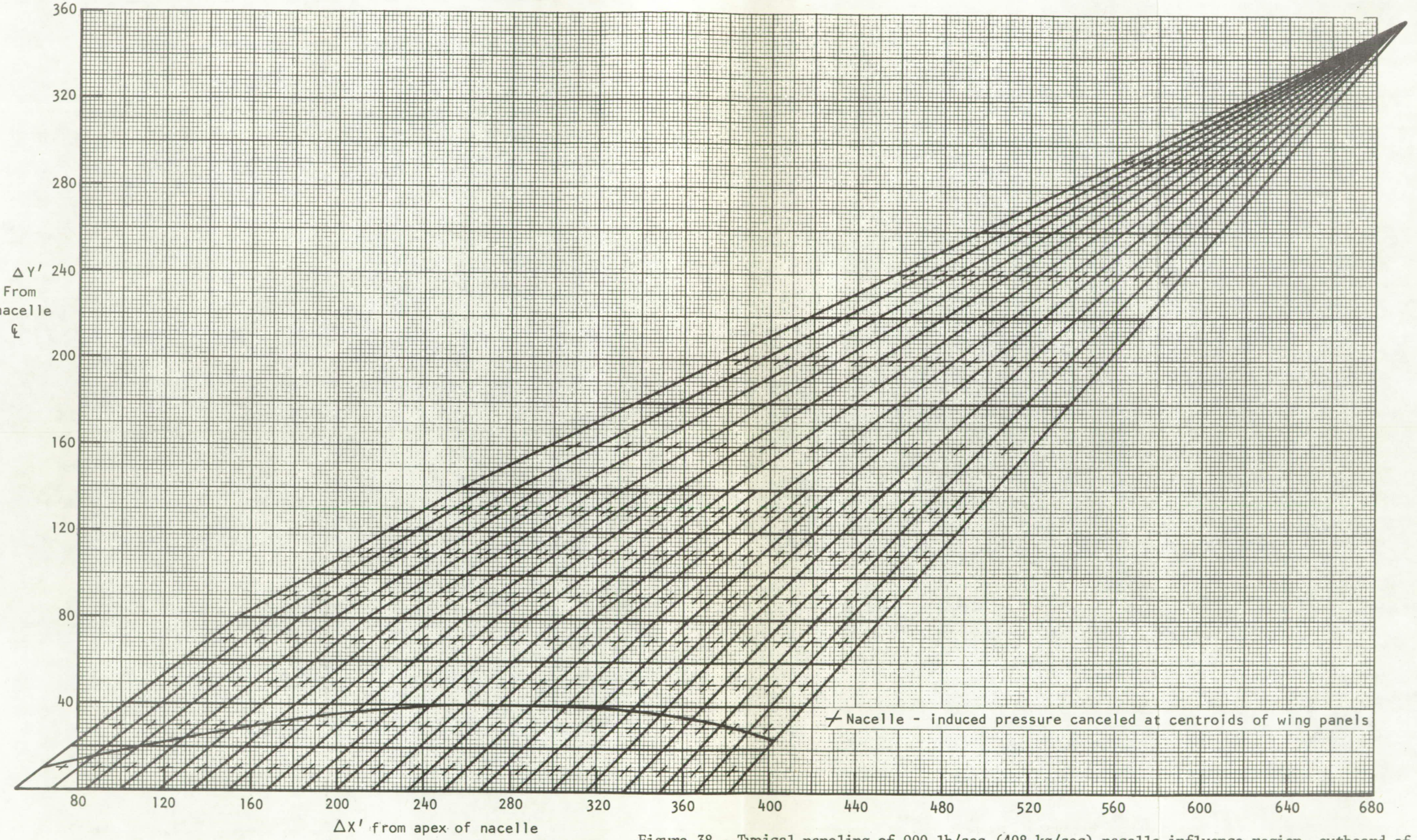

Figure 38.- Typical paneling of 900 lb/sec (408 kg/sec) nacelle influence region, outboard of outboard nacelle.

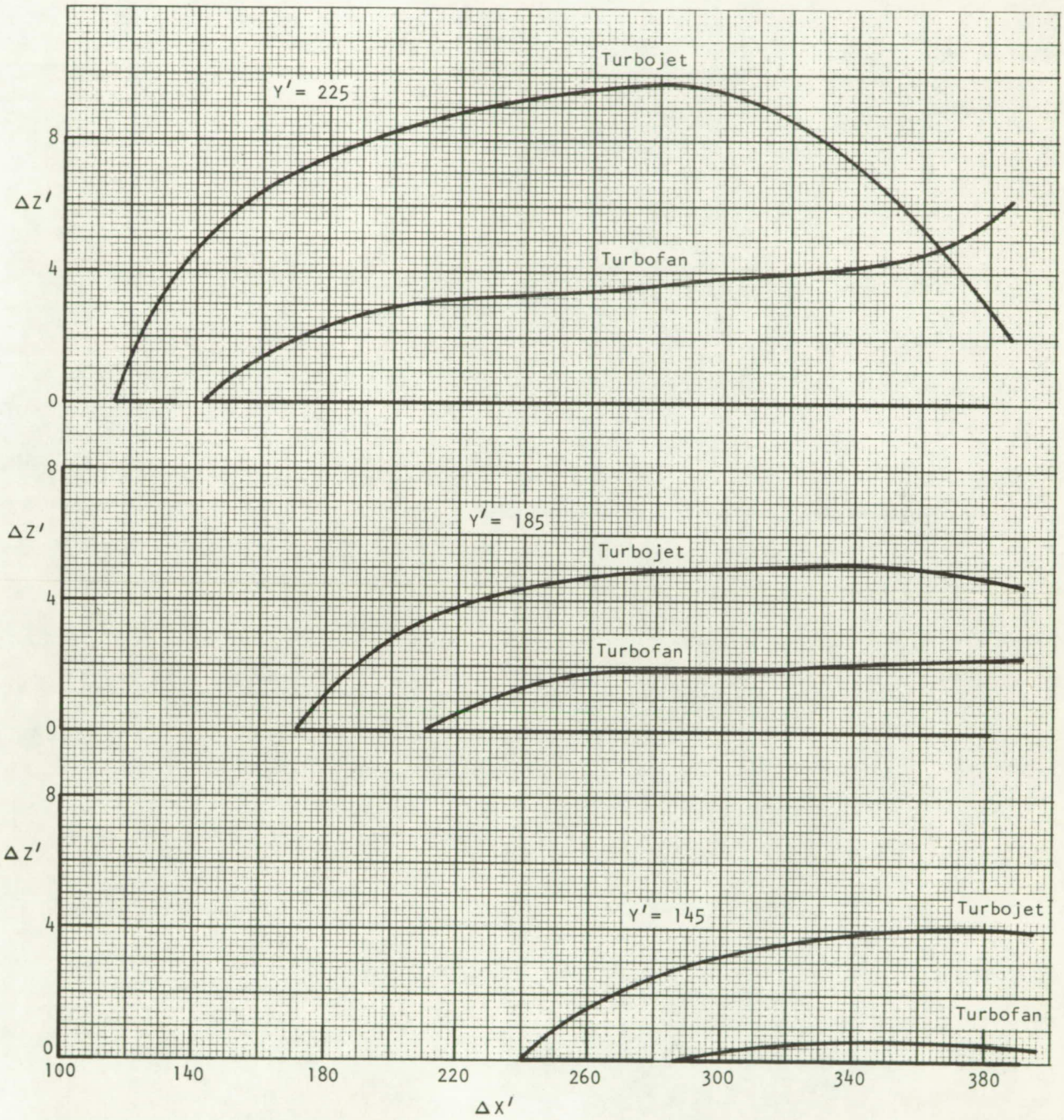

Figure 39.- Comparison of 900 lb/sec (408 kg/sec) turbojet and turbofan wing distortions required to cancel nacelle-induced pressures, inboard of inboard nacelle.

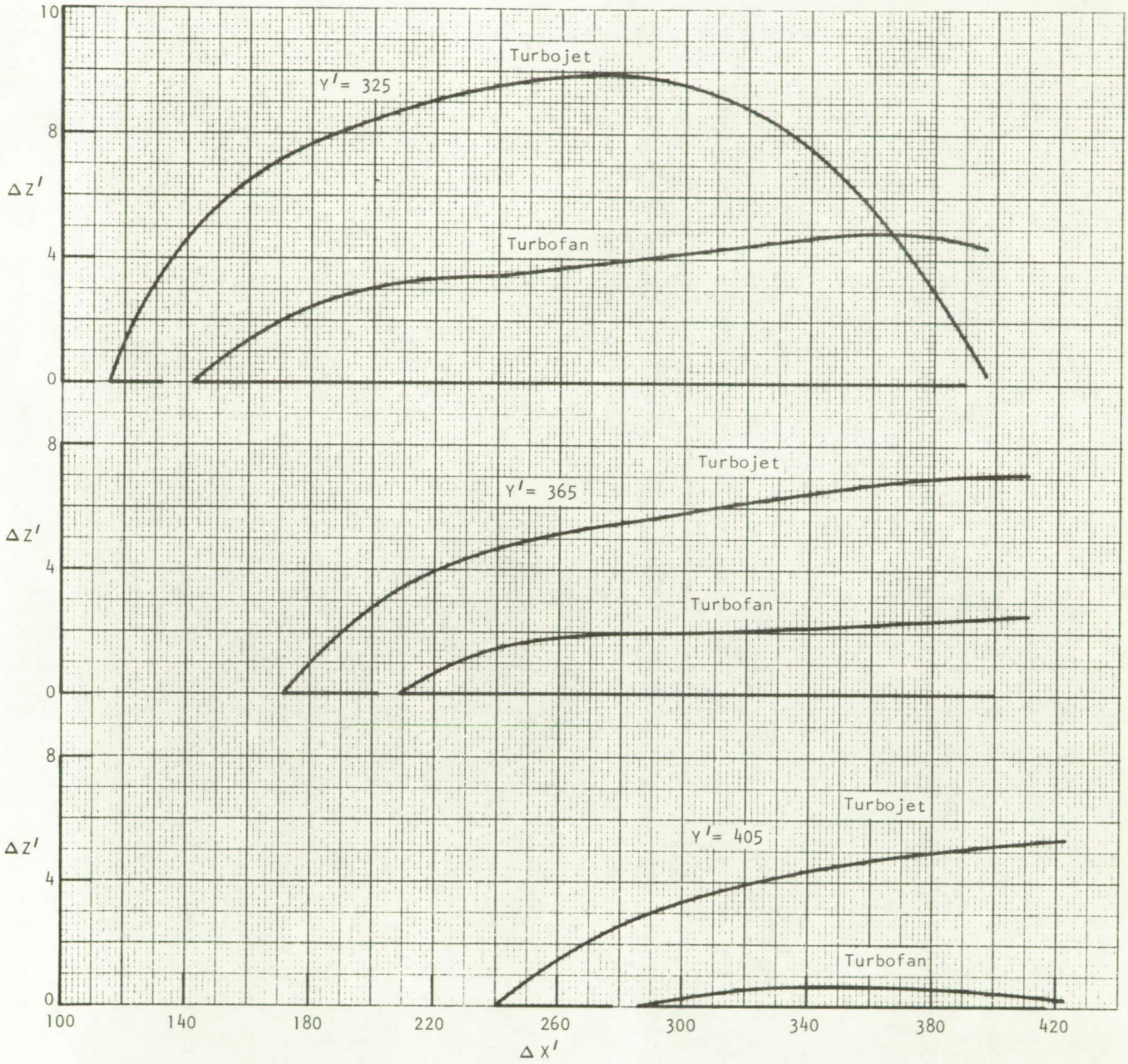

Figure 40.- Comparison of 408 kg/sec (900 lb/sec) turbojet and turbofan wing distortions required to cancel nacelle induced pressures, outboard of inboard nacelle.

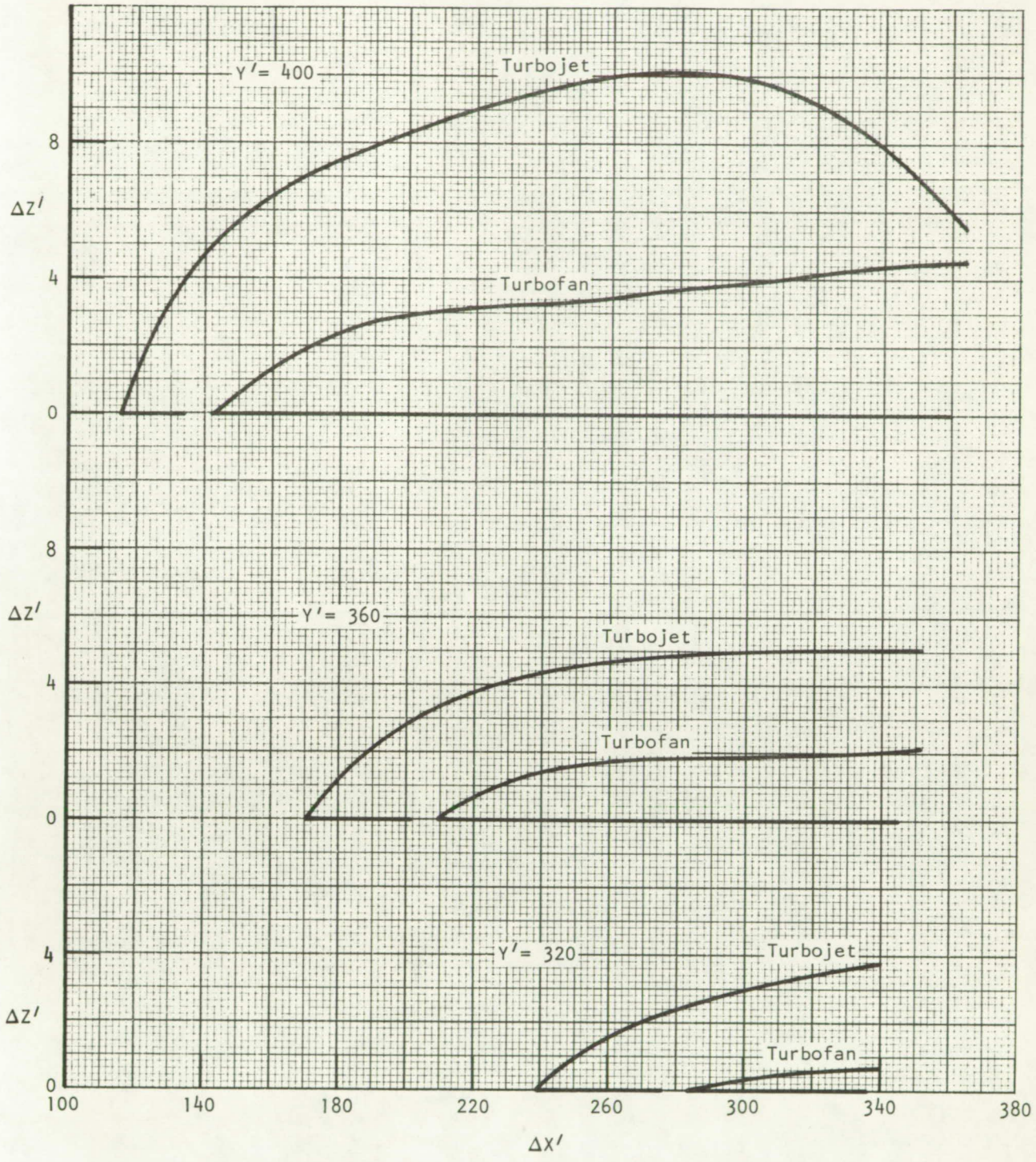

Figure 41.- Comparison of 900 lb/sec (408 kg/sec) turbojet and turbofan wing distortions required to cancel nacelle-induced pressures, inboard of outboard nacelle.

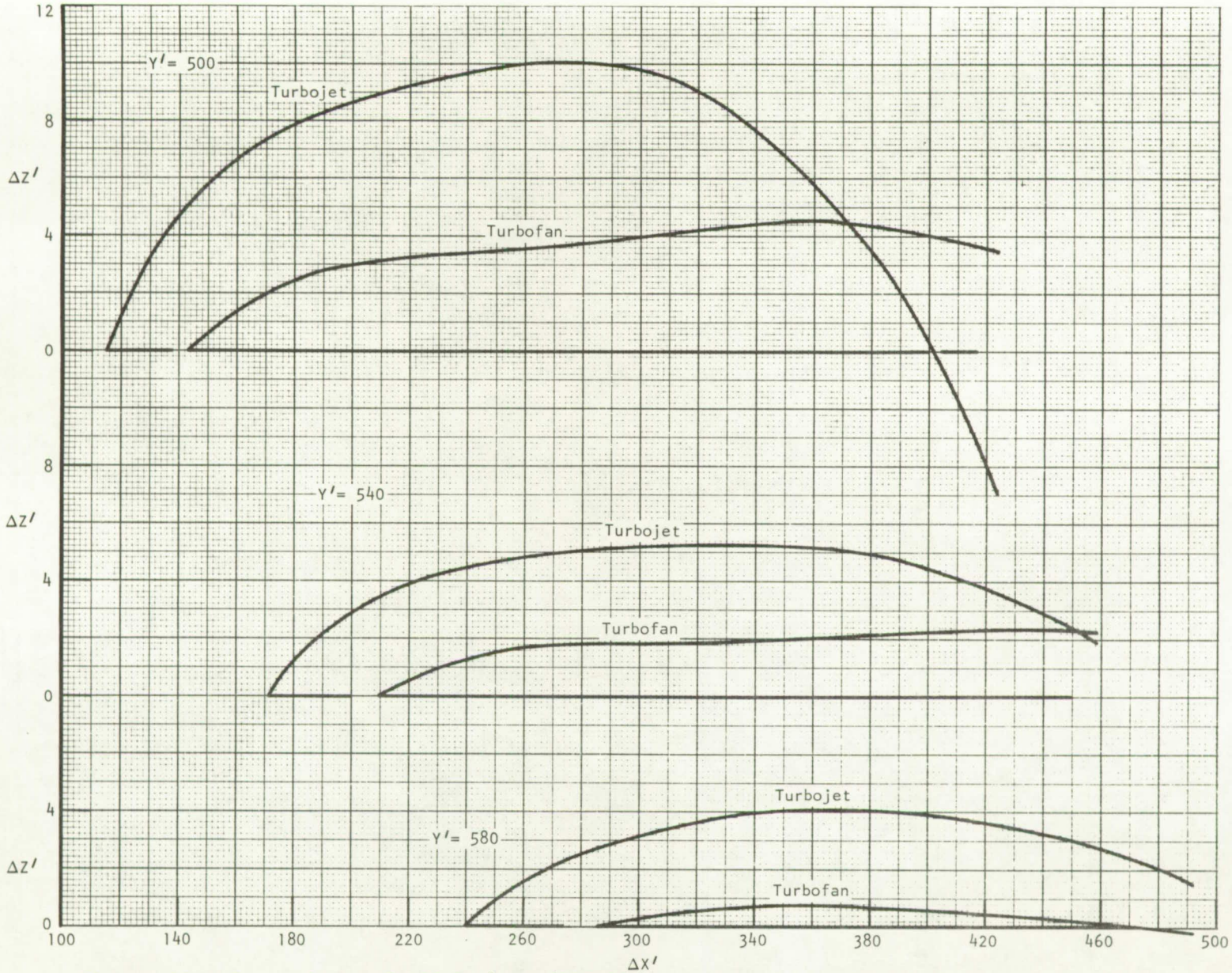

Figure 42.- Comparison of 408 kg/sec (900 lb/sec) turbojet and turbofan wing distortions required to cancel nacelle-induced pressures, outboard of outboard nacelle.

spanwise constant pressure panel is concentrated in regions of large disturbance and rapid attenuation. The linearized deformation calculation results for the basepoint propulsion systems are presented in figures 39 through 42. Between the nacelles, figures 40 and 41 must be linearly combined to establish the total solution. In this regard, the analysis in this region has not been adjusted for shock wave reflection off the side of the adjacent nacelle. Examination of the results indicates that the extent and maximum magnitude of the required wing camber plane deformation is greatest for the turbojet cycle and reflects the fact that the bow shock was stronger (and hence stood ahead of the turbofan shock), and the overall compressive field disturbances were larger for the installation. The previously cited figures indicate the adjustments in wing camber plane shape are relatively modest (with the possible exception of regions immediately next to the turbojet nacelle midway along its length) and appear to be practical to incorporate into the design*. Alternatively, limitations on the magnitude of the deformation allowable may necessitate the acceptance of nonzero drag due to the lift penalty for the turbojet. For this study, it was assumed that full cancellation of the nacelle thickness induced disturbance field is relizable for lack of information to the contrary.

Detailed engine scaling was carried through for the turbofan and turbojet cycles for the minimum 272 kg/sec (600 lb/sec) and maximum 544 kg/sec (1200 lb/sec) airflow range of this study to ascertain whether the 408 kg/sec (900 lb/sec) induced flow field could be treated as a universal function; i.e., $Cp(\frac{\Delta X}{L}, \frac{\Delta Y}{L}) \neq f(Wa)$. On the basis of the results of table IV, which have been discussed in more detail previously, it is concluded that adjustment of the median-size nacelle detailed layout linear dimensions by square root of the airflow ratio is reasonable, and consequently the 408 kg/sec (900 lb/sec) interference flow field of figures 36 and 37 will be utilized in normalized form for the 272 and 544 kg/sec (600 and 1200 lb/sec) camber plane deformation analysis. The intermediate airflows are obtained by interpolation of these results.

Typical scaled influence regions of various-size nacelles having coincident apexes are shown in figure 43. Linearized supersonic wing theory was used to calculate the wing deformation ΔZ required to cancel the nacelle-induced pressures within region ABC for the 408 kg/sec (900 lb/sec) size nacelle. Scaling ΔX, ΔY, and ΔZ as square root of the airflow gives the corresponding wing deformations within region DEF for the 272 kg/sec (600 lb/sec) nacelle and within region GHI for the 544 kg/sec (1200 lb/sec) nacelle. This scaling is possible because shock wave reflection effects were neglected between the nacelles, the physical location of the inboard and outboard nacelles apex was assumed to be invariant with airflow, and the rule of forbidden signals applies to the linear theory at supersonic speeds. Although this scaling is clear for

*The incremental corrections are to be applied to the optimum wing fuselage design and not the reference configuration, which has already been adjusted for the effect of the presence of 278 kg/sec (633 lb/sec) axisymmetric nacelles.

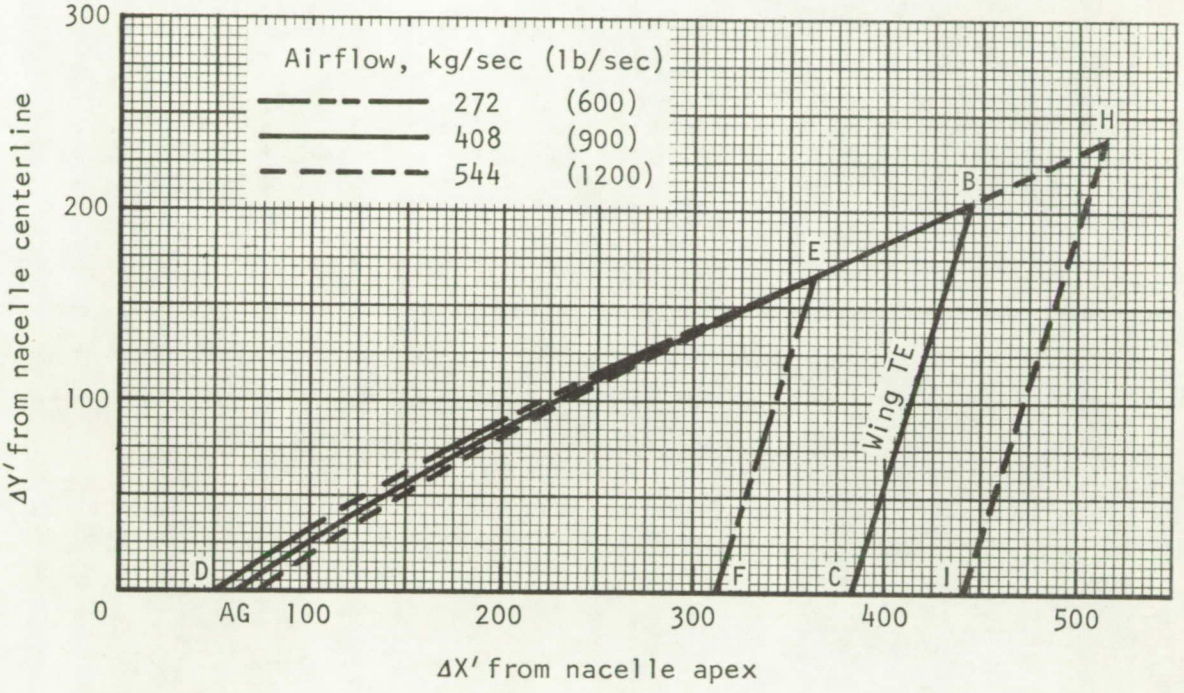

Figure 43.- Influence regions of various size nacelles having coincident apexes.

ΔX and ΔY, a brief discussion is required to show that it also applies to ΔZ as well. Consider that ΔX, ΔY, and ΔZ are normalized by some nacelle linear dimension. The linearized supersonic wing theory used here to calculate $(d\bar{Z}/d\bar{X})$ gives a universal variation with $\Delta\bar{X}$ and $\Delta\bar{Y}$. Consider the integrals used to evaluate $\Delta\bar{Z}$ at $\Delta\bar{Y}$ and $\Delta\bar{X}$, and ΔZ at ΔY and ΔX:

$$\Delta\bar{Z} = \int_{\bar{X}_o}^{\bar{X}} \left(\frac{d\bar{Z}}{d\bar{X}}\right) d\bar{X}$$

$$\Delta Z = \int_{X_o}^{X} \left(\frac{dZ}{dX}\right) dX$$

Since $(d\bar{Z}/d\bar{X}) = (dZ/dX)$ at corresponding points, it follows that ΔX, ΔY, and ΔZ all scale similarly with nacelle size as proportional to square root of the airflow.

One further consideration arises, since the distance from the nacelle apex to the wing trailing edge does not scale as square root of the airflow. Consider, initially, that this distance from the nacelle apex to the wing trailing edge remains fixed as the nacelle size is varied and regard the wing trailing edge to be along BC in figure 43. For the 544 kg/sec (1200 lb/sec) nacelle, required wing deformations are given within region GBC by the square root of the airflow scaling procedure. For the 272 kg/sec (600 lb/sec) nacelle, required wing deformations within region EBCF can be obtained by extrapolation or by further longitudinal calculation of the nacelle flow field and of the canceling wing slopes and deformations. Results from the performance sizing task in the present study (table XXV) indicate that the wing size decreases with decreasing engine size. For the 272 kg/sec (600 lb/sec) nacelle, it was considered appropriate to present wing deformations scaled as square root of the airflow within the region of definition DEF of figure 43 and to extrapolate, if necessary, to reach the trailing edge.

Influence regions are sketched in figure 44 for the 272 kg/sec (600 lb/sec) turbojet nacelle. Wing distortions required to cancel the nacelle-induced pressures are shown in figure 45, inboard of the inboard nacelle; in figure 46, between the nacelles; and in figures 47 and 48, outboard of the outboard nacelle. These spanwise sections can be located in figure 44. Similar data are shown in figures 47 through 68 for other size nacelles and for the turbofan engine cycle. Table XXVI presents an index to these wing distortion data. All of these results are presented for the study basepoint wing area of 995 sq m (10 713 sq ft) and nacelle apex locations. They

apply equally well to the resized configurations if the wing trailing edge is located relative to the nacelle apex in accordance with figure 31, and the absolute lateral locations of the calculation are reinterpreted to account for inboard movement of the nacelle in accordance with table XVIII.

TABLE XXVI.- INDEX TO WING DISTORTION DATA

Fig. No.	Airflow kg/sec (lb/sec)	Nacelle	Sketch	Distortions		
				Inbd	Between	Outbd
43	272 (600)	TJ	X			
44				X		
45					X	
46, 47						X
48	408 (900)	TJ	X			
49				X		
50					X	
51						X
52	544 (1200)	TJ	X			
53				X		
54					X	
55						X
56	272 (600)	DHTF	X			
57				X		
58					X	
59						X
60	408 (900)	DHTF	X			
61				X		
62					X	
63						X
64	544 (1200)	DHTF	X			
65				X		
66					X	
67						X

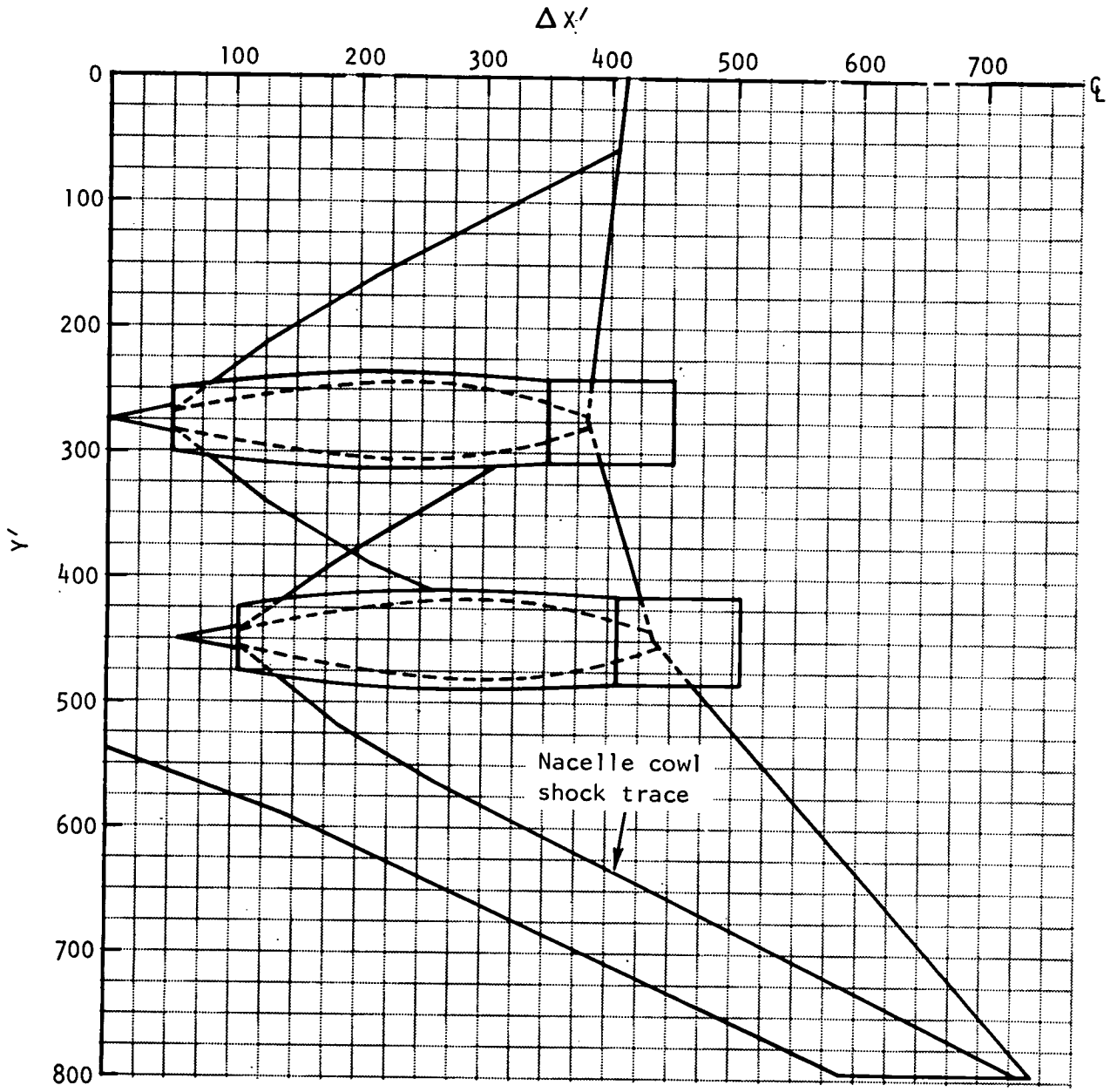

Figure 44.- Influence region for 272 kg/sec (600 lb/sec) turbojet nacelles.

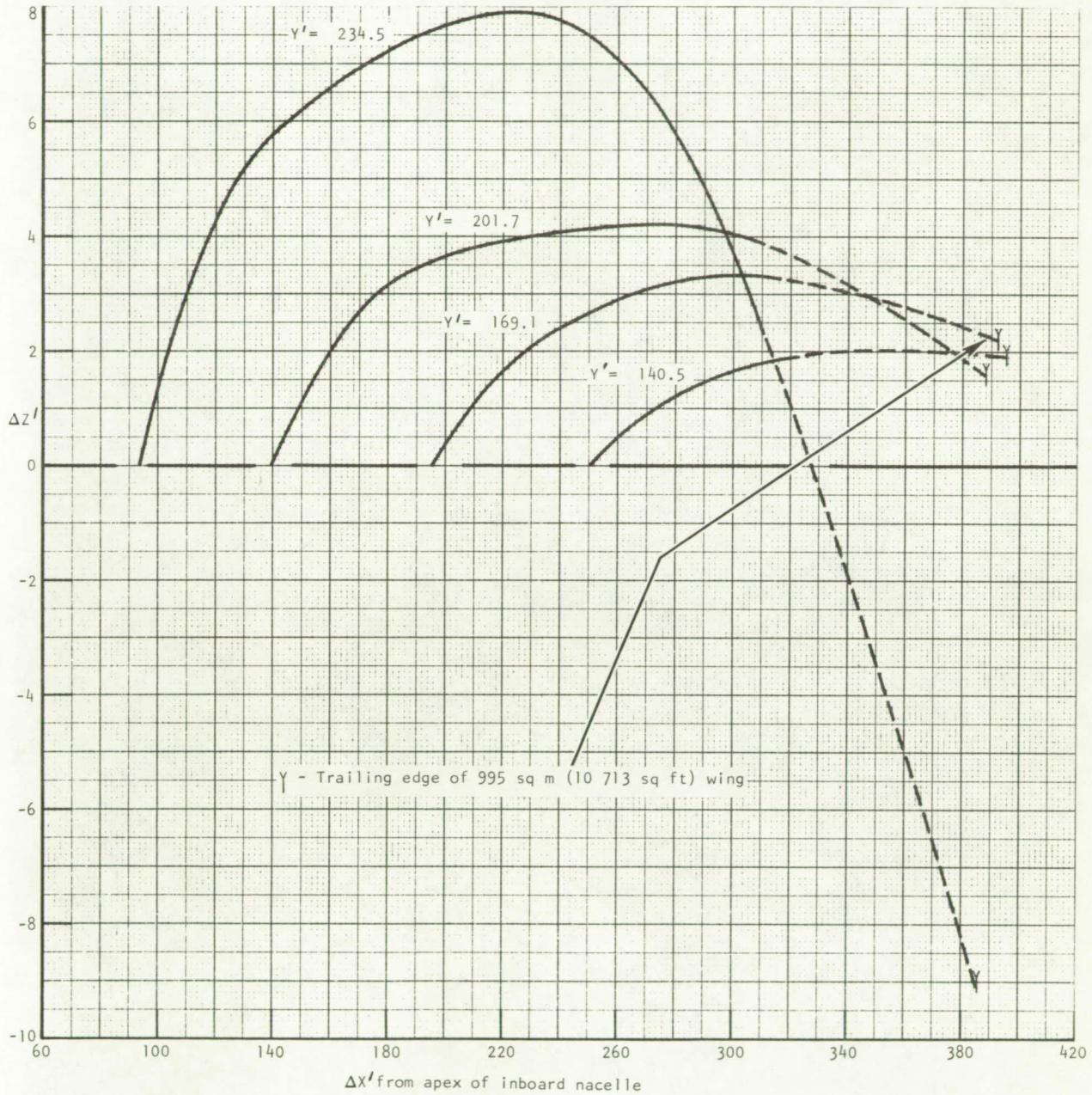

Figure 45.- Wing distortion required to cancel 272 kg/sec (600 lb/sec) turbojet nacelle-induced pressures, inboard of inboard nacelle.

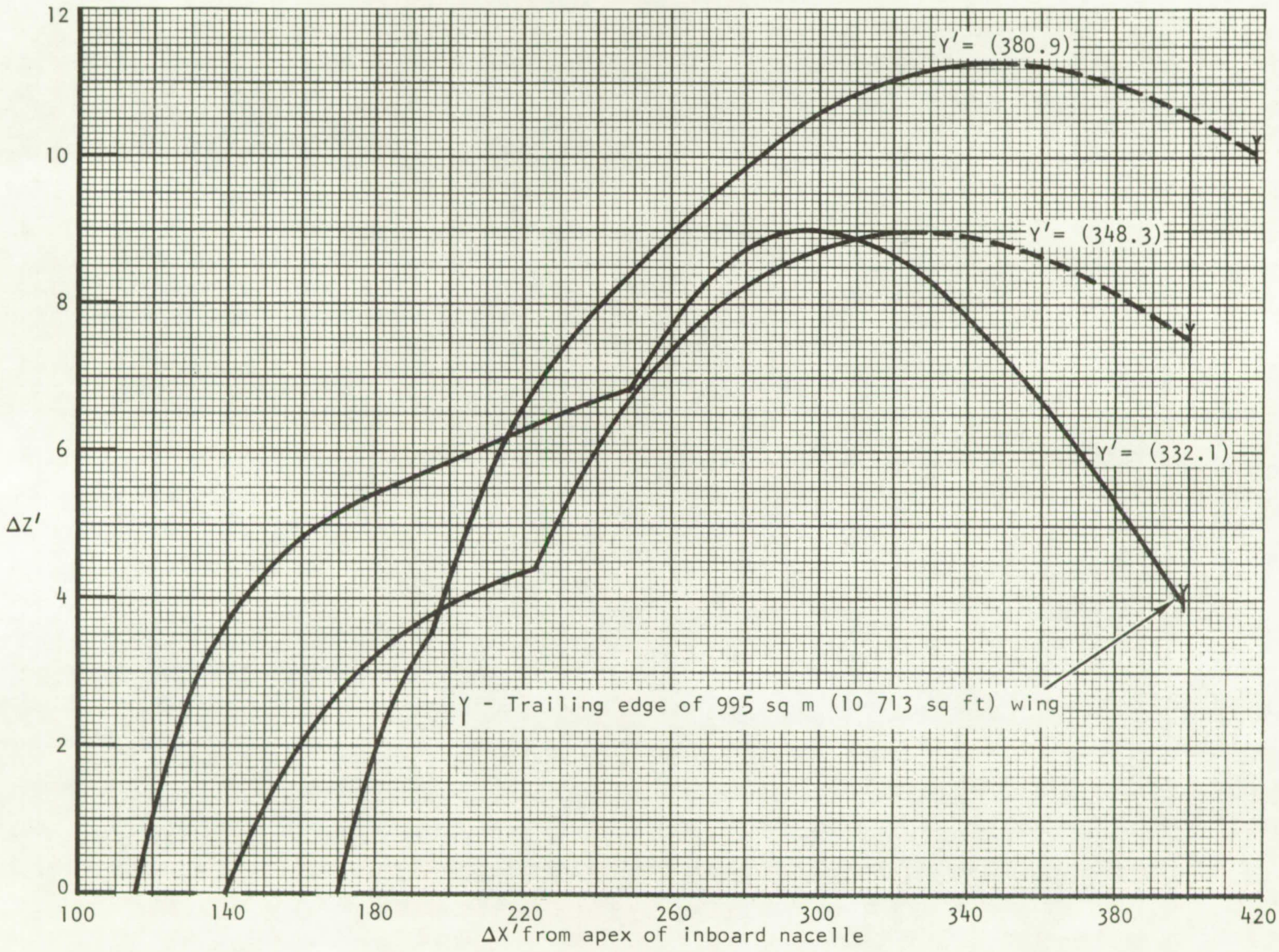

Figure 46.- Wing distortion required to cancel 272 kg/sec (600 lb/sec) turbojet nacelle-induced pressures, between nacelles.

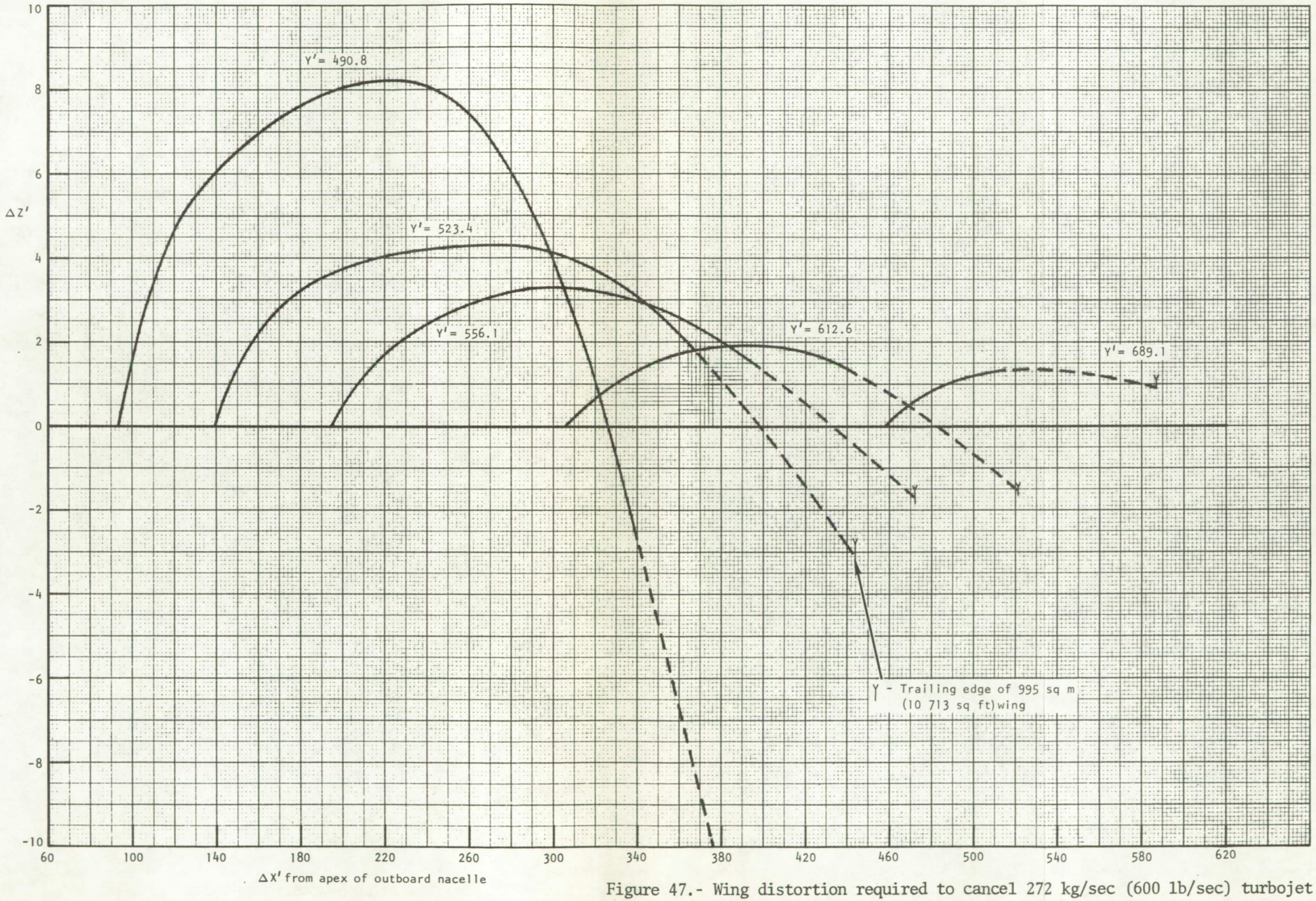

Figure 47.- Wing distortion required to cancel 272 kg/sec (600 lb/sec) turbojet nacelle-induced pressures, outboard of outboard nacelle.

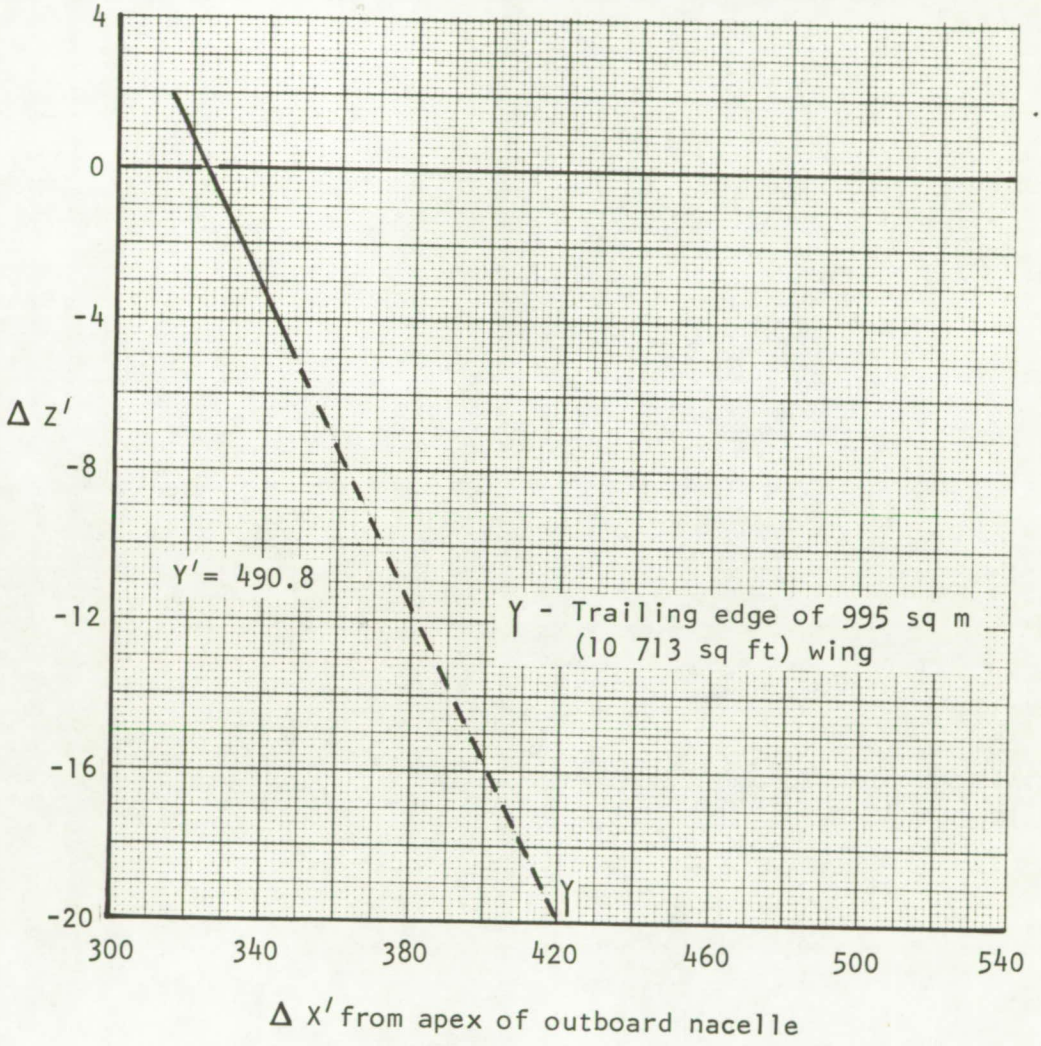

Figure 48.- Wing distortion required to cancel 408 kg/sec (900 lb/sec) turbojet nacelle induced pressures, outboard of outboard nacelle.

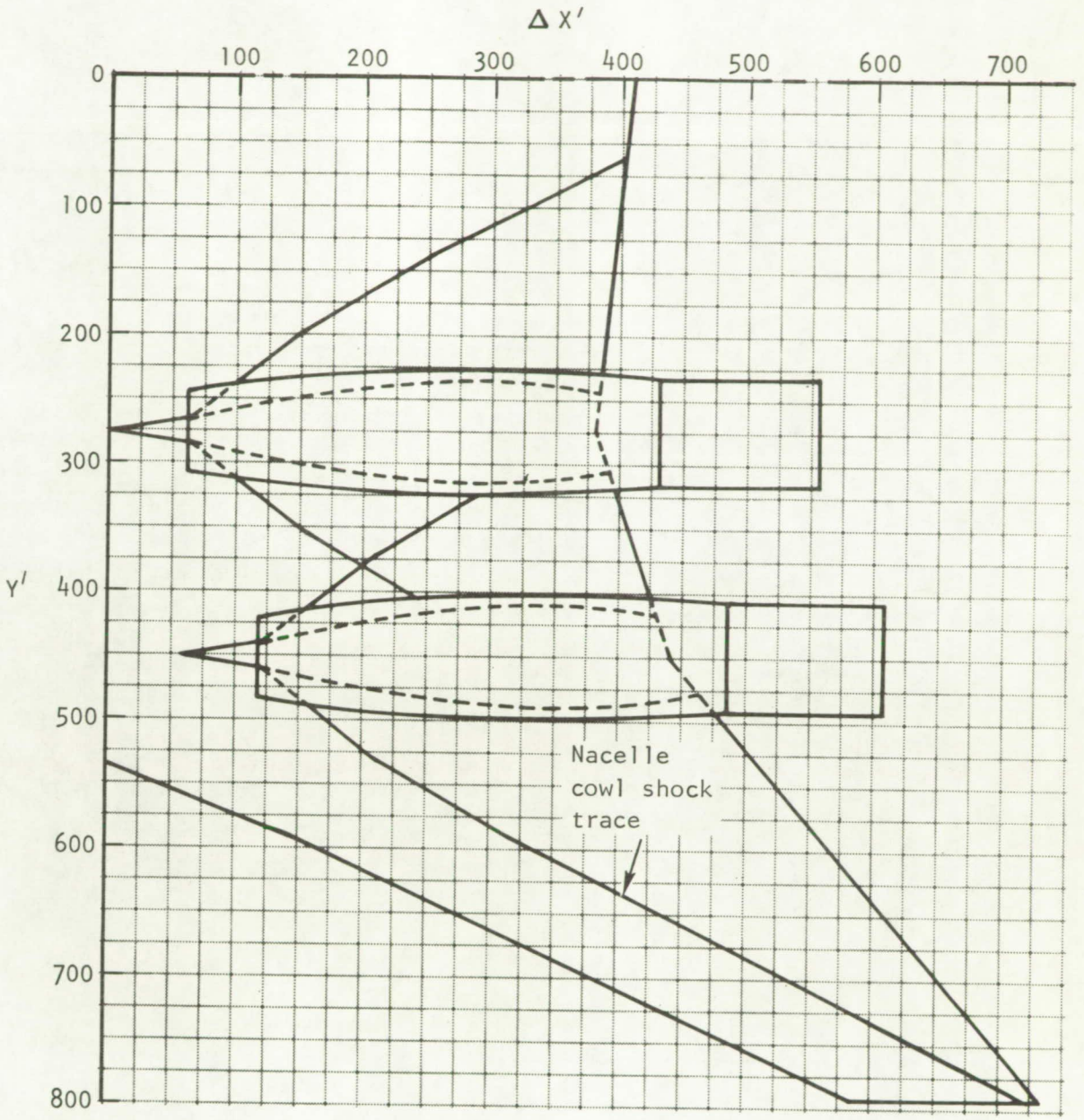

Figure 49.- Influence region for 408 kg/sec (900 lb/sec) turbojet nacelles.

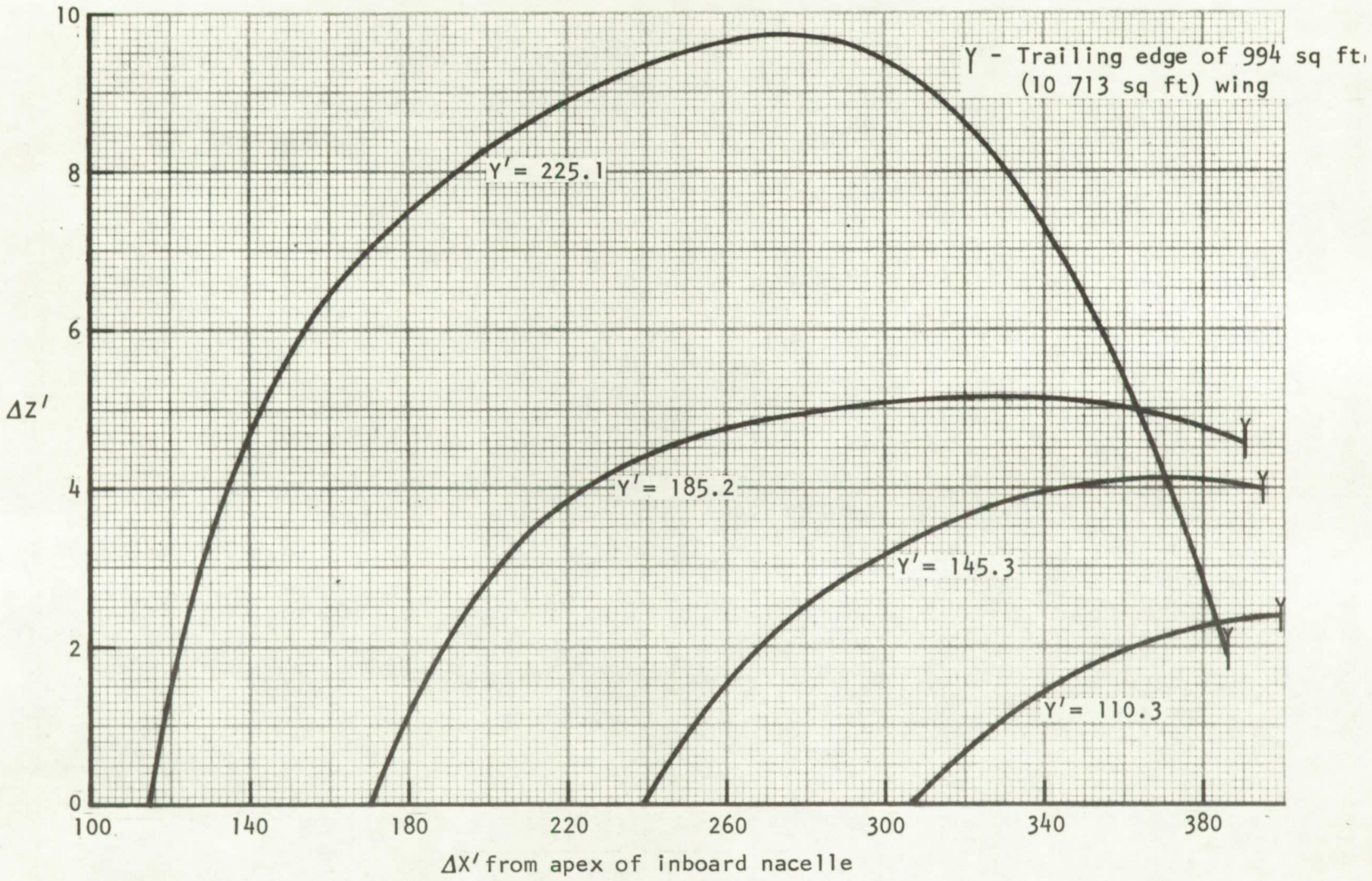

Figure 50.- Wing distortion required to cancel 408 kg/sec (900 lb/sec) turbojet nacelle-induced pressures, inboard of inboard nacelle.

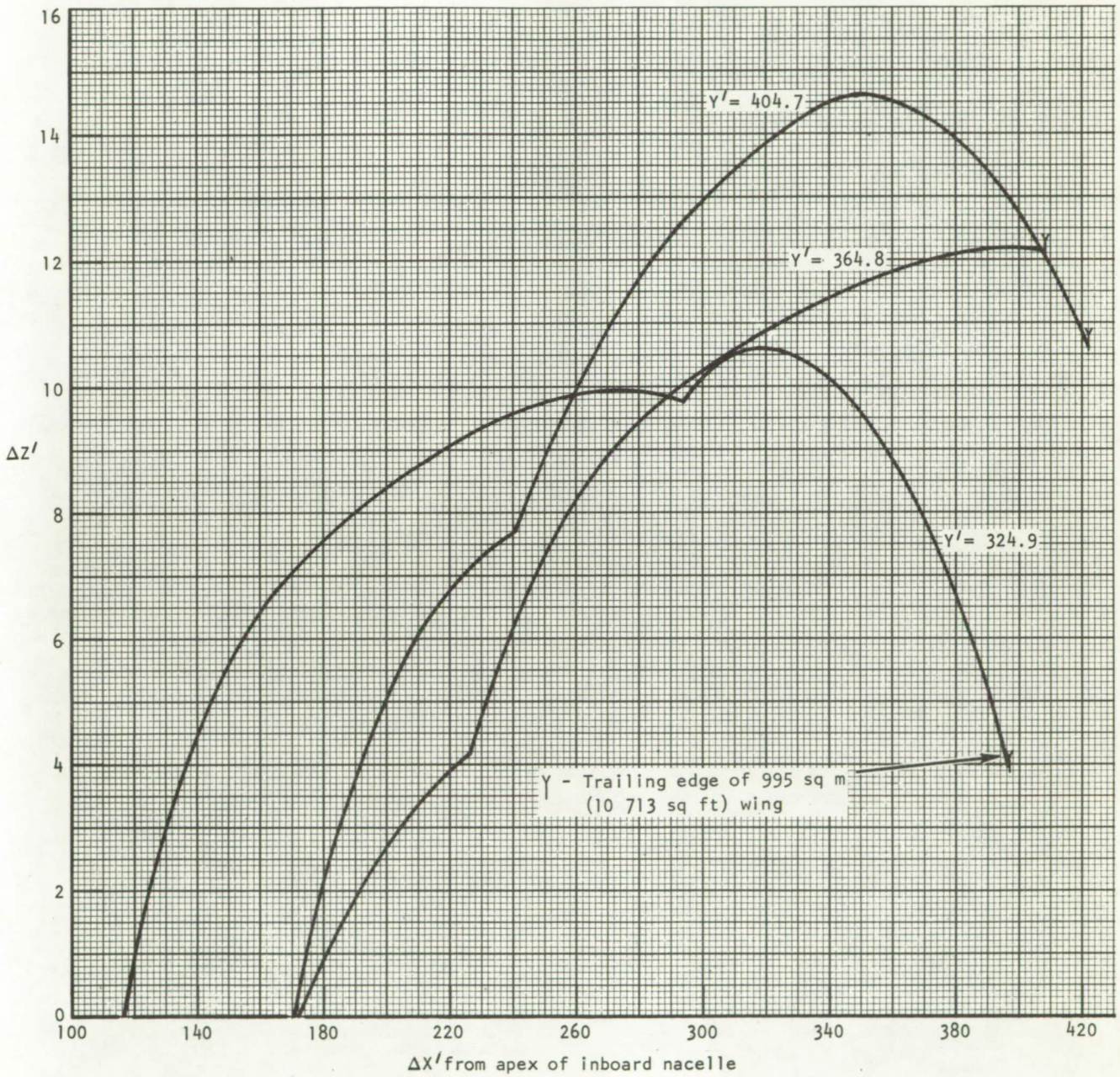

Figure 51.- Wing distortion required to cancel 408 kg/sec (900 lb/sec) turbojet nacelle-induced pressures, between nacelles.

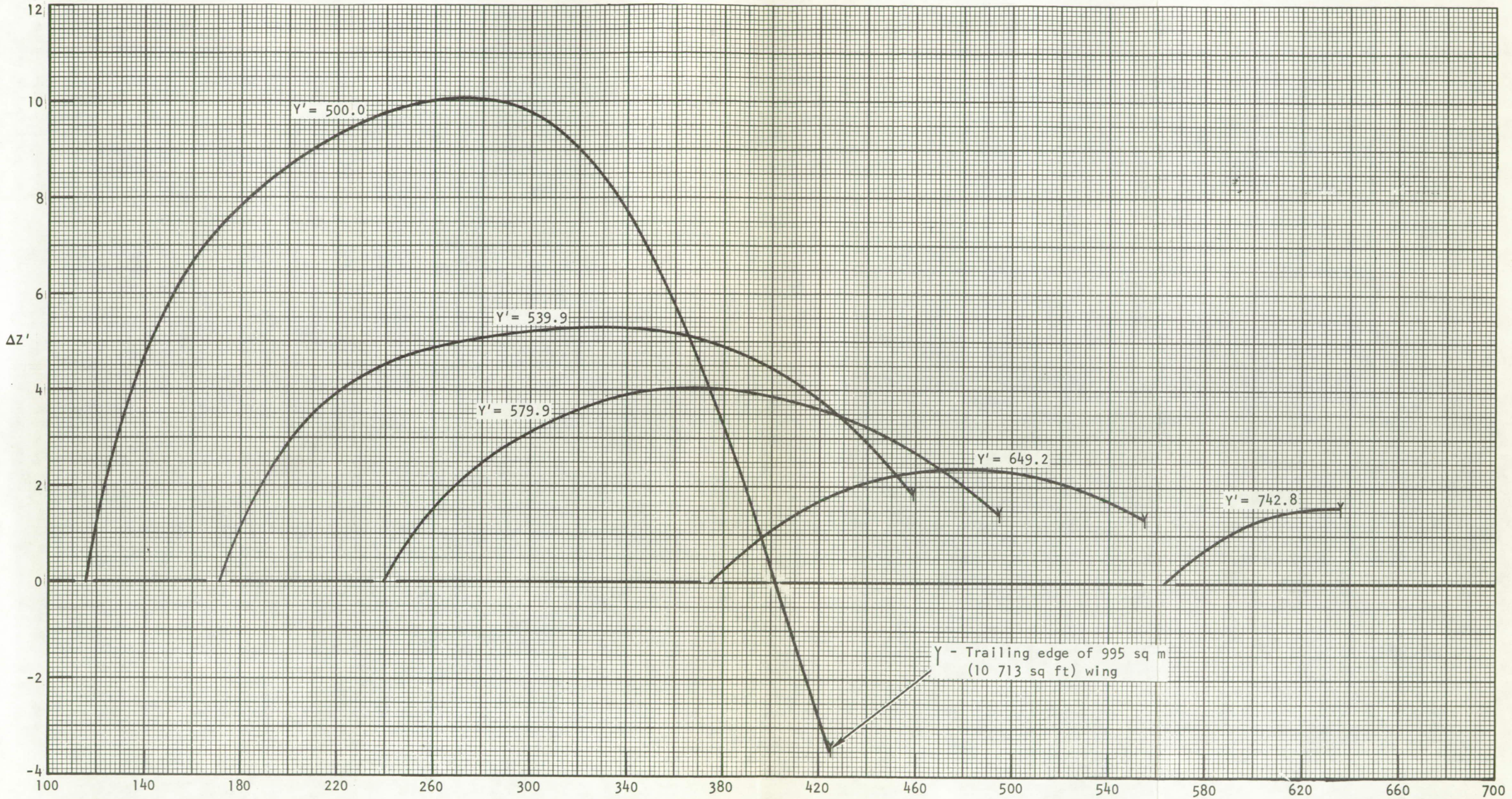

Figure 52.- Wing distortion required to cancel 408 kg/sec (900 lb/sec) turbojet nacelle-induced pressures, outboard of outboard nacelle.

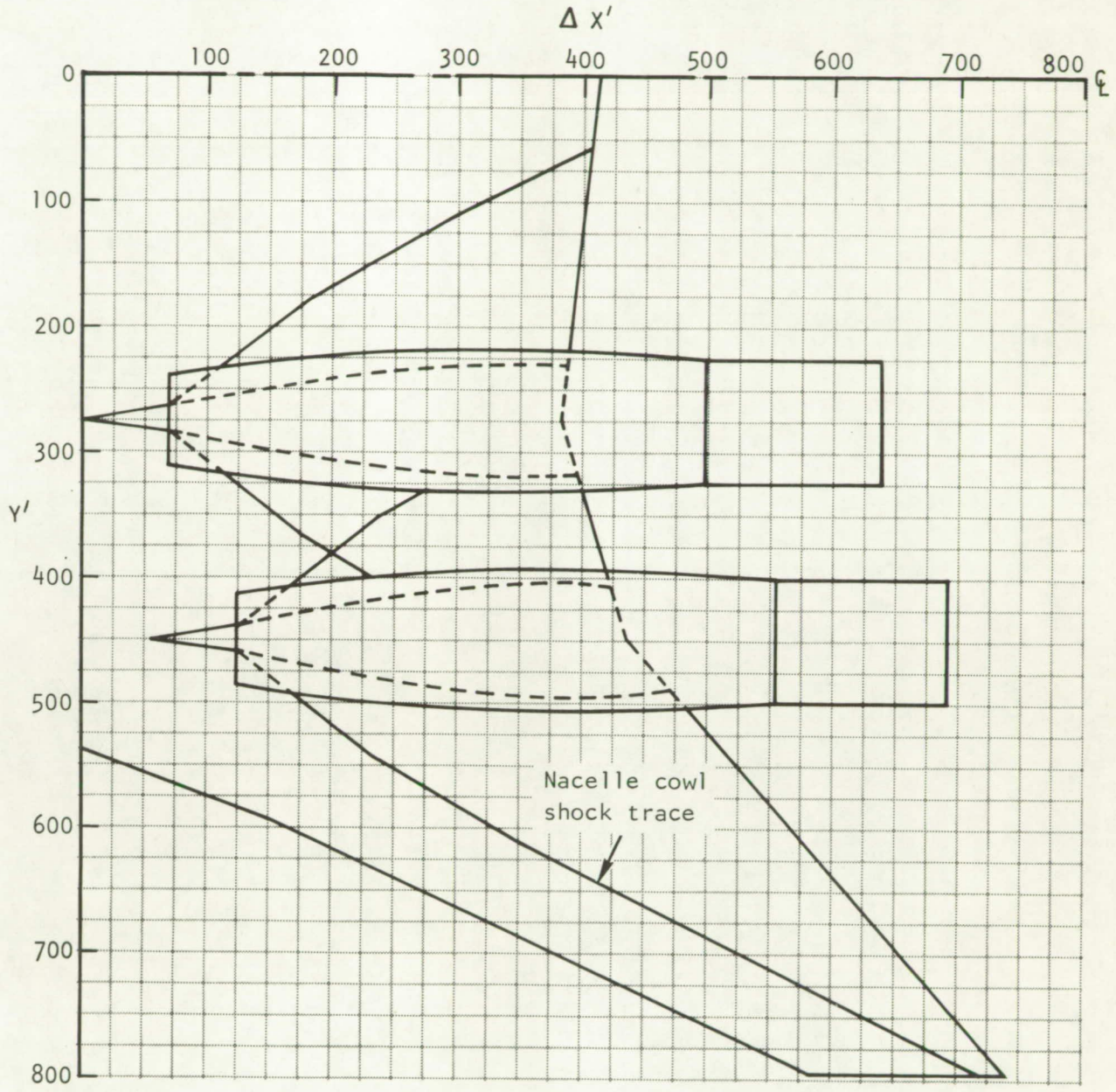

Figure 53.- Influence region for 544 kg/sec (1200 lb/sec) turbojet nacelles.

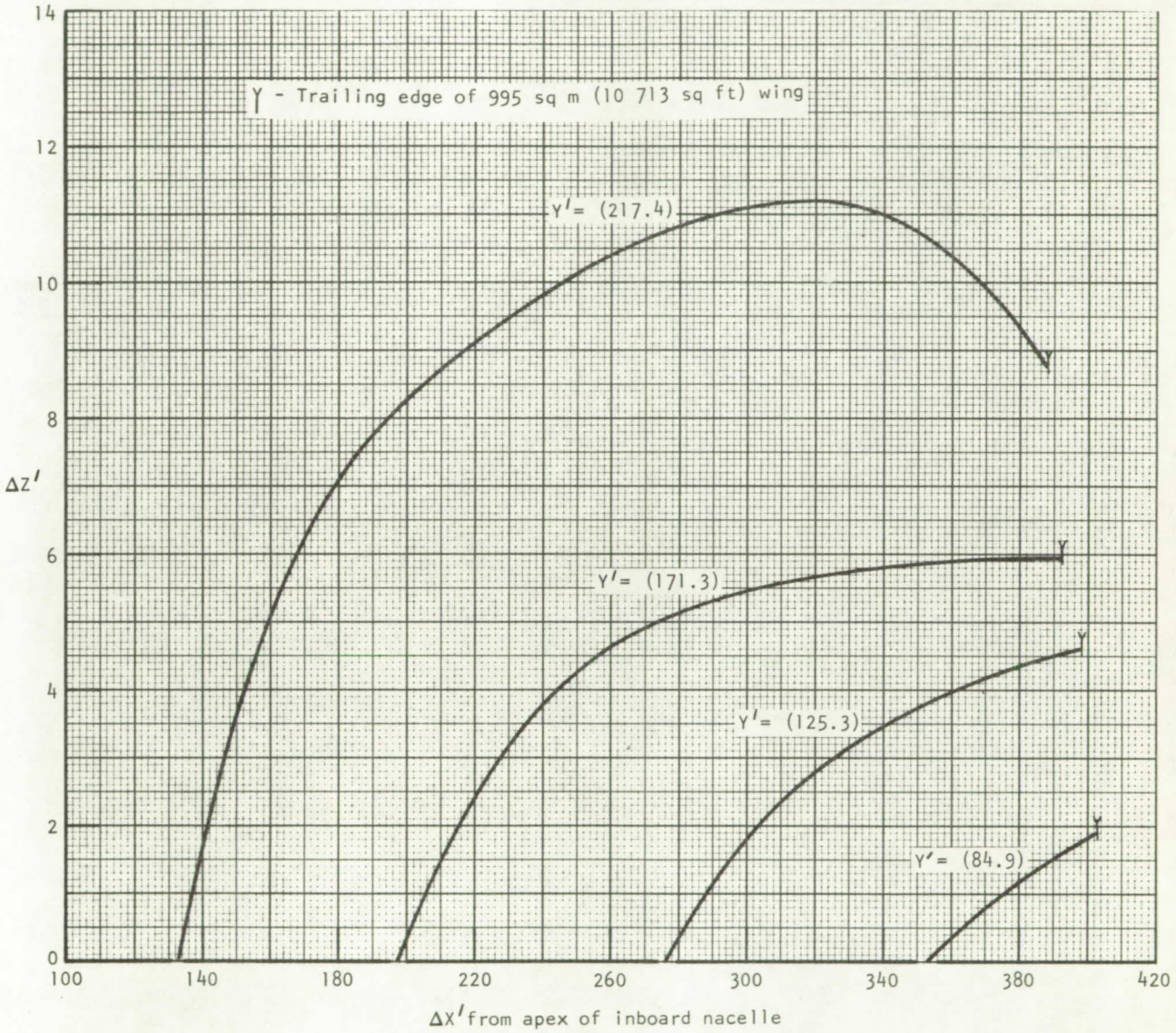

Figure 54.- Wing distortion required to cancel 544 kg/sec (1200 lb/sec) turbojet nacelle-induced pressures, inboard of inboard nacelle.

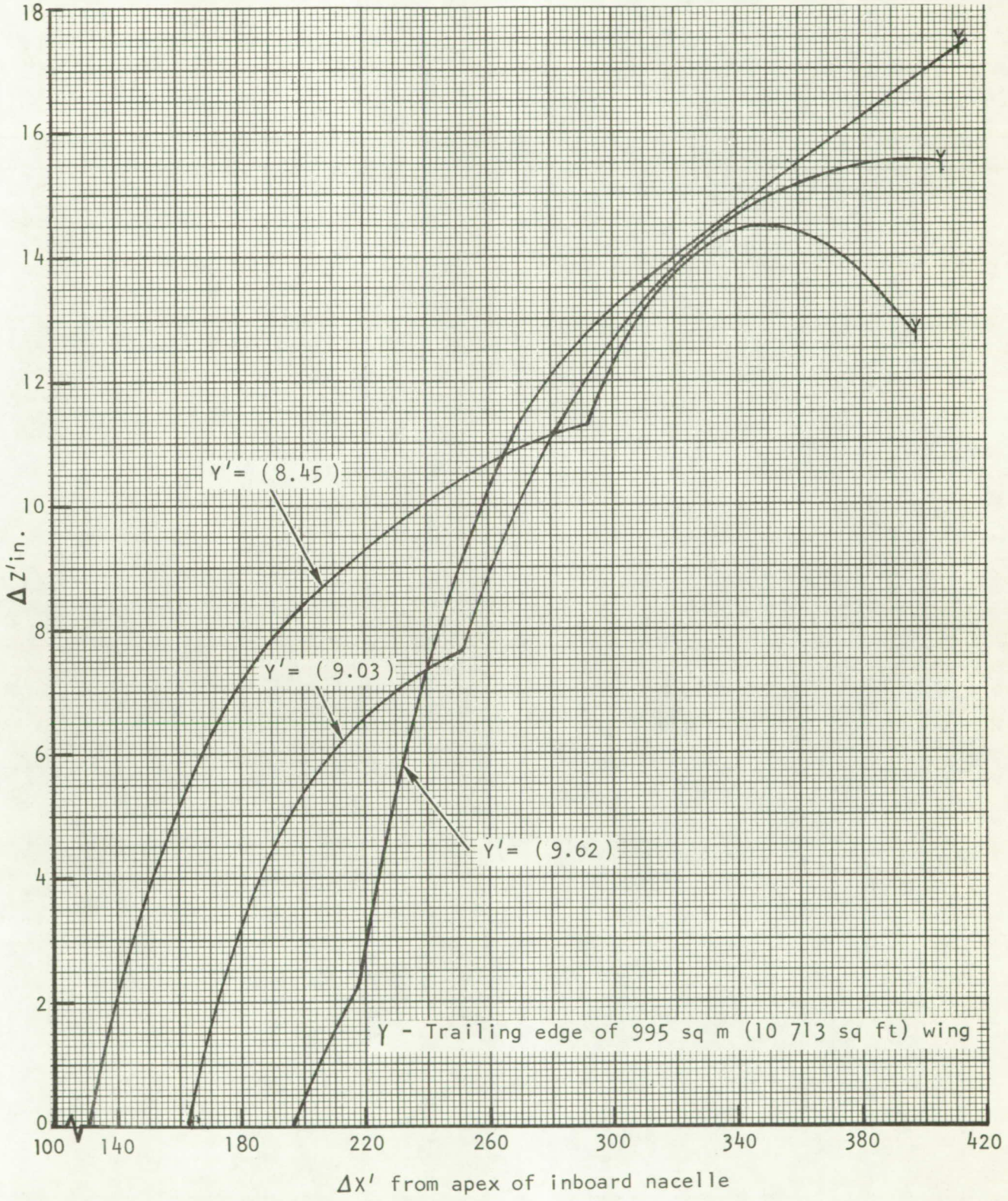

Figure 55.- Wing distortion required to cancel 544 kg/sec (1200 lb/sec) turbojet nacelle-induced pressures, between nacelles.

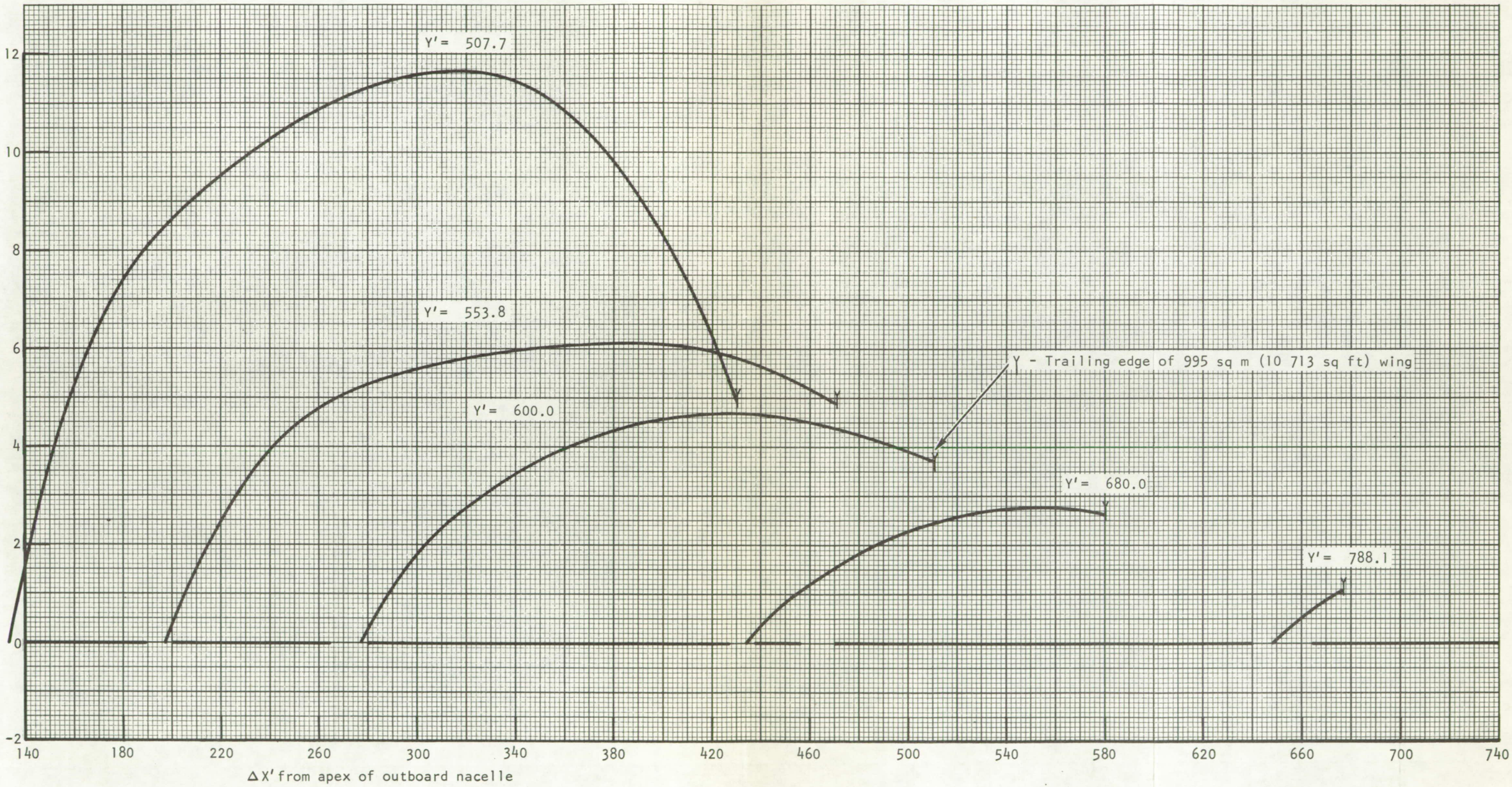

Figure 56.- Wing distortion required to cancel 544 kg/sec (1200 lb/sec) turbojet nacelle-induced pressures, outboard of outboard nacelle.

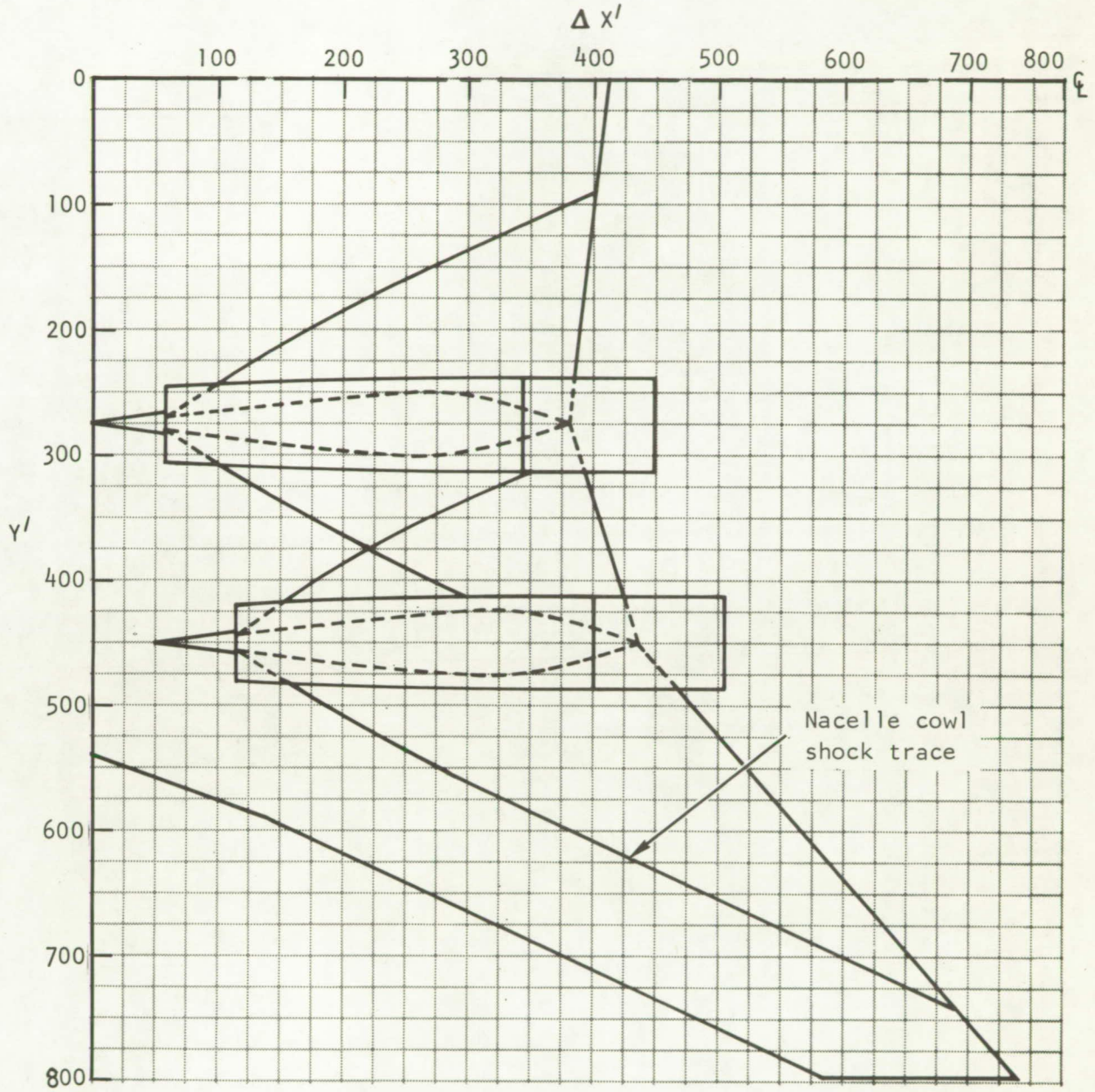

Figure 57.- Influence region for 272 kg/sec (600 lb/sec) turbofan nacelles.

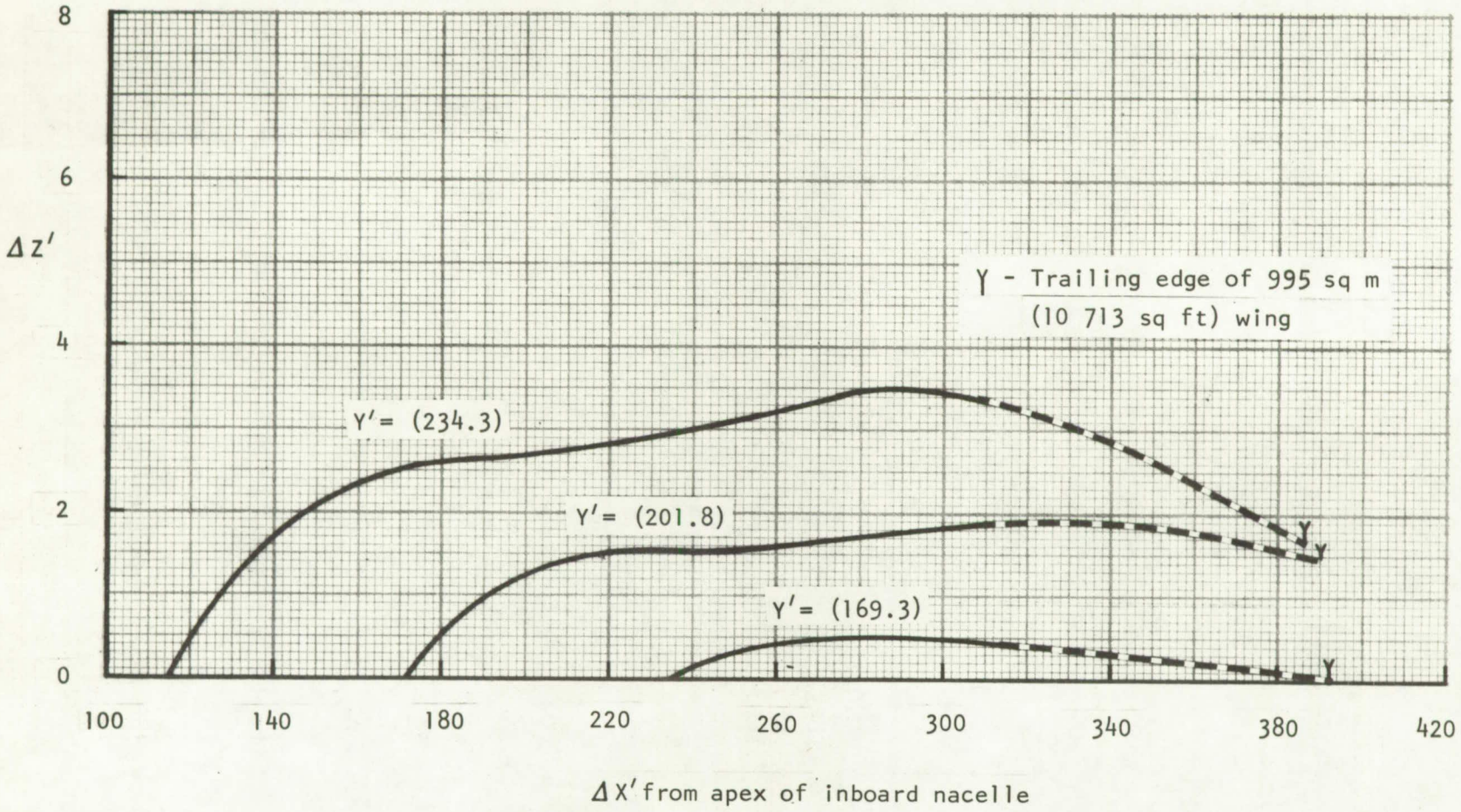

Figure 58.- Wing distortion required to cancel 272 kg/sec (600 lb/sec) turbofan nacelle-induced pressures, inboard of inboard nacelle.

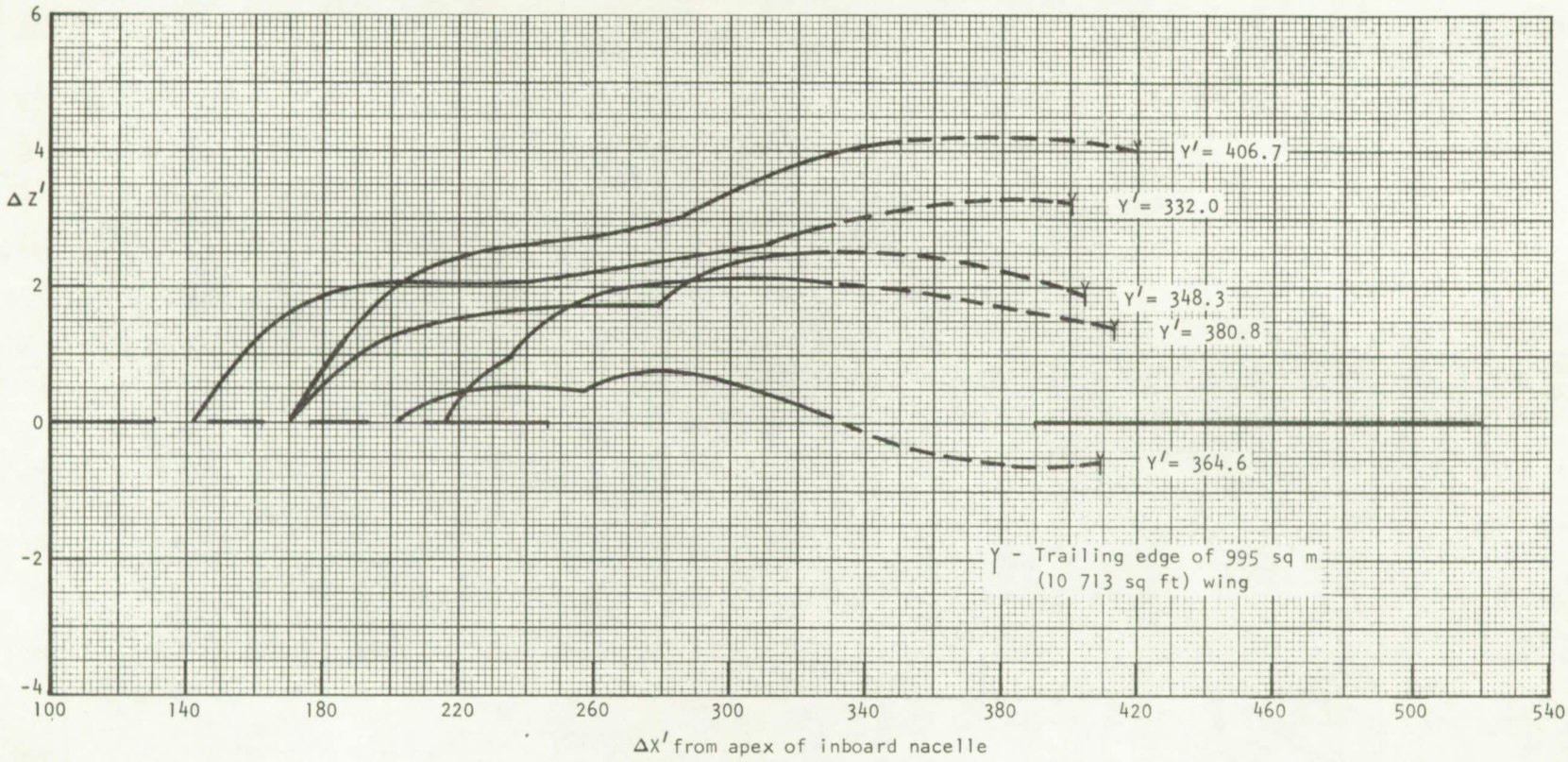

Figure 59.- Wing distortion required to cancel 272 kg/sec (600 lb/sec) turbofan nacelle-induced pressures, between nacelles.

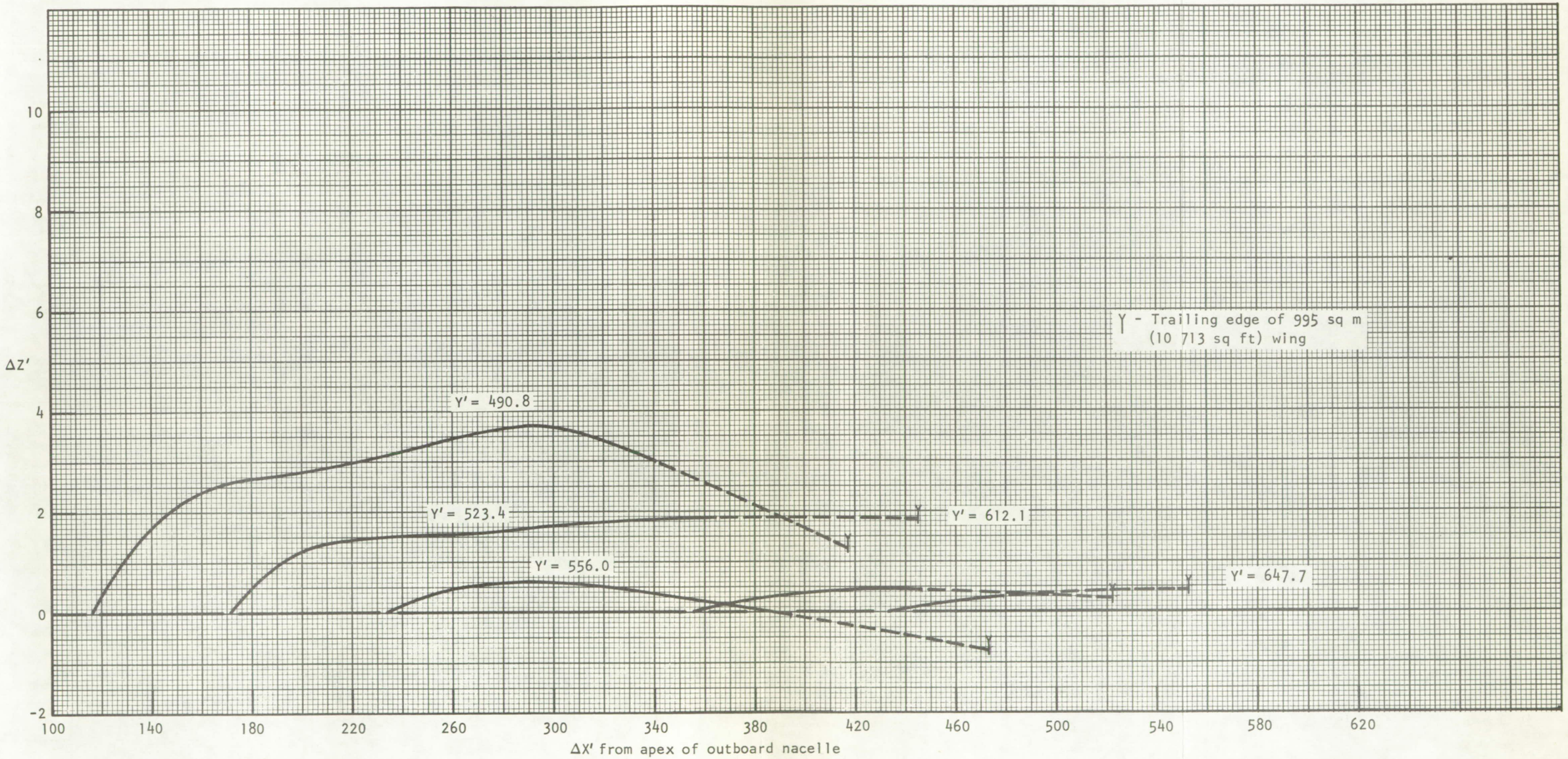

Figure 60.- Wing distortion required to cancel 272 kg/sec (600 lb/sec) turbofan nacelle-induced pressures, outboard of outboard nacelle.

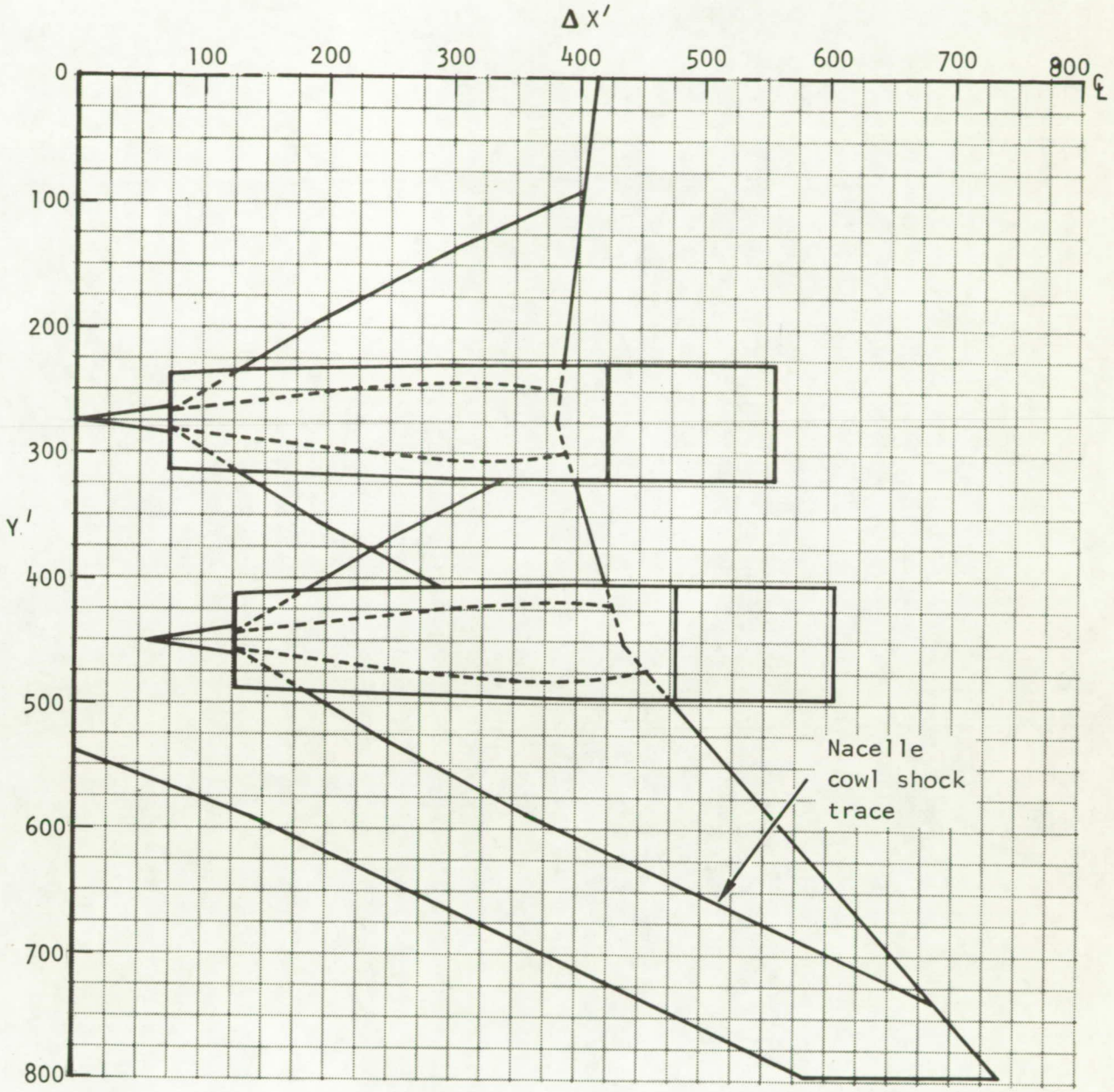

Figure 61.- Influence region for 408 kg/sec (900 lb/sec) turbofan nacelle.

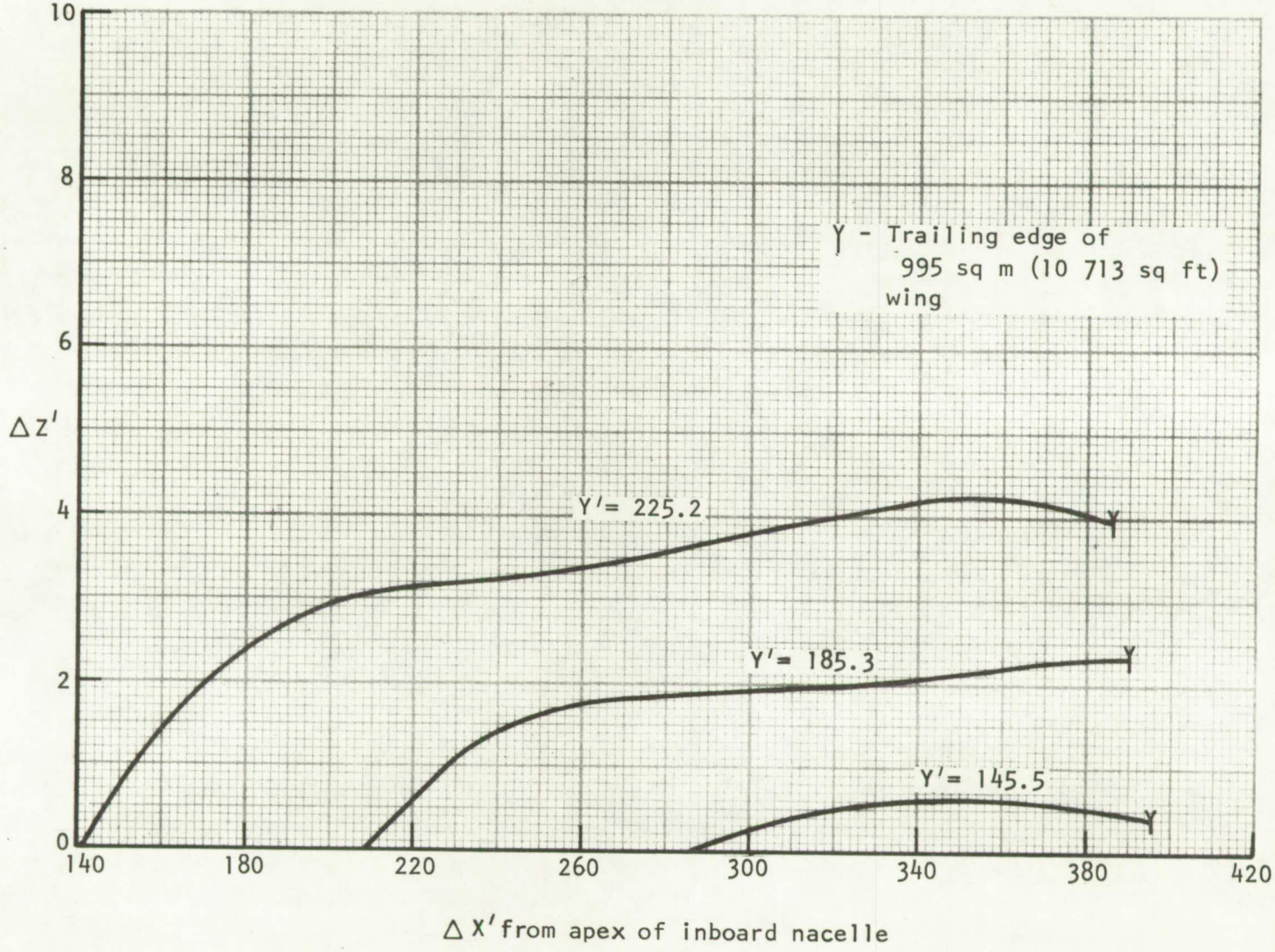

Figure 62.- Wing distortion required to cancel 408 kg/sec (900 lb/sec) turbofan nacelle-induced pressures, inboard of inboard nacelle.

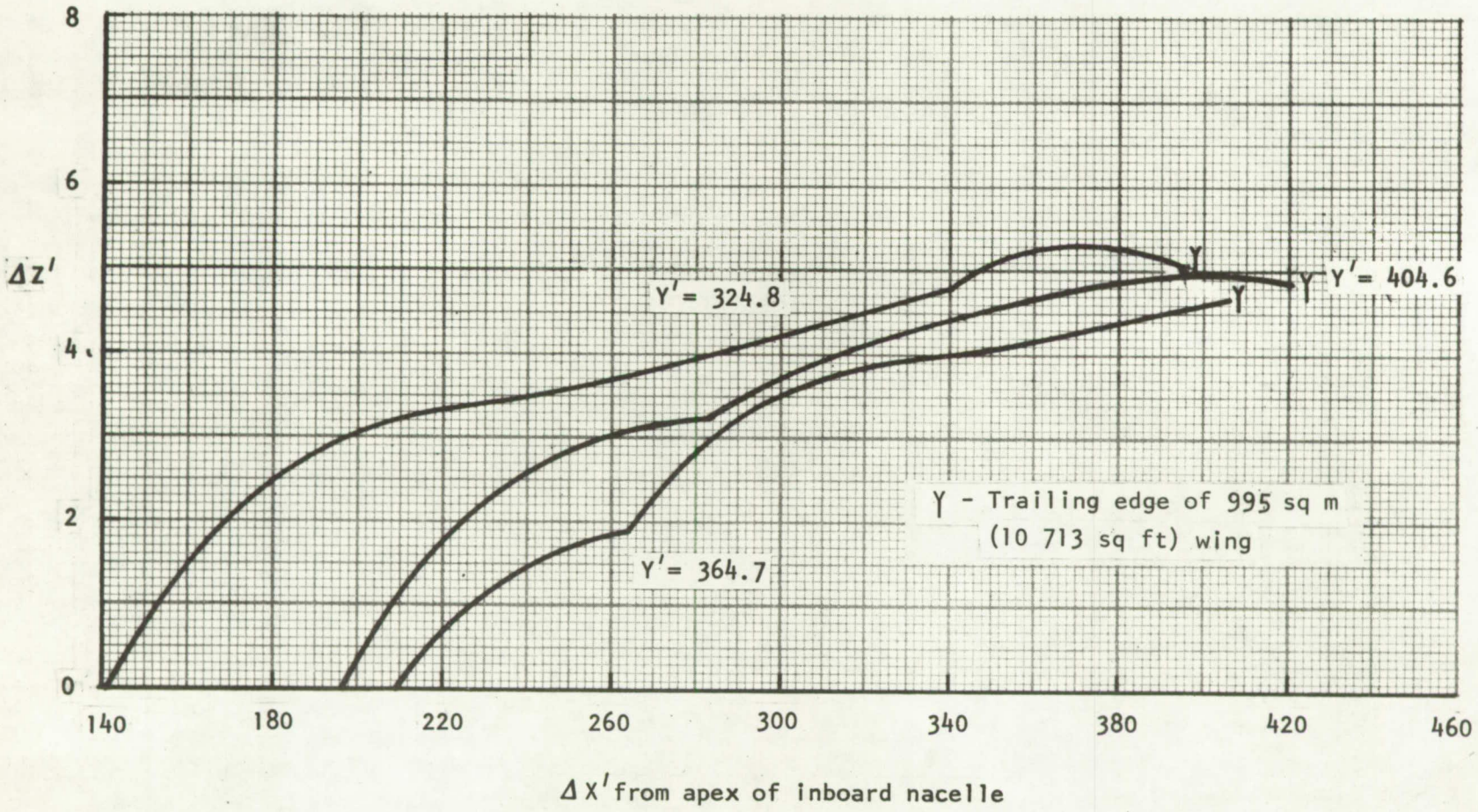

Figure 63.- Wing distortion required to cancel 408 kg/sec (900 lb/sec) turbofan nacelle-induced pressures, between nacelles.

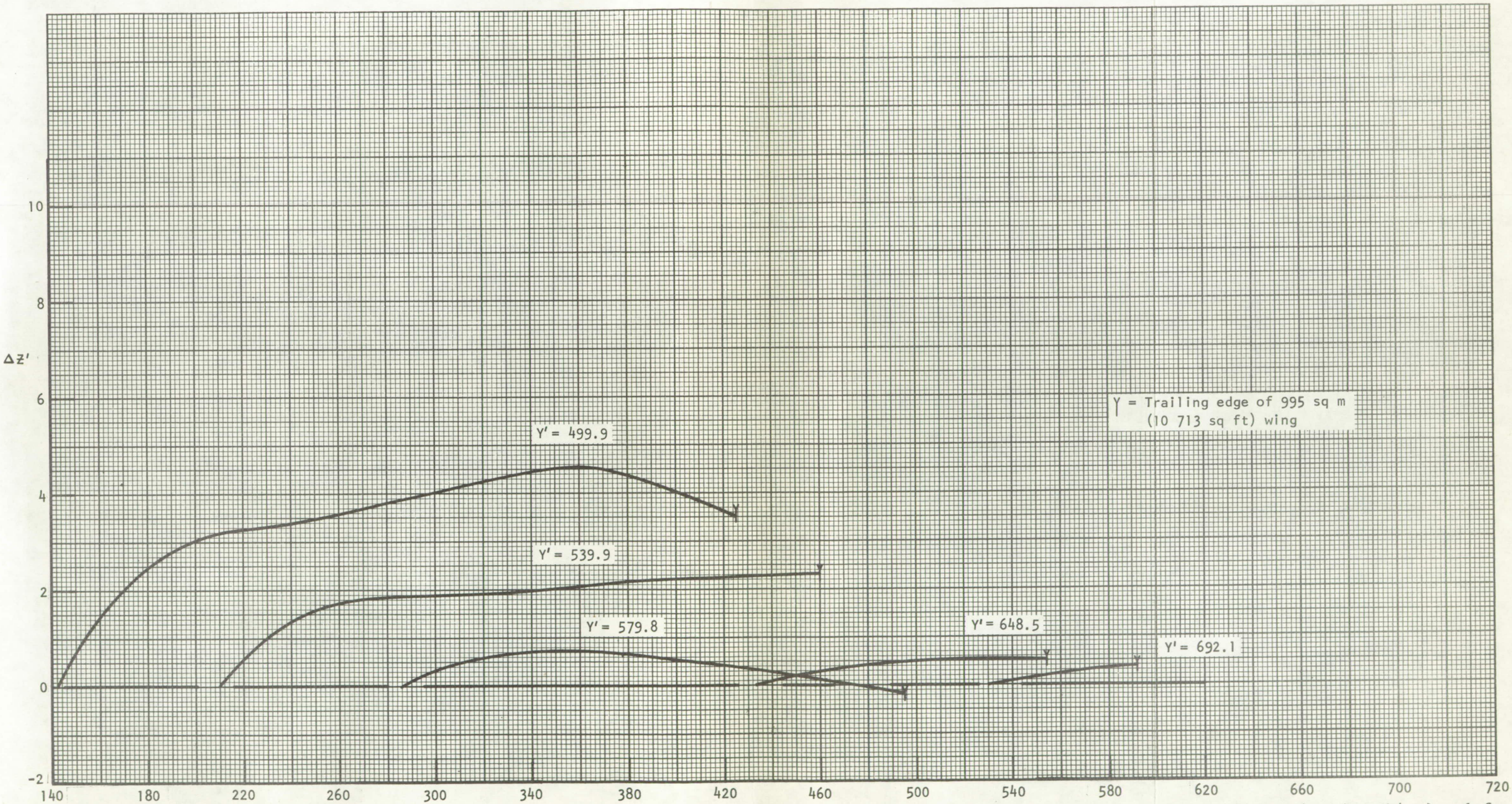

Figure 64.- Wing distortion required to cancel 408 kg/sec (900 lb/sec) turbofan nacelle-induced pressures, outboard of outboard nacelle.

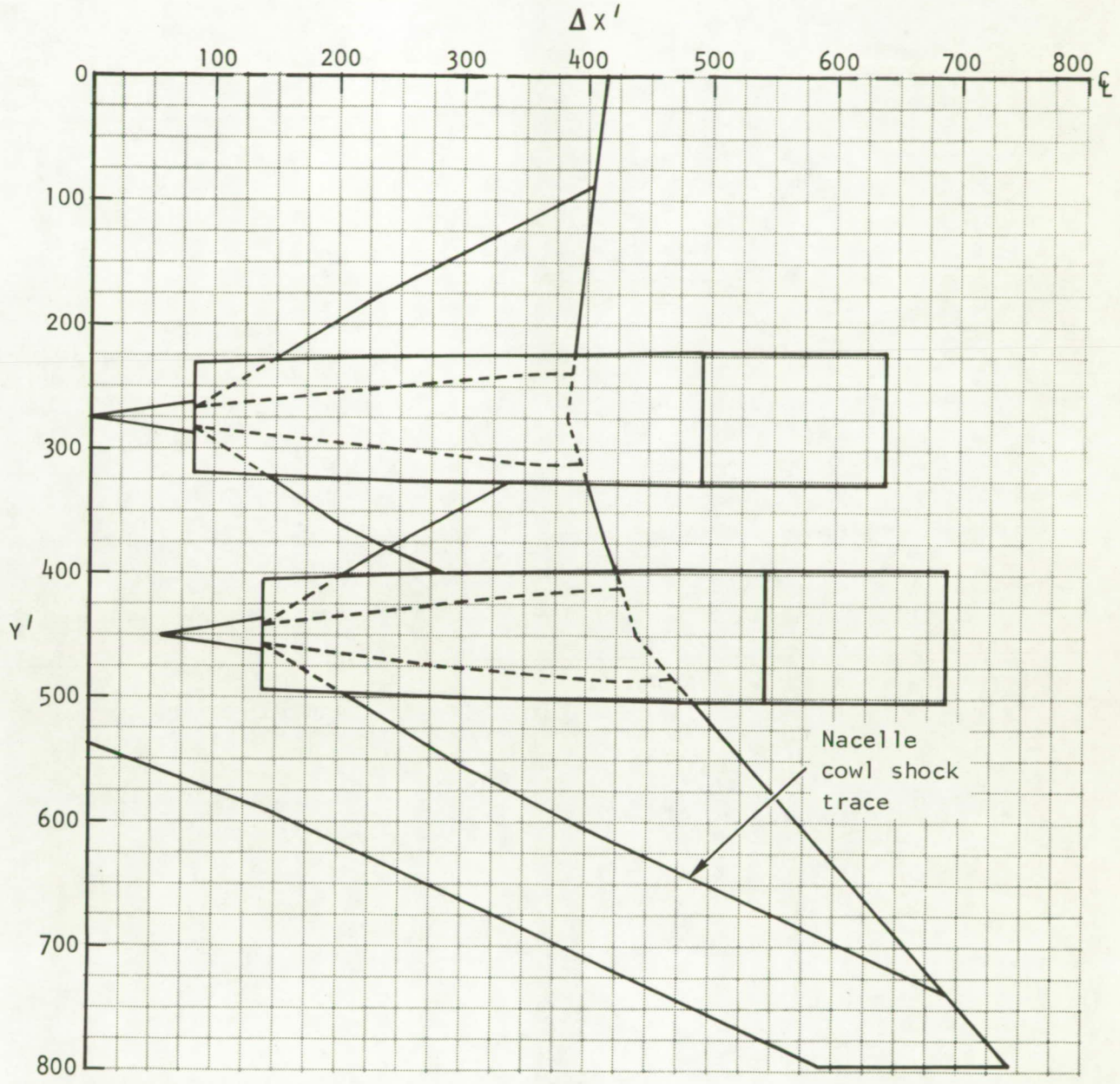

Figure 65.- Influence region for 544 kg/sec (1200 lb/sec) turbofan nacelles.

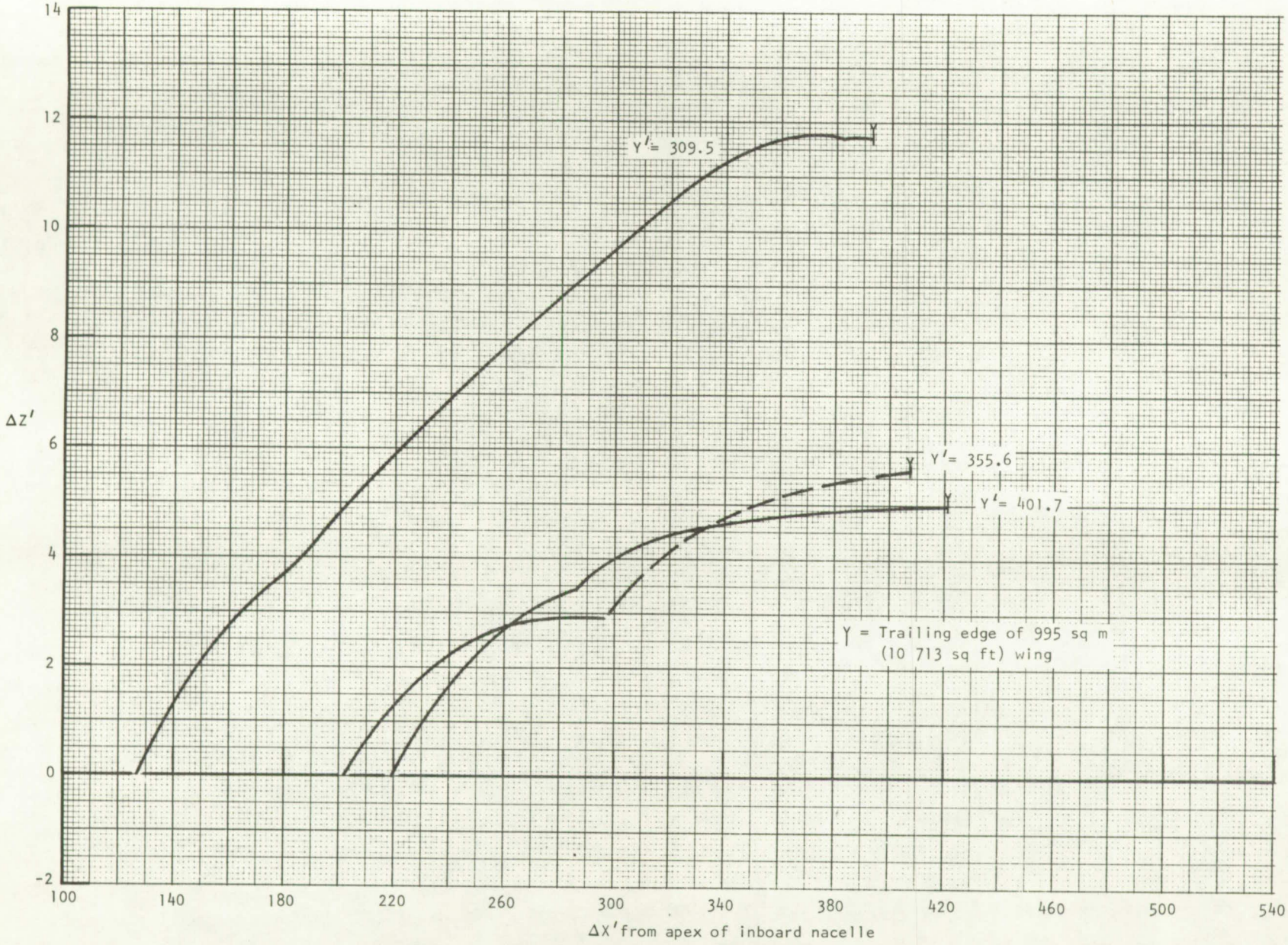

Figure 66.- Wing distortion required to cancel 544 kg/sec (1200 lb/sec) turbofan nacelle-induced pressures, between nacelles.

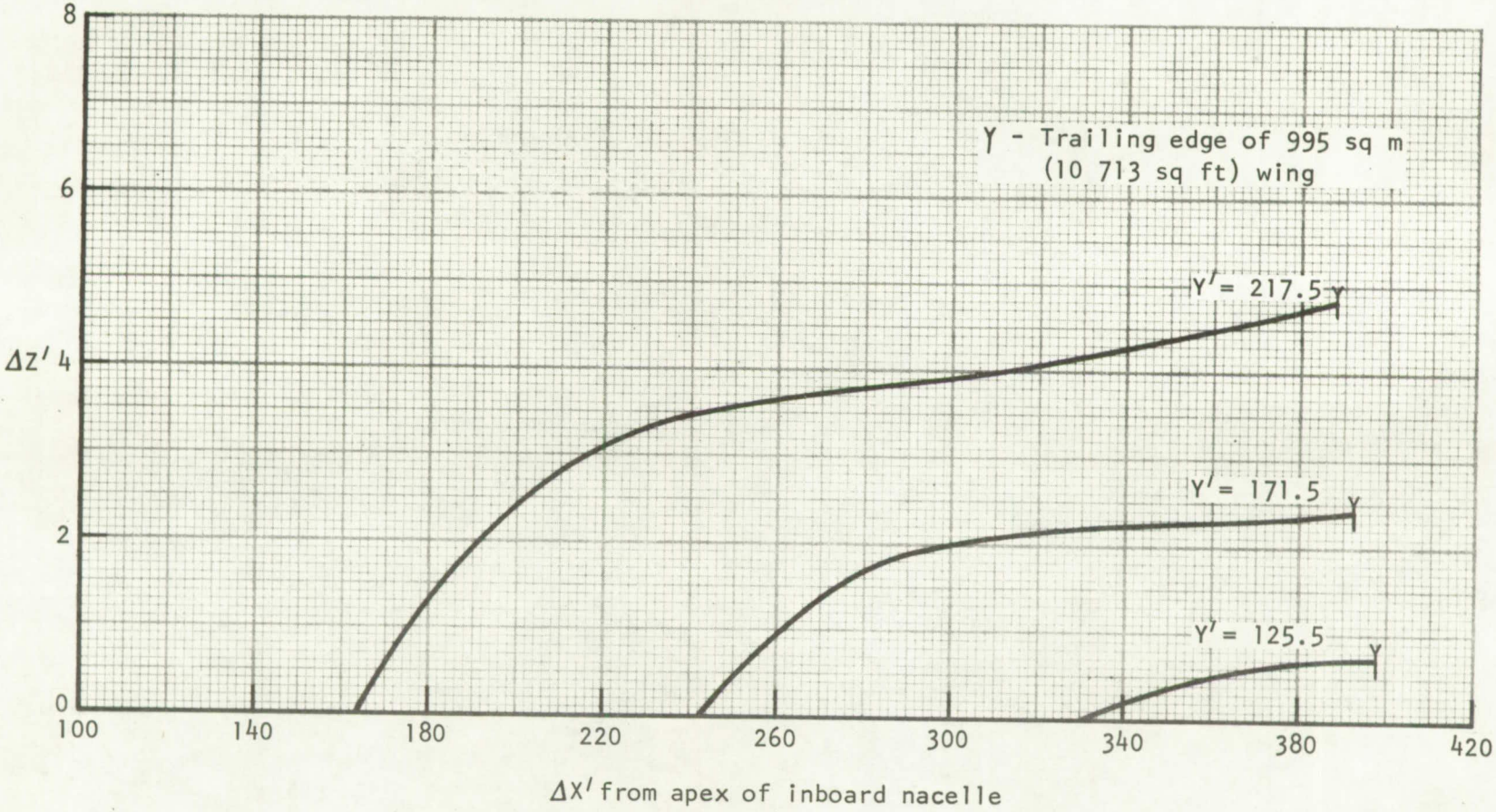

Figure 67.- Wing distortion required to cancel 544 kg/sec (1200 lb/sec) turbofan nacelle-induced pressures, inboard of inboard nacelle.

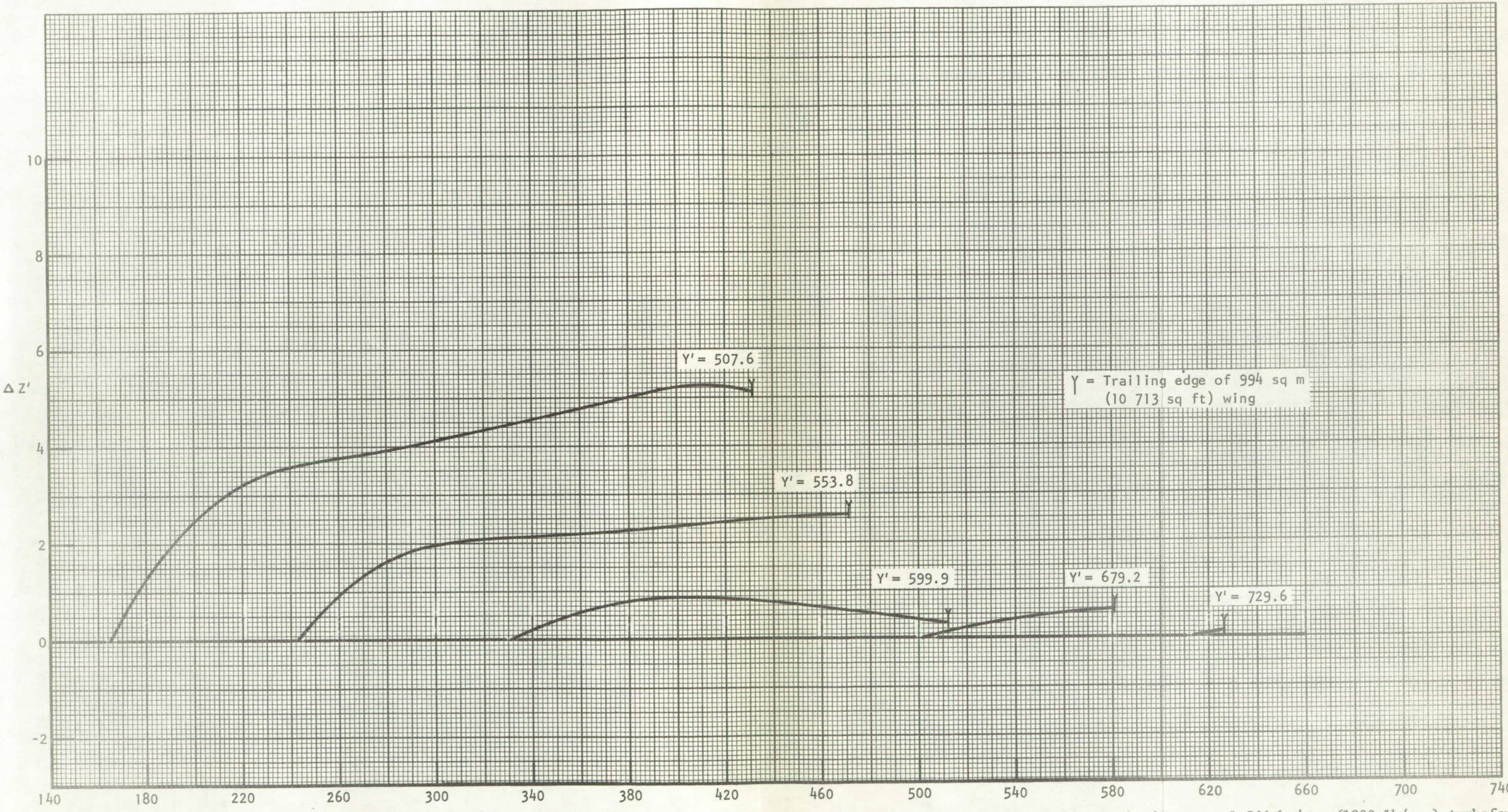

Figure 68.- Wing distortion required to cancel 544 kg/sec (1200 lb/sec) turbofan nacelle-induced pressures, outboard of outboard nacelle.

Airplane Performance and Sizing

All performance and sizing calculations were made using the Rockwell Vehicle Sizing and Performance Evaluation Program (VSPEP). This computer program is a design tool capable of scaling a known basepoint vehicle according to specified values of several different design parameters. These include vehicle gross weight (or fuel weight), thrust-to-weight ratio (or engine size), wing-loading (or wing area), and payload or fixed equipment weight and volume. A search routine permits automatic sizing of the vehicle gross weight such that a specified radius or range of the design mission is satisfied, or performance may be determined at a specified gross weight.

Vehicle performance is calculated internally from a set of subroutines programmed according to a detailed performance analysis model. The subroutines are general in nature and permit calculation of a wide variety of mission profiles. Several mission profiles may be calculated simultaneously. Takeoff and landing distances and maneuvering capability may also be determined. Figure 69 illustrates the evaluation process.

Typical mission legs which may be calculated include warmup, taxi, takeoff, climb, descent, cruise, and loiter operations. Climb and descent performance are determined by numerical integration of the equations of motion along a specified flight schedule. Internally generated schedules are also available, including minimum time and minimum fuel flight paths as defined by the energy method. Constraints on the allowable flight regime are included. Cruises and loiters may be determined at fixed or optimum speeds and altitudes. Numerical searches are used to determine optimum speeds and altitudes at the beginning and end of each of these legs.

Data input to the VSPEP for each of the AST concepts include:

- Weights broken down by major component, along with scaling information on the wing and the engines
- Drags broken down by major component and by type; e.g., friction drag, wave drag, drag due to lift, and base drag
- Installed propulsion data, including thrust and fuel flow as functions of speed, altitude, and power setting
- Dimensional data such as lengths, areas, and volumes for major components and the total vehicle

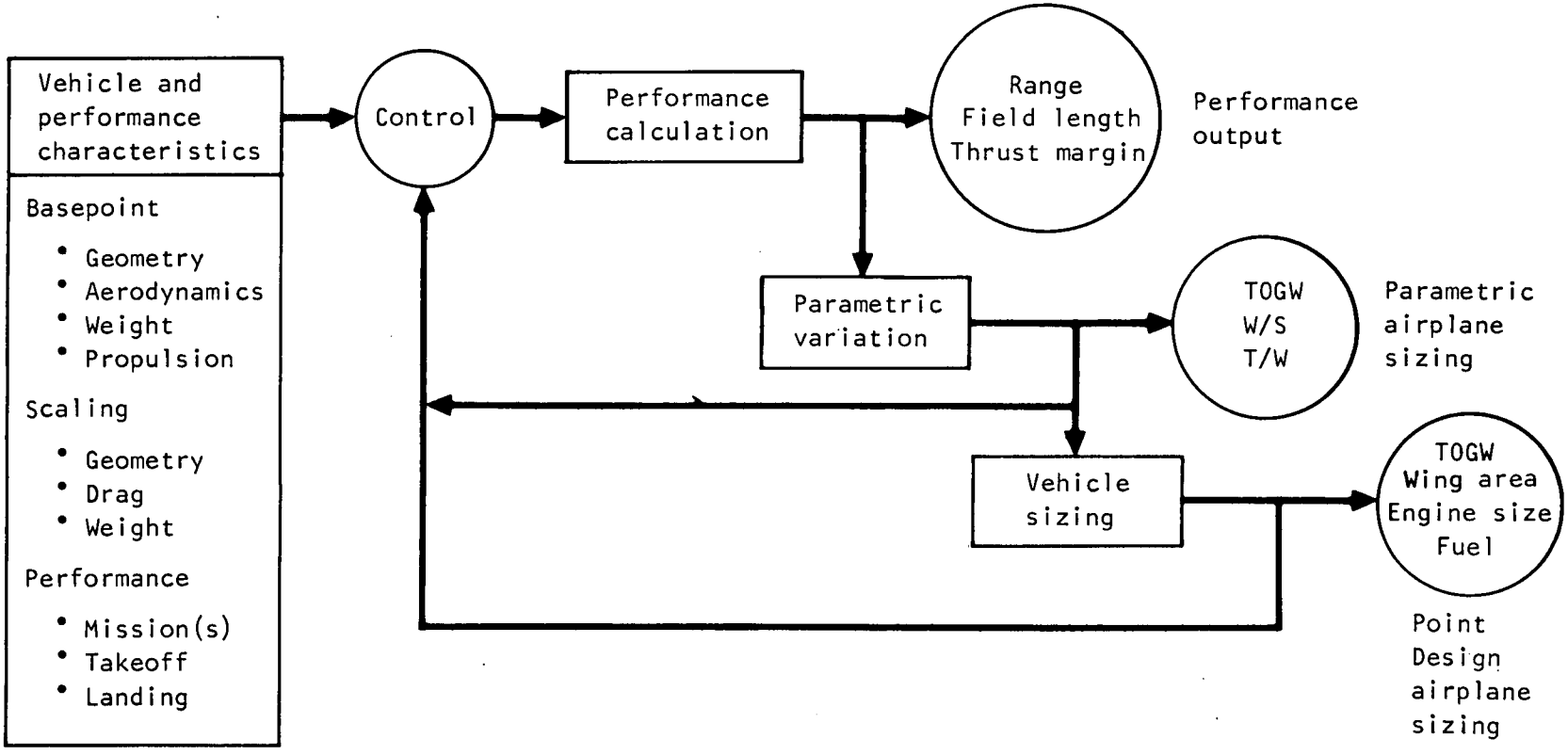

Figure 69.- Vehicle sizing and performance evaluation program.

Performance items calculated by the VSPEP program for the basepoint and resized vehicles for this study consist of the following:

1. Design mission range

2. Alternate mission range

3. FAR 36 takeoff distance

4. Balanced field takeoff distance

5. Thrust-to-drag ratio at 2.7M/18 300 m (60 000 ft)

A description of each of these performance items is given in the following paragraph.

Design mission.- A profile of the design mission is shown in figure 2. This mission consists mainly of a 2.7 Mach cruise. Fuel reserves as recommended in reference 2 are calculated for an alternate airport located 460 km (250 n. mi.) from the destination airport.

Design mission description:

1. Warmup and takeoff - 10 minutes at idle power plus 1 minute at maximum power

2. Climb - Maximum power climb and accelerate to cruise altitude and Mach No.

3. Cruise - Cruise at Mach 2.7 at altitude for best cruise range

4. Descent - Descend and decelerate to Mach 0.5 and 457 m (1500 ft) using idle power

5. Approach and land - Descend to Mach 0.3 at sea level using idle power

6. Taxi - 5 minutes at idle power

7. Reserve allowance - 5 percent of total fuel used in all previous legs

8. Reserve climb - Maximum power climb to subsonic cruise conditions

9. Reserve cruise - Subsonic cruise at Mach No. and altitude for best range

10. Reserve descent - Descend and decelerate to holding altitude and Mach No. using idle power

11. Reserve hold - Loiter for 30 minutes at 3048 m (10 000 ft) at the Mach No. for best endurance

12. Reserve approach and land - Descend to sea level using idle power

Alternate mission.- A profile of the alternate mission is shown in figure 3. The first half of the alternate is identical to the first half of the design mission. At the point corresponding to the midpoint of the design mission, a failure is assumed to occur in the most critical engine. At that point, the airplane descends and continues to cruise subsonically with one engine windmilling. The fuel reserve remaining at the end of this mission is equal to the reserve fuel as calculated for the design mission.

Alternate mission description:

1. Warmup and takeoff - Same as design mission

2. Climb - Same as design mission

3. Cruise - Same as design mission

4. Descent - Descend and decelerate to subsonic cruise conditions using idle power, following failure of most critical engine

5. Cruise - Subsonic cruise at Mach No. and altitude for best range with one engine inoperative

6. Descend and land - Descend to sea level using idle power

7. Reserve - Allow total reserve fuel equal to that calculated for design mission (legs 7 through 12)

FAR 36 takeoff.- Takeoff distance is calculated over a 10.7 m (35 ft) obstacle using takeoff thrust which has been suppressed and throttled so that FAR 36 sideline noise requirements are not exceeded.

Balanced field takeoff.- The balanced field length is defined such that segments B + C = D + E as shown in figure 70. The speed at which the engine failure occurs (i.e., V_1) is varied until this definition is satisfied to a reasonable tolerance. The balanced field length is then taken as the larger of the total takeoff distance or the accelerate-stop distance. Thrust data which are suppressed and throttled to meet FAR 36 noise requirements are used up to the point of engine failure. From this point on, the remaining engines are

operated at maximum power for takeoff without regard for noise requirements. For the stop distance calculation, the remaining engines are cut to idle power.

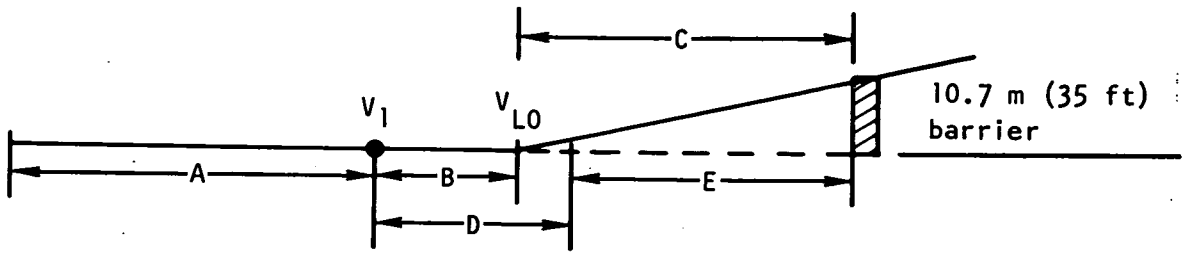

A - Distance up to critical engine failure speed V_1

B - 3-engine acceleration distance from V_1 to V_{LO}

C - 3-engine lift-off to barrier distance

D - Distance gained after engine failure before full brake application

E - Stopping distance

V_1 - Critical engine failure speed

V_{LO} - Lift-off velocity

Figure 70.- Balanced field length definition.

Thrust-to-drag (T/D) ratio.- T/D is calculated using maximum available thrust at 2.7 Mach, 18 300 m (60 000 ft). Drag is that for level flight at the same conditions. Airplane weight is that at the start of the supersonic cruise as calculated for the design mission.

Baseline airplane performance.- Performance was calculated for the base-point airplanes with engine airflow of 408 kg/sec (900 lb/sec) for both the turbojet and duct-heating turbofan engine cycles. Tables XXVII and XXVIII present a leg-by-leg summary of both the design and alternate missions.

Engine airflow was then varied from 272 kg/sec (600 lb/sec) to 544 kg/sec (1200 lb/sec), maintaining a fixed airplane gross weight of 340 198 kg (750 000 lb), fixed wing area of 995 sq m (10 713 sq ft), and a fixed payload of 234 passengers. Airplane performance is shown plotted versus engine airflow in figures 71 through 75 for both engine cycles.

Figure 76 shows airplane thrust-to-weight ratio using maximum installed thrust at sea level static conditions as a reference and weight equal to take-off gross weight. Note that the actual thrust-to-weight for takeoff is approximately 81 percent of this value, due to noise suppression and throttling to meet FAR 36 noise requirements. L/D and SFC values attained at the start of the supersonic cruise leg are shown in figures 77 and 78. For comparison purposes, the optimum values (i.e., maximum L/D and minimum SFC) are also shown.

TABLE XXVII.- MISSION SUMMARY FOR BASEPOINT AIRPLANE WITH 408 KG/SEC (900 LB/SEC) TURBOJET ENGINES

Design mission summary

Leg description	Weight		Altitude		Mach No.	Fuel used		Time, min	Total time, min	Range		Total range	
	kg	lb	m	ft		kg	lb			km	n. mi.	km	n. mi.
Initial weight	340 197	750 000											
1. Warmup and takeoff	335 232	739 053	0	0	0.30	4 965	10 947	11.00	11.00	0	0	0	0
2. Climb and accelerate	303 324	668 710	19 038	62 961	2.7	31 907	70 343	20.56	31.56	626.1	338.1	626.1	338.1
3. Cruise at 2.7 M	210 087	463 159	21 260	69 752	2.7	93 237	205 551	126.05	157.61	6029.4	3255.9	6655.5	3594.0
4. Descend to 457 m (1500 ft)	208 459	459 570	457	1 500	0.50	1 627	3 589	17.66	175.27	356.8	192.7	7012.4	3786.7
5. Approach and land	207 996	458 550	0	0	0.30	462	1 020	1.77	177.04	14.6	7.9	7027.0	3794.6
6. Taxi allowance	206 507	455 267	0	0	0	1 489	3 283	5.00	182.04	0	0	7027.0	3794.6
7. 5% fuel allowance	199 823	440 530	0	0	0	6 684	14 737	0	182.04	0	0	7027.0	3794.6
8. Climb	193 891	427 454	12 866	42 212	0.95	5 931	13 076	3.17	185.21	43.3	23.4	7070.3	3818.0
9. Subsonic cruise	188 330	415 193	13 063	42 860	0.95	5 561	12 261	17.31	202.52	291.1	157.2	7361.4	3975.2
10. Descend to 3048 m (10 000 ft)	187 145	412 581	3 048	10 000	0.40	1 184	2 612	10.60	213.12	131.4	71.0	7492.9	4046.2
11. Hold at 3048 m (10 000 ft)	177 263	390 795	3 048	10 000	0.40	9 882	21 786	30.00	243.12	0	0	7492.9	4046.2
12. Descend and land	176 416	388 927	0	0	0.30	847	1 868	3.63	246.75	32.0	17.3	7525.0	4063.5

Total fuel used = 163 781 kg (361 073 lb)

Alternate mission summary

Leg description	Weight		Altitude		Mach No.	Fuel used		Delta time, min	Total total, min	Delta range		Total range	
	kg	lb	m	ft		kg	lb			km	n. mi.	km	n. mi.
Initial weight	340 197	750 000											
1. Warmup and takeoff	335 232	739 053	0	0	0.30	4 965	10 947	11.00	11.00	0	0	0	0
2. Climb and accelerate	303 324	668 710	19 038	62 461	2.7	31 907	70 343	20.56	31.56	626.1	338.1	626.1	338.1
3. Cruise at 2.7 M	254 923	562 004	20 017	65 675	2.7	48 401	106 706	60.41	91.97	2887.4	1559.2	3513.5	1897.3
4. Descend to subsonic cruise	254 614	561 323	11 160	36 617	0.95	308	681	7.76	99.73	236.4	127.7	3750.0	2025.0
5. Subsonic cruise	207 605	457 688	12 463	40 891	0.95	47 008	103 635	116.10	215.83	1952.5	1054.4	5702.5	3079.4
6. Descend and land	206 505	455 262	0	0	0.30	1 100	2 426	11.28	227.11	133.5	72.1	5836.1	3151.5
7. FAR 121 receiver	176 416	388 927	0	0	0	30 089	66 335	64.71	291.82	497.9	268.9	6334.0	3420.4

Total fuel used = 163 781 kg (361 073 lb)

operated at maximum power for takeoff without regard for noise requirements. For the stop distance calculation, the remaining engines are cut to idle power.

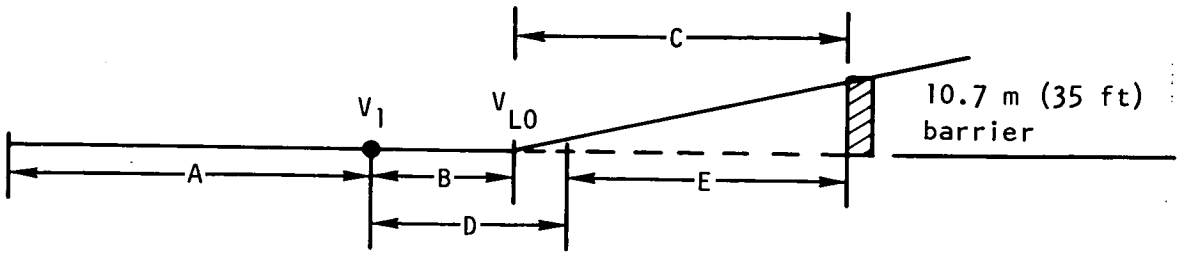

A - Distance up to critical engine failure speed V_1

B - 3-engine acceleration distance from V_1 to V_{LO}

C - 3-engine lift-off to barrier distance

D - Distance gained after engine failure before full brake application

E - Stopping distance

V_1 - Critical engine failure speed

V_{LO} - Lift-off velocity

Figure 70.- Balanced field length definition.

Thrust-to-drag (T/D) ratio.- T/D is calculated using maximum available thrust at 2.7 Mach, 18 300 m (60 000 ft). Drag is that for level flight at the same conditions. Airplane weight is that at the start of the supersonic cruise as calculated for the design mission.

Baseline airplane performance.- Performance was calculated for the base-point airplanes with engine airflow of 408 kg/sec (900 lb/sec) for both the turbojet and duct-heating turbofan engine cycles. Tables XXVII and XXVIII present a leg-by-leg summary of both the design and alternate missions.

Engine airflow was then varied from 272 kg/sec (600 lb/sec) to 544 kg/sec (1200 lb/sec), maintaining a fixed airplane gross weight of 340 198 kg (750 000 lb), fixed wing area of 995 sq m (10 713 sq ft), and a fixed payload of 234 passengers. Airplane performance is shown plotted versus engine airflow in figures 71 through 75 for both engine cycles.

Figure 76 shows airplane thrust-to-weight ratio using maximum installed thrust at sea level static conditions as a reference and weight equal to take-off gross weight. Note that the actual thrust-to-weight for takeoff is approximately 81 percent of this value, due to noise suppression and throttling to meet FAR 36 noise requirements. L/D and SFC values attained at the start of the supersonic cruise leg are shown in figures 77 and 78. For comparison purposes, the optimum values (i.e., maximum L/D and minimum SFC) are also shown.

TABLE XXVIII.- MISSION SUMMARY FOR BASEPOINT AIRPLANE WITH 408 KG/SEC (900 LB/SEC) TURBOFAN ENGINES

Design mission summary

Leg description	Weight		Altitude		Mach No.	Fuel used		Time, min	Total time, min	Range		Total range	
	kg	lb	m	ft		kg	lb			km	n. mi.	km	n. mi.
Initial weight	340 197	750 000											
1. Warmup and takeoff	336 771	742 946	0	0	0.30	3 426	7 554	11.00	11.00	0	0	0	0
2. Climb and accelerate	302 468	666 823	18 471	60 603	2.7	34 302	75 623	12.83	23.83	315.4	170.3	315.4	170.3
3. Cruise at 2.7 M	201 693	444 654	21 344	70 029	2.7	100 777	222 169	135.93	159.76	6502.0	3511.1	6817.4	3681.4
4. Descend to 457 m (1500 ft)	199 847	440 584	457	1 500	0.50	1 846	4 070	19.70	179.46	391.1	211.2	7208.5	3892.6
5. Approach and land	199 546	439 921	0	0	0.30	300	663	1.91	181.37	15.9	8.6	7224.4	3901.2
6. Taxi allowance	198 876	438 444	0	0	0	669	1 477	5.00	186.37	0	0	7224.4	3901.2
7. 5% fuel allowance	188 984	416 635	0	0	0	9 892	21 809	0	186.37	0	0	7224.4	3901.2
8. Climb	182 922	403 272	12 554	41 188	0.91	6 061	13 363	9.33	195.70	131.1	70.8	7355.6	3972.0
9. Subsonic cruise	179 912	396 635	12 655	41 521	0.91	3 010	6 637	11.88	207.58	190.6	102.9	7546.1	4074.9
10. Descend to 3048 m (10 000 ft)	178 687	393 934	3 048	10 000	0.38	1 225	2 701	11.88	219.46	145.7	78.7	7691.9	4153.6
11. Hold at 3048 m (10 000 ft)	172 171	379 570	3 048	10 000	0.38	6 575	14 364	30.00	249.46	0	0	7691.9	4153.6
12. Descend and land	171 586	378 280	0	0	0.3	585	1 290	3.93	253.39	34.6	18.7	7726.5	4172.3

Total fuel used = 168 611 kg (371 720 lb)

Alternate mission summary

Leg description	Weight		Altitude		Mach No.	Fuel used		Delta time, min	Total time, min	Delta range		Total range	
	kg	lb	m	ft		kg	lb			km	n. mi.	km	n. mi.
Initial weight	340 197	750 000											
1. Warmup and takeoff	336 771	742 446	0	0	0.30	3 426	7 554	11.00	11.00	0	0	0	0
2. Climb and accelerate	302 468	666 823	18 471	60 603	2.7	34 302	75 623	12.83	23.83	315.4	170.3	315.4	170.3
3. Cruise at 2.7 M	246 941	544 408	20 007	65 641	2.7	55 527	122 415	68.98	92.81	3296.9	1780.3	3612.2	1950.6
4. Descend to subsonic cruise	246 403	543 222	9 675	31 743	0.90	537	1 186	9.47	102.28	275.7	148.9	3888.0	2099.5
5. Subsonic cruise	199 847	440 583	11 005	36 106	0.88	46 556	102 639	139.87	242.15	2228.5	1203.4	6116.5	3302.9
6. Descend and land	198 876	438 443	0	0	0.30	970	2 140	11.44	253.59	130.2	70.3	6246.7	3373.2
7. FAR 121 receiver	171 585	378 278	0	0	0	27 290	60 165	67.02	320.61	502.0	271.1	6748.7	3644.3

Total fuel used = 168 612 kg (371 722 lb)

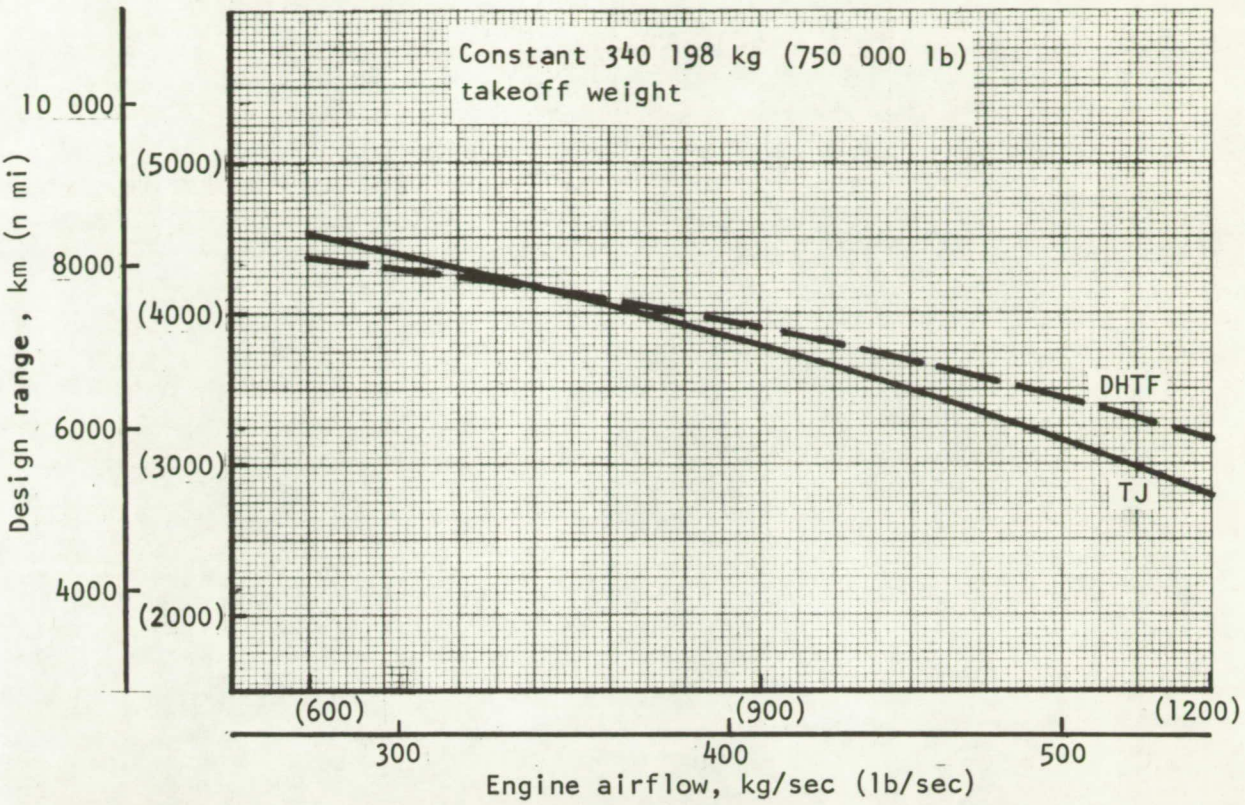

Figure 71.- Design range versus airflow for baseline airplanes.

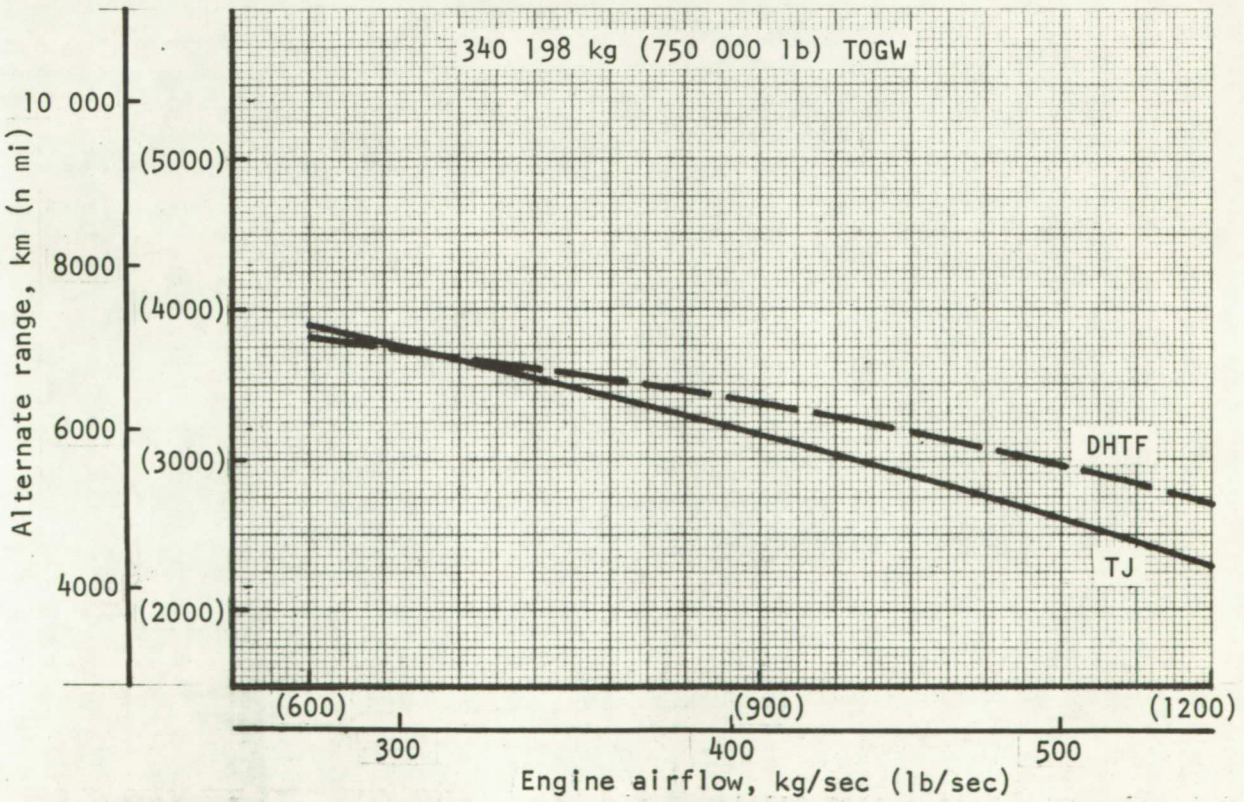

Figure 72.- Alternate range versus airflow for baseline airplanes.

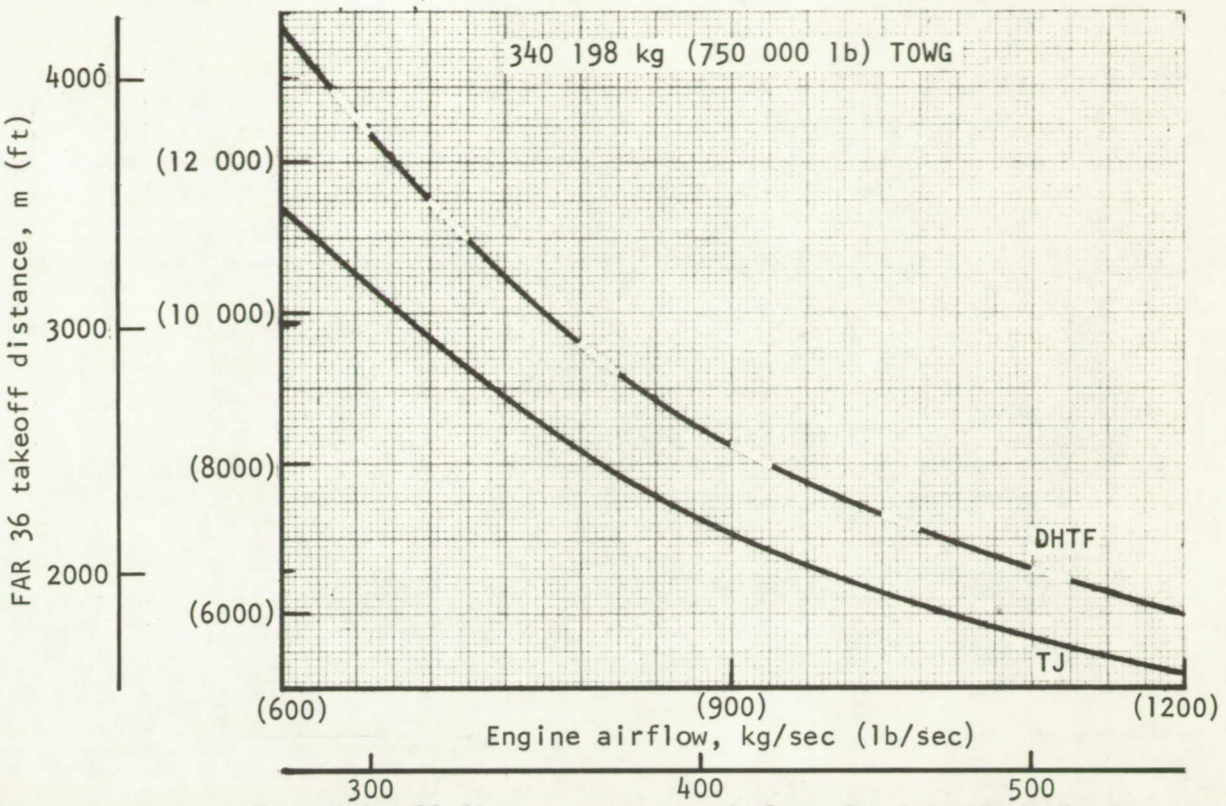

Figure 73.- Takeoff distance versus airflow for baseline airplanes.

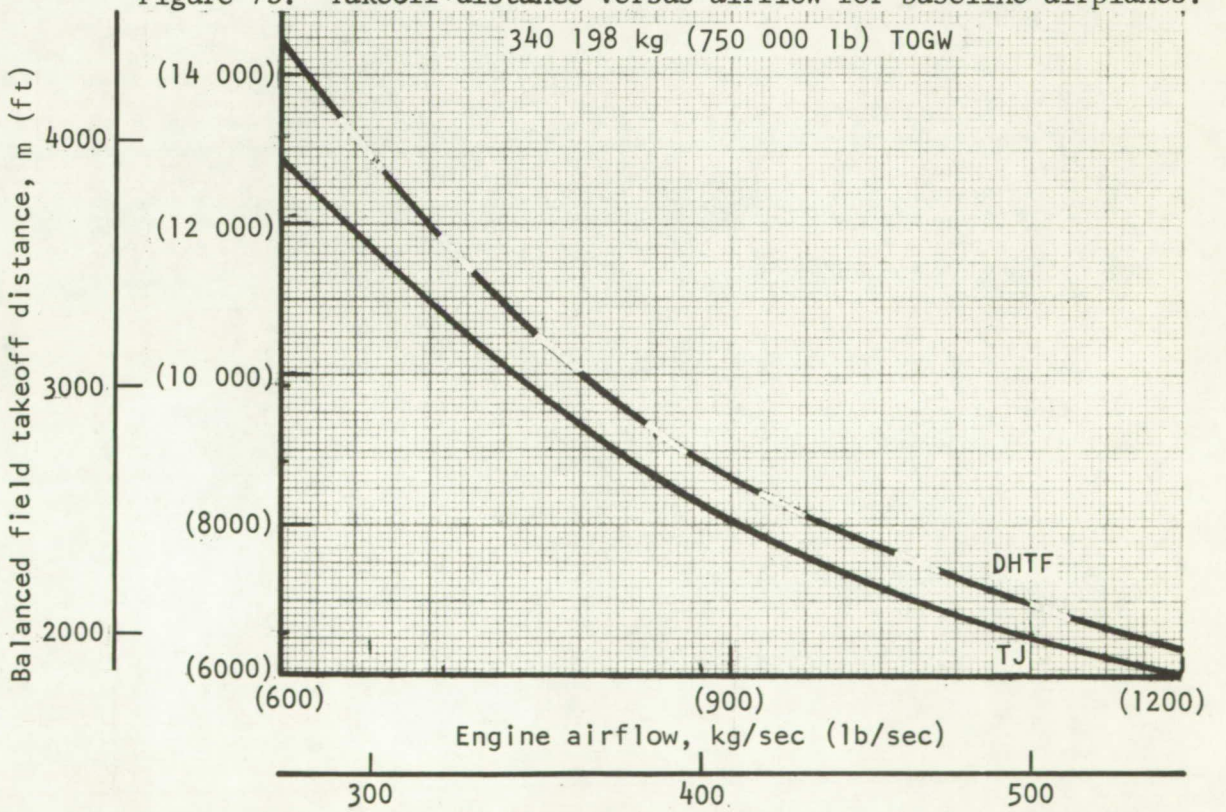

Figure 74.- Balanced field takeoff distance versus airflow for baseline airplanes.

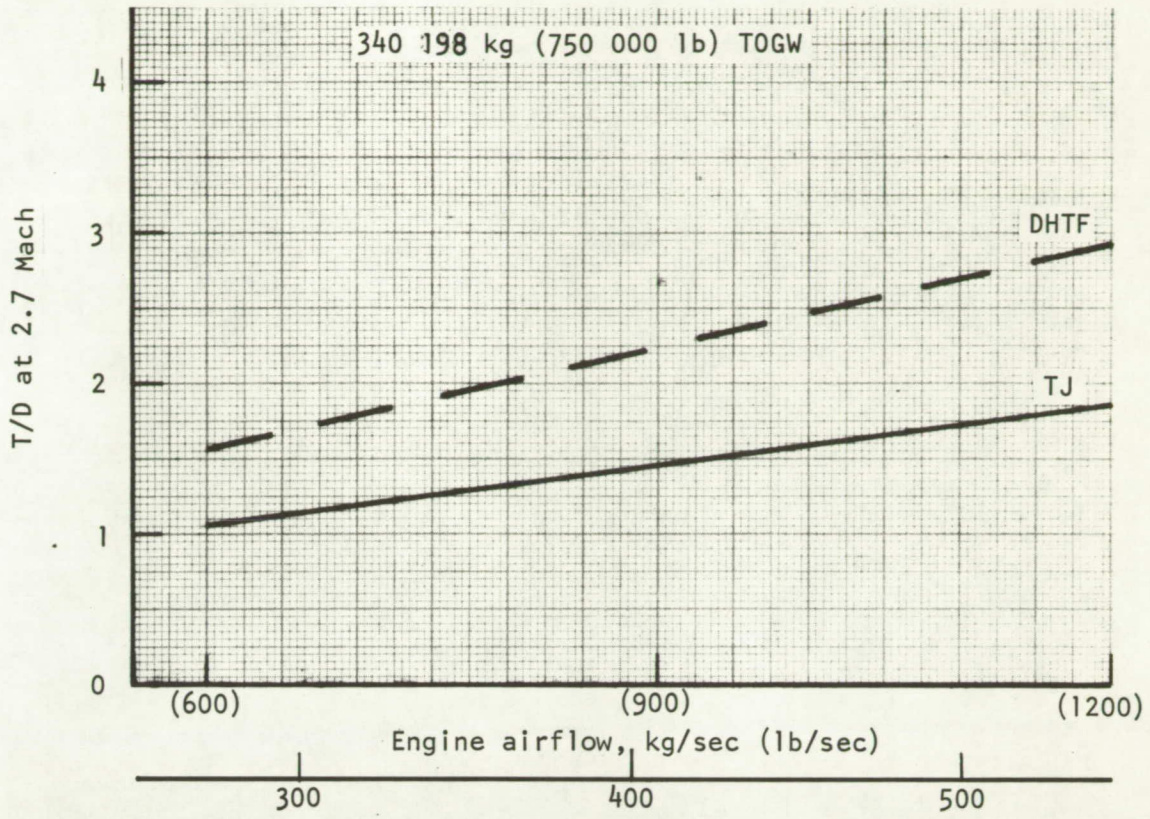

Figure 75.- T/D at 2.7M versus airflow for baseline airplanes.

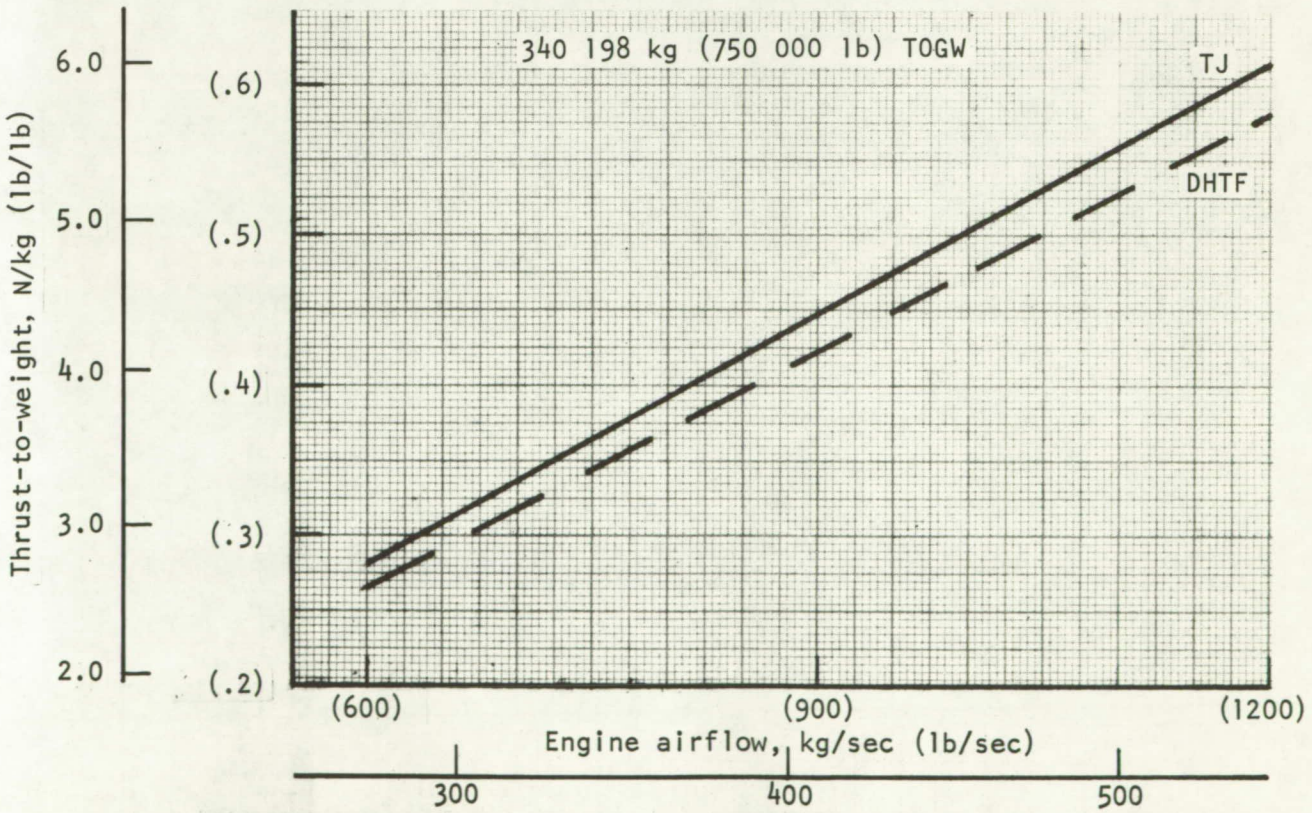

Figure 76.- Thrust-to-weight versus airflow for baseline airplanes.

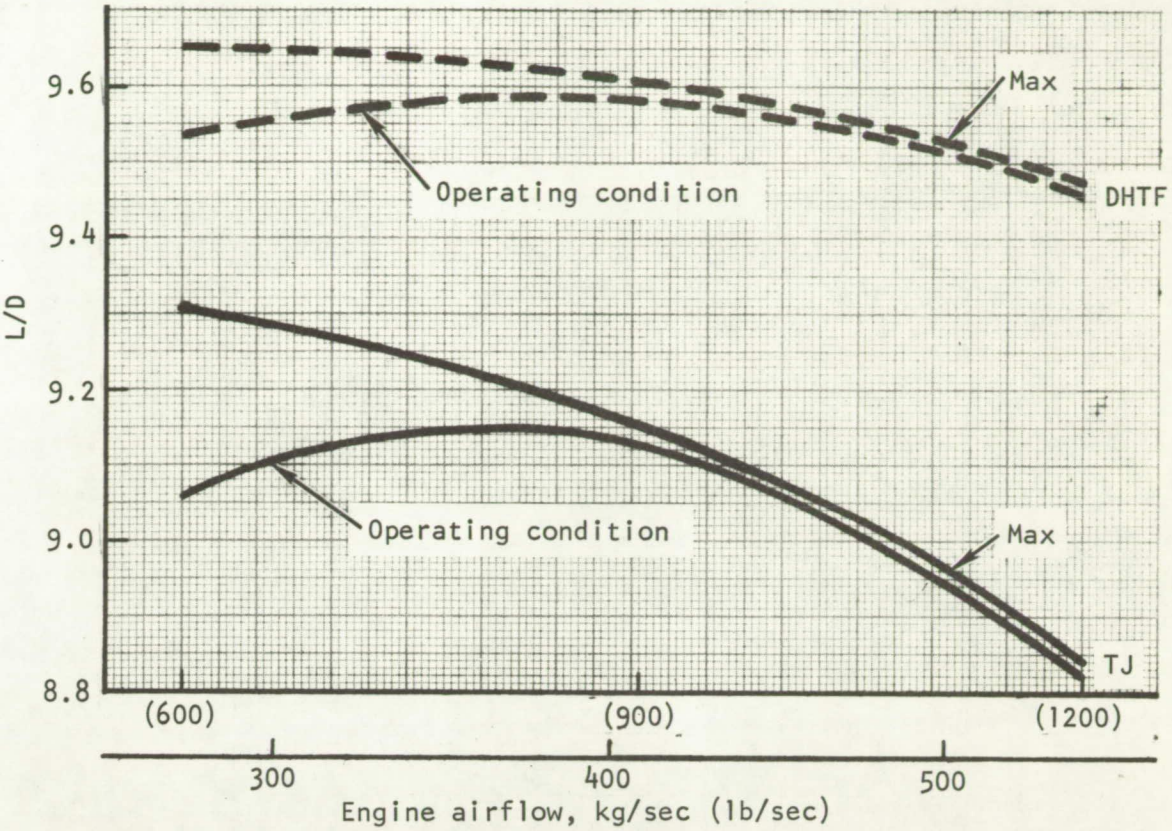

Figure 77.- Cruise L/D versus airflow for baseline airplanes.

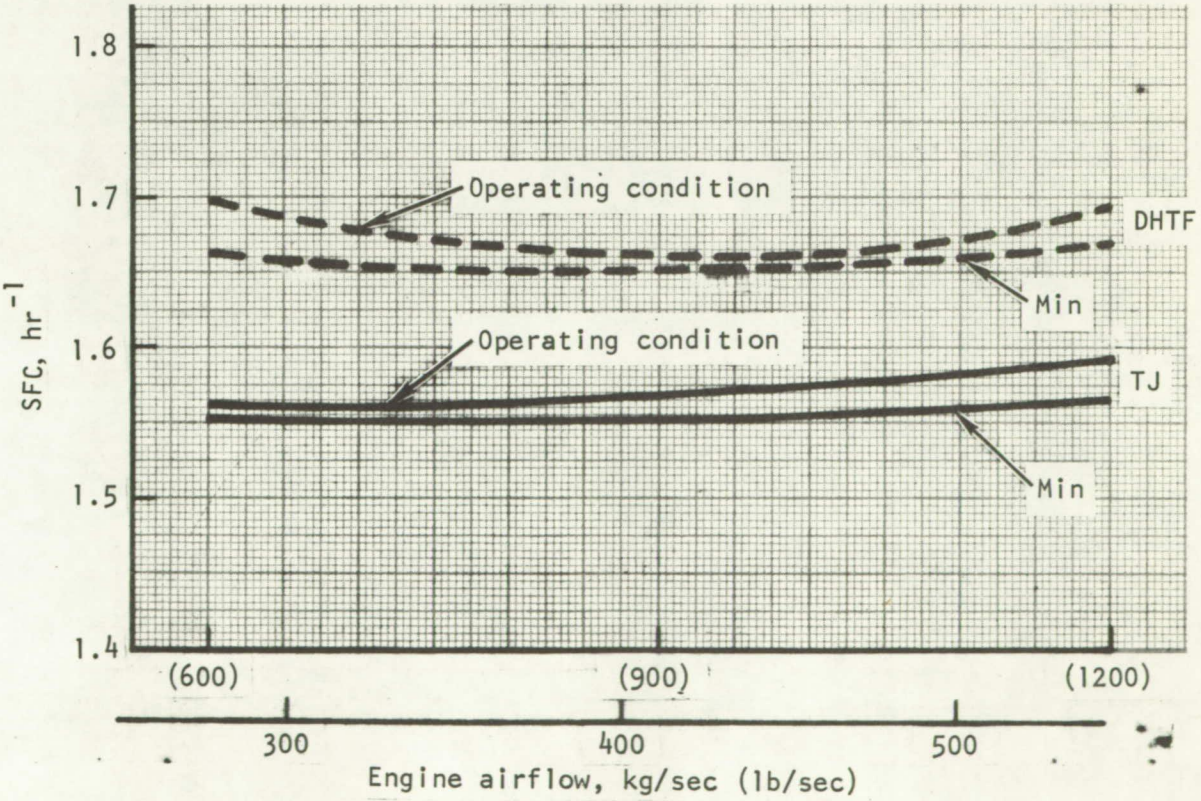

Figure 78.- Cruise SFC versus airflow for baseline airplanes.

Figure 79 shows the Mach 2.7 cruise efficiency factor, $\frac{L/D}{SFC}$, for each airplane, while figure 80 shows the total propulsion weight versus engine airflow. The latter includes engines, nozzles, nacelles, air induction system, engine controls, and accessories.

The relative shape and level of these curves are responsible for the difference in shape and magnitude of the design range curve for the turbojet and turbofan cycle of figure 71. The airplane for the smaller engine sizes is operating progressively off the maximum cruise efficiency point for both cycles as a result of incorrect sizing.

Airplane Sizing.- Airplane sizing was performed in two iterations. For the first iteration, wave drag coefficient was varied as a function of engine airflow only in accordance with figure 29. Three vehicles were resized for each engine cycle having engine airflows of 272, 408, and 544 kg/sec (600, 900, and 1200 lb/sec). These resized vehicles were then rebalanced and wave drag values re-evaluated as described in the following pages. A second sizing interation was then performed using the revised wave drag estimates. A discussion of the preliminary sizing (i.e., first iteration) follows. The second iteration is discussed under "Sizing of Rebalanced Airplane."

Preliminary sizing: For each engine airflow, a wing-loading trade was performed to obtain the optimum airplane for that airflow. Optimum, in this case, is defined as the minimum gross weight airplane that will make the required design mission range of 6481 km (3500 n. mi.). All other performance items are allowed to vary. For each wingloading, the VSPEP program was allowed to iterate to arrive at the gross weight such that design mission range is equal to the required value.

The wingloading that yields the minimum gross weight is approximately 464 kg/m^2 (95 lb/sq ft) for all cases. However, these wings are too small to carry the full fuel load as calculated for the scaled airplane. This physical restriction forces a second sizing criterion to be imposed. This criterion is that the wing must contain enough available fuel volume to carry the design mission fuel load plus an incremental volume for payload-range trade use, taken as an amount equal to one-half the payload (i.e., 11 113 kg (24 500 lb)).

Gross weight is plotted versus wingloading for a constant range of 6481 km (3500 n. mi.) in figure 81 for the turbojet-powered airplane. Figure 82 shows the corresponding plots of fuel used and fuel for which wing volume is available minus 11 113 kg (24 500 lb) versus wing loading. The intersection point of these curves indicates the maximum wingloading for which sufficient fuel volume is available in the wing. These points are spotted on the gross weight curves and represent the selected vehicles as obtained by the preliminary sizing

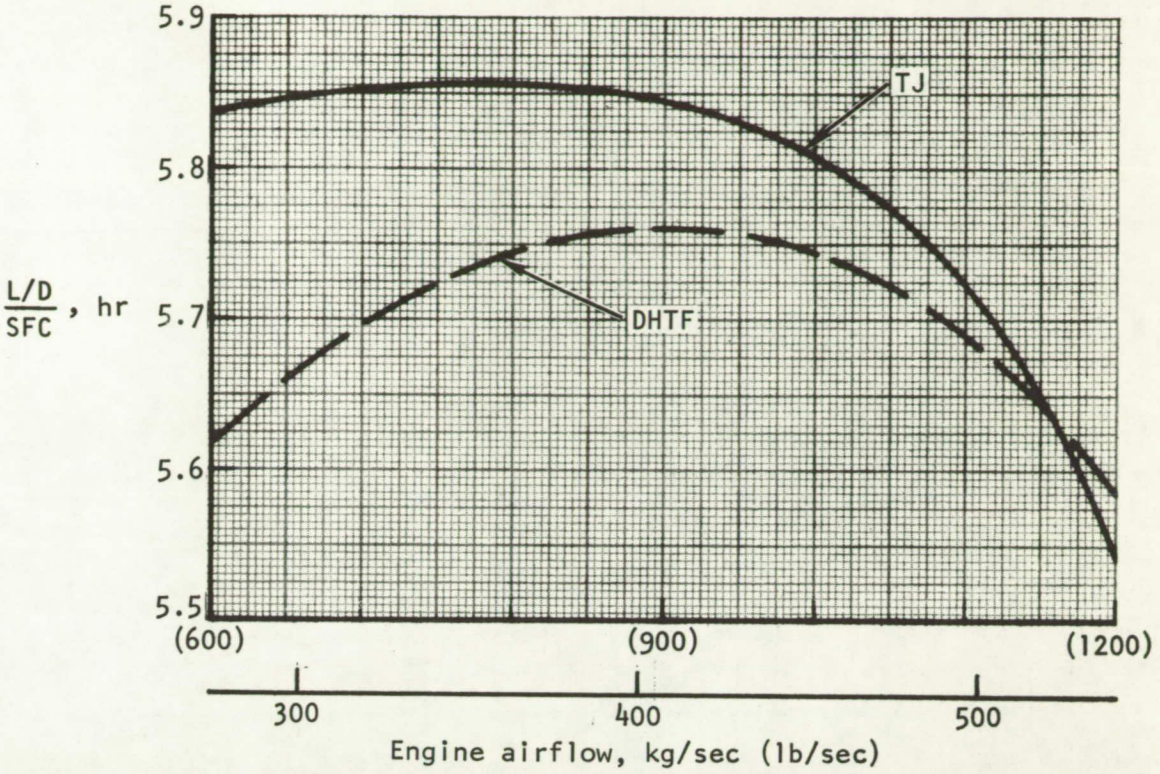

Figure 79.- Operating cruise efficiency versus airflow for baseline airplane.

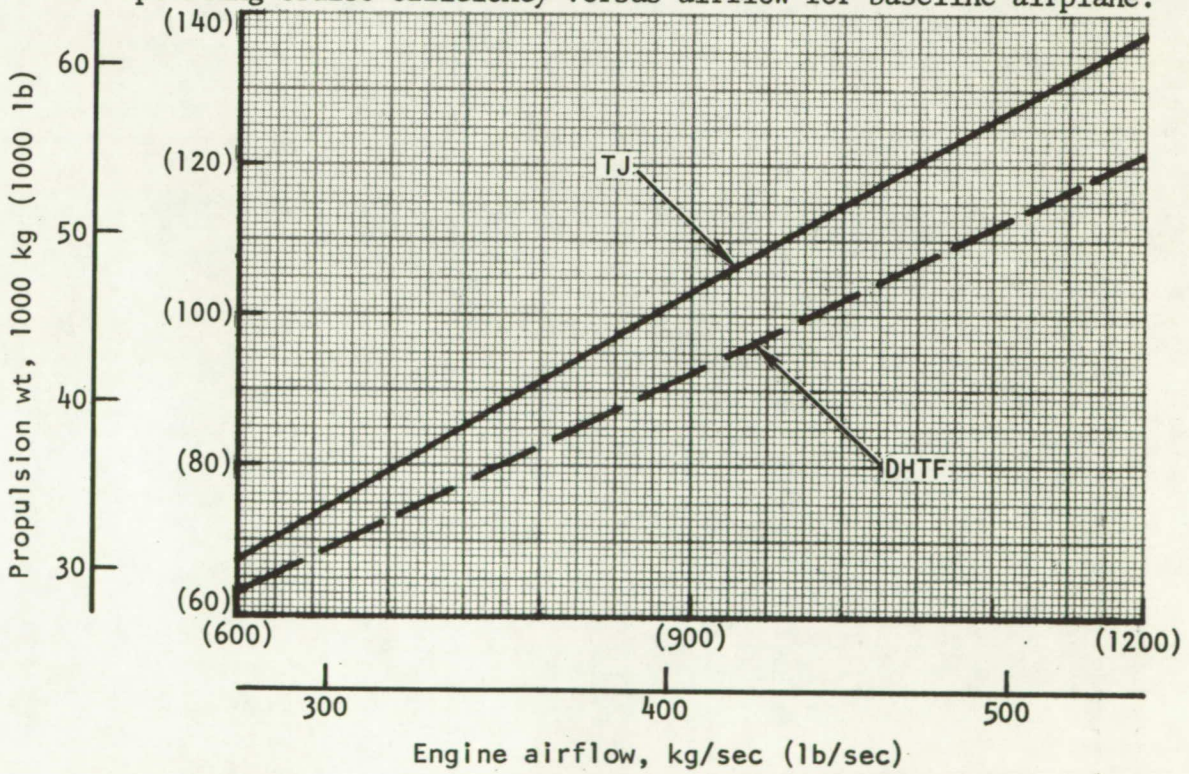

Figure 80.- Propulsion weight versus airflow for baseline airplanes.

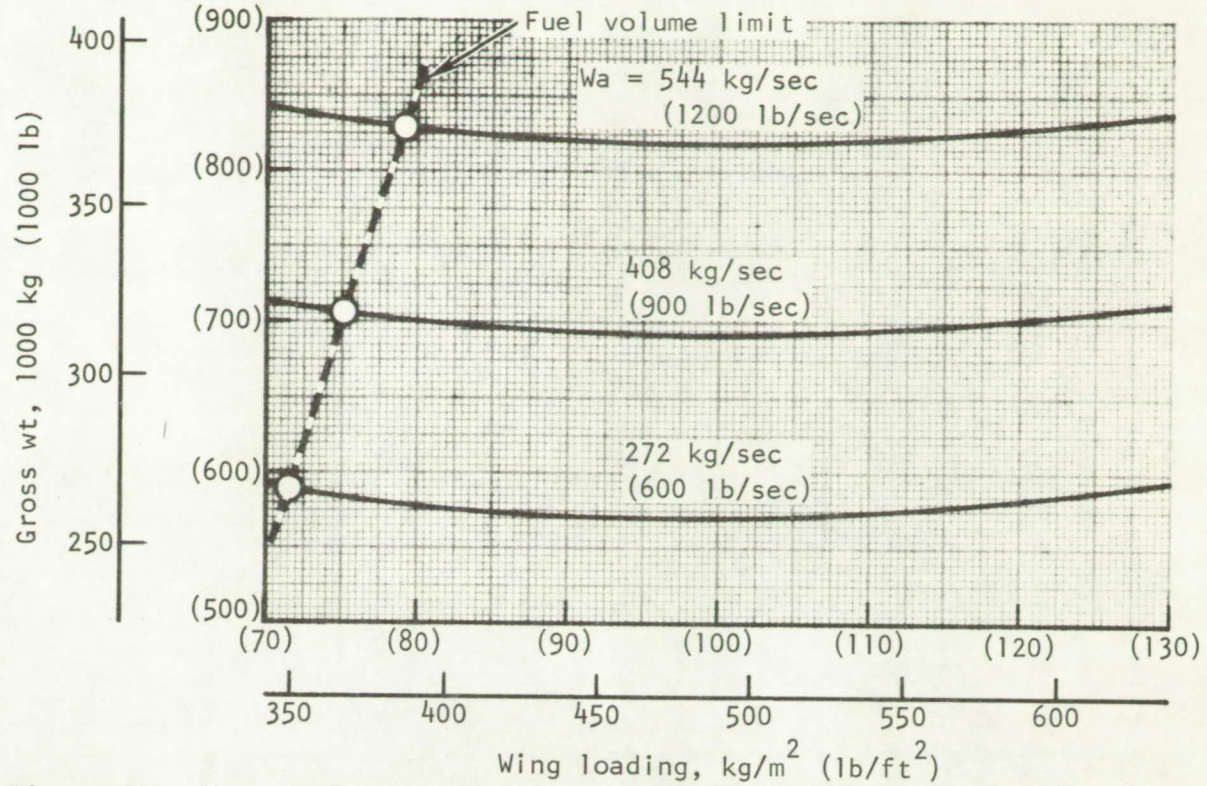

Figure 81.- Gross weight versus wing loading for turbojet airplanes.

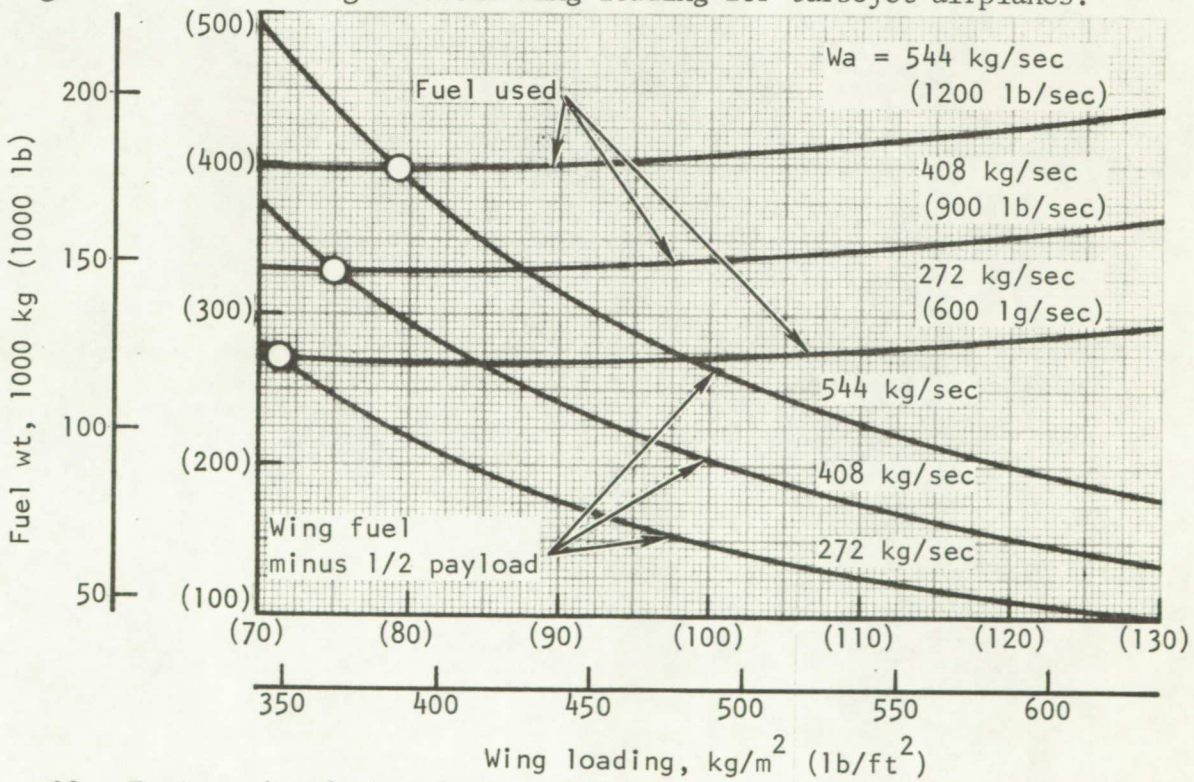

Figure 82.- Fuel used and wing fuel available versus wing loading for turbojet airplanes.

process. Similar sizing curves are shown in figures 83 and 84 for the duct-heating turbofan engine.

The selected wing-loading values are plotted versus design engine airflow for both engine cycles in figure 85. For comparison purposes, the wingloading which would have resulted had fuel volume been ignored is also shown. Figure 86 shows the airplane gross weight penalty paid as a result of the fuel volume sizing criterion.

Airplane balance.- Aerodynamic rebalance of the minimum takeoff gross weight configuration was based on the previously described first-iteration sizing wing area and fuel weight results in conjunction with the nacelle wing relocation data of figures 31, 32, and table XVIII. The resulting impact on wing location and wave drag are presented in table X and figure 33, respectively. The latter is used in the following paragraphs to make a second evaluation of the vehicle size as a function of engine airflow for constant range performance.

Sizing of rebalanced airplane.- As described under "Preliminary Sizing," the sizing process was performed in two iterations. The process used in the first iteration is described under that heading. The following paragraphs detail the final iteration and present final results in plotted form.

Revised estimates for wave drag as detailed previously were used. For each engine airflow, the optimum airplane was chosen as that having the minimum gross weight and still meeting the design mission range requirement of 6481 km (3500 n. mi.) while maintaining sufficient wing volume to carry the entire fuel load plus an amount equal to one-half the payload.

Wing-loading trades performed exactly as described for preliminary sizing were performed for several airplanes. However, it was soon discovered that, due to the small changes from the preliminary sizing results, virtually no change occurred in the wingloading required to maintain sufficient fuel volume in the wing. The final sizing process, therefore, was reduced to the simpler problem of scaling airplane gross weight to that required to meet the range requirement while maintaining wingloading at that value calculated during preliminary sizing.

Leg-by-leg summaries of the design and alternate missions are presented in tables XXIX and XXX for the resized airplanes having an engine airflow of 408 kg/sec (900 lb/sec). Resized vehicle characteristics may be found plotted versus engine airflow for both engine cycles in figures 87 through 91. Note that thrust-to-weight ratio is calculated using maximum sea level static installed thrust and weight equal to takeoff gross weight. The actual thrust-to-weight for takeoff is approximately 81 percent of this value, due to noise suppression and throttling to meet FAR 36 sideline noise requirements.

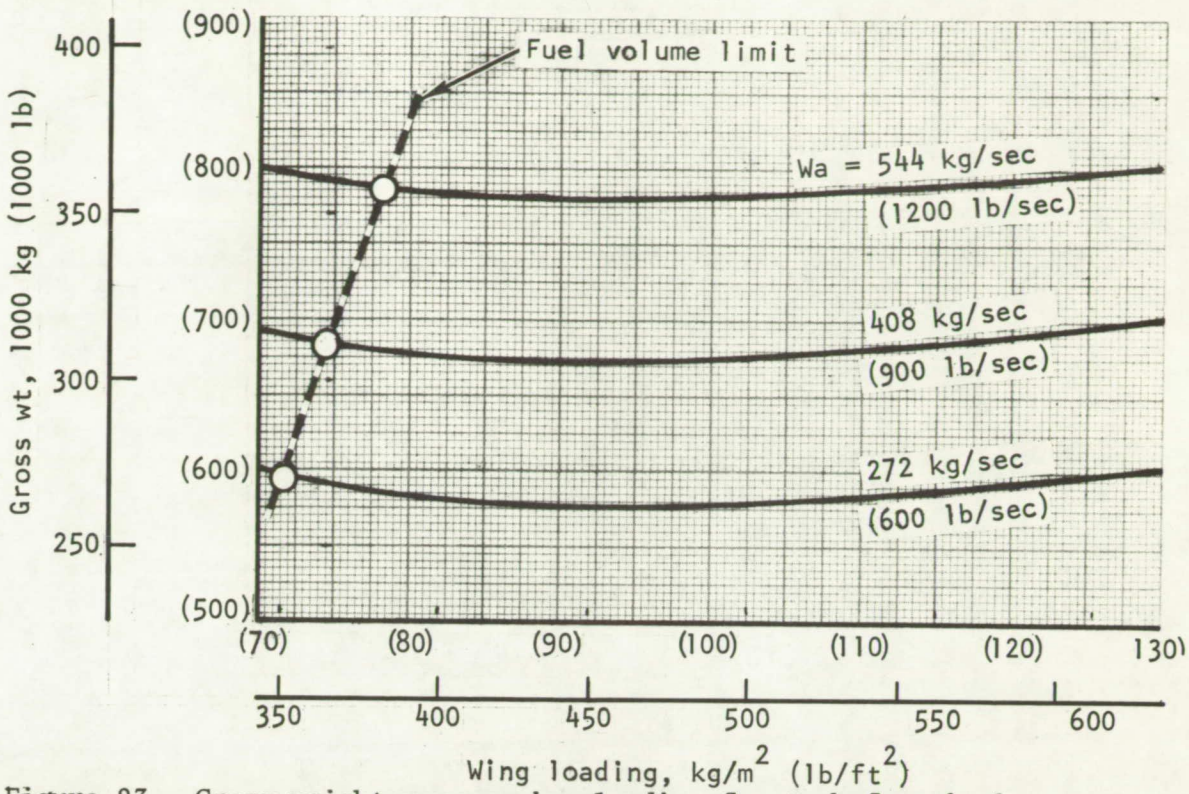

Figure 83.- Gross weight versus wing loading for turbofan airplanes.

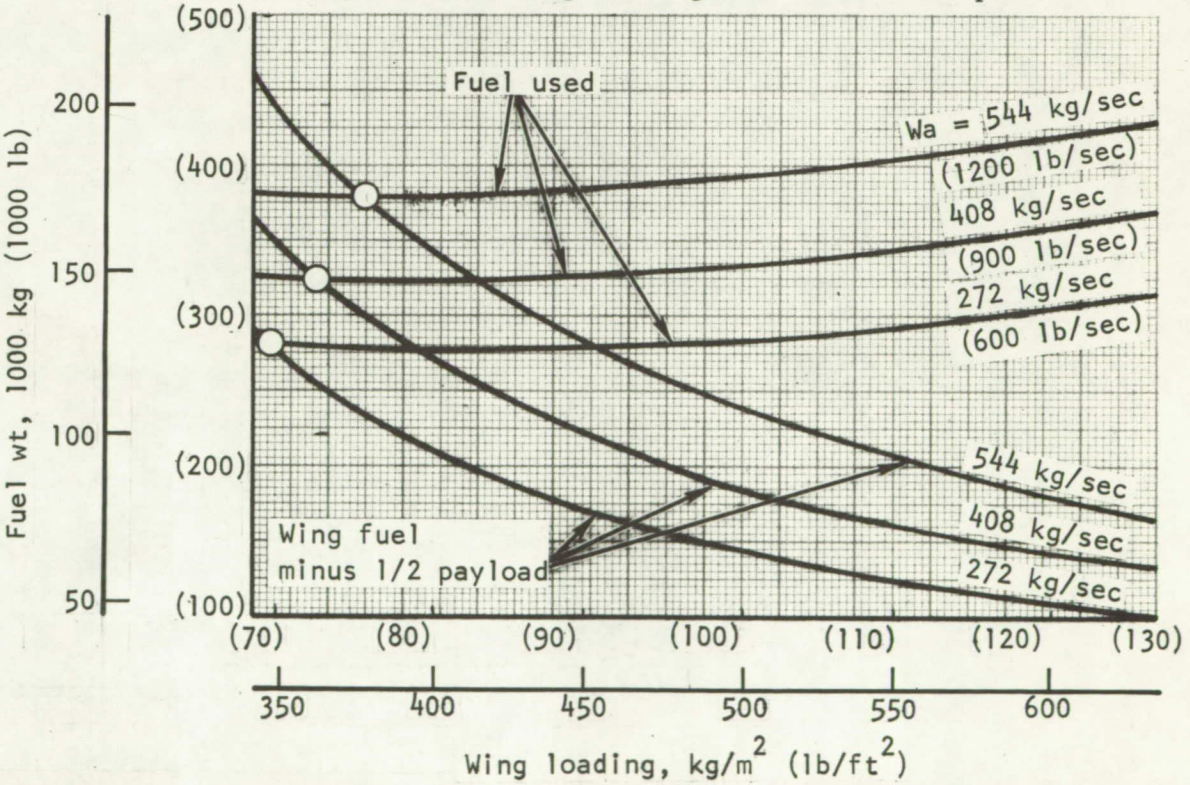

Figure 84.- Fuel used and wing fuel available versus wing loading for turbofan airplanes.

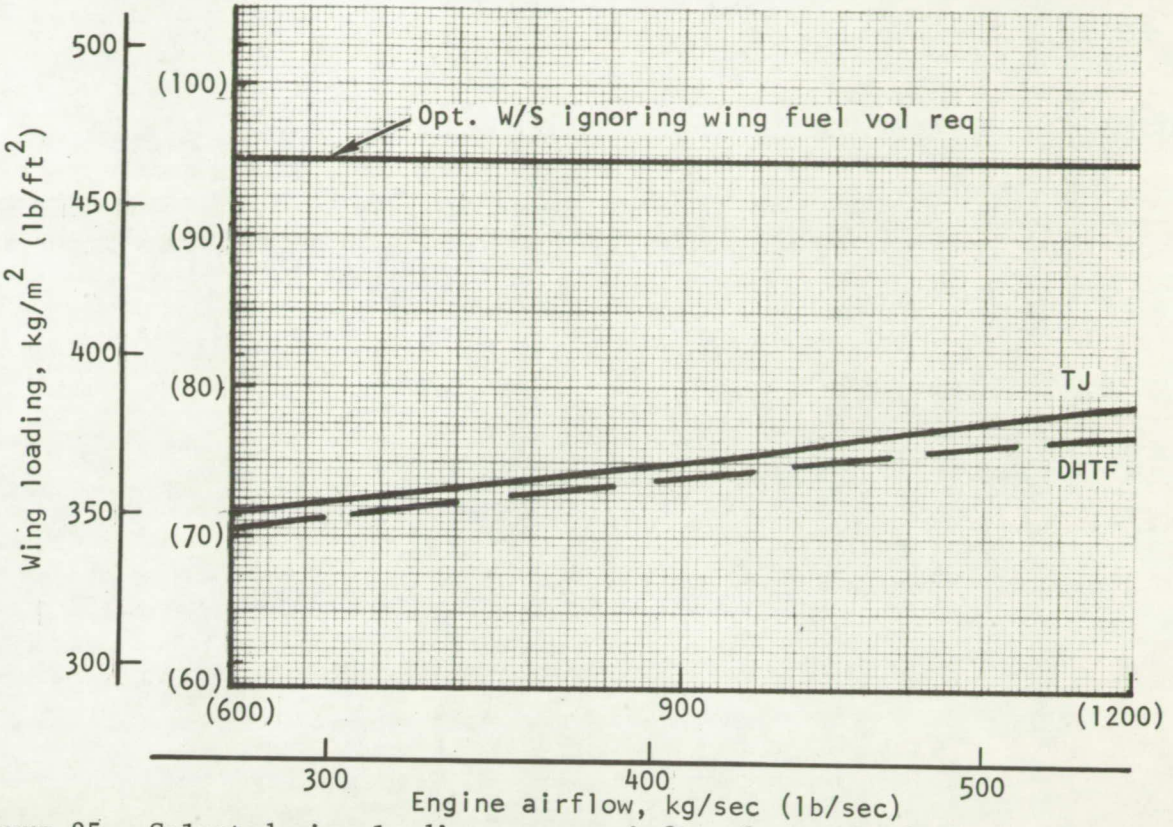

Figure 85.- Selected wing loading versus airflow for resized airplanes.

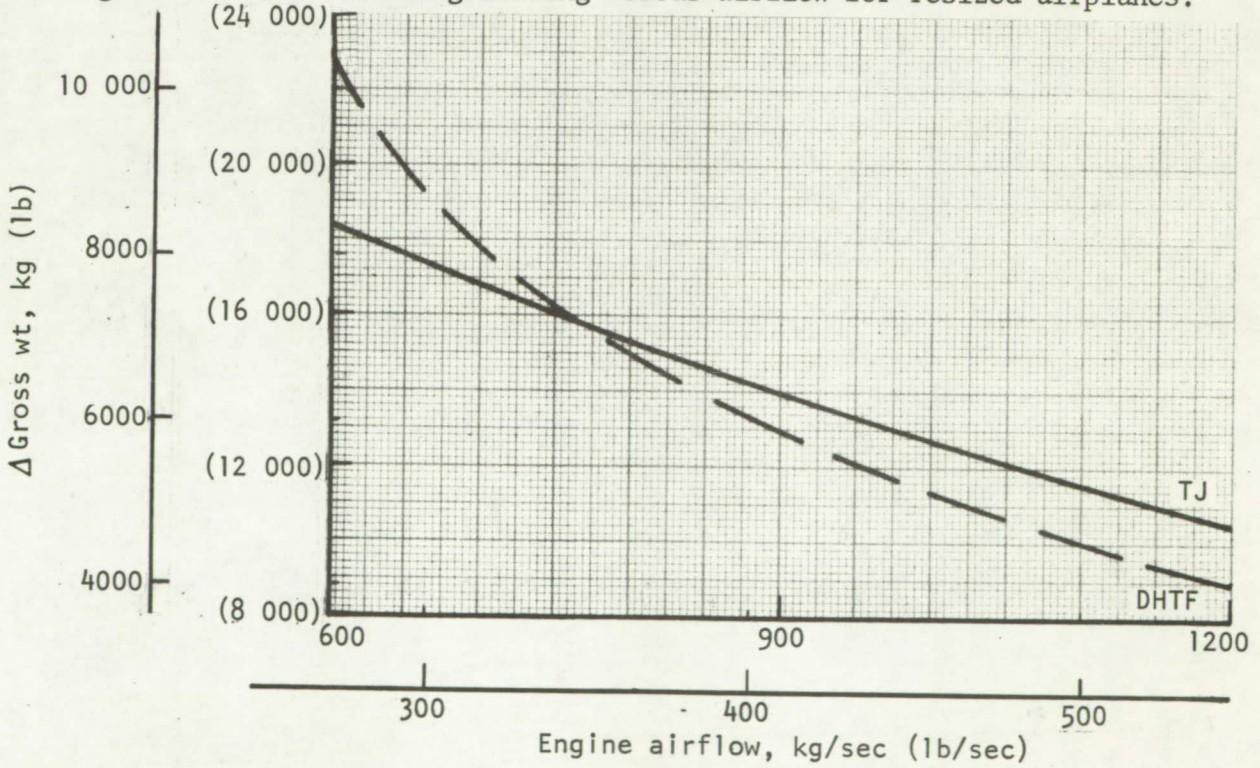

Figure 86.- Gross weight penalty due to wing fuel volume requirement.

TABLE XXIX.- MISSION SUMMARY FOR RESIZED AIRPLANE WITH 408 KG/SEC (900 LB/SEC) TURBOJET ENGINES

Design mission summary

Leg description	Weight		Altitude		Mach No.	Fuel used		Time, min	Total time, min	Range		Total range	
	kg	lb	m	ft		kg	lb			km	n. mi.	km	n. mi.
Initial weight	320 118	705 734											
1. Warmup and takeoff	315 153	694 787	0	0	0.30	4 965	10 947	11.00	11.00	0	0	0	0
2. Climb and accelerate	287 031	632 789	18 647	61 180	2.7	28 122	61 998	17.91	28.91	533.0	287.8	533.0	287.8
3. Cruise at 2.7 M	202 818	447 134	20 897	68 560	2.7	84 212	185 655	116.89	145.80	5589.8	3018.5	6122.8	3306.3
4. Descend to 457 m (1500 ft)	201 264	443 708	457	1 500	0.50	1 554	3 426	16.94	162.79	345.0	186.3	6467.8	3492.6
5. Approach and land	200 820	442 728	0	0	0.30	444	980	1.71	164.45	14.3	7.7	6482.0	3500.3
6. Taxi allowance	199 330	439 444	0	0	0	1 489	3 284	5.00	169.45	0	0	6482.0	3500.3
7. 5% fuel allowance	193 291	426 130	0	0	0	6 039	13 314	0	169.95	0	0	6482.0	3500.3
8. Climb	187 725	413 859	12 562	41 214	0.95	5 566	12 271	2.93	172.38	39.3	21.2	6521.3	3521.5
9. Subsonic cruise	181 917	401 056	12 750	41 833	0.95	5 807	12 803	17.88	190.26	300.7	162.4	6822.0	3683.9
10. Descend to 3048 m (10 000 ft)	180 758	398 501	3 048	10 000	0.42	1 158	2 555	10.22	200.48	125.9	68.0	6948.0	3751.9
11. Hold at 3048 m (10 000 ft)	170 738	376 409	3 048	10 000	0.42	10 020	22 092	30.00	230.48	0	0	6948.0	3751.9
12. Descend and land	169 891	374 532	0	0	0.30	846	1 866	3.64	239.12	32.4	17.5	6980.4	3769.4

Total fuel used = 150 227 kg (331 191 lb)

Alternate mission summary

Leg description	Weight		Altitude		Mach No.	Fuel used		Delta time, min	Total time, min	Delta range		Total range	
	kg	lb	m	ft		kg	lb			km	n. mi.	km	n. mi.
Initial weight	320 118	705 734											
1. Warmup and takeoff	315 153	694 787	0	0	0.30	4 965	10 947	11.00	11.00	0	0	0	0
2. Climb and accelerate	287 031	632 789	18 647	61 180	2.7	28 122	61 998	17.91	28.91	533.0	287.8	533.0	287.8
3. Cruise at 2.7 M	243 033	535 791	19 747	64 788	2.7	43 998	96 998	56.66	85.57	2708.0	1462.3	3240.9	1750.1
4. Descend to subsonic cruise	242 734	535 133	10 992	36 066	0.95	298	658	7.48	93.05	227.8	123.0	3468.7	1873.1
5. Subsonic cruise	200 403	441 810	12 039	39 500	0.95	42 331	93 323	104.10	197.15	1750.9	945.5	5219.6	2818.6
6. Descend and land	199 339	439 463	0	0	0.30	1 064	2 347	10.69	207.84	125.0	67.5	5344.6	2886.1
7. Reserve	169 900	374 562	0	0	0	29 438	64 901	64.68	272.52	498.1	269.0	5842.8	3155.1

Total fuel used = 150 218 kg (331 172 lb)

TABLE XXX.- MISSION SUMMARY FOR RESIZED AIRPLANE WITH 408 KG/SEC (900 LB/SEC) TURBOFAN ENGINES

Design mission summary

Leg description	Weight		Altitude		Mach No.	Fuel used		Time, min	Total time, min	Range		Total range	
	kg	lb	m	ft		kg	lb			km	n. mi.	km	n. mi.
Initial weight	313 648	691 468											
1. Warmup and takeoff	310 221	683 914	0	0	0.30	3 426	7 554	11.00	11.00	0	0	0	0
2. Climb and accelerate	279 634	616 482	18 291	60 011	2.7	30 587	67 432	11.44	22.44	278.7	150.5	278.7	150.5
3. Cruise at 2.7 M	192 820	425 092	20 911	68 605	2.7	86 814	191 390	121.54	143.98	5811.9	3138.4	6090.6	3288.9
4. Descend to 457 m (1500 ft)	191 047	421 183	457	1 500	0.50	1 773	3 909	18.89	162.87	376.7	203.4	6467.2	3492.3
5. Approach and land	190 757	420 542	0	0	0.30	291	641	1.85	164.72	15.4	8.3	6482.6	3500.6
6. Taxi allowance	190 087	419 065	0	0	0	670	1 477	5.00	169.72	0	0	6482.6	3500.6
7. 5% fuel allowance	181 437	399 997	0	0	0	8 649	19 068	0	169.72	0	0	6482.6	3500.6
8. Climb	175 916	387 824	12 293	40 330	0.91	5 522	12 173	8.17	177.89	115.6	62.4	6598.1	3563.0
9. Subsonic cruise	172 556	380 416	12 418	40 743	0.91	3 360	7 408	13.05	190.94	211.1	114.0	6809.3	3677.0
10. Descend to 3048 m (10 000 ft)	171 363	377 786	3 048	10 000	0.39	1 193	2 630	11.51	202.45	140.6	75.9	6949.8	3752.9
11. Hold at 3048 m (10 000 ft)	164 721	363 144	3 048	10 000	0.39	6 642	14 642	30.00	232.45	0	0	6949.8	3752.9
12. Descend and land	164 133	361 847	0	0	0.30	588	1 297	3.95	236.40	35.0	18.9	6984.8	3771.8

Total fuel used = 149 515 kg (329 621 lb)

Alternate mission summary

Leg description	Weight		Altitude		Mach No.	Fuel used		Delta time, min	Total time, min	Delta range		Total range	
	kg	lb	m	ft		kg	lb			km	n. mi.	km	n. mi.
Initial weight	313 648	691 468											
1. Warmup and takeoff	310 221	683 914	0	0	0.30	3 426	7 554	11.00	11.00	0	0	0	0
2. Climb and accelerate	279 634	616 482	18 291	60 011	2.7	30 587	67 432	11.44	22.44	278.7	150.5	278.7	150.5
3. Cruise at 2.7 M	231 909	511 267	19 408	63 673	2.7	47 725	105 215	61.98	84.42	2962.6	1599.8	3241.3	1750.3
4. Descend to subsonic cruise	231 412	510 171	9 878	32 407	0.90	497	1 096	8.81	93.23	257.6	139.1	3498.9	1889.4
5. Subsonic cruise	191 031	421 146	11 120	36 483	0.90	40 381	89 025	122.63	215.86	1970.4	1064.0	5469.3	2953.4
6. Descend and land	190 091	419 075	0	0	0.30	939	2 071	11.13	226.99	127.4	68.8	5596.7	3022.2
7. Reserve	164 137	361 856	0	0	0	25 954	57 219	66.69	293.68	502.2	271.2	6098.9	3293.4

Total fuel used = 149 511 kg (329 612 lb)

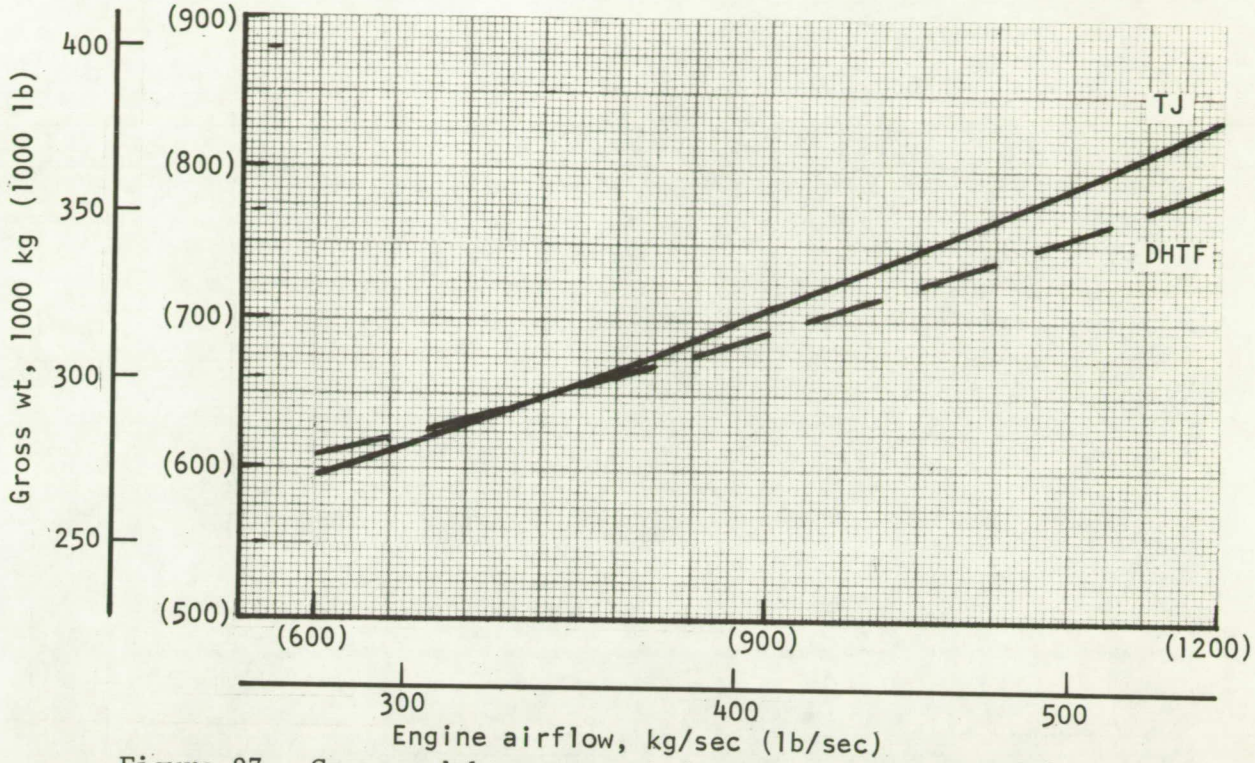

Figure 87.- Gross weight versus airflow for resized airplanes.

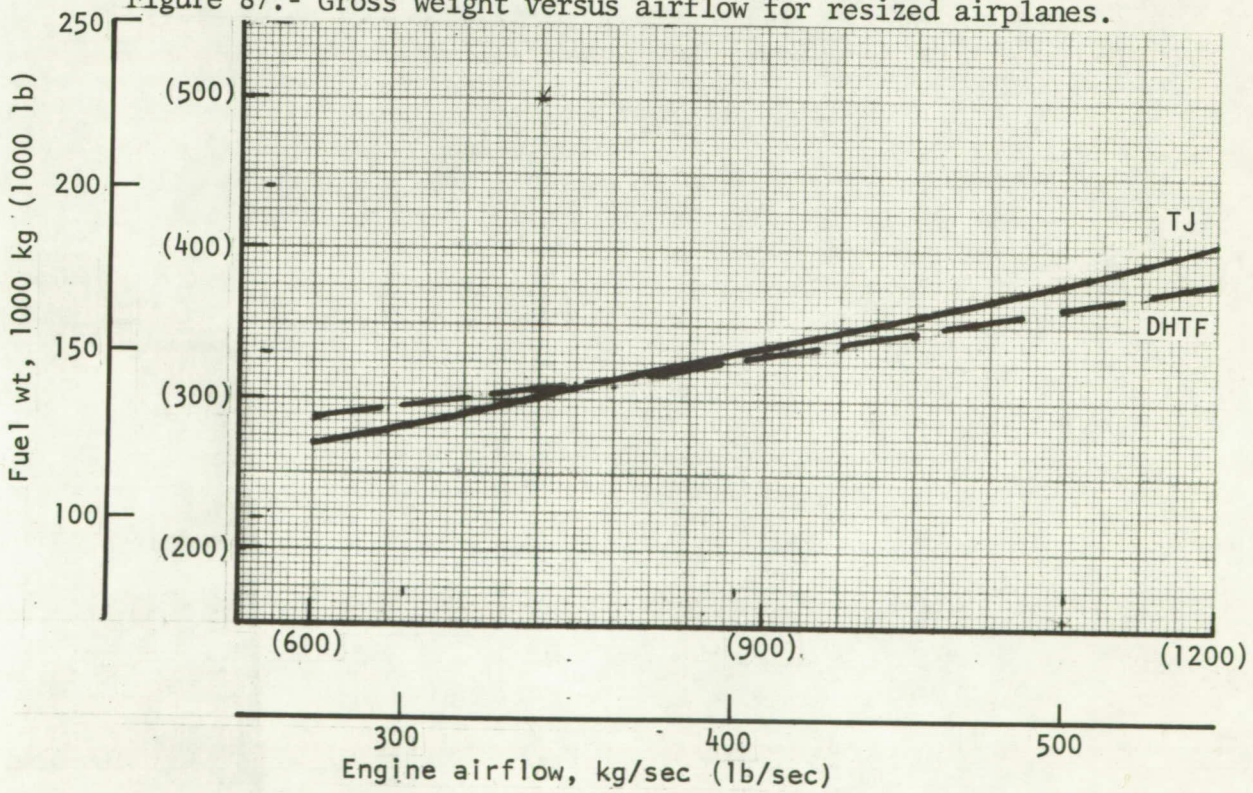

Figure 88.- Fuel weight versus airflow for resized airplanes.

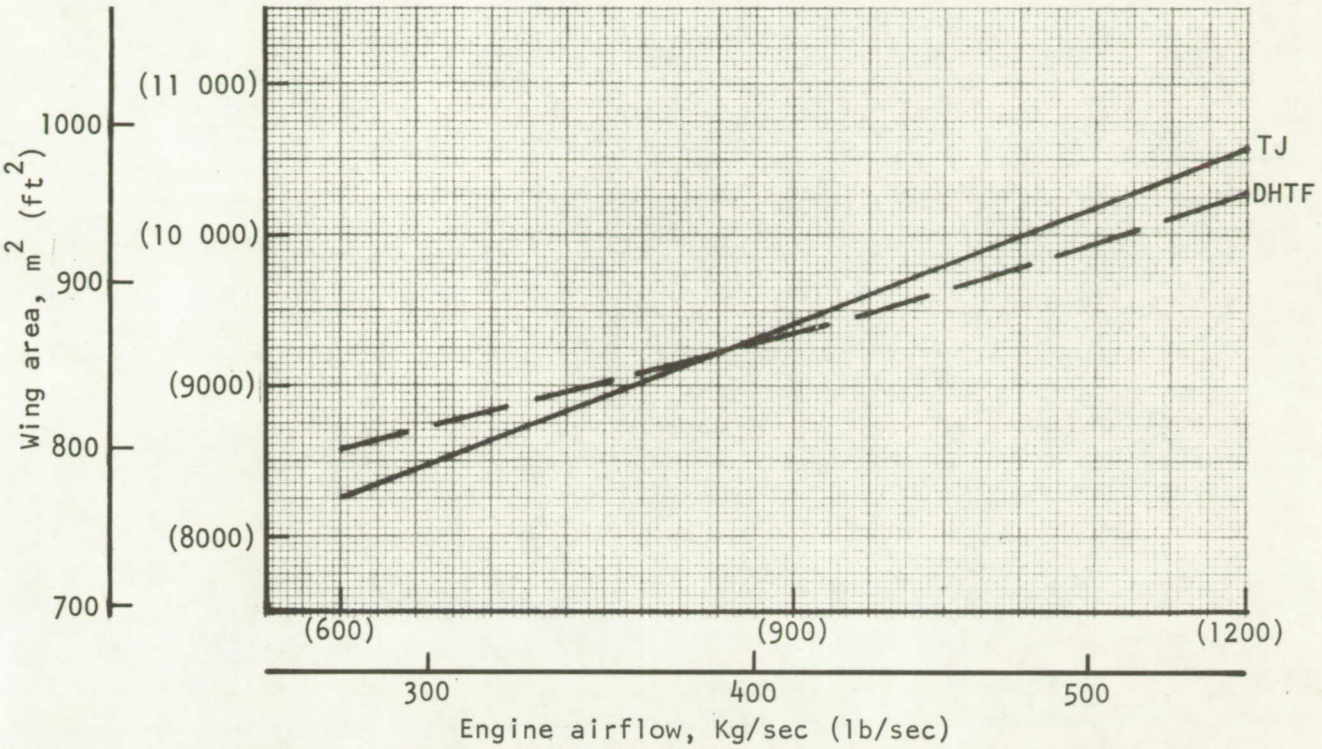

Figure 89.- Wing area versus airflow for resized airplanes.

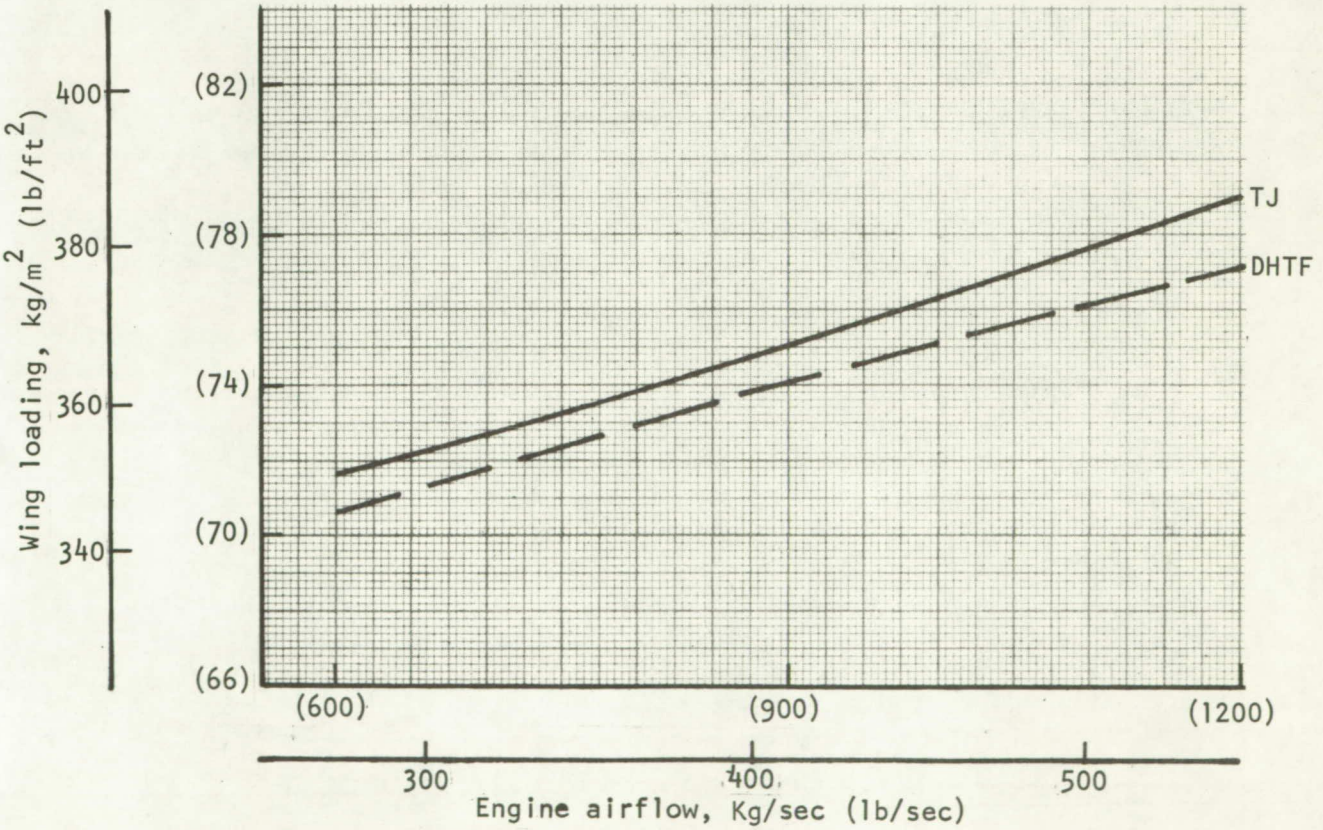

Figure 90.- Wing loading versus airflow for resized airplanes.

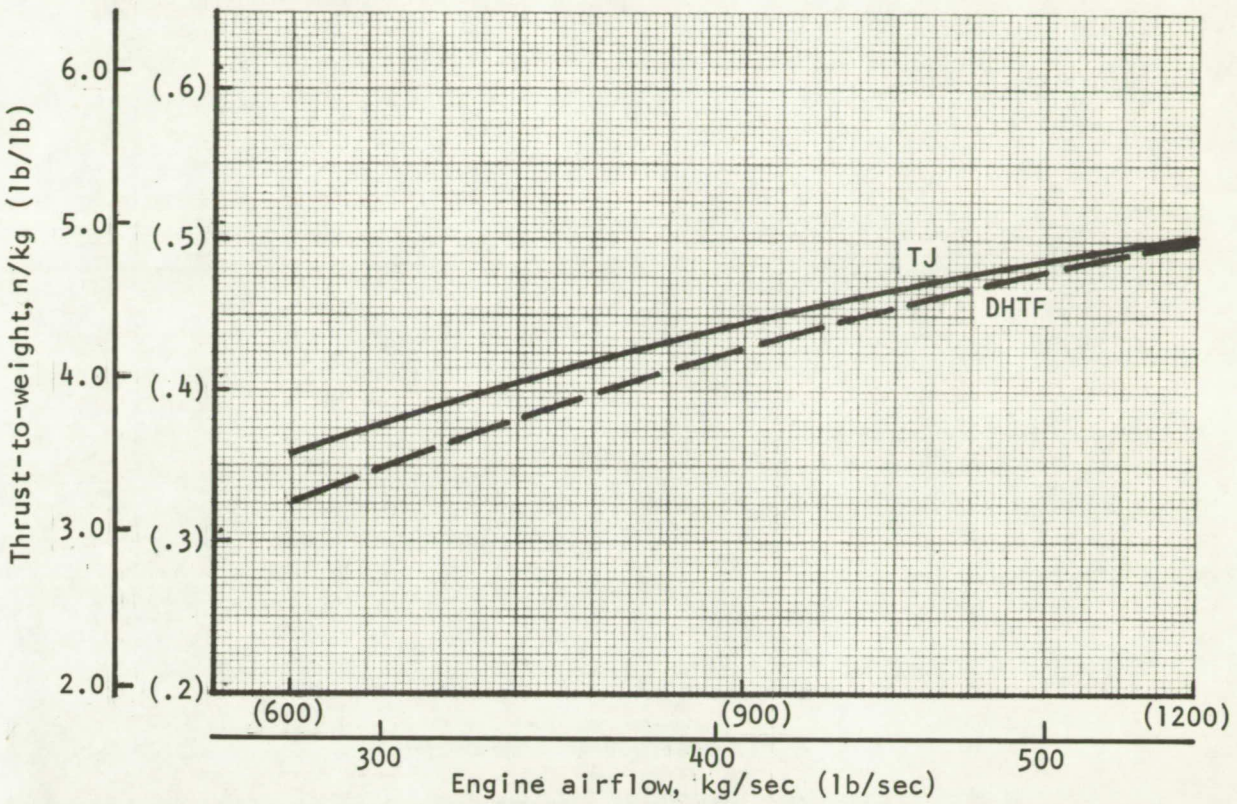

Figure 91.- Thrust-to-weight versus airflow for resized airplanes.

Performance items allowed to vary are shown in figures 92 through 95. All airplanes shown on these plots have a design mission range of 6481 km (3500 n. mi.) and have sufficient fuel volume available in the wing. Figures 96 and 97 show L/D and SFC values obtained at the start of the supersonic cruise. For comparison purposes, values of maximum L/D and minimum SFC are also shown for each airplane. Figure 98 shows the Mach 2.7 cruise efficiency factor, $\frac{L/D}{SFC}$, for each airplane, while figure 99 shows the total propulsion weight versus engine airflow. The latter includes engines, nozzles, nacelles, air induction system, engine controls, and accessories. Differences in the rate of change of the cruise efficiency with engine size and the increment in propulsion system weight between the turbofan and turbojet cycle are the cause of the relative shape change and magnitude of the gross weight curves of figure 87. The mismatch between operating and maximum cruise efficiency factor previously found for the constant takeoff gross weight performance has largely been eliminated by vehicle wing resizing. Calculation intervals for the final sizing were made for each 45.4 kg/sec (100 lb/sec) change in engine airflow, ranging from 272 kg/sec (600 lb/sec) to 544 kg/sec (1200 lb/sec).

The results of the second iteration may be readily compared to those of the first iteration by comparing the final gross weight values as shown in figure 87 with those indicated in figures 81 and 83. All results of the second iteration are within approximately 1 percent of the first iteration results. It was therefore concluded that the analysis had converged and that negligible refinement would result by performing further iterations.

Although there were no performance requirements to be met other than design mission range, there are desired levels of performance for takeoff and supersonic (T/D) ratio. These values are indicated on the respective plots. It is observed that all airplanes meet the desired balanced field takeoff distance of 3200 m (10 500 ft), except those turbofan-powered vehicles with engine airflow values below 286 kg/sec (630 lb/sec). Similarly, the desired all-engine takeoff distance of 2783 m (9130 ft) is met in all cases, except the turbofan-powered airplanes below 327 kg/sec (720 lb/sec) airflow. The desired value of T/D at 2.7 Mach, 18 300 m (60 000 ft) is met in all cases.

DISCUSSION OF RESULTS

An investigation has been made of the effects of various propulsion system parameters on the characteristics of a supersonic transport. The effects of engine size on wave drag, friction drag, drag-due-to-lift, wing sizing, airplane balance, and airplane weight were studied. These evaluations were made for two engine cycles, which further provided information on the effects of

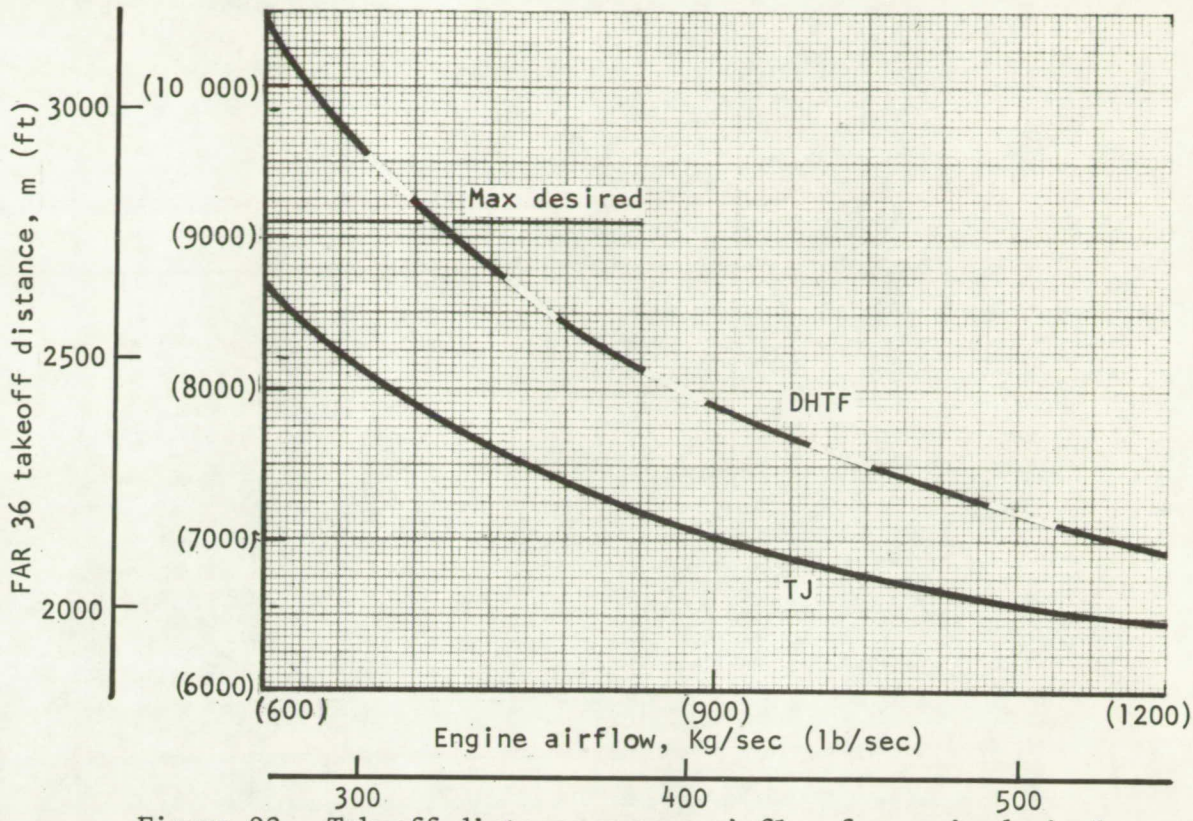

Figure 92.- Takeoff distance versus airflow for resized airplanes.

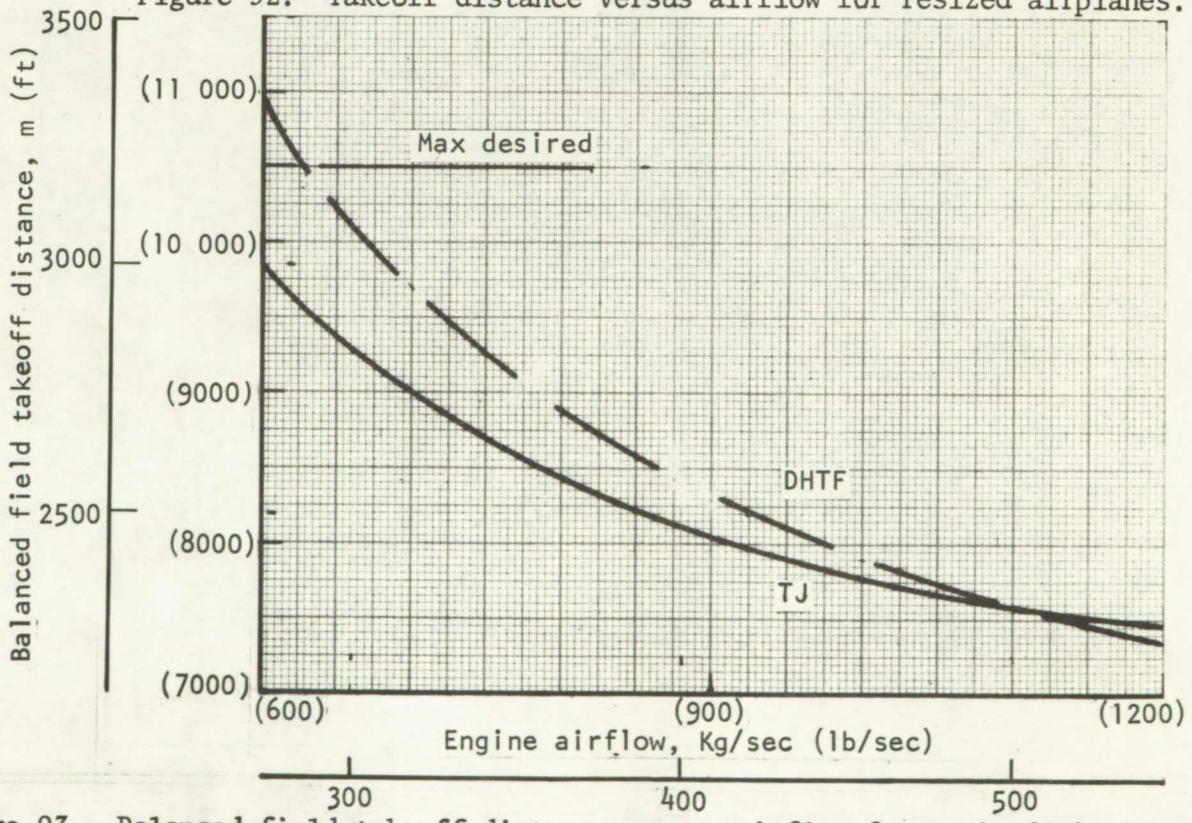

Figure 93.- Balanced field takeoff distance versus airflow for resized airplanes.

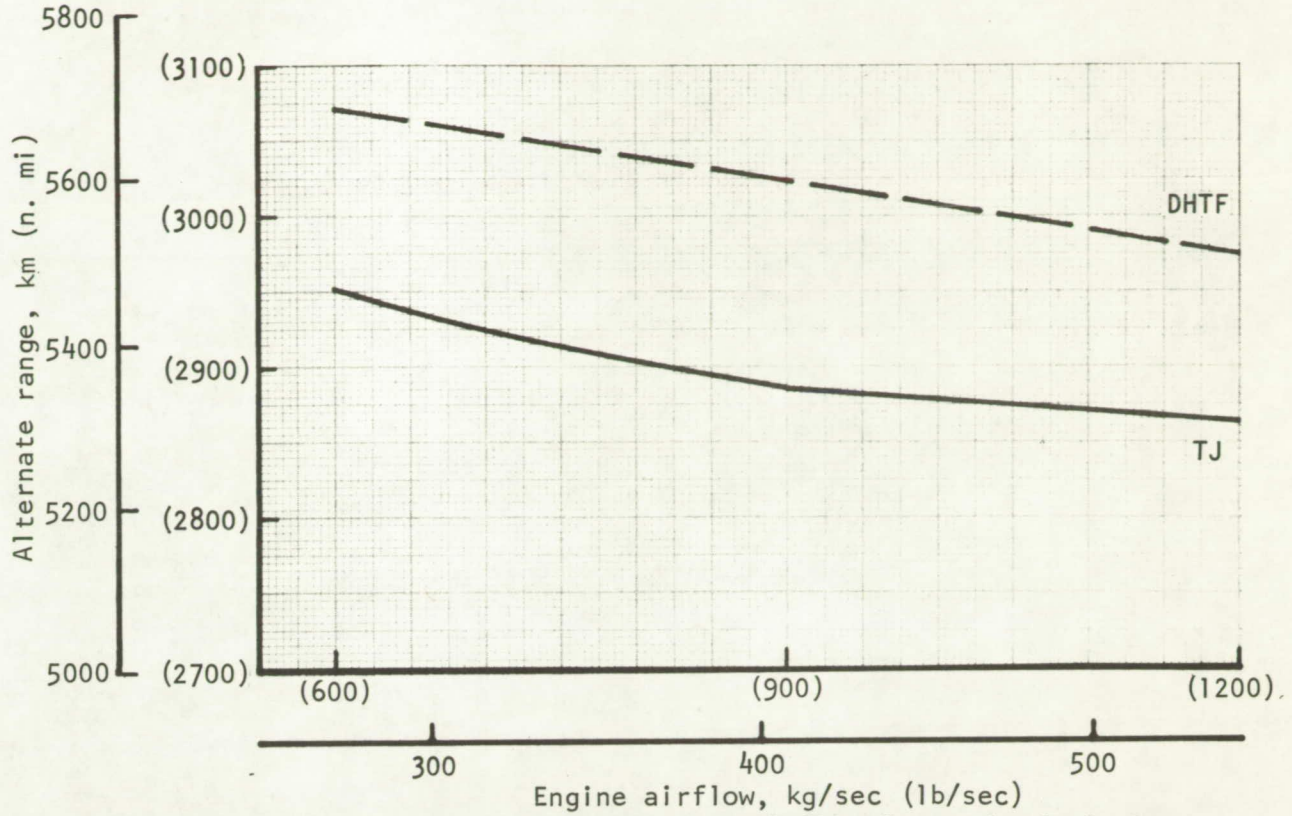

Figure 94.- Alternate mission range versus airflow for resized airplanes.

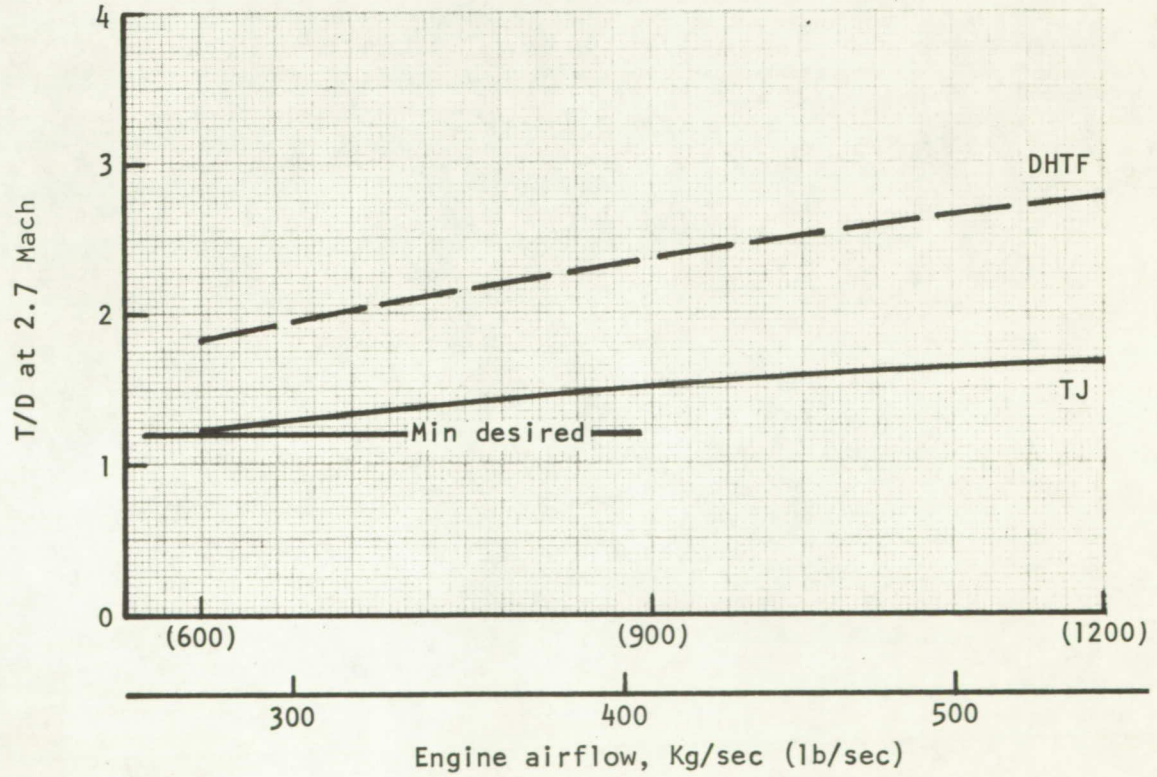

Figure 95.- T/D at 2.7 M versus airflow for resized airplanes.

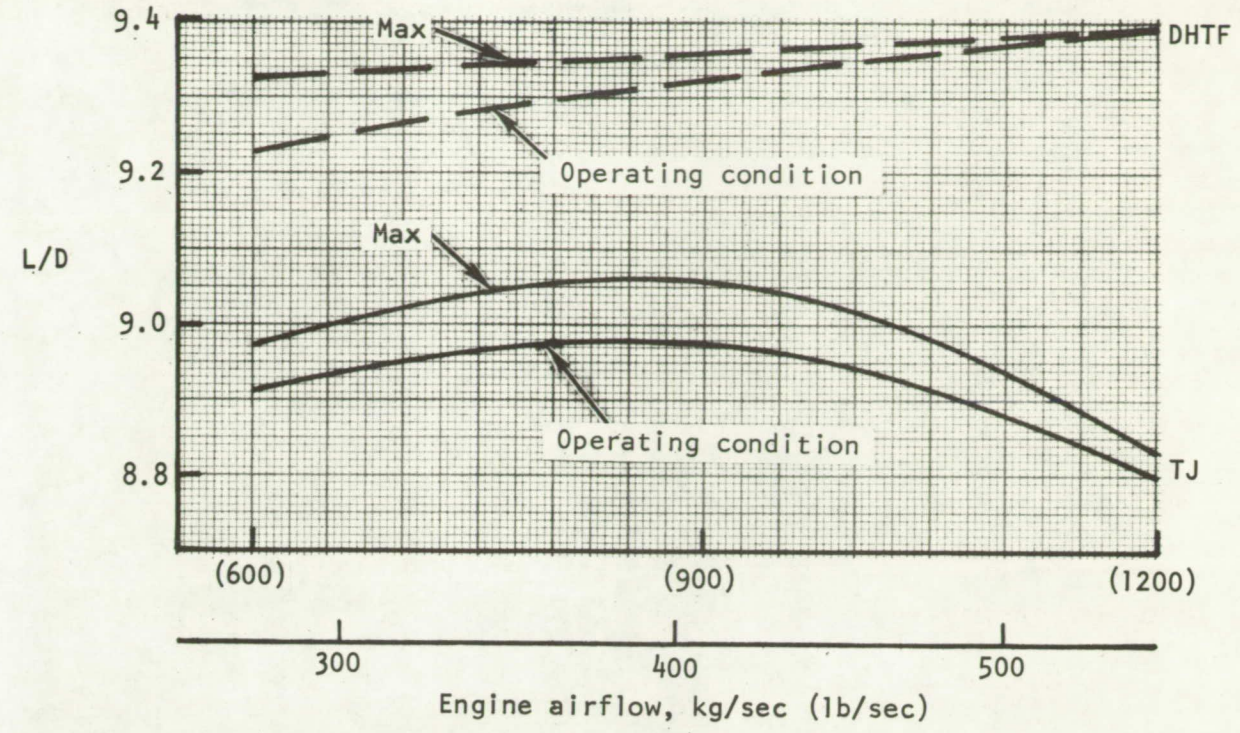

Figure 96.- Cruise L/D versus airflow for resized airplanes.

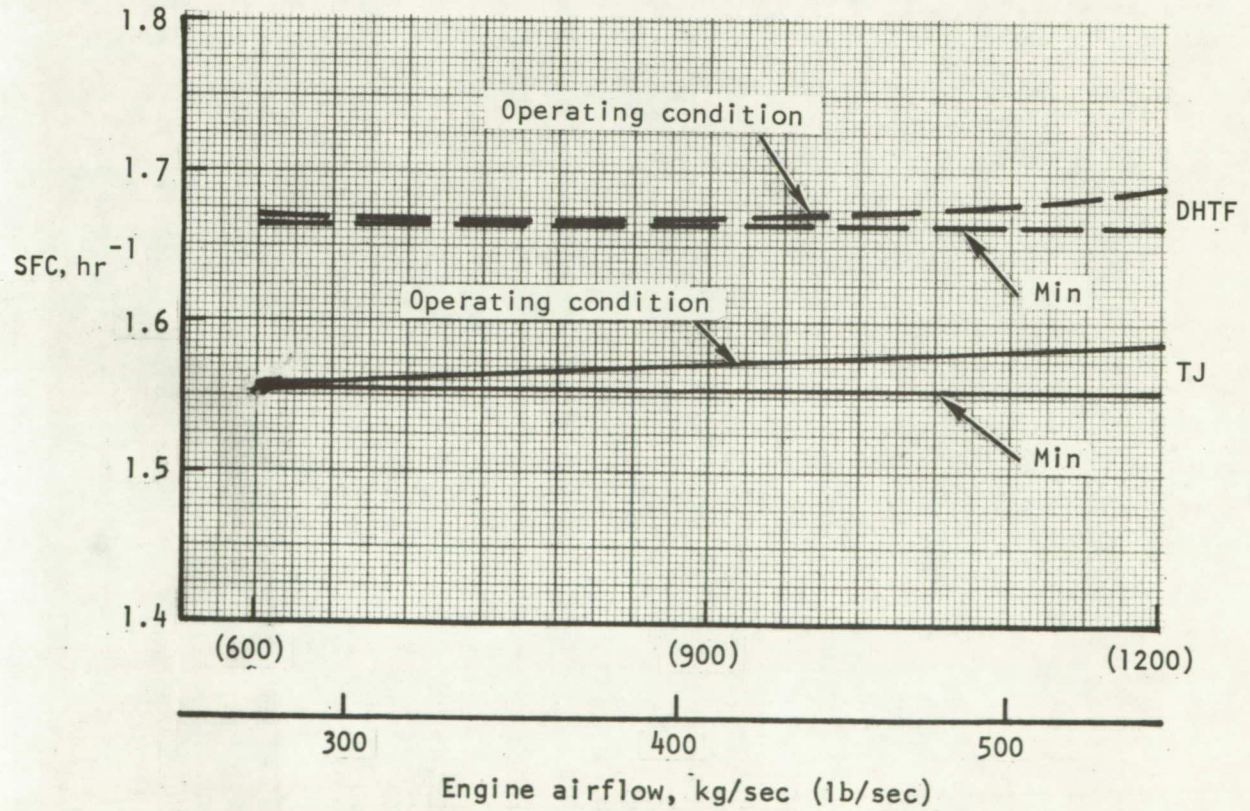

Figure 97.- Cruise SFC versus airflow for resized airplanes.

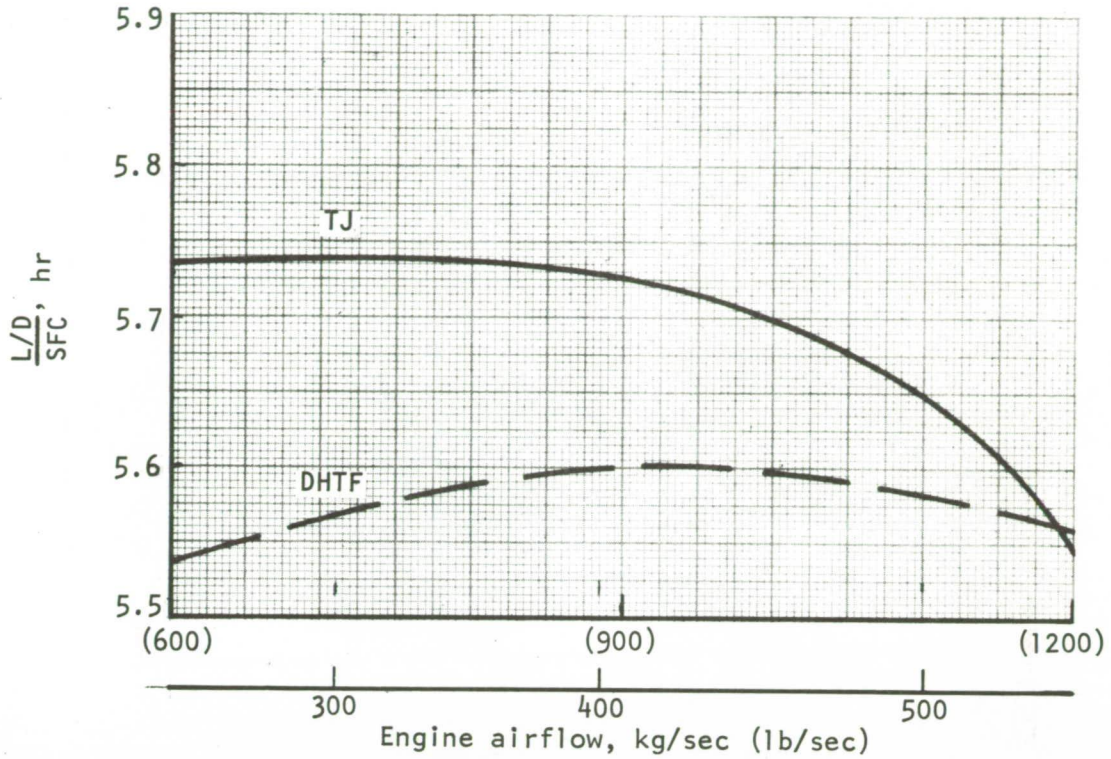

Figure 98.- Cruise efficiency versus airflow for resized airplanes.

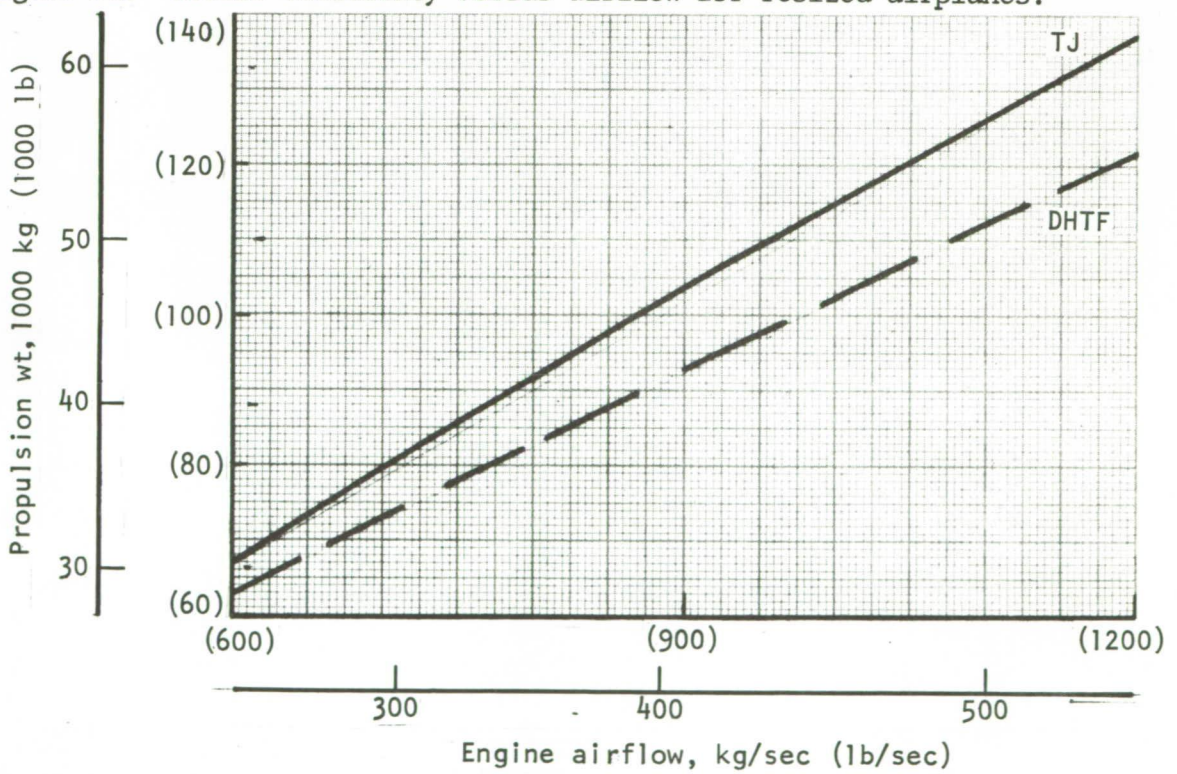

Figure 99.- Propulsion weight versus airflow for resized airplanes.

nacelle shape. Also, a comparison was made to illustrate the effects of using a slightly underexpanded nozzle as opposed to a fully expanded nozzle.

Cruise Drag Effects of Engine Mass Flow Rate and Nacelle Shape

A summary of the turbofan and turbojet nacelle installation drag for the balanced S_W = 995 sq m (10 713 sq ft) configuration is presented in figure 100 at Mach 2.7 as a function of engine size. These results are relative to the reference configuration nacelle installation. Absolute levels may be established by use of table III. The positive slope of the total incremental curves is a consequence of wetted area increases. The impact of nacelle shape on wave drag is clearly visible from these results, and is of equal or greater importance than the effect of engine size and the associated considerations of aerodynamic balance for the arrangement under consideration. Skin friction drag is primarily dependent on the engine size, as would be expected. The associated variation of L/D with engine size is presented in figure 77. The degradation of maximum L/D with increasing airflow is a result of increasing nacelle wetted area.

A summary of resized total configuration skin friction and wave drag characteristics is presented in figure 101 at Mach 2.7 as a function of airflow. All coefficients are based on their own wing area, in accordance with the table in the upper right-hand corner. Each analysis point has been balanced to neutral pitch stability at takeoff and has the same tail volume as the reference configuration. The variation of operating and maximum cruise L/D with engine size is presented in figure 96. The decrease above 408 kg/sec (900 lb/sec) airflow for the turbojet cycle is a result of the increased wave drag and wetted area.

Cruise Drag Effects of Nacelle Location

It was known, from the results of the earlier configuration studies from which the baseline configuration of this study was evolved, that the nacelles of the baseline airplane were favorably located, from the viewpoint of cruise wave drag. To examine the sensitivity of cruise drag to changes in nacelle location, wave drag increments were determined for three different manipulations of the longitudinal placement of the nacelles. In one case, all nacelles were moved forward and aft in unison. In the other cases, the inboard and outboard nacelles were moved independently of the other.

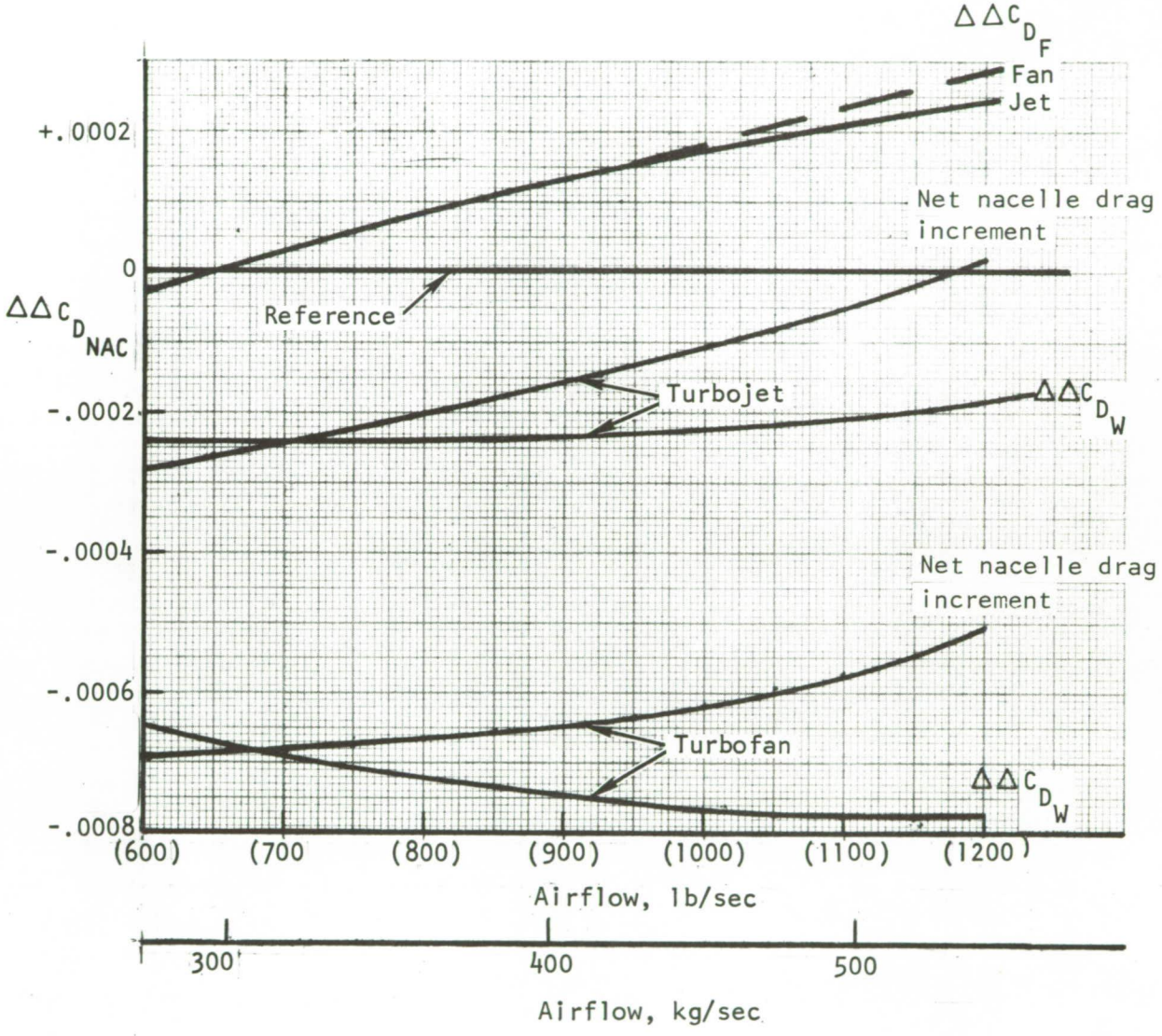

Figure 100.- Relative incremental nacelle drag as a function of design airflow.

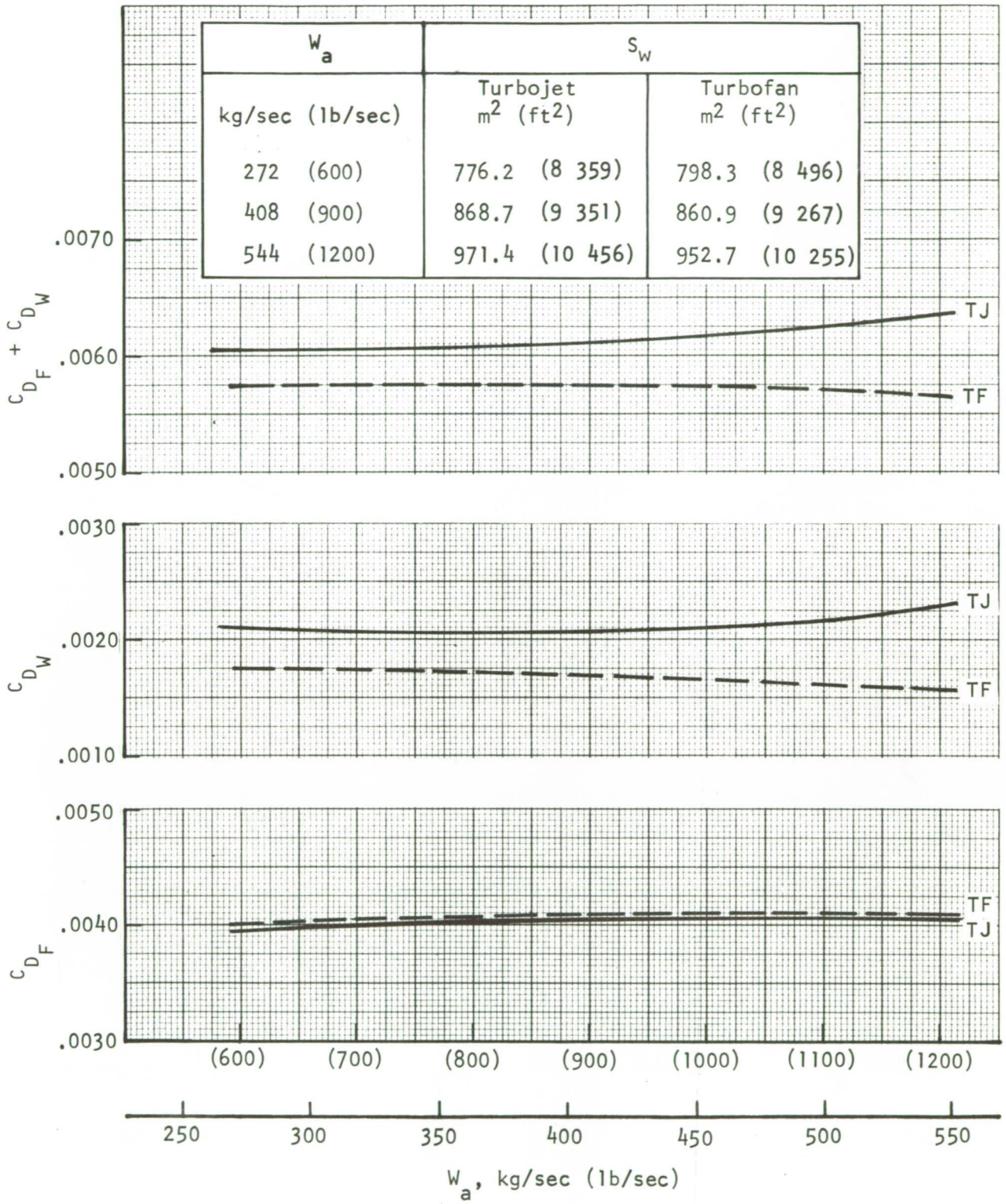

Figure 101.- Effect of engine size on preliminary resized configuration cruise drag.

The results of this evaluation of the effects of nacelle location on wave drag at Mach 2.7 are shown in figure 102 for the turbojet nacelle, and in figure 103 for the turbofan nacelle. The trend for both nacelles is seen to be that of increasing drag as the nacelles move forward and decreasing drag as they move aft, for a limited extent of movement. Further aft movement is restricted, of course, by the allowable extent of overhang of the nacelle beyond the wing structure.

The drag sensitivity of the location of the turbofan nacelle is seen to be much smaller than that of the turbojet nacelle, which is consistent with the weaker pressure field of the turbofan nacelle, as discussed previously.

Wing Camber Plane Deformation, Effects of Mass Flow Rate and Nacelle Shape

The effects of engine size on the incremental wing distortions required to cancel propulsion system induced disturbances due to thickness at the Mach 2.7 cruise condition are summarized in figure 104 for the turbojet nacelle, and in figure 105 for the turbofan nacelle. Three typical spanwise stations are shown: one station inboard of the inboard nacelle, one station between nacelles, and one station outboard of the outboard nacelle. In general, larger wing distortions are required to cancel pressures induced by the larger nacelles and for the turbojet cycle. The discontinuity in the deformation between the nacelles corresponds to the location of the second shock. The largest corrections are required between the nacelles as a result of both pods influencing this region.

Typical location of the nacelle influence field relative to the wing spar is presented in figure 106 for the baseline turbofan nacelle installation. Variations of required wing distortion along the rear spar are presented in figure 107 for two engine cycles and for three engine sizes. The reductions in the deformations required between the nacelles correspond to regions in which the nacelle thickness disturbance are either not felt (region A of figure 106) or are weak. In the case of the turbojet, the shock is stronger and consequently stands ahead of that for the turbofan, to the extent that the intersection point of the two shocks between the nacelles is located ahead of the spar.

Examination of the previous results indicates that nacelle shapes of high-volumetric efficiency (low wave drag) are compatible with small wing camber plane corrections required to maintain wing-body design cruise lifting efficiency.

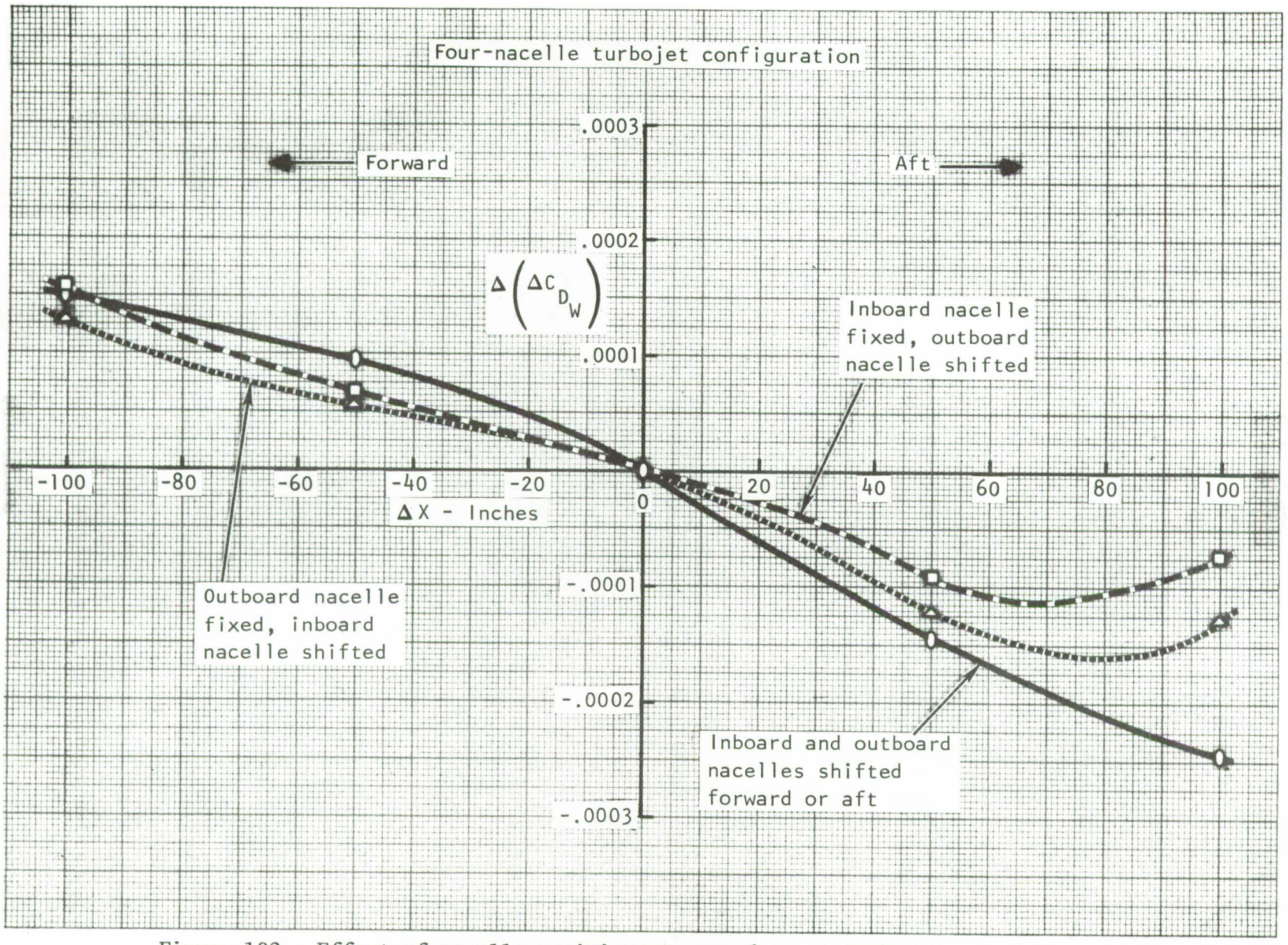

Figure 102.- Effect of nacelle position on wave drag at Mach 2.7 - turbojet nacelles.

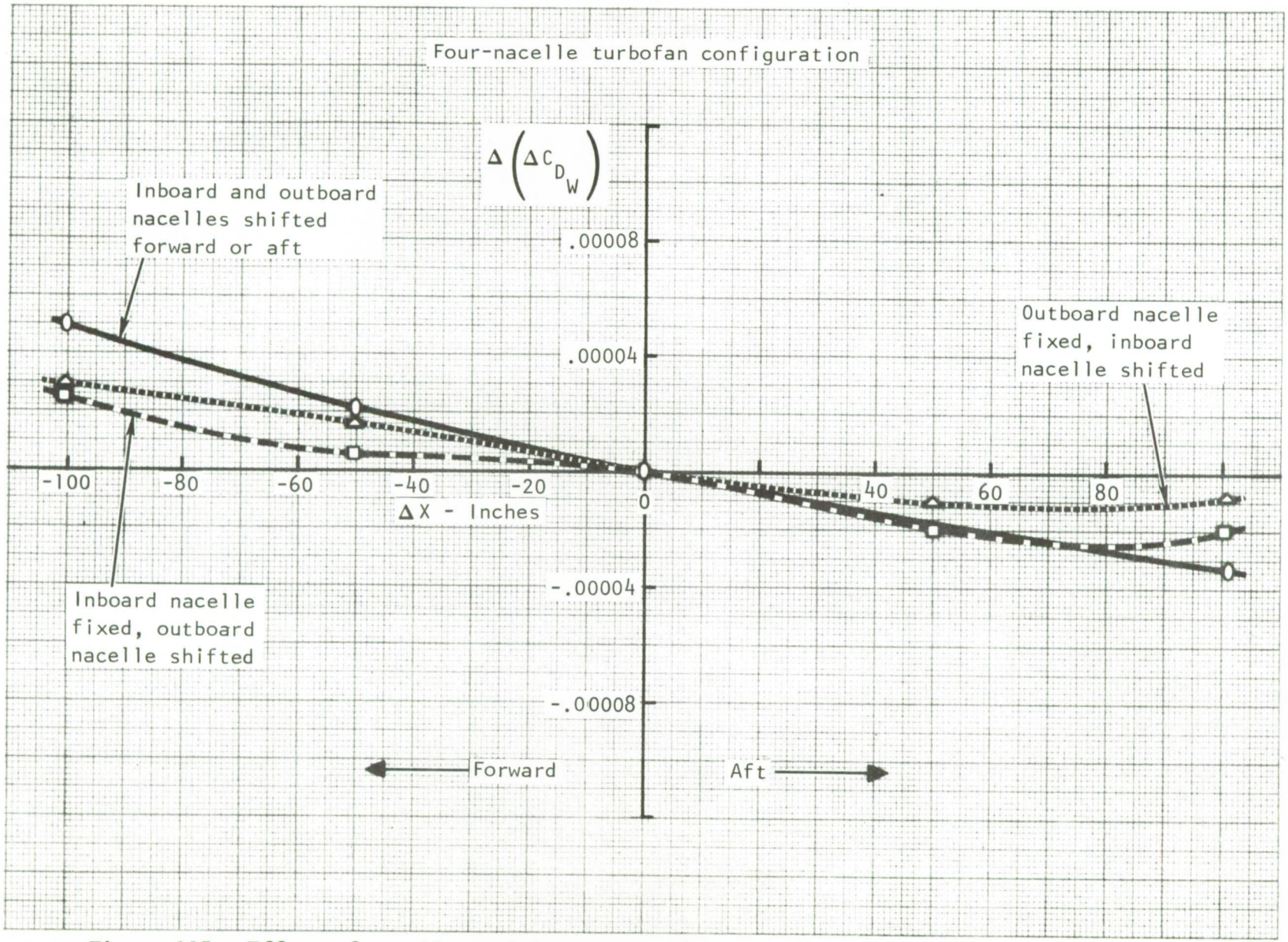

Figure 103.- Effect of nacelle position on wave drag at Mach 2.7 - turbofan nacelles.

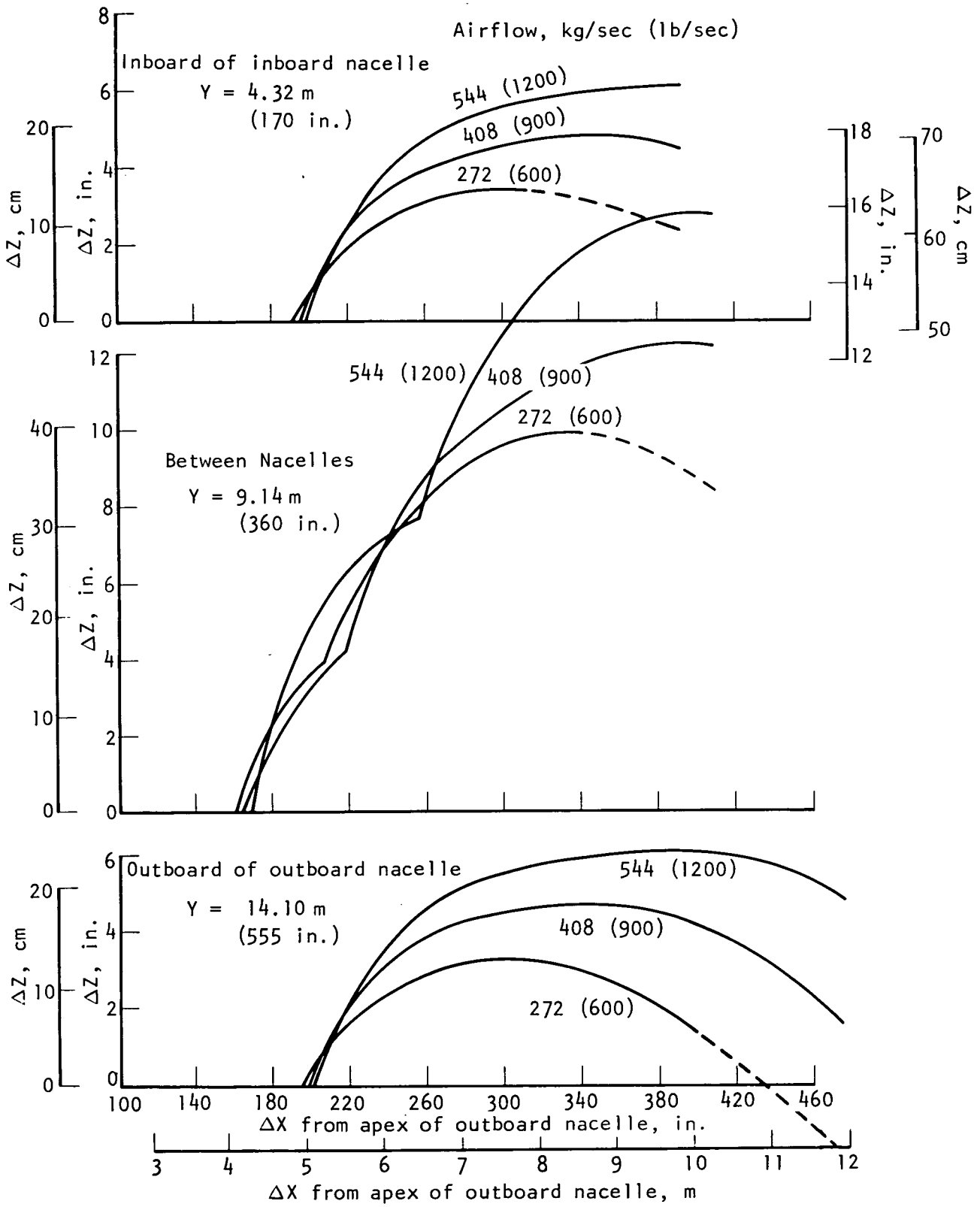

Figure 104.- Effect of engine size on wing distortion required to cancel turbojet nacelle-induced pressures.

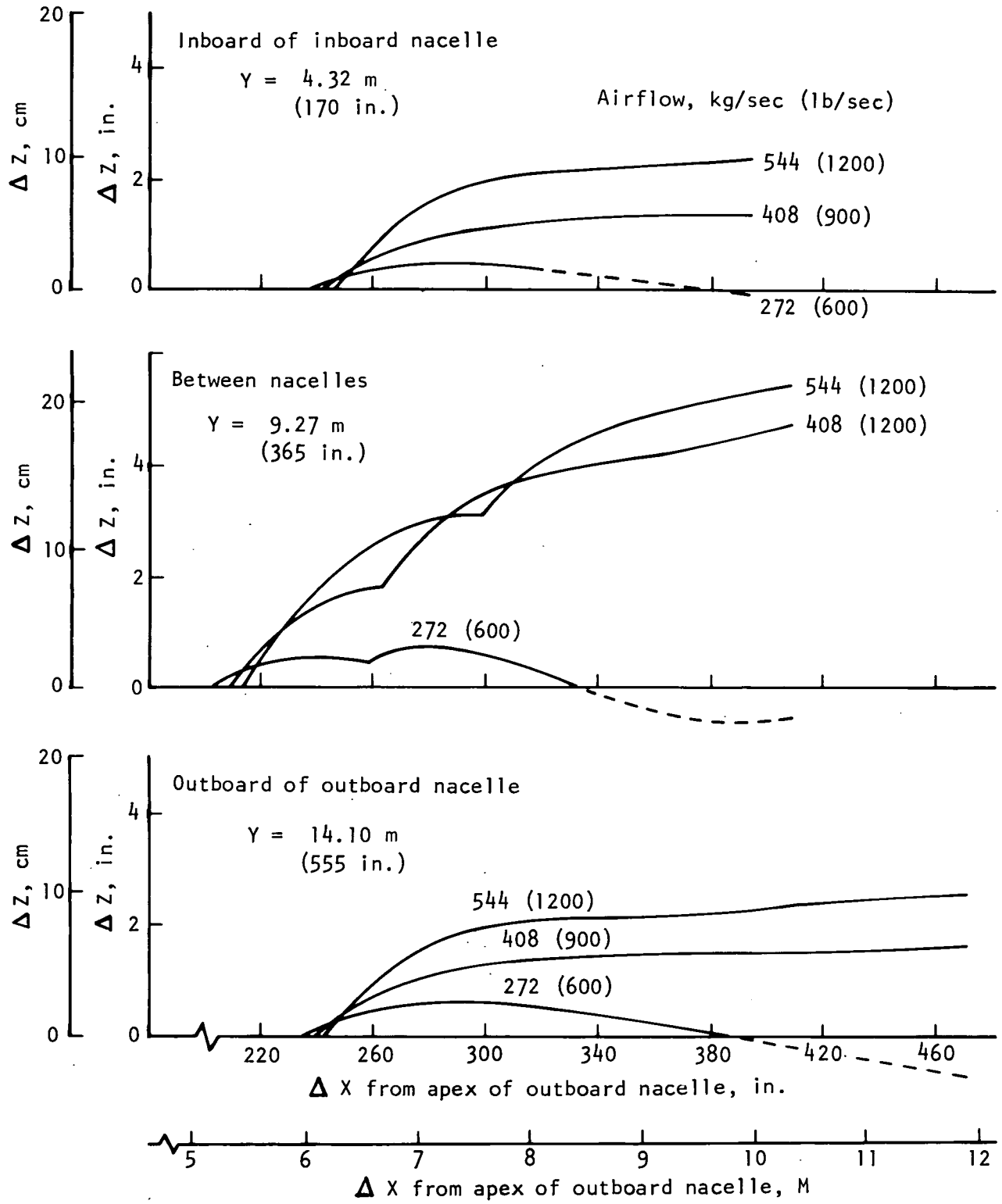

Figure 105.- Effect of engine size on wing distortion required to cancel turbofan nacelle-induced pressures.

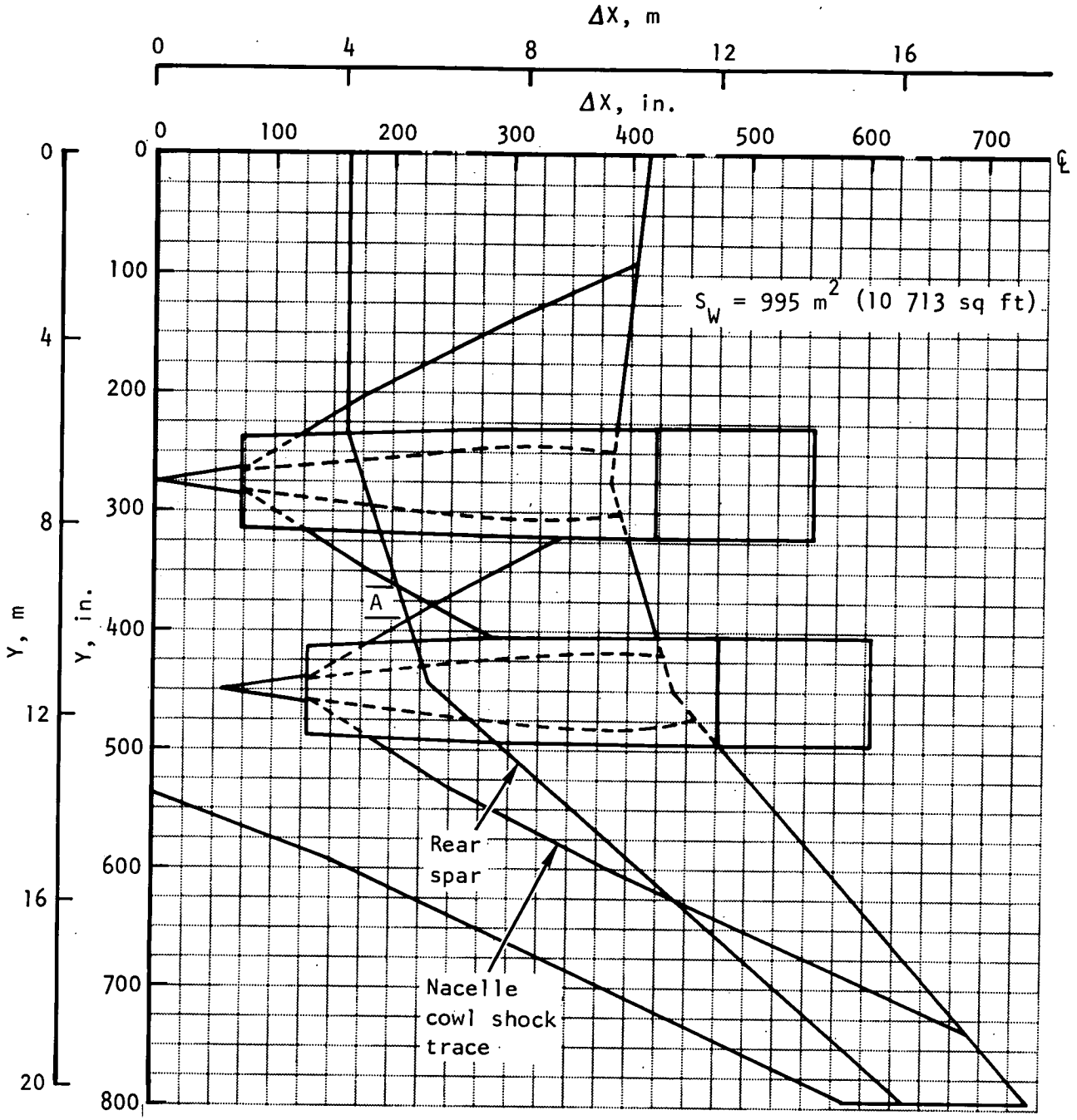

Figure 106.- Typical location of rear wing spar relative to 408 kg/sec (900 lb/sec) nacelle influence region.

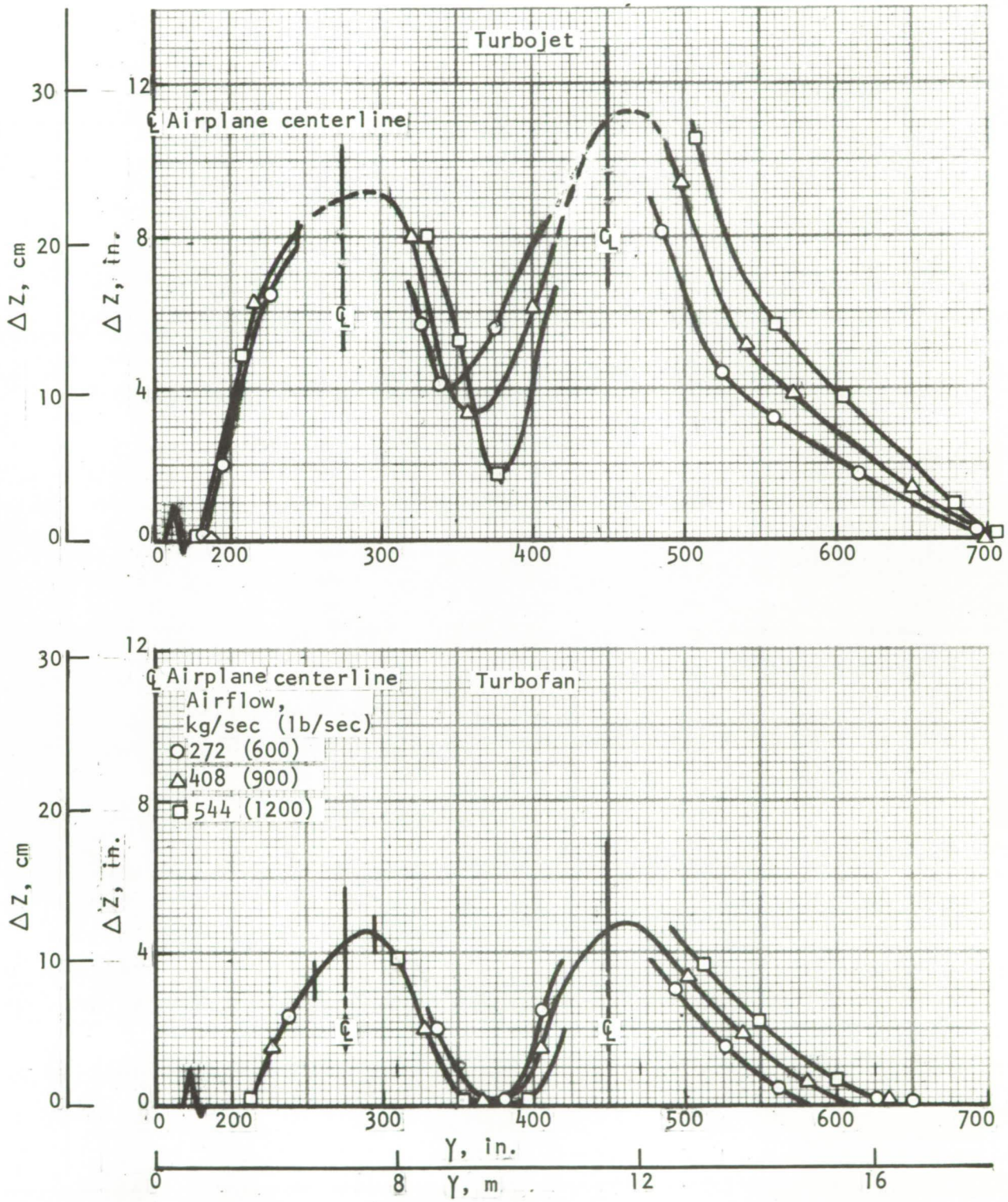

Figure 107. - Required wing distortion along rear spar to cancel nacelle thickness disturbance at 2.7 Mach.

Airplane Gross Weight Effects of Mass Flow Rate

The most pronounced effect of engine size found during the current study is the impact on TOGW for constant range performance. Increasing the airflow from 272 to 408 kg/sec (600 to 900 lb/sec) resulted in an increase in airplane weight (figure 87) of 43 000 to 55 000 kg (95 000 to 120 000 lb) and corresponds to a 16- to 20-percent increase for the same mission task. Examination of figures 98 and 99 indicates that the dominant controlling factor is the increased structural weight of the propulsion system and its multiplying effect on required fuel weight and wing size.

The difference in rate of growth between the turbojet and turbofan cycles of figure 87 is a result of (1) the more efficient installation of the latter from a wave drag point of view, and (2) the reduced rate of the propulsion system structural weight growth (figure 99) for the turbofan. The crossover point of about 340 kg/sec (750 lb/sec) airflow could undoubtedly be delayed by reducing the maximum nacelle cross-sectional area of the turbojet installation relative to the capture and exit area. Possible means of accomplishing this have been discussed briefly under "Propulsion," page 61.

Application to Preliminary Design Studies

From the viewpoint of external aerodynamic drag, the most meaningful characteristic of a nacelle installation is the axial distribution of nacelle cross-sectional area. The cross-sectional area of the nacelle is, of course, dictated by the external geometry of the engine and accessories, installation requirements, and the nacelle structure. Favorable trends in drag were shown in this study to result from reducing the maximum nacelle cross-sectional area relative to the inlet capture area, and by increasing the nozzle exit area relative to the capture area. Referring to the nacelle cross-sectional area distribution curves in figure 16, the wave drag at Mach 2.7 of the nacelle labeled "SF74-19" is five drag counts less than that of the nacelle labeled "TJ73-02." This increment of five drag counts amounts to 25 percent of the wave drag of the entire airplane at cruise speed, which is quite significant. A comparison of the nacelle envelopes, shown in figure 13a, illustrates the differences in capture area, maximum cross-sectional area, and nozzle exit area, which contribute to the substantial wave drag difference.

The more favorable design characteristics are obtained by eliminating, wherever possible, protuberances from the engine envelope, and by utilizing a fully expanded nozzle at cruise conditions. For both nacelles considered here, the maximum cross-sectional area was reduced as much as possible by moving the accessories from the engine case into the wing, and by submerging the engine as deeply as possible into the wing contour. Other trades in the engine design that would reduce the maximum cross-sectional area of the engine relative to the capture area should be investigated with respect to the effects on engine performance, engine weight, and airplane drag.

Other nacelle design considerations that affect the nacelle geometry, and which might be manipulated to improve the cross-sectional area distribution, are thrust reversers, noise suppressors, secondary and tertiary air, bleed ducts, compartment cooling, insulation, clearance allowances, mounting arrangements, pylon effects, and accessibility.

From a quantitative viewpoint, then, if a favorable nacelle cross-sectional area distribution (similar to that of SF74-19 in figure 16) is achieved, and if the nacelle is favorably located relative to the wing thickness distribution (as in the NASA arrow wing - SCAT 15F- configuration), it can be assumed, as a minimum, that there is no wave drag penalty at the design cruise Mach number due to the nacelle installation. Also, for a well-shaped nacelle, it can be assumed that the nacelle interference effects on drag-due-to-lift can be eliminated at the same condition by proper wing camber plane warping.

A less conservative assumption is warranted under the circumstances that favorable nacelle shaping is achieved and that the twist and camber of the wing is optimized with the nacelle interference effects included. If these conditions are met, the nacelle can be added to the wing-body configuration with a net reduction of pressure drag of a magnitude that would largely offset the friction drag of the nacelle at the supersonic cruise condition. (For the baseline airplane of this study, it is believed that this assumption would apply to nacelle sizes up to that of the 900 lb/sec engine.)

The foregoing clearly does not apply to less well-shaped nacelle area distributions, as evidenced by the results of figure 17. If the nacelle shape does not meet the aforementioned criteria for favorable cross-sectional area distribution characteristics, then the effects of the nacelle on cruise drag must be determined by specific analysis of the resulting configuration.

The effect of engine size on airplane weight is about 4.1 pounds increase in takeoff gross weight per pound increase in bare engine weight. This value pertains to the design mission of 234 passengers and 3500 n mi range, and will be greater if the design range is increased.

RECOMMENDATIONS

Propulsion system size and nacelle shaping have been shown to have significant effects on the drag and performance of a supersonic cruising airplane. Because of the sensitivity of the drag of supersonic airplanes to nacelle shaping, and because of the dependence of nacelle shape on details of the engine cycle, it is recommended that further effort be directed toward optimization of the supersonic transport configuration through engine cycle-engine packaging studies. For example, addition of variable geometry (variable turbine area and additional variable compressor and fan stators) should improve both

turbojet-and turbofan-powered aircraft. The turbojet nacelle arrangement could be improved with variable geometry because the airflow demand (and, thus, the inlet shape) and the exhaust nozzle area could be tailored to better match the nacelle maximum cross-sectional area. This would result in reduced aircraft drag. Also, addition of variable geometry to the turbofan should improve its specific fuel consumption at supersonic cruise. Further integration work with variable-cycle engines (with multiple flow paths) is also believed warranted due to their potential of reduced takeoff noise, improved subsonic cruise fuel consumption, and supersonic fuel consumption near that of a turbojet.

REFERENCES

1. Tyson, Ray M., et al, "Study of a Multimode Intergrated Propulsion System in an Advanced Supersonic Transport," NASA Contract NAS1-12245, February 1974.

2. Lockheed-California Company Report LR 26133 (Prepared under Consultation agreement by Trans World Airlines, Inc),"An Airline's View of Reserve Fuel Requirements for the Supersonic Transport," 19 September 1973.

3. Boeing Document D 6A 11666-1.

4. Sommer, S., and Short, B., "Free Flight Measurements of Turbulent Boundary Layer Skin Friction in the Presence of Severe Aerodynamic Heating at Mach Numbers From 2.8 to 7.0," NACA TN 3391, 1955.

5. Schoenherr, K. E., "Resistance of Flat Plates Moving Through a Fluid," Transactions of Society of Naval Architects and Marine Engineers, Vol 40, pp 279-313, 1952.

6. Jones, R. T., "Theory of Wing-Body Drag at Supersonic Speeds," NACA RM A53H18a, 1953 (Also NACA TR 1284).

7. Bonner, E., "Theoretical Prediction of Supersonic Pressure Drag," NA-66-862, Rockwell International, 1966. (Also refer to AIAA Paper 69-1132.)

8. "Advanced Supersonic Technology Concept Study Reference Characteristics," NASA CR-132377, December 1973.

9. Williston, K. W., "Advanced Supersonic Technology Integrated Variable Cycle Propulsion System Performance Analysis," NA-73-818, Rockwell International, November 1973.

10. Williston, K. W., "Duct Heating Turbofan Propulsion Data for Advanced Supersonic Technology Study," TFD-74-887, Rockwell International.

11. Nichols, Mark R., "Aerodynamics of Airframe-Engine Integration of Supersonic Aircraft," NASA TN D-3390, August 1966.

12. Sigalla, A., and Hallstaff, T. H., "Aerodynamics of Powerplant Installation on Supersonic Aircraft," AIAA Journal of Aircraft, July-August 1967, pp 273-277.

13. Baals, D. D., Robins, A. W., and Harris, R. V., "Aerodynamic Design Integration of Supersonic Aircraft," AIAA paper 68-1018, 1968.

14. Mack, R. J., "A Numerical Method for Evaluation and Utilization of Supersonic Nacelle-Wing Inteference," NASA TN D-5057, 1969.

15. Kutler, P., et al, "Numerical Computation of Multishock Three-Dimensional Supersonic Flow Fields With Real Gas Effects," AIAA Paper 72-702, 1972.

16. Woodward, F. A., "Analysis and Design of Wing-Body Combinations at Subsonic and Supersonic Speeds," AIAA J. of Aircraft, Vol 5, No. 6, November 1968.